November 2020

Synthesis and Investigation of Amphiphilic Polypeptoids for Environmental and Biological Applications

Tianyi Yu
Louisiana State University and Agricultural and Mechanical College

SYNTHESIS AND INVESTIGATION OF AMPHIPHILIC POLYPEPTOIDS FOR ENVIRONMENTAL AND BIOLOGICAL APPLICATIONS

A Dissertation

Submitted to the Graduate Faculty of the
Louisiana State University and
Agricultural and Mechanical College
in partial fulfillment of the
requirements for the degree of
Doctor of Philosophy

in

The Department of Chemistry

by
Tianyi Yu
M.S., The University of Akron, 2013
B.Eng., East China University of Science and Technology, 2012
December 2020

ACKNOWLEDGEMENTS

First, I would like to express my great gratitude to my advisor Prof. Donghui Zhang for all her guidance, mentoring and strong support throughout my graduate studies. Dr. Zhang is a talented and passionate scientist, and her enthusiasm for research and constant encouragement energized me to continue in academic research. I feel very privileged to have her as my supervisor.

My thanks also go to my research committee Prof. Gerald J. Schneider, Prof. M. Graça H. Vicente, and Prof. Christopher G. Arges for all the intellectual contributions to my thesis.

I am very grateful to my collaborators and this work cannot be achieved without their contribution and assistance. I would like to express my great gratitude to Prof. Vijay John in Department of Chemical & Biomolecular Engineering at Tulane University, who offered me a lot of suggestions and tremendous support on my research. Also, I would like to thank his group members Marzhana Omarova, Igor Kevin Mkam Tsengam, and Dr. Jiangqiang Chen for their help with my research and many discussions about my projects. I would like to take this opportunity to sincerely thank to Prof. Diane A. Blake in School of Medicine at Tulane University and her graduate student Lauren T. Swientoniewski for their great help with the bacterial cell growth study. Also, I would like to thank to Prof. Yuri M. Lvov in Institute for Micromanufacturing at Louisiana Tech University and his student Abishek Panchal for their help with my research.

I would like to especially thank to Dr. Naisheng Jiang, who was a postdoc associate in our group and currently is a professor in Beijing University of Science and Technology, for all of his teaching and training on SANS and SAXS experiments.

I have been feeling super lucky to have an outstanding undergrad researcher, Omead A. Darvish, who worked with me for more than two years and made very important contributions in monomer synthesis and polymer characterizations for my research projects.

I would like to thank to Dr. Jibao He in Microscopy Laboratory at Tulane University and Dr. Ying Xiao in Shared Instrumentation Facility (SIF) at LSU for the assistance with cryo-TEM experiments. I am very thankful to Dr. Cueto in Polymer Analysis Lab (PAL) at LSU for the help with TGA experiments and all the valuable suggestions on DLS analysis.

I would like to thank all my lab-mates, Dr. Brandon A. Chan, Dr. Xin Li, Dr. Sunting Xuan, Zhaoyuan Liu, Dr. Ang Li, Dr. Jinbao Cao, Dr. Lu Lu, Dr. Albert Chao, Dr. Jessica M. Simpson, Dr. Garrett L. Sternhagen, David Siefker, Meng Zhang, Bailee N. Barrett, Md. Asmat Ullah, Erin H. Tsai for their camaraderie and support during this research journey.

Most importantly, I would like to express my deeply gratitude to my parents for their unconditional love and endless support throughout my life. I am truly blessed to be their daughter.

In the end, I would express my special thanks to my husband, your everyday encouragement and love give me the most strength.

I dedicate this work to you all.

TABLE OF CONTENTS

TABLE OF ABBREVIATIONS

NMR	nuclear magnetic resonance
FT-IR	Fourier-transform infrared spectroscopy
DLS	dynamic light scattering
SLS	static light scattering
Cryo-TEM	cryogenic transmission electron microscopy
TGA	thermogravimetric analysis
M_n	number-average molecular weight
DP_n	number-average degree of polymerization
MEM	maximum entropy method
PDI	polydispersity index
DCM	dichloromethane
$CDCl_3$	deuterated chloroform
CD_2Cl_2	deuterated dichloromethane
DMSO	dimethyl sulfoxide
R-NCA	*N*-substituted glycine derived *N*-carboxyanhydride
DRI	differential refractive index
SEC	size exclusion chromatography
SANS	small-angle neutron scattering
SAXS	small-angle X-ray scattering
T_{gel}	gelation temperature

ABSTRACT

Polypeptoids are an emerging class of peptidomimetic polymers featuring *N*-substituted polyglycine backbones. Polypeptoids are cyto-compatible and backbone degradable, making them appealing to many biological applications. When the highly polar polyamide backbone is coupled with non-polar aliphatic side chains, polypeptoids can be considered as facial amphiphiles. Without extensive hydrogen bonding along the backbone, the conformation of polypeptoid is largely controlled by the *N*-substituent structures. The hydrophobicity-lipophilicity balance of polypeptoids can be readily tuned with the *N*-substituent structures as well as the molar ratio between the hydrophilic and hydrophobic segments in their copolymers. In view of these combined attributes, amphiphilic polypeptoids represent an attractive polymer platform to systematically investigate the effect of polymer composition and *N*-substituent structures on their performance as facial amphiphiles. This dissertation includes four chapters introducing the use of facially amphiphilic polypeptoids towards environmental and biological applications.

Chapter 1 gives a general introduction to the recent development on the materials and methods used in the isolation and stabilization of membrane proteins in aqueous solutions.

Chapter 2 presents the investigation of fragmentation of synthetic liposomes using hydrophobically modified polypeptoids (HMP) towards membrane protein extraction. The effects of molecular characteristics of polypeptoids on the relative rate and extent of liposome fragmentation were elucidated by using a combination of SLS, DLS and cryo-TEM methods.

Chapter 3 reports the design and synthesis of amphiphilic polypeptoids-functionalized Halloysites nanotubes (HNTs), a class of naturally occurring clay nanotubes, as Pickering emulsions stabilizers towards oil-spill remediation application. The effects of polypeptoid grafting

and the molecular characteristics of grafted polypeptoids on HNTs on emulsion performances and the cell proliferation of hydrocarbon degrading bacteria were also investigated.

Chapter 4 presents a work on the synthesis, characterization and investigation of structural change of ABC thermo-responsive triblock copolypeptoids during the reversible sol-gel transition in water. The temperature-dependent structural evolution and the effect of polymer hydrophobic fraction on the polymer self-assembly were investigated by SANS and cryo-TEM method.

CHAPTER 1. RECENT DEVELOPMENTS ON ISOLATION AND STABILIZATION OF MEMBRANE PROTEINS IN AQUEOUS SOLUTIONS FOR STRUCTURAL AND FUNCTIONAL STUDIES

1.1 Challenges in characterization of membrane proteins

Approximately 30% proteins in eukaryotic cells are membrane proteins (MP) which can function as transporters, receptors, anchors and enzymes. Membrane proteins represent over 60% of the drug targets, [32] and the structures of membrane protein are critical for understanding the cellular function associated with many diseases, *e.g*. cystic fibrosis, obesity, *etc*. Whereas till 2015, structures of only less than 2% membrane protein have been deposited,[37,38] which strongly limits our understanding on cellular membrane biology thus the development of drugs targeted on membrane protein. The major challenge for membrane protein characterization is due to the intrinsic high hydrophobicity of membrane proteins and the requirement of membrane environment for their functional stability. Recent developments on isolation and stabilization of membrane proteins in aqueous solution for their structural and functional studies will be discussed in this chapter.

1.2 Detergent micelles in stabilizing membrane protein

Traditional detergents (*a.k.a.* head-to-tail detergents) are amphiphilic molecules with one side having hydrophilic head groups and another side with long hydrophobic tails. “Head-to-tail” detergent have been widely used in membrane protein isolation and characterization by extracting the membrane protein from phospholipid bilayer into a protein-detergent complex. Various types of “head-to-tail” detergents (*e.g*. nonionic, sulfonated, and zwitterionic detergents) have been applied for membrane protein characterization. Sugar based detergent n-octyl-β-d-glucoside (β-OG) nonionic detergents with structures shown in Figure 1.1 (c), is one of the most commonly

used detergents which are effective in breaking lipid-lipid and lipid-protein interactions with retaining protein-protein interactions.[81]

Recently, a new class of structurally unique detergent, known as facial amphiphiles, has been designed and developed. Different from "head-to-tail" structure of traditional surfactant, the polar and non-polar segments in facial amphiphiles point to opposite face of a conformationally rigid molecular motif. For example, as shown in Figure 1.1(d), steroid-based amphiphiles are representative facial amphiphiles having non-polar backbone and polar side chains. As compared to traditional "head-to-tail detergents, facial amphiphiles stabilize membrane proteins with fewer molecules with enhanced thermostability. [87, 88]

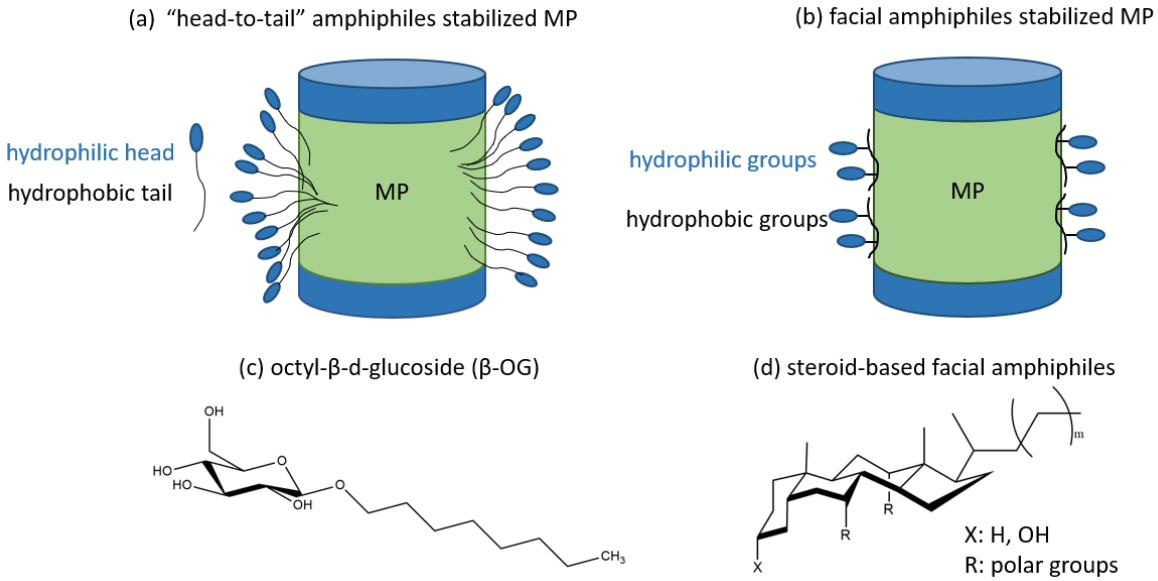

Figure 1.1. Membrane protein (MP) stabilized by (a) "head-to-tail" amphiphiles and (b) facial amphiphiles. (c) Octyl-β-d-glucoside and (d) steroid-based facial amphiphiles are shown as representatives to "head-to-tail" amphiphiles and facial amphiphiles respectively.

However, there are some general disadvantages in membrane protein isolation using detergents. First, the folding structures and physiochemical properties of membrane proteins are different in detergent micelles as compared with in native membrane. In addition, a monomer-micelle equilibrium was present above the critical micelle concentration (CMC) of detergent which

result in an unfavorable dynamic environment for stabilizing membrane protein. In addition, CMC is sensitive to temperature, pH, ionic strength, *etc*., leading to a poor structural stability of membrane proteins in the micelles due to the changes of environmental conditions. Furthermore, the long-term stability of membrane proteins in detergent micelle is limited resulting in possible protein aggregation and denaturing.[80]

1.3 Amphipols in stabilizing membrane protein

Many efforts have been dedicated to designing new solubilizing agents with enhanced structural stability of encapsulated membrane protein and one class of materials that have received increasing attention is amphipol. Amphipols are short amphiphilic polymers capable to keep individual membrane protein soluble in the form of small complex. Several types of amphipols have been designed and synthesized to replace traditional detergents in stabilizing membrane proteins, e.g. A8-35,[82] glucose-based amphipols,[83] α-helical or β-sheet peptide,[84] *etc*. The advantage of amphipols over traditional surfactants in stabilizing MP are: 1) amphipols can stabilize MP at relatively low concentration; 2) the stability of most MPs in amphipols are enhanced, and the functional states (*e.g*. folding structures, oligomeric states) of MPs were better retained in amphipols as compared to those in detergent micelles. However, the major limitation of using of amphipols in MPs extraction is that most of the amphipols are not able to directly solubilize biological membranes without the assistance of detergent even though the amphipols can partition to the lipid membrane. There is still a risk of protein aggregation and denaturing when using detergents to solubilize target MPs prior to the addition of amphipols.[85]

1.4 Membrane scaffold protein (MSP) stabilized lipid nanodisc

As the structure and biological function of membrane proteins are often coupled to their native lipid environment, there is a strong need to develop new membrane mimetic platform for

studying and analyzing the structural and functional properties of membrane proteins. While liposomes and vesicles have been used to mimic the cellular lipid environment, they are not ideally suited for many biophysical and analytical techniques due to the their large sizes, structural heterogeneity, limited stabilities over time, high viscosity and turbidity in solution, *etc*.[12] Alternative membrane mimetic system for reconstitution of membrane proteins has been investigated. Segrest et al. reported the naturally occurring human plasma lipoprotein, apolipoprotein A-I, can assemble with synthetic phosphorous lipid to form nanoscale water-soluble lipid/protein supramolecular complexes.[5,13,14,20] The scaffold protein and lipid complex is also known as nanodisc which is a non-covalent assembly of discoidal phospholipids bilayer with encircling apolipoprotein.[1,9,11,12] However, the size of natural occurring apolipoprotein A-I stabilized lipid nanodiscs is not well-defined.[6,7] To better control the size and homogeneity of protein stabilized nanodisc, Sligar and coworkers designed and synthesized genetically engineered apolipoprotein, also known as membrane scaffold proteins (MSP), using apolipoprotein A-I as a model template to produce lipid nanodisc.[8,22] The rim of the lipid patch was encircled and stabilized with two belts of helical proteins.[19,21] Before incorporating membrane proteins into MSP stabilized lipid nanodisc, many research efforts have been devoted to optimize the protocol for preparation of empty MSP stabilized nanodisc with well-defined size. Briefly, detergent-solubilized phospholipids were mixed with MSP under optimized concentration and molar ratio, and the self-assembly of MSP stabilized nanodiscs were initiated by gradual removal of detergent using dialysis or hydrophobic adsorption (*e.g*. biobead) methods.[86] The size homogeneity can be controlled by optimizing the stoichiometry between phospholipid, MSP and lipid solubilizing detergent.[23] Based on the result from small angle x-ray scattering (SAXS) analysis, it was found that the size of nanodisc can be controlled via tuning the sequence and chain length of MSP and

the diameter of resultant nanodiscs varied in the 10-17 nm range with different sequence-engineered MSP.[23,31] The size-defined MSP nanodiscs can serve as a water-soluble platform for membrane protein reconstitution and characterization. The target membrane proteins were first extracted and pre-dissolved in optimized detergents before the addition of detergent-solubilized lipids and MSP, and the nanodisc self-assembly protocol is the same as that for the empty MSP-nanodiscs.

As MSP-stabilized nanodisc are colloidally stable in water with embedded membrane proteins in their native lipid environment, a variety of molecular characterization and structure-function studies of the target membrane proteins can be carried out using NMR,[1] surface plasmon resonance (SPR),[2,3,] cryo-TEM,[4] MALDI-TOF-MS,[24] *etc*. MSP-stabilized nanodiscs have been demonstrated to successfully reconstitute various membrane proteins, such as SecYEG peptide translocon complex,[25,26] receptor tyrosine kinase Epidermal growth factor receptor (EGFR),[27] bacteriorhodopsin (bR),[8] G-protein coupled receptors,[28] cytochrome P450,[29,30] *etc*.

When compared to the traditional detergent method, the MSP-nanodisc method affords better control over protein oligomeric state[34,35] with enhanced long-term structural stability.[39] However, there remains some limitations in using MSP-nanodisc for membrane protein extraction: 1) MSP has strong UV absorption in the same region as membrane proteins which interfere with the membrane protein characterization; 2) in reconstitution of membrane protein embedded MSP-nanodiscs, the rate of detergent removal and nanodisc formation need to be carefully designed to prevent the protein aggregation and denaturing, and the detergents used for protein solubilization also need to be optimized due to the competition between protein-MSP, protein-detergent and lipid-detergent, which varies with specific structures and compositions of target membrane

proteins.[12,19,3] 3) Moreover, the size of MSP-nanodiscs is generally small with diameter ~10 nm which are not suitable for large size proteins or protein-protein complex.

1.5 Styrene-co-maleic acid (SMA) copolymer stabilized lipid nanodisc

Tonge et al. reported that styrene-maleic acid (SMA) amphiphilic copolymer can solubilize lipid bilayer structures. In contrast to MSP-nanodiscs, SMA copolymers with styrene/maleic acid(molar ratio = 2:1 and 3: 1) enable the detergent-free extraction of lipids and membrane proteins from both natural and artificial phosphorous lipid bilayer at neutral pH.[40] As shown in Scheme 1.1, SMA is composed with hydrophobic styrene and hydrophilic carboxyl/carboxylate ([COOH]/[COO^-]) moieties. The hydrophobicity and solubility of the polymer was determined by both molar ratio between the two monomeric units and the solution pH. The extent of de-protonation of carboxyl groups at different pH strongly affects the solubility and conformation of the polymer in polymer-lipid assembly.[41] In most application cases, the pH used were adjusted in the range between 7-8 and the polymer adopted random coil conformation with electrostatic interactions dominating the polymer-lipid interactions.

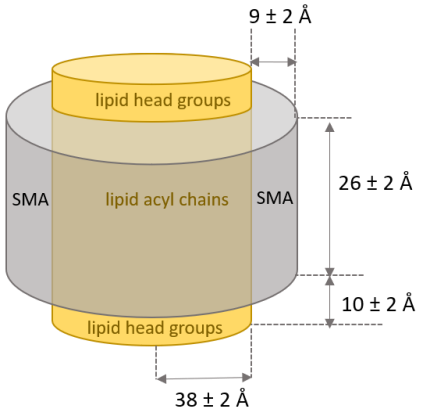

Figure 1.2. Structural dimensions of styrene–maleic acid/lipid particles (SMALPs) determined from SANS analysis. SMALP is composed with DMPC lipids and SMA copolymer with [Sty] : [MA] = 2 and MW = 9.5 kDa.[43]

1.5.1 Structure and formation mechanism of SMA stabilized lipid particles (SMALP)

The structure of SMA-stabilized lipid particles (SMALP) has been determined using dipalmitoylphosphatidylcholine (DMPC) vesicles as a lipid membrane model by small-angle neutron scattering analysis as shown in Figure 1.2. The molecular weight of SMA is 9.5 kDa and Sty/MA molar ratio is 2:1. The analysis results show SMALP are in discoidal shape with diameter at ~ 10 nm and thickness at ~ 4.6 nm, which is the thickness of DMPC bilayer in fluid phase. The thickness of the polymer belt was ~ 0.9 nm which is consistent with the thickness of one SMA molecule. [42,43] Based on the result from NMR and FT-IR analysis, it was found the phenyl group in SMA perpendicularly inserted between the lipid acyl chains and the COO^- electrostatically interacted with the phosphorous head group of the lipid. In differential scanning calorimetry (DSC) analysis, the melting temperature of lipids decrease from 24 ˚C to 23˚C with broader distribution after the formation of SMALP, suggesting the conservation of lipid bilayer packing with minimal perturbation in the presence of belted SMA.[43]

1.5.2 MD simulation studies on SMA induced nanodisc formation

Detailed mechanism of early stage SMALP assembly is further investigated using SMA periodic copolymers by coarse-grained (CG) molecular dynamics (MD) simulation.[40,50] Interaction of lipid bilayers with periodic copolymers having repeating unit of [SSM] and [SSSM] with varying molecular weight (MW) were investigated, and two lipid fragmentation pathways (*i.e.* "water-pore formation" and "direct extraction" mechanisms) have been identified, which will be discussed later in details.

Water-pore formation fragmentation mechanism: 1) As shown in Figure 1.3, before binding to the lipid membrane, SMA copolymers adopted a disordered conformation in the aqueous solution and SMA copolymers self-assembled into small clusters. Driven by the

hydrophobic interactions, the hydrophobic phenyl groups inserted between the acyl chain of the lipid, and no detachment was observed afterwards indicating the strong hydrophobic interactions between SMA polymer and lipid acyl chains. The rate and binding efficiency are affected by many factors, *e.g.* salt concentration, electrostatic repulsion between COO^- in SMA and PO_4^- in phosphorous lipid. The polymer binding efficiency was found to increase with higher salt concentration and lower anionic lipid content in the lipid system. Upon binding to the lipid membranes, the polymer clusters dissociated with polymer conformation becoming more extended, as supported by the analysis of polymer's radius of gyration (r_g).

In this step, the lipid packing was more readily disrupted at or above gel-liquid phase transition temperature, at which the gel-phase domains transferred into liquid-crystalline phase and the lipid packing are less ordered and more likely to form structural packing defects.[45] The packing of lipids with short acyl chains are more readily perturbed due to the lack of extensive hydrophobic interactions relative to lipids with long acyl chains. High saturated lipids were more readily

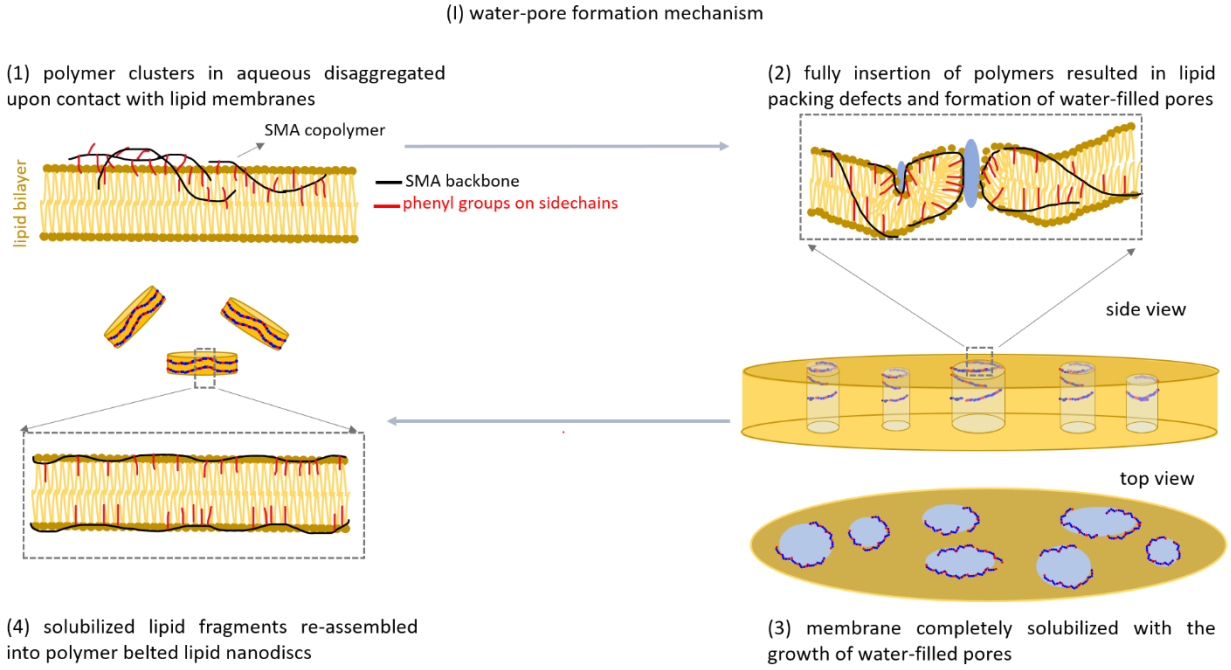

Figure 1.3. Water-pore formation mechanism of lipid membrane fragmentation using SMA copolymers based on MD simulation study.

solubilized in the presence of SMA polymers relative to the unsaturated lipids, which is attributed to the unsaturated double bonds having more lateral pressure along the acyl-chain inhibiting the polymer insertion.[46,48] Therefore, it was also concluded that lipids with saturated and short acyl chains allow for greater extent of polymer insertion.

2) After the fully insertion of SMA copolymers into lipid membranes, transmembrane pores were formed with penetration of water molecules into the lipid. The water pore rim was stabilized with SMA copolymers by intercalating the hydrophobic phenyl group among the lipid acyl chains and orienting the hydrophilic COO^- towards water pore.

3) The final formation of nanodiscs was not observed due to the size limitation of the simulation box. It was proposed that the further growth of the transmembrane water-filled pores drives the eventual membrane disruption and induces the formation of SMA-stabilized discoidal lipid nanodisc.

Direct extraction mechanism: SMA periodic copolymers with higher hydrophobicity (*e.g.* $[SSSM]_{13}$, MW = 1.5 kDa) was found to fragment lipids bilayers by a direct extraction mechanism, as shown in Figure 1.4.

1) Different from the previous water-pore formation mechanism, the polymer clusters formed in aqueous solution do not disassociate upon interacting with the lipid surface. The higher hydrophobicity of the polymers enables a greater extent of local contacts between polymers and lipids, resulting in a local lipid binding and membrane deformation.

2) Next, the polymer clusters can directly sequester lipid protrusion from the lipid membranes, which was stabilized by a single layer of SMA copolymer.

3) The extracted lipid patch was re-organized into SMA copolymer belted lipid nanodisc.

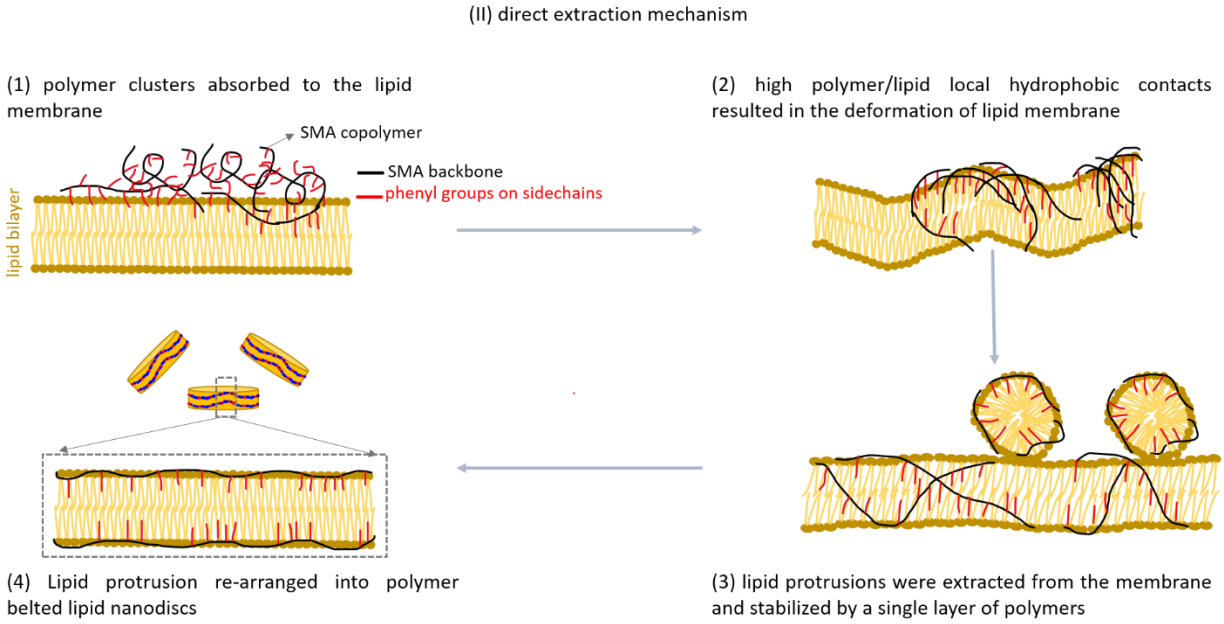

Figure 1.4. Direct extraction mechanism of lipid membrane fragmentation using SMA copolymers based on MD simulation study.

From MD simulation study, it was observed that the molecular weight (MW) and hydrophobicity of polymers affect the type of fragmentation mechanism and the fragmentation efficiency. To study the effect of molecular weight on lipid fragmentation and nanodisc formation, periodic polymers with identical hydrophobicity (Sty/MA ratio = 3:1) and varying molecular weight, $[SSSM]_{13}$ and $[SSSM]_3$, were compared. It was observed that both $[SSSM]_{13}$ and $[SSSM]_3$ fragment the lipid bilayers by the direct extraction mechanism. The stability of extracted lipid protrusion varies with the MW of polymer. Lipid protrusion wrapped with longer polymer ($[SSSM]_{13}$) are stable over time, allowing the lipid and polymer in the assemblies to re-organize into polymer belted lipid nanodisc. By contrast, the lipid protrusion with shorter polymer ($[SSSM]_3$) was found to form transiently and eventually merge back into the original lipid membranes with short polymer evenly distributed at the surface of the membrane. This indicates short-chain polymer has limited capacity in stabilizing lipid patches relative to long-chain polymer.

To investigate the effect of polymer hydrophobicity on lipid fragmentation, periodic polymers with similar molecular weight but varying hydrophobicity ($[SSSM]_{13}$ with MW = 1.5 kDa and [Sty]/[MA] = 3, $[SSM]_{17}$ with MW = 1.8 kDa and [Sty]/[MA] =2) were investigated. It was observed that due to the high local concentration of the hydrophobic groups, polymer with higher hydrophobicity ($[SSSM]_{13}$) adopt the direct extraction mechanism with faster lipid fragmentation, whereas the polymer with lower hydrophobicity ($[SSM]_{17}$) adopted the water pore formation with slower lipid fragmentation, and the final lipid solubilization to form nanodiscs was not observed within the similar simulation time scale.

Lipid to polymer number ratio (lipid/polymer) also affect the nanodisc formation. For example, with lipid/polymer molar ratio = 150, the resultant lipid nanodiscs are surrounded with one single SMA polymer belt from both MD simulation and SANS analysis. However, with lipid/polymer = 75:1 and 75:2, each nanodisc has multiple belting SMA copolymers, suggesting that the belting SMA polymer number in each SMALP can vary with different lipid/polymer ratio.[58,59]

Overall, it was concluded that the polymer hydrophobicity (mainly determined by Sty/MA ratio), chain length, monomer sequence as well as polymer concentration are all critical factors for effectively inducing the formation of stable SMALP.[40]

It has been demonstrated that a wide variety of biological membranes can be fragmented into SMA stabilized lipid nanodiscs and a number of membrane proteins ranging from single membrane spanning α-helix to oligomeric complexes with 36 transmembrane helices have been directly extracted from native cell membranes *(e.g.* bacteria,[51,52,54,55, 56] yeast,[58] cultures of insect,[57] human cells,[57-58] *etc.*) using SMA polymer without detergent.[51-54] The size of nanodisc was analyzed using electron microscopy,[43,59, 68] dynamic light scattering,[59,60,69] small angle neutron

scattering (SANS),[43] and size exclusion chromatography.[43] A variety of protein structures were resolved using SMALP, *e.g.* bacteriorhodopsins,[59,60,61] G-protein-coupled receptors,[58,62] neucleoside transporter hENT1,[38] light-harvesting complex II,[51] potassium channels,[55,63] ABC-transporters.[57,64]

1.5.3 Advantages of SMALPs over detergent micelles and MSP-nanodisc in membrane protein isolation application

Relative to detergent-solubilized membrane protein micelles, SMALP provide a better mimetic of native lipid environment of target membrane proteins, which is beneficial to maintain its native structures and biological function. Secondly, it has been reported that the stability of membrane proteins is enhanced when stabilized in SMALP relative to in detergent micelles.[36]

The advantages of SMALP over MSP-nanodisc are: 1) the preparation of SMALP is more cost effective and less complex relative to that of MSP-nanodisc, as no detergent required for membrane protein reconstitution in the former, which ensure the preservation of the local lipid environment for the target membrane proteins. 2) The size of SMALP can be readily modulated by tuning the initial feeding ratio between the two monomers,[67] polymer to lipid ratio,[63, 65, 66] as well as the monomer sequence in the polymer by using different synthetic methods,[65] which is critical in solubilizing membrane proteins with larger sizes.

Besides the advantages mentioned above, the limitation of SMALP include: 1) SMA polymer has strong UV absorption which can interfere with the signal of membrane proteins, adding complication to certain spectroscopic characterization of the MPs (*e.g.*, CD spectroscopy). 2) The stability and solubility of SMA copolymer in water is highly sensitive to pH and the concentration of divalent metals. One example is SMA polymer precipitated from the solution with Mg^{2+} concentration above10 mM at pH < 6,[36] and the poor stability at high divalent cations render the incompatibility with many metal cation dependent protein assays.[36,74,75]

1.6 SMA derivatives stabilized lipid nanodisc

SMA-derivative polymers have been developed to enhance the stability of SMA over pH and divalent metal ions. Ramamoorthy and coworkers developed pH resistant SMA derived copolymer by functionalizing SMA moieties with ethanolamine (SMA-EA)[70] quaternary ammonium (SMA-QA).[71] The sizes of both SMA-EA and SMA-QA stabilized nanodiscs can be controlled by tuning the polymer to lipid ratio, whereas the size distribution of SMA-QA nanodiscs is narrower as compared to SMA-EA nanodiscs at the same lipid to polymer ratio, indicating that the charge content in the polymer plays a role in the polymer lipid interaction and self-assembly. Furthermore, SMA-QA resulted in the formation of nanodiscs in the pH at 2-10 with good stability in the presence of divalent metal ions at concentration up to 200 mM. Another recent study on SMA derivative polymer where maleic anhydride units are functionalized with varying nucleophiles, *e.g.* aminoethanol, *N,N*-dimethylethylenediamine, *etc*. The introduction of nucleophiles can induce more stable nanodisc in the presence of bivalent Mg^{2+} cations with concentration up to 100 mM relative to 20-40 mM for SMA before modification. The resultant nanodisc also exhibit good stability over a broader pH range (pH = 3-9) relative to SMA.[72]

The nature of the charge group of SMA derivatives is also important in the application of membrane protein reconstitution due to the electrostatic interactions between polymer and target proteins. For example, cytochrome P450 (CytP450) is a positively charged membrane protein at neutral pH which can be successfully extracted using positively charged polymer SMA-QA yielding stable CytP450 encased nanodiscs. By contrast, the protein reconstitution into nanodiscs was unsuccessful using a negatively charged SMA-EA under same incubation conditions due to the strong electrostatic interactions between the negatively charged polymer and positively charged protein resulting in the formation of ill-defined polymer-protein aggregates.[73] To resolve

this problem, the salt concentrations in the buffer for membrane protein extraction need to be carefully optimized to screen the unfavorable electronic interactions between the charged polymer and membrane proteins.

1.7 Styrene-free copolymer based lipid nanodisc

Even though the polymer tolerance to a broader pH range and higher divalent metal cations can be achieved by SMA functionalization, the SMA derivatives still have strong UV absorbance which interfere with certain spectroscopic characterization of membrane proteins and pose challenges to quantify the amount of the embedded membrane protein in each nanodisc. The challenges were addressed by replacing lipid nanodisc scaffold with styrene-free polymers. Alternating copolymer of maleic acid and diissobutylene (DIBMA) with molecular weight ~ 8.4 kDa has been demonstrated to induce the formation of DIBMA stabilized lipid nanodisc (DIBMALP) and enable the isolation of membrane proteins with varying sizes from native membranes.[77] DIBMALP also shows much higher tolerance to Ca^{2+} relative to SMALP which is very critical for Ca^{2+} mediated phospholipase activation,[78] and the absence of UV-absorbing moieties in polymer enable the characterization of membrane protein conformation and stability using CD spectroscopy.

A random copolymer of butyl methacrylate and cationic methacroylcholine chloride with varying molecular weight and compositions have been designed and synthesized using free radical polymerization method.[76] The hydrophobic fraction (f) of the polymer was defined as the molar ratio between hydrophobic butyl methacrylate over hydrophilic cationic methacroylcholine chloride segment, which can be controlled by varying the initial feeding ratio of the two monomers. The effect of polymer molecular weight (MW) on nanodisc formation was investigated by comparing polymers with comparable hydrophobic fraction (f) but varying MW. Polymers with

MW lower than 3 kDa can't effectively induce nanodisc formation, which is attributed to inability of the low MW polymers to cover ~ 3 nm thickness of the DMPC lipid bilayer. Next, the effect of polymer hydrophobicity (f) on nanodisc formation was analyzed using polymers with similar MW but varying hydrophobicity to optimize the hydrophobicity required for effective nanodisc formation. Polymers with hydrophobicity (f) in the 0.4-0.6 range were found to induce the formation of stable polymer bounded nanodiscs. Thus, it was concluded that the hydrophobicity and molecular weight are both critical in the design of nanodisc-inducing polymers. Furthermore, the optimized copolymers were successfully used to fragment the intact *E. coli* cell membranes into polymer bounded lipid nanodiscs without the assistance of detergents.[76]

Another styrene-free nanodisc-forming polymer, alkyl polyacrylic acid copolymers (APAA), has been designed and synthesized by functionalizing polyacrylic acid polymers with varying alkyl side chains (*e.g*. butyl, pentyl, and hexyl).[79] At pH > 6.5, all the polymers with varying side chains can solubilize the liposomes. The polymer with the longest side chain, hexyl substituted PAA, was shown to extract membrane proteins from *E Coli.* membranes with the highest yield that is comparable with that obtained using SMA (3:1) copolymer.

1.8 Amphiphilic polypeptoid copolymers for lipid membrane fragmentation

For all the nanodisc forming polymers discussed before, due to the high hydrophobicity of the polymer backbone, the compositional range to form colloidal stable polymer is very limited. There is a clear need to develop more water-soluble nanodisc-forming amphiphilic polymers. Polypeptoid, a structurally mimic of α-polypeptide, is a facially amphiphilic polymer with polar polyamide backbone and *N*-substitution with tunable hydrophilicity-lipophilicity balance (HLB). The highly polar polymer backbones can enhance the polymer solubility in aqueous solution with a broader compositional range relative to the traditional nanodisc forming vinyl polymers. In

addition, without extensive hydrogen bonding along the backbone, polypeptoid backbone is more flexible and the polymer conformation can be readily tuned with *N*-substituents via initial monomer design, relative to other facially amphiphilic detergent (*e.g*. steroid based amphiphiles, short peptides). The synthetic methods for well-defined polypeptoids with a range of *N*-substituent structures have been well established. Previous studies by Zuckermann and co-workers have shown that polypeptoids with optimized sequence and sidechain structures can adopt an extended conformation at oil/water interfaces.[90,91] It is hypothesized that poly[(*N*-methoxyethyl glycine)-*r*-(*N*-decyl glycine)] copolypeptoids (*a.k.a.* hydrophobically modified polypeptoid (HMPs)) may adopt the extended polymer conformation with enhanced polymer facial amphiphilicity, thus favor the formation of polymer belted lipid nanodisc analogously to the twisted α-helical membrane scaffold protein (MSP). Recently Zhang et al. reported HMPs can fragment synthetic liposomes and assemble into nanoscale polymer-lipid complexes,[80] but the detailed relationship between the molecular characteristics of HMP and polymer-liposome interactions have not been systematically investigated. In this work, a series of HMP copolymers with varying molecular weight and hydrophobicity were designed and synthesized to investigate their effects on liposome fragmentation. The polymer induced lipid fragmentation was fully characterized using SLS/DLS, cryo-TEM, and negative stained TEM. The newly developed polypeptoid stabilized lipid complex is a promising platform for membrane protein isolation and protein structural and functional studies.

1.9 References

1. Hagn, F.; Etzkorn, M.; Raschle, T.; Wagner, G., Optimized Phospholipid Bilayer Nanodiscs Facilitate High-Resolution Structure Determination of Membrane Proteins. *Journal of the American Chemical Society* **2013,** *135* (5), 1919-1925.

2. Borch, J.; Torta, F.; Sligar, S. G.; Roepstorff, P., Nanodiscs for Immobilization of Lipid Bilayers and Membrane Receptors: Kinetic Analysis of Cholera Toxin Binding to a Glycolipid Receptor. *Analytical Chemistry* **2008,** *80* (16), 6245-6252.

3. Glück, J. M.; Koenig, B. W.; Willbold, D., Nanodiscs allow the use of integral membrane proteins as analytes in surface plasmon resonance studies. *Analytical Biochemistry* **2011,** *408* (1), 46-52.

4. Gao, Y.; Cao, E.; Julius, D.; Cheng, Y., TRPV1 structures in nanodiscs reveal mechanisms of ligand and lipid action. *Nature* **2016,** *534* (7607), 347-351.

5. Jonas, A., [32] Reconstitution of high-density lipoproteins. In *Methods in Enzymology*, Academic Press: 1986; Vol. 128, pp 553-582.

6. Durbin, D. M.; Jonas, A., The Effect of Apolipoprotein A-II on the Structure and Function of Apolipoprotein A-I in a Homogeneous Reconstituted High Density Lipoprotein Particle. *Journal of Biological Chemistry* **1997,** *272* (50), 31333-31339.

7. Li, L.; Chen, J.; Mishra, V. K.; Kurtz, J. A.; Cao, D.; Klon, A. E.; Harvey, S. C.; Anantharamaiah, G. M.; Segrest, J. P., Double Belt Structure of Discoidal High Density Lipoproteins: Molecular Basis for Size Heterogeneity. *Journal of Molecular Biology* **2004,** *343* (5), 1293-1311.

8. Bayburt, T. H.; Sligar, S. G., Self-assembly of single integral membrane proteins into soluble nanoscale phospholipid bilayers. *Protein Science* **2003,** *12* (11), 2476-2481.

9. Nath, A.; Atkins, W. M.; Sligar, S. G., Applications of Phospholipid Bilayer Nanodiscs in the Study of Membranes and Membrane Proteins. *Biochemistry* **2007,** *46* (8), 2059-2069.

10. Shen, P. S.; Yang, X.; DeCaen, P. G.; Liu, X.; Bulkley, D.; Clapham, D. E.; Cao, E., The Structure of the Polycystic Kidney Disease Channel PKD2 in Lipid Nanodiscs. *Cell* **2016,** *167* (3), 763-773.e11.

11. Denisov, I. G.; Sligar, S. G., Nanodiscs for structural and functional studies of membrane proteins. *Nature Structural & Molecular Biology* **2016,** *23* (6), 481-486.

12. Denisov, I. G.; Sligar, S. G., Nanodiscs in Membrane Biochemistry and Biophysics. *Chemical Reviews* **2017,** *117* (6), 4669-4713.

13. Silva, R. A. G. D.; Huang, R.; Morris, J.; Fang, J.; Gracheva, E. O.; Ren, G.; Kontush, A.; Jerome, W. G.; Rye, K.-A.; Davidson, W. S., Structure of apolipoprotein A-I in spherical high density lipoproteins of different sizes. *Proceedings of the National Academy of Sciences* **2008,** *105* (34), 12176.

14. Matz, C. E.; Jonas, A., Micellar complexes of human apolipoprotein A-I with phosphatidylcholines and cholesterol prepared from cholate-lipid dispersions. *Journal of Biological Chemistry* **1982,** *257* (8), 4535-4540.

15. Zhang, M.; Huang, R.; Ackermann, R.; Im, S.-C.; Waskell, L.; Schwendeman, A.; Ramamoorthy, A., Reconstitution of the Cytb5–CytP450 Complex in Nanodiscs for Structural Studies using NMR Spectroscopy. *Angewandte Chemie International Edition* **2016,** *55* (14), 4497-4499.

16. Barnaba, C.; Sahoo, B. R.; Ravula, T.; Medina-Meza, I. G.; Im, S.-C.; Anantharamaiah, G. M.; Waskell, L.; Ramamoorthy, A., Cytochrome-P450-Induced Ordering of Microsomal Membranes Modulates Affinity for Drugs. *Angewandte Chemie International Edition* **2018,** *57* (13), 3391-3395.

17. Prade, E.; Mahajan, M.; Im, S.-C.; Zhang, M.; Gentry, K. A.; Anantharamaiah, G. M.; Waskell, L.; Ramamoorthy, A., A Minimal Functional Complex of Cytochrome P450 and FBD of Cytochrome P450 Reductase in Nanodiscs. *Angewandte Chemie International Edition* **2018,** *57* (28), 8458-8462.

18. Ravula, T.; Ishikuro, D.; Kodera, N.; Ando, T.; Anantharamaiah, G. M.; Ramamoorthy, A., Real-Time Monitoring of Lipid Exchange via Fusion of Peptide Based Lipid-Nanodiscs. *Chemistry of Materials* **2018,** *30* (10), 3204-3207.

19. Bayburt, T. H.; Sligar, S. G., Membrane protein assembly into Nanodiscs. *FEBS Letters* **2010,** *584* (9), 1721-1727.

20. Brouillette, C. G.; Jones, J. L.; Ng, T. C.; Kercret, H.; Chung, B. H.; Segrest, J. P., Structural studies of apolipoprotein A-I/phosphatidylcholine recombinants by high-field proton NMR, nondenaturing gradient gel electrophoresis, and electron microscopy. *Biochemistry* **1984,** *23* (2), 359-367.

21. May, S., Protein-induced bilayer deformations: the lipid tilt degree of freedom. *European Biophysics Journal* **2000,** *29* (1), 17-28.

22. Bayburt, T. H.; Grinkova, Y. V.; Sligar, S. G., Self-Assembly of Discoidal Phospholipid Bilayer Nanoparticles with Membrane Scaffold Proteins. *Nano Letters* **2002,** *2* (8), 853-856.

23. Denisov, I. G.; Grinkova, Y. V.; Lazarides, A. A.; Sligar, S. G., Directed Self-Assembly of Monodisperse Phospholipid Bilayer Nanodiscs with Controlled Size. *Journal of the American Chemical Society* **2004,** *126* (11), 3477-3487.

24. Marin, V. L.; Bayburt, T. H.; Sligar, S. G.; Mrksich, M., Functional Assays of Membrane-Bound Proteins with SAMDI-TOF Mass Spectrometry. *Angewandte Chemie International Edition* **2007,** *46* (46), 8796-8798.

25. Alami, M.; Dalal, K.; Lelj-Garolla, B.; Sligar, S. G.; Duong, F., Nanodiscs unravel the interaction between the SecYEG channel and its cytosolic partner SecA. *The EMBO Journal* **2007,** *26* (8), 1995-2004.

26. Dalal, K.; Nguyen, N.; Alami, M.; Tan, J.; Moraes, T. F.; Lee, W. C.; Maurus, R.; Sligar, S. S.; Brayer, G. D.; Duong, F., Structure, Binding, and Activity of Syd, a SecY-interacting Protein. *Journal of Biological Chemistry* **2009,** *284* (12), 7897-7902.

27. Mi, L.-Z.; Grey, M. J.; Nishida, N.; Walz, T.; Lu, C.; Springer, T. A., Functional and Structural Stability of the Epidermal Growth Factor Receptor in Detergent Micelles and Phospholipid Nanodiscs. *Biochemistry* **2008,** *47* (39), 10314-10323.

28. Leitz, A. J.; Bayburt, T. H.; Barnakov, A. N.; Springer, B. A.; Sligar, S. G., Functional reconstitution of β2-adrenergic receptors utilizing self-assembling Nanodisc technology. *BioTechniques* **2006,** *40* (5), 601-612.

29. Denisov, I. G.; Baas, B. J.; Grinkova, Y. V.; Sligar, S. G., Cooperativity in Cytochrome P450 3A4: LINKAGES IN SUBSTRATE BINDING, SPIN STATE, UNCOUPLING, AND PRODUCT FORMATION. *Journal of Biological Chemistry* **2007,** *282* (10), 7066-7076.

30. Duan, H.; Civjan, N. R.; Sligar, S. G.; Schuler, M. A., Co-incorporation of heterologously expressed Arabidopsis cytochrome P450 and P450 reductase into soluble nanoscale lipid bilayers. *Archives of Biochemistry and Biophysics* **2004,** *424* (2), 141-153.

31. Grinkova, Y. V.; Denisov, I. G.; Sligar, S. G., Engineering extended membrane scaffold proteins for self-assembly of soluble nanoscale lipid bilayers. *Protein Engineering, Design and Selection* **2010,** *23* (11), 843-848.

32. Overington, J. P.; Al-Lazikani, B.; Hopkins, A. L., How many drug targets are there? *Nature Reviews Drug Discovery* **2006,** *5* (12), 993-996.

33. Park, S. H.; Berkamp, S.; Cook, G. A.; Chan, M. K.; Viadiu, H.; Opella, S. J., Nanodiscs versus Macrodiscs for NMR of Membrane Proteins. *Biochemistry* **2011,** *50* (42), 8983-8985.

34. Boldog, T.; Grimme, S.; Li, M.; Sligar, S. G.; Hazelbauer, G. L., Nanodiscs separate chemoreceptor oligomeric states and reveal their signaling properties. *Proceedings of the National Academy of Sciences* **2006,** *103* (31), 11509.

35. Shi, L.; Shen, Q.-T.; Kiel, A.; Wang, J.; Wang, H.-W.; Melia, T. J.; Rothman, J. E.; Pincet, F., SNARE Proteins: One to Fuse and Three to Keep the Nascent Fusion Pore Open. *Science* **2012,** *335* (6074), 1355.

36. Dörr, J. M.; Scheidelaar, S.; Koorengevel, M. C.; Dominguez, J. J.; Schäfer, M.; van Walree, C. A.; Killian, J. A., The styrene–maleic acid copolymer: a versatile tool in membrane research. *European Biophysics Journal* **2016,** *45* (1), 3-21.

37. Ravula, T.; Hardin, N. Z.; Ramamoorthy, A., Polymer nanodiscs: Advantages and limitations. *Chemistry and Physics of Lipids* **2019,** *219*, 45-49.

38. Ravula, T.; Hardin, N. Z.; Di Mauro, G. M.; Ramamoorthy, A., Styrene maleic acid derivates to enhance the applications of bio-inspired polymer based lipid-nanodiscs. *European Polymer Journal* **2018,** *108*, 597-602.

39. Rouck, J. E.; Krapf, J. E.; Roy, J.; Huff, H. C.; Das, A., Recent advances in nanodisc technology for membrane protein studies (2012–2017). *FEBS Letters* **2017,** *591* (14), 2057-2088.

40. Orekhov, P. S.; Bozdaganyan, M. E.; Voskoboynikova, N.; Mulkidjanian, A. Y.; Steinhoff, H.-J.; Shaitan, K. V., Styrene/Maleic Acid Copolymers Form SMALPs by Pulling Lipid Patches out of the Lipid Bilayer. *Langmuir* **2019,** *35* (10), 3748-3758.

41. Banerjee, S.; Pal, T. K.; Guha, S. K., Probing molecular interactions of poly(styrene-co-maleic acid) with lipid matrix models to interpret the therapeutic potential of the co-polymer. *Biochimica et Biophysica Acta (BBA) - Biomembranes* **2012,** *1818* (3), 537-550.

42. Nagle, J. F.; Tristram-Nagle, S., Structure of lipid bilayers. *Biochimica et Biophysica Acta (BBA) - Reviews on Biomembranes* **2000,** *1469* (3), 159-195.

43. Jamshad, M.; Grimard, V.; Idini, I.; Knowles, T. J.; Dowle, M. R.; Schofield, N.; Sridhar, P.; Lin, Y.; Finka, R.; Wheatley, M.; Thomas, O. R. T.; Palmer, R. E.; Overduin, M.; Govaerts, C.; Ruysschaert, J.-M.; Edler, K. J.; Dafforn, T. R., Structural analysis of a nanoparticle containing a lipid bilayer used for detergent-free extraction of membrane proteins. *Nano Research* **2015,** *8* (3), 774-789.

44. Scheidelaar, S.; Koorengevel, Martijn C.; Pardo, Juan D.; Meeldijk, Johannes D.; Breukink, E.; Killian, J. A., Molecular Model for the Solubilization of Membranes into Nanodisks by Styrene Maleic Acid Copolymers. *Biophysical Journal* **2015,** *108* (2), 279-290.

45. Noordam, P. C.; Killian, A.; Oude Elferink, R. F. M.; de Gier, J., Comparative study on the properties of saturated phosphatidylethanolamine and phosphatidylcholine bilayers: Barrier characteristics and susceptibility to phospholipase A2 degradation. *Chemistry and Physics of Lipids* **1982,** *31* (2), 191-204.

46. Frolov, V. A.; Shnyrova, A. V.; Zimmerberg, J., Lipid Polymorphisms and Membrane Shape. *Cold Spring Harbor Perspectives in Biology* **2011,** *3* (11).

47. Cantor, R. S., Lipid Composition and the Lateral Pressure Profile in Bilayers. *Biophysical Journal* **1999,** *76* (5), 2625-2639.

48. Mouritsen, O. G., Lipids, curvature, and nano-medicine. *European Journal of Lipid Science and Technology* **2011,** *113* (10), 1174-1187.

49. Gruner, S. M., Intrinsic curvature hypothesis for biomembrane lipid composition: a role for nonbilayer lipids. *Proceedings of the National Academy of Sciences* **1985,** *82* (11), 3665.

50. Xue, M.; Cheng, L.; Faustino, I.; Guo, W.; Marrink, S. J., Molecular Mechanism of Lipid Nanodisk Formation by Styrene-Maleic Acid Copolymers. *Biophysical Journal* **2018,** *115* (3), 494-502.

51. Swainsbury, D. J. K.; Scheidelaar, S.; Foster, N.; van Grondelle, R.; Killian, J. A.; Jones, M. R., The effectiveness of styrene-maleic acid (SMA) copolymers for solubilisation of integral membrane proteins from SMA-accessible and SMA-resistant membranes. *Biochimica et Biophysica Acta (BBA) - Biomembranes* **2017,** *1859* (10), 2133-2143.

52. Postis, V.; Rawson, S.; Mitchell, J. K.; Lee, S. C.; Parslow, R. A.; Dafforn, T. R.; Baldwin, S. A.; Muench, S. P., The use of SMALPs as a novel membrane protein scaffold for structure study by negative stain electron microscopy. *Biochimica et Biophysica Acta (BBA) - Biomembranes* **2015,** *1848* (2), 496-501.

53. Lee, S. C.; Khalid, S.; Pollock, N. L.; Knowles, T. J.; Edler, K.; Rothnie, A. J.; R.T.Thomas, O.; Dafforn, T. R., Encapsulated membrane proteins: A simplified system for molecular simulation. *Biochimica et Biophysica Acta (BBA) - Biomembranes* **2016,** *1858* (10), 2549-2557.

54. Paulin, S.; Jamshad, M.; Dafforn, T. R.; Garcia-Lara, J.; Foster, S. J.; Galley, N. F.; Roper, D. I.; Rosado, H.; Taylor, P. W., Surfactant-free purification of membrane protein complexes from bacteria: application to the staphylococcal penicillin-binding protein complex PBP2/PBP2a. *Nanotechnology* **2014,** *25* (28), 285101.

55. Dörr, J. M.; Koorengevel, M. C.; Schäfer, M.; Prokofyev, A. V.; Scheidelaar, S.; van der Cruijsen, E. A. W.; Dafforn, T. R.; Baldus, M.; Killian, J. A., Detergent-free isolation, characterization, and functional reconstitution of a tetrameric K⁺ channel: The power of native nanodiscs. *Proceedings of the National Academy of Sciences* **2014,** *111* (52), 18607.

56. Prabudiansyah, I.; Kusters, I.; Caforio, A.; Driessen, A. J. M., Characterization of the annular lipid shell of the Sec translocon. *Biochimica et Biophysica Acta (BBA) - Biomembranes* **2015,** *1848* (10, Part A), 2050-2056.

57. Gulati, S.; Jamshad, M.; Knowles, Timothy J.; Morrison, Kerrie A.; Downing, R.; Cant, N.; Collins, R.; Koenderink, Jan B.; Ford, Robert C.; Overduin, M.; Kerr, Ian D.; Dafforn, Timothy R.; Rothnie, Alice J., Detergent-free purification of ABC (ATP-binding-cassette) transporters. *Biochemical Journal* **2014,** *461* (2), 269-278.

58. Jamshad, M.; Charlton, J.; Lin, Y.-P.; Routledge, Sarah J.; Bawa, Z.; Knowles, Timothy J.; Overduin, M.; Dekker, N.; Dafforn, Tim R.; Bill, Roslyn M.; Poyner, David R.; Wheatley, M.,

G-protein coupled receptor solubilization and purification for biophysical analysis and functional studies, in the total absence of detergent. *Bioscience Reports* **2015,** *35* (2).

59. Knowles, T. J.; Finka, R.; Smith, C.; Lin, Y.-P.; Dafforn, T.; Overduin, M., Membrane Proteins Solubilized Intact in Lipid Containing Nanoparticles Bounded by Styrene Maleic Acid Copolymer. *Journal of the American Chemical Society* **2009,** *131* (22), 7484-7485.

60. Orwick-Rydmark, M.; Lovett, J. E.; Graziadei, A.; Lindholm, L.; Hicks, M. R.; Watts, A., Detergent-Free Incorporation of a Seven-Transmembrane Receptor Protein into Nanosized Bilayer Lipodisq Particles for Functional and Biophysical Studies. *Nano Letters* **2012,** *12* (9), 4687-4692.

61. Lindhoud, S.; Carvalho, V.; Pronk, J. W.; Aubin-Tam, M.-E., SMA-SH: Modified Styrene–Maleic Acid Copolymer for Functionalization of Lipid Nanodiscs. *Biomacromolecules* **2016,** *17* (4), 1516-1522.

62. Logez, C.; Damian, M.; Legros, C.; Dupré, C.; Guéry, M.; Mary, S.; Wagner, R.; M'Kadmi, C.; Nosjean, O.; Fould, B.; Marie, J.; Fehrentz, J.-A.; Martinez, J.; Ferry, G.; Boutin, J. A.; Banères, J.-L., Detergent-free Isolation of Functional G Protein-Coupled Receptors into Nanometric Lipid Particles. *Biochemistry* **2016,** *55* (1), 38-48.

63. Zhang, R.; Sahu, I. D.; Bali, A. P.; Dabney-Smith, C.; Lorigan, G. A., Characterization of the structure of lipodisq nanoparticles in the presence of KCNE1 by dynamic light scattering and transmission electron microscopy. *Chemistry and Physics of Lipids* **2017,** *203*, 19-23.

64. Rothnie, A. J., Detergent-Free Membrane Protein Purification. In *Heterologous Expression of Membrane Proteins: Methods and Protocols*, Mus-Veteau, I., Ed. Springer New York: New York, NY, 2016; pp 261-267.

65. Craig, A. F.; Clark, E. E.; Sahu, I. D.; Zhang, R.; Frantz, N. D.; Al-Abdul-Wahid, M. S.; Dabney-Smith, C.; Konkolewicz, D.; Lorigan, G. A., Tuning the size of styrene-maleic acid copolymer-lipid nanoparticles (SMALPs) using RAFT polymerization for biophysical studies. *Biochimica et Biophysica Acta (BBA) - Biomembranes* **2016,** *1858* (11), 2931-2939.

66. Vargas, C.; Arenas, R. C.; Frotscher, E.; Keller, S., Nanoparticle self-assembly in mixtures of phospholipids with styrene/maleic acid copolymers or fluorinated surfactants. *Nanoscale* **2015,** *7* (48), 20685-20696.

67. Smith, A. A. A.; Autzen, H. E.; Laursen, T.; Wu, V.; Yen, M.; Hall, A.; Hansen, S. D.; Cheng, Y.; Xu, T., Controlling Styrene Maleic Acid Lipid Particles through RAFT. *Biomacromolecules* **2017,** *18* (11), 3706-3713.

68. Orwick, M. C.; Judge, P. J.; Procek, J.; Lindholm, L.; Graziadei, A.; Engel, A.; Gröbner, G.; Watts, A., Detergent-Free Formation and Physicochemical Characterization of Nanosized Lipid–Polymer Complexes: Lipodisq. *Angewandte Chemie International Edition* **2012,** *51* (19), 4653-4657.

69. Zhang, R.; Sahu, I. D.; Liu, L.; Osatuke, A.; Comer, R. G.; Dabney-Smith, C.; Lorigan, G. A., Characterizing the structure of lipodisq nanoparticles for membrane protein spectroscopic studies. *Biochimica et Biophysica Acta (BBA) - Biomembranes* **2015,** *1848* (1, Part B), 329-333.

70. Ravula, T.; Ramadugu, S. K.; Di Mauro, G.; Ramamoorthy, A., Bioinspired, Size-Tunable Self-Assembly of Polymer–Lipid Bilayer Nanodiscs. *Angewandte Chemie International Edition* **2017,** *56* (38), 11466-11470.

71. Ravula, T.; Hardin, N. Z.; Ramadugu, S. K.; Cox, S. J.; Ramamoorthy, A., Formation of pH-Resistant Monodispersed Polymer–Lipid Nanodiscs. *Angewandte Chemie International Edition* **2018,** *57* (5), 1342-1345.

72. Burridge, K. M.; Harding, B. D.; Sahu, I. D.; Kearns, M. M.; Stowe, R. B.; Dolan, M. T.; Edelmann, R. E.; Dabney-Smith, C.; Page, R. C.; Konkolewicz, D.; Lorigan, G. A., Simple Derivatization of RAFT-Synthesized Styrene–Maleic Anhydride Copolymers for Lipid Disk Formulations. *Biomacromolecules* **2020,** *21* (3), 1274-1284.

73. Ravula, T.; Hardin, N. Z.; Bai, J.; Im, S.-C.; Waskell, L.; Ramamoorthy, A., Effect of polymer charge on functional reconstitution of membrane proteins in polymer nanodiscs. *Chemical Communications* **2018,** *54* (69), 9615-9618.

74. Lee, S. C.; Knowles, T. J.; Postis, V. L. G.; Jamshad, M.; Parslow, R. A.; Lin, Y.-p.; Goldman, A.; Sridhar, P.; Overduin, M.; Muench, S. P.; Dafforn, T. R., A method for detergent-free isolation of membrane proteins in their local lipid environment. *Nature Protocols* **2016,** *11* (7), 1149-1162.

75. Rothnie, A. J., Detergent-Free Membrane Protein Purification. *Methods Mol Biol* **2016,** *1432*, 261-7.

76. Yasuhara, K.; Arakida, J.; Ravula, T.; Ramadugu, S. K.; Sahoo, B.; Kikuchi, J.-i.; Ramamoorthy, A., Spontaneous Lipid Nanodisc Fomation by Amphiphilic Polymethacrylate Copolymers. *Journal of the American Chemical Society* **2017,** *139* (51), 18657-18663.

77. Dekker, N.; Merck, K.; Tommassen, J.; Verheij, H. M., In Vitro Folding of Escherichia Coli Outer-Membrane Phospholipase A. *European Journal of Biochemistry* **1995,** *232* (1), 214-219.

78. Oluwole, A. O.; Danielczak, B.; Meister, A.; Babalola, J. O.; Vargas, C.; Keller, S., Solubilization of Membrane Proteins into Functional Lipid-Bilayer Nanodiscs Using a Diisobutylene/Maleic Acid Copolymer. *Angewandte Chemie International Edition* **2017,** *56* (7), 1919-1924.

79. Hardin, N. Z.; Ravula, T.; Mauro, G. D.; Ramamoorthy, A., Hydrophobic Functionalization of Polyacrylic Acid as a Versatile Platform for the Development of Polymer Lipid Nanodisks. *Small* **2019,** *15* (9), 1804813.

80. Seddon, A. M.; Curnow, P.; Booth, P. J., Membrane proteins, lipids and detergents: not just a soap opera. *Biochimica et Biophysica Acta (BBA) - Biomembranes* **2004,** *1666* (1), 105-117.

81. Vanaken, T.; Foxall-Vanaken, S.; Castleman, S.; Ferguson-Miller, S., [3] Alkyl glycoside detergents: Synthesis and applications to the study of membrane proteins. In *Methods in Enzymology*, Academic Press: 1986; Vol. 125, pp 27-35.

82. Tribet, C.; Audebert, R.; Popot, J.-L., Amphipols: Polymers that keep membrane proteins soluble in aqueous solutions. *Proceedings of the National Academy of Sciences* **1996,** *93* (26), 15047.

83. Bazzacco, P.; Sharma, K. S.; Durand, G.; Giusti, F.; Ebel, C.; Popot, J.-L.; Pucci, B., Trapping and Stabilization of Integral Membrane Proteins by Hydrophobically Grafted Glucose-Based Telomers. *Biomacromolecules* **2009,** *10* (12), 3317-3326.

84**.** Tao, H.; Lee, S. C.; Moeller, A.; Roy, R. S.; Siu, F. Y.; Zimmermann, J.; Stevens, R. C.; Potter, C. S.; Carragher, B.; Zhang, Q., Engineered nanostructured β-sheet peptides protect membrane proteins. *Nature Methods* **2013,** *10* (8), 759-761.

85. Popot, J. L.; Althoff, T.; Bagnard, D.; Banères, J. L.; Bazzacco, P.; Billon-Denis, E.; Catoire, L. J.; Champeil, P.; Charvolin, D.; Cocco, M. J.; Crémel, G.; Dahmane, T.; de la Maza, L. M.; Ebel, C.; Gabel, F.; Giusti, F.; Gohon, Y.; Goormaghtigh, E.; Guittet, E.; Kleinschmidt, J. H.; Kühlbrandt, W.; Le Bon, C.; Martinez, K. L.; Picard, M.; Pucci, B.; Sachs, J. N.; Tribet, C.; van Heijenoort, C.; Wien, F.; Zito, F.; Zoonens, M., Amphipols From A to Z. *Annual Review of Biophysics* **2011,** *40* (1), 379-408.

86. Rigaud, J. L.; Levy, D.; Mosser, G.; Lambert, O., Detergent removal by non-polar polystyrene beads. *European Biophysics Journal* **1998,** *27* (4), 305-319.

87. Zhang, Q.; Ma, X.; Ward, A.; Hong, W.-X.; Jaakola, V.-P.; Stevens, R. C.; Finn, M. G.; Chang, G., Designing Facial Amphiphiles for the Stabilization of Integral Membrane Proteins. *Angewandte Chemie International Edition* **2007,** *46* (37), 7023-7025.

88. Chae, P. S.; Gotfryd, K.; Pacyna, J.; Miercke, L. J. W.; Rasmussen, S. G. F.; Robbins, R. A.; Rana, R. R.; Loland, C. J.; Kobilka, B.; Stroud, R.; Byrne, B.; Gether, U.; Gellman, S. H., Tandem Facial Amphiphiles for Membrane Protein Stabilization. *Journal of the American Chemical Society* **2010,** *132* (47), 16750-16752

89. Zhang, Y.; Xuan, S.; Owoseni, O.; Omarova, M.; Li, X.; Saito, M. E.; He, J.; McPherson, G. L.; Raghavan, S. R.; Zhang, D.; John, V. T., Amphiphilic Polypeptoids Serve as the Connective Glue to Transform Liposomes into Multilamellar Structures with Closely Spaced Bilayers. *Langmuir* **2017,** *33* (11), 2780-2789.

90. Robertson, E. J.; Olivier, G. K.; Qian, M.; Proulx, C.; Zuckermann, R. N.; Richmond, G. L., Assembly and molecular order of two-dimensional peptoid nanosheets through the oil–water interface. *Proceedings of the National Academy of Sciences* **2014,** *111* (37), 13284.

91. Sanii, B.; Haxton, T. K.; Olivier, G. K.; Cho, A.; Barton, B.; Proulx, C.; Whitelam, S.; Zuckermann, R. N., Structure-Determining Step in the Hierarchical Assembly of Peptoid Nanosheets. *ACS Nano* **2014,** *8* (11), 11674-11684.

CHAPTER 2. FRAGMENTATION OF LIPOSOMES BY HYDROPHOBICALLY-MODIFIED POLYPEPTOIDS: ELUCIDATING THE ROLE OF MOLECULAR CHARACTERISTICS

2.1 Experimental

2.1.1 General considerations

All the chemicals and solvents were purchased from Sigma Aldrich and used as received unless otherwise noted. The solvents used for polymerization were further purified by using alumina columns under argon protection. CD_2Cl_2 and $CDCl_3$ were purchased from Cambridge Isotope laboratories. L-α-Phosphatidylcholine (PC) and liposome extrusion setup were purchased from Avanti Polar Lipids. Polycarbonate membranes and membrane filter support were purchased from EMD Millipore. Deionized water used for DLS and SLS was further purified by Nanopure Bioresearch water purification system with a resistance of 17.8-17.9 MΩ·cm from Barnstead Lab Water Products. ^{1}H NMR was collected by Bruker AV-400 III spectrometer at 298K and analyzed using Topspin software. Chemical shifts (δ) given in parts per million (ppm) were referenced to protio impurities.

2.1.2 Synthesis and characterization of *N*-substituted *N*-carboxyanhydride (R-NCA) monomers and HMP copolypeptoids

N-decyl glycine derived *N*-carboxyanhydride (De-NCA) and *N*-methoxyethyl glycine derived *N*-carboxyanhydride (MeOEt-NCA) monomers were synthesized by published procedure.[80] ^{1}H NMR spectra of these monomers were shown in Figure 2.1 and Figure 2.2.

HMP random copolypeptoids were synthesized by primary amine-initiated ring-opening polymerization (ROP) of MeOEt-NCA and De-NCA monomers as shown in Scheme 2.1.

A representative procedure for synthesizing PNMeOEtG$_{75}$-*r*-PNDG$_{25}$ is shown as followed. In the glovebox, stock solutions of MeOEt-NCA (M_1, 640 mg, $[M_1]_0$ = 0.4 M) and De-NCA (M_2,

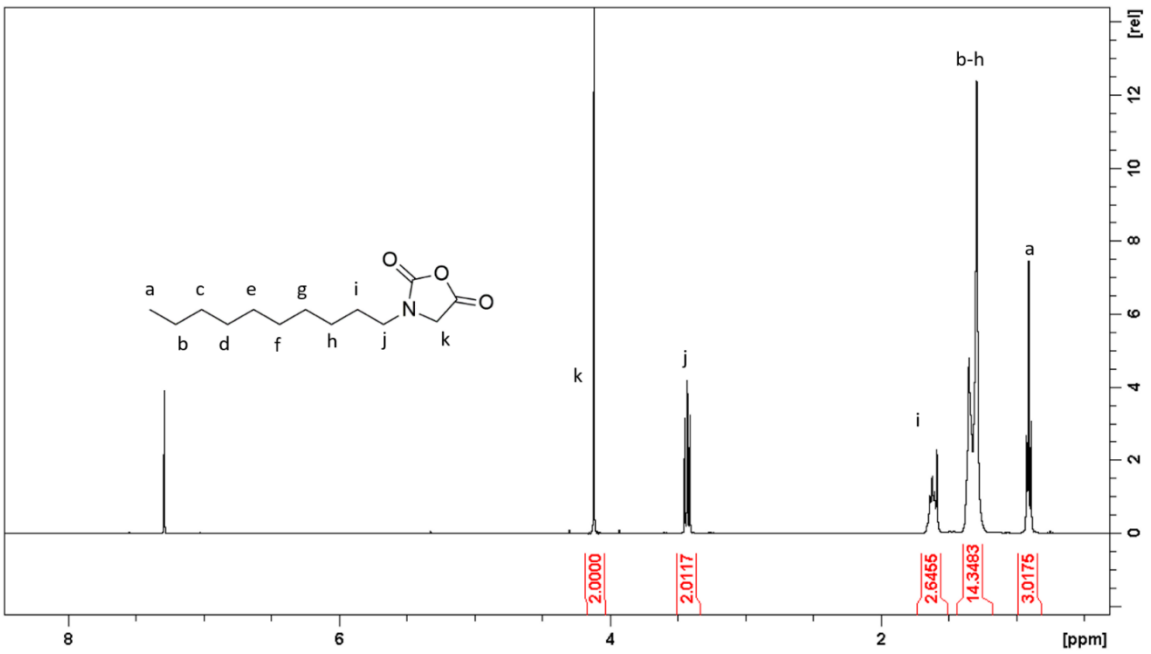

Figure 2.1. ^{1}H NMR spectrum of De-NCA monomer in $CDCl_3$.

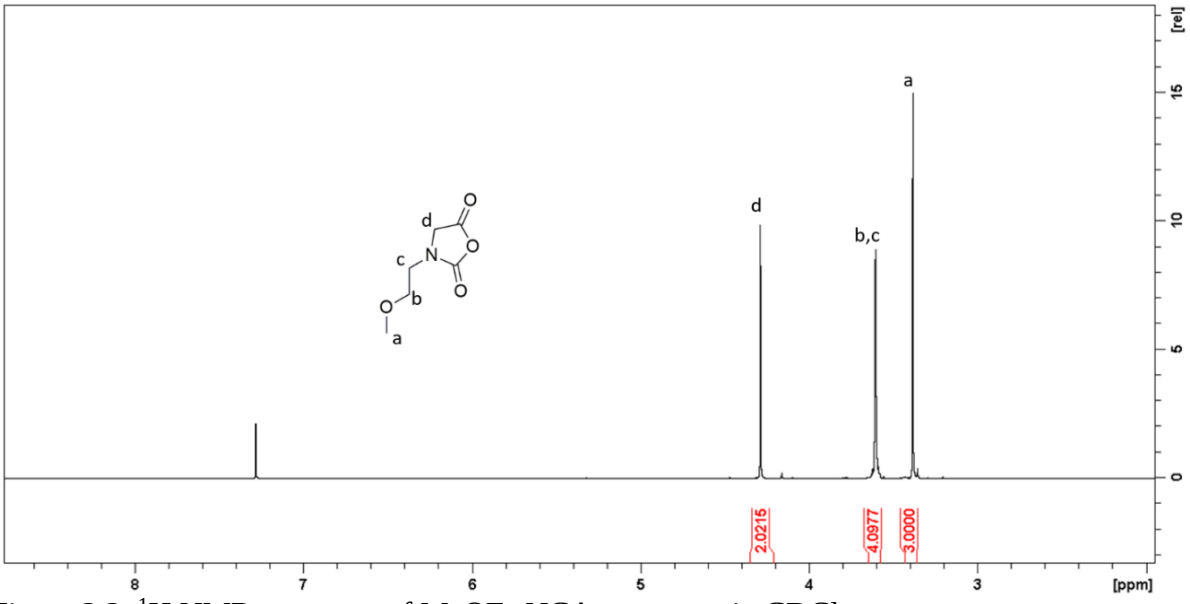

Figure 2.2. ^{1}H NMR spectrum of MeOEt-NCA monomer in $CDCl_3$.

Scheme 2.1. Synthesis of $PNMeOEt_x$-*r*-$PNDG_y$ random copolypeptoids

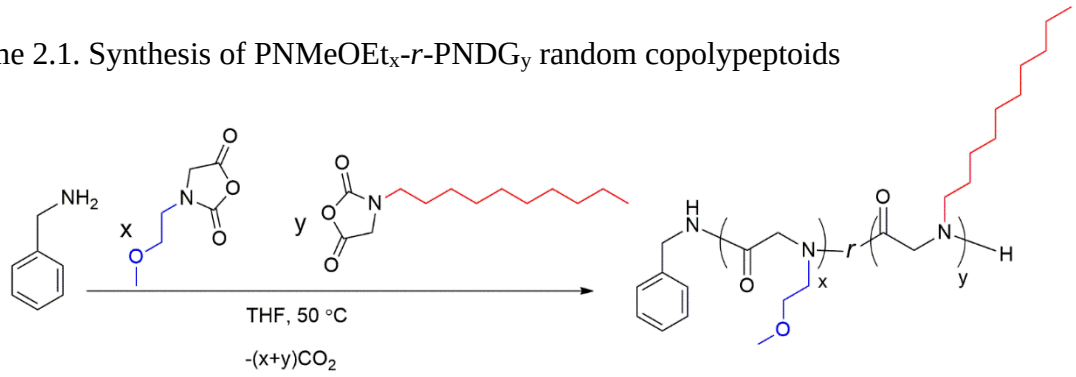

968 mg, $[M_2]_0$ = 0.4 M) monomers in anhydrous THF were prepared respectively in 10 ml volumetric flasks. Benzyl amine stock solution (I_0, 55 mg, $[I]_0$ = 0.102 M) in anhydrous THF was prepared using a 5 ml volumetric flask. 2812 µl M_1 (0.18 g, 1.13 mmol, $[M_1]_0$ = 0.4 M) and 939 µl M_2 (0.09 g, 0.39 mmol, $[M_2]_0$ = 0.4) stock solutions were fully mixed prior to the addition of initiator stock solution I_0 (148 µl, 0.015 mmol, $[M_1+M_2]_0$: $[I]_0$ = 100). Polymerization mixture was stirred at 50 °C under nitrogen atmosphere for 96 h to reach complete conversion (Note: polymerization time varied depending on different $[M_1]_0$:$[M_2]_0$ and $[M_1+M_2]_0$:$[I]_0$). The polymerization conversion was tracked by monitoring the disappearance of -C=O peak at 1780 cm^{-1} and 1740 cm^{-1} in the reaction aliquots taken over time using FT-IR spectroscopy. The volatiles were removed under vacuum using Schlenk line. The crude polymer was further purified by re-dissolved in DCM and precipitated with ample hexanes twice. The polymer was isolated by centrifugation and dried under vacuum to yield a white powder (0.19 g, 93 %). ^{1}H NMR spectrum of PNMeOEtG$_{73}$-*r*-PNDG$_{27}$ is shown in Figure 2.3, and ^{1}H NMR spectra for other HMP copolymers were shown in Figure S2.1-S2.5. ^{1}H NMR spectra of PNMeOEtG$_{73}$-*r*-PNDG$_{27}$ (CD_2Cl_2, 400 MHz) δ (ppm): 7.23-7.18 (m, C_6H_5-, 5H), 4.34-4.02 (m, -$COCH_2$-), 3.40-3.19 (m, -$CH_2CH_2OCH_3$, -NCH_2- (NDG)), 1.50-1.36 (m, -NCH_2 CH_2-, NDG), 1.18 (m, -NCH_2 CH_2 $(CH_2)_6$ CH_2-, NDG), 0.81 (t, -CH_3, NDG). The polymer compositions were determined by end-group analysis. The number-averaged degree of polymerization (DP_n) for PNDG segment (y in Scheme 2.1) was determined by integrating the methyl protons of PNDG segment centered at 0.81 ppm (p, Figure 2.3) relative to the phenyl protons of the benzyl amine end-group at 7.23-7.18 ppm (r, Figure 2.3). The DP_n for PNMeOEtG segment (x in Scheme 2.1) was determined from the integration of -$COCH_2$- backbone methylene protons for x + y at 4.34- 4.02 ppm (b, f in Figure 2.3) subtracted by the integration of methyl protons at 0.81 ppm for y. More specifically, if the

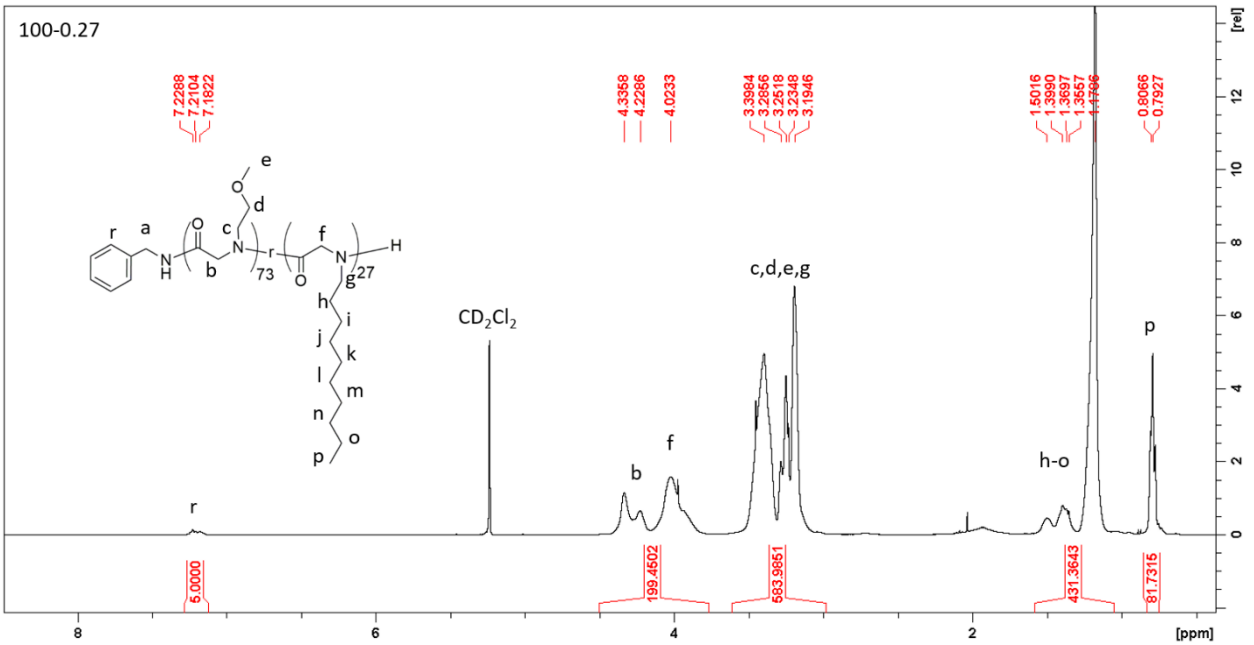

Figure 2.3. Representative ^{1}H NMR spectrum of PNMeOEGt$_{73}$-*r*-PNDG$_{27}$ (100-0.27) random copolypeptoid in CD_2Cl_2.

integration of end phenyl protons (C_6H_5-) were set as 5, DP_n (y) = integration of CH_3(p)/3; DP_n (x) = (integration of ^{b,f}-$COCH_2$- 2 × y)/2, where p refers to the end methyl group in PNDG segment, and b f refer to the methylene groups of –$COCH_2$ on polymer backbones. The molecular characteristics of HMP copolypeptoids were summarized and listed in Table 2.1.

2.1.3 Size-exclusion chromatography

SEC experiments were performed in DMF with 0.1 M LiBr at 25 ℃ with a flow rate of 0.5 ml/min. HMP polymerization solution (0.1 ml) was mixed with a DMF solution (0.6 ml) containing LiBr (0.1M) and left to stand overnight. The polymer solutions were filtered with 0.45 μm PTFE filters before injecting into the SEC system. SEC analysis of the hydrophobically modified polypeptoids was performed using an Agilent 1200 system equipped with three Phenomenex 5 μm, 300 × 7.8 mm columns, a Wyatt DAWN EOS multiangle light scattering (MALS) detector (GaAs 30mW laser at λ = 690 nm) and Wyatt OptilabrEX differential refractive index (DRI) detector. The data analysis was performed using Wyatt Astra V 5.3 software. The

PDI were obtained using polystyrene standards. The results of SEC analysis for varying HMPs were shown in Figure 2.4 and the size information were summarized in Table 2.1.

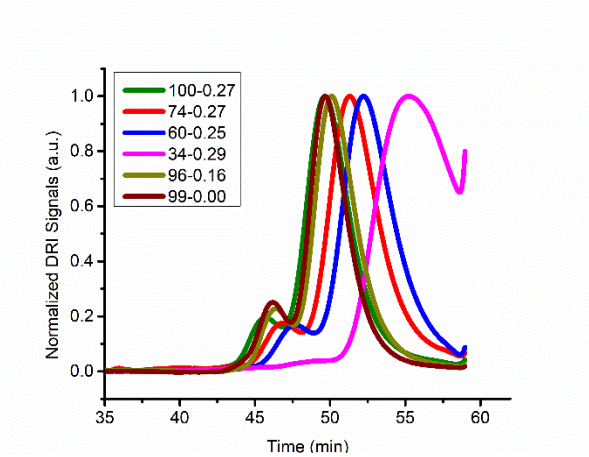

Figure 2.4. SEC-DRI chromatograms of HMP copolypeptoids in DMF with 0.1 M LiBr at 25℃.

Table 2.1. Molecular parameters of PNMeOEtG$_x$-*r*-PNDG$_y$ (HMP) copolypeptoids.

Entry #	Sample Name (DP$_n$-PNDG%) [a.]	Polymer Composition [a.]	M_n (kDa)[a.]	PDI[b.]	PNDG molar % [a.]
1	34-0.29	PNMeOEt$_{24}$-PNDG$_{10}$	4.7	1.13	29
2	60-0.25	PNMeOEt$_{45}$-PNDG$_{15}$	8.1	1.14	25
3	74-0.27	PNMeOEt$_{54}$-PNDG$_{20}$	10.2	1.36	27
4	100-0.27	PNMeOEt$_{73}$-PNDG$_{27}$	13.7	1.13	27
5	96-0.16	PNMeOEt$_{81}$- PNDG$_{15}$	12.3	1.07	16
6	99-0.00	PNMeOEt$_{99}$	11.4	1.07	0

[a.] Sample composition and molecular weight (M_n[a]) were determined by ^{1}H NMR spectroscopy. DP$_n$ signifies the number average degree of polymerization determined by end group analysis; PNDG% refers to the molar percentage of PNDG segment in HMP copolypeptoids; [b.] Polydispersity (PDI) was determined using SEC in DMF with 0.1 M LiBr at 25℃ with a flow rate of 0.5 ml/min.

2.1.4 Liposome preparation

PC lipids (20 mg) were dissolved in a mixture of chloroform and methanol (5 ml, v/v = 2:1) and gently swirled till the lipid was fully dissolved. The sample was then mixed using rotovap at 25 ℃ for 10 min with rotation rate at 120 rpm before turning on vacuum at 150 mbar for 3 h to slowly remove the volatile. The vacuum was then increased up to 80 mbar for another 1 h to completely remove all the volatiles, yielding a transparent thin film coated inside of the flask. Nano-pure water (5 ml) was added to hydrate the thin film at 50 ℃ for 2 h with rotation rate at 80 rpm. The hydration solution was extruded at 50℃ for 20 times with polycarbonate membrane (pore size = 0.1 μm) to afford translucent liposome solutions with a 5 mg/ml concentration. An aliquot of extruded liposome solution was taken and diluted by 40 times to perform DLS measurement. The DLS exponential decay curve was fitted using maximum entropy method (MEM) analysis to obtain the information of hydrodynamic radius (r_h) and size homogeneity of liposomes.[1]

2.1.5 Liposome stability test

The effect of agitation on liposome size stability was assessed by measuring the liposome size change with or without agitation over 3 days. First, the freshly extruded 5 mg/ml liposome aqueous solution was diluted into 1.25 mg/ml which is the liposome concentration used for further studying the polymer induced liposome fragmentation in section 2.2.4 and 2.2.5. Liposome size was measured by DLS at 25 ℃ and the exponential decay curve G(t) was analyzed using MEM analysis method to obtain the average hydrodynamic radius (R_h). The liposome solution was then incubated at 25 ℃ for 3 days with magnetic stirring rate at 150 rpm. The R_h was re-analyzed using DLS. For comparison, same experiment was also conducted to monitor the change of liposome size for 3 days without agitation.

2.1.6 Polymer aqueous solution preparation

A representative procedure for the preparation of 100-0.27 HMP polymer aqueous solution (100 signifies the DP_n of the polymer, and 0.27 refers to the molar percentage of the PNDG hydrophobic segment over the entire polymer) at a 5 mg/ml concentration is shown as followed. In a clean scintillation vial, 100-0.27 polymer powder (10 mg) was dissolved in dichloromethane (DCM, ~1 ml) for overnight without agitation. The solution was dried by blowing nitrogen over it to form a transparent polymer thin film, which was hydrated with nano-pure water (2 ml). The resultant solution was then stirred at 25℃ overnight with a stirring rate at 350 rpm, yielding a visually clear polymer solution. The polymer solution was passed through a polyethersulfone (PES) syringe filter (pore size = 0.45 μm) prior to DLS measurement. All the vials, spatulas and stirring bars used were pre-cleaned with nano-pure water and air-dried before using.

2.1.7 Polymer and liposome complex preparation

A representative procedure for the preparation of 100-0.27 polymer and liposome complex (100-0.27+lip) is given as followed. A known volume of 100-0.27 polymer solution (5 mg/ml) was first filtered through a PES filter (pore size = 0.45 μm) and then added into a freshly extruded liposome aqueous solution (2.5 mg/ml, liposome hydrodynamic diameter = ~ 0.1 μm) in equal volume (v/v = 1:1). The solution was gently mixed 10 times with a plastic pipette and further stirred at 25℃ with a stirring rate at 150 rpm over a period of 3 days. An aliquot of the above solution (0.2 ml) was taken at a controlled time points and diluted 10 times with nano-pure water prior to DLS measurement.

2.1.8 Sample preparation for cryo-TEM and negative stained TEM analyses

Cryo-TEM imaging was conducted using a FEI G2 F30 Tecnai TEM operated at 200 kV. The 5 mg/ml HMP and 2.5 mg/ml liposome aqueous solutions prepared using the method

described in section 2.1.4 and 2.1.6 were mixed in equal volume (v/v = 1:1) and incubated at 25˚C for overnight before imaging. 5 µl of the sample solution was transferred to a 200-mesh lacey carbon coated copper grid (Electron Microscopy Sciences) mounted on the FEI Vitrobot and blotted for 2 s to generate a sample thin film before plunging into liquid ethane.

The morphology of HMP and liposome complex (HMP+lip) was also analyzed using negative stained TEM. The 200 mesh carbon coated copper grid was pre-treated with a glow-discharger (LEICA EM ACE 600) for 30s to yield a negatively charged hydrophilic surface. Sample solution (5 µl) was placed on the grid and left for about 5 min before blotted with a filter paper to remove excess solution. 2 wt % uranyl acetate (5 µl) aqueous solution was subsequently added on the grid and left for 20 s before botted using a filter paper.

2.1.9 Sample preparation for dynamic light scattering and static light scattering analyses

DLS and SLS measurements were performed on Wyatt DAWN HELEOS-II instrument with a laser wavelength of 658 nm at 25 ˚C. The polymer solution was passed through a polyethersulfone (PES) syringe filter (pore size = 0.45 µm) into pre-cleaned scintillation vial, and the sample vial was equilibrium at 25 ˚C for 5 min before each measurement. The collection time for each sample is 5 min with collection interval of 5 s and 2 s for DLS and SLS measurements respectively.

2.1.10 Maximum entropy method (MEM)

The correlation function obtained from DLS measurement was fitted using maximum entropy method (MEM) to obtain the size and distribution information of hydrodynamic radius (R_h). A decay time distribution can be generated using MEM analysis which was performed using the Clementine (v1.2) package in Igor Pro (v 6.37) software. The hydrodynamic radius (R_h) can be calculated using the Stokes-Einstein equation (eq. 2.2), where k is Boltzmann's constant, T is

absolute temperature, ŋ is the solvent viscosity and D is the diffusion constant which can be calculated using equation 2.3. In equation 2.3, q is the scattering vector which is calculated using equation 2.4, where n_0 is the solvent refraction index, λ_0 is the vacuum wavelength of the incident light, and θ is the scattering angle, Γ is the decay rate which can be obtained from the correlation function in DLS measurement (eq. 2.1). R_h distribution curve can be further fitted with a lognormal distribution function in Origin software to obtain the average R_h.

$$G_1(t) = exp^{-\Gamma t} \quad \text{(eq. 2.1)}$$

$$R_h = \frac{kT}{6\pi ŋ D} \quad \text{(eq. 2.2)}$$

$$D = \frac{\Gamma}{q^2} \quad \text{(eq. 2. 3)}$$

$$q = \frac{4\pi n_0}{\lambda_0} \times sin(\frac{\theta}{2}) \quad \text{(eq. 2.4)}$$

2.2 Results and discussion

2.2.1 Liposome stability with or without agitation

The change of normalized exponential decay G(t) of liposomes over 3 days with (c) or without (a) agitation were shown in Figure 2.5 (a) and (c) and analyzed by the maximum entropy method (MEM) to obtain the corresponding mean hydrodynamic radius (R_h) and distributions in Figure 2.5 (b) and (d). Over a course period of 3 days, a minor reduction of hydrodynamic radius by ~ 8 nm with a narrow distribution was observed without agitation (Figure 2.5 b). By contrast, a relatively large increase of hydrodynamic radius by ~ 26 nm and a broader size distribution were observed under agitation (Figure 2.5 d). This clearly indicates that agitation of the solution under a stirring rate of 150 rpm can increase the size and heterogeneity of liposomes. The bright field cryo-TEM images and negative stained TEM images of freshly prepared liposomes were shown in Figure 2.6 (a)-(b) and (c)-(d), respectively.

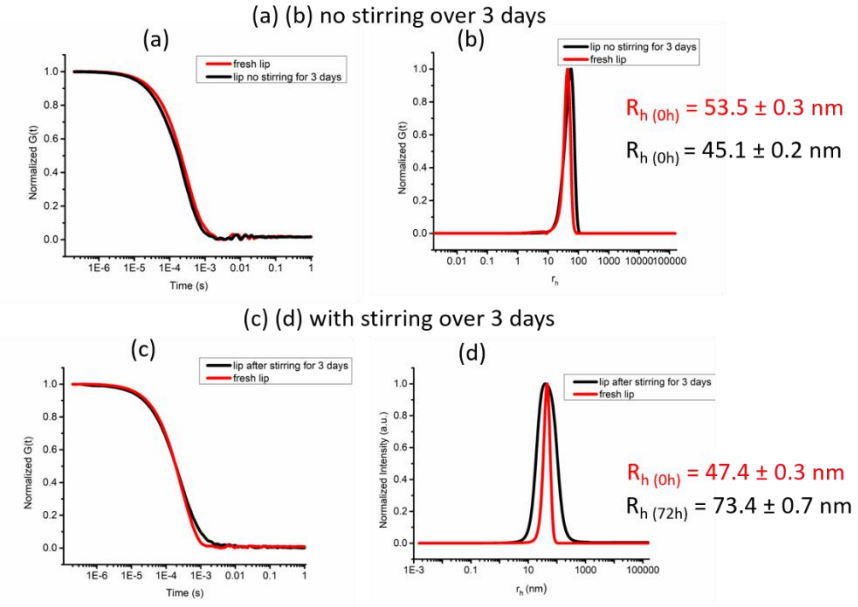

Figure 2.5. Change of normalized exponential decay curves G(t) and hydrodynamic radius distribution for liposomes with (c, d) or without stirring (a, b) for 3 days. R_h indicated hydrodynamic radius at designated measurement time point.

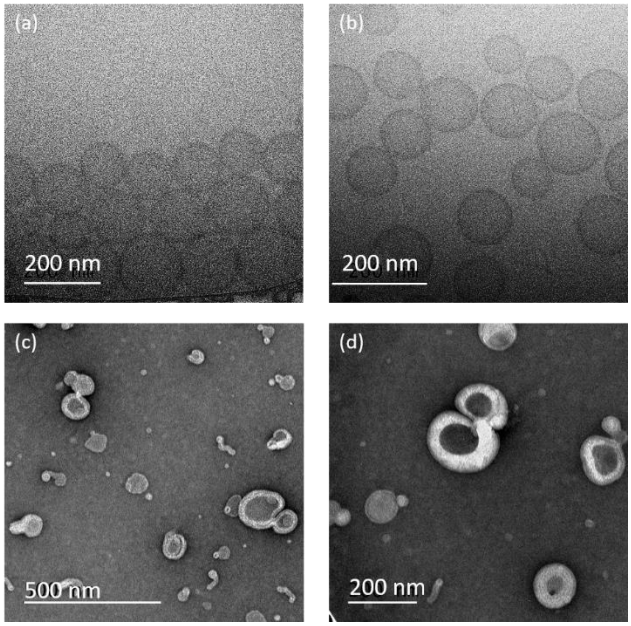

Figure 2.6. (a)-(b) Cryo-TEM and (c)-(d) negative stained TEM images of freshly prepared liposome.

2.2.2 Polymer concentration effect on polymer induced liposome fragmentation

HMP sample 100-0.27 was selected to investigate the impact of polymer concentration on polymer induced liposome fragmentation. First, a 100-0.27 polymer aqueous solution (5 mg/ml)

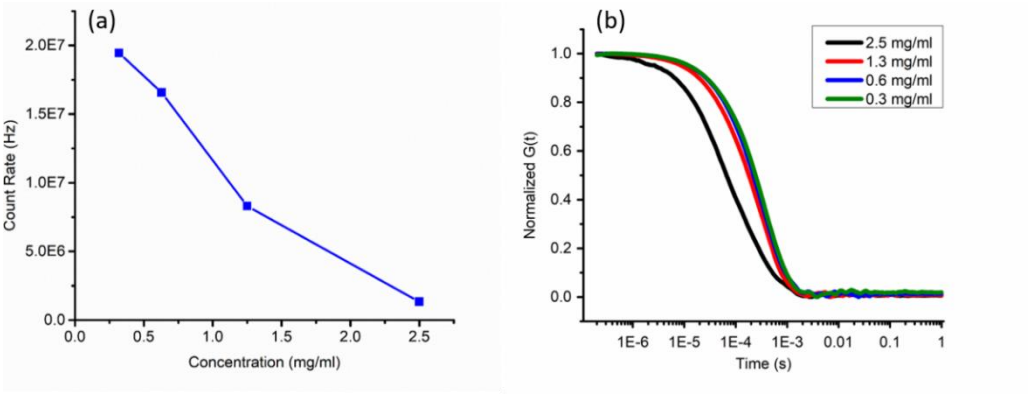

Figure 2.7. Results of SLS and DLS studies on the size of 100-0.27 and liposome complex (100-0.27+lip) with varying polymer concentrations. Figure (a) shows the total scattered light intensity versus polymer concentration measured by SLS after 2 days, and figure (b) displays the normalized DLS decay curves of 100-0.27 after 48 h.

was prepared using the DCM thin film hydration method as described in section 2.1.6. The polymer solution was sequentially diluted into 2.5, 1.3, 0.6 and 0.3 mg/ml concentrations. These polymer solutions with varying polymer concentrations were each mixed with a freshly prepared liposome solution (2.5 mg/ml) in equal volume (v/v = 1:1). The resultant polymer and liposome mixtures (100-0.27+lip) were allowed to stand at 25℃ for 2 days. The addition of HMP polymers into liposome solutions resulted in a gradual reduction of solution turbidity, which is presumably associated with the liposome fragmentation. This can be characterized by monitoring the change of total light scattering intensity versus time using static light scattering (SLS). After incubating the polymer and liposome mixtures for 48 h, the final photon count rate (I in Hz), which corresponds to the total scattered light intensity per unit time, was plotted versus final polymer concentrations in Figure 2.7(a). The initial count rates (I_0) for all the samples remained in a range of $1.8 \times 10^7 \sim 2.0 \times 10^7$ Hz and the final count rates (I_{48h}) steadily decreased with increasing polymer concentrations as shown in Figure 2.7 (a). This indicates that the higher polymer concentration can more effectively induce liposome fragmentation. The final size of 100-0.27+lip with varying polymer concentrations were characterized using DLS, as shown in Figure 2.7 (b). By comparison

of normalized G(t) over 48 h at different polymer concentrations, it was found that G(t) at high polymer concentration ($c_{polymer}$ = 2.5 mg/ml) afforded a notable shift toward low decay time range relative to those with low polymer concentrations ($c_{polymer}$ = 1.3 - 0.3 mg/ml), indicating an enhanced fragmentation of liposomes at higher polymer concentration ($c_{polymer}$ = 2.5 mg/ml) which is consistent with the observation from SLS study. DLS G(t) curves were fitted and analyzed using MEM (Figure 2.8). In all samples, two size populations with varying relative abundance were observed. The population appeared at the longer decay time is attributed to the liposomes or larger reconstructed liposomes by HMP. The population at shorter decay time is attributed to the fragmented liposomal pieces. It is clear that high polymer concentration ($c_{polymer}$ = 2.5 mg/ml) is most effectively in inducing the liposome fragmentation, evidenced by the significantly enhanced intensity of the population at short decay time relative to that at long decay time. Based on the SLS and DLS results, 2.5 mg/ml is used as a standard polymer concentration for further study on the polymer induced liposome fragmentation with other HMP polymers.

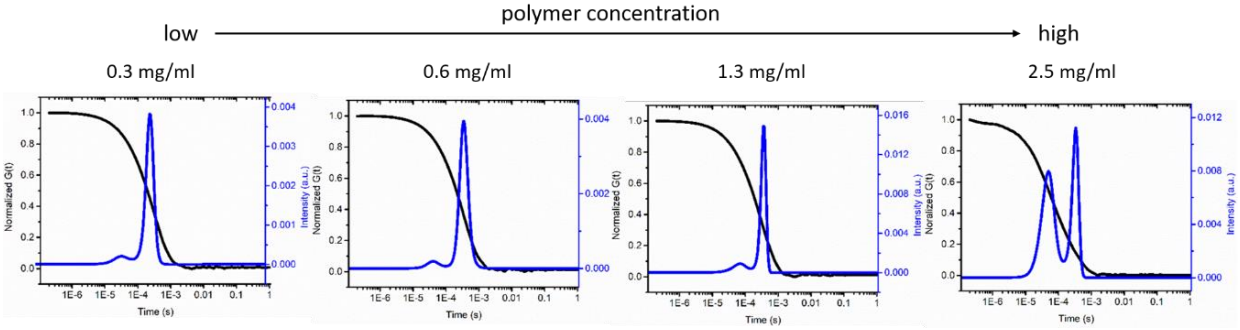

Figure 2.8. DLS decay time distribution with G(t) for 100-0.27+lip with varying polymer concentrations ($c_{polymer}$ = 0.3-2.5 mg/ml) after incubating for 2 days. Size distribution was analyzed using MEM analysis method.

2.2.3 Analysis of HMP polymer size in aqueous solution

Before studying the impact of polymer molecular characteristics (*e.g.* molecular weight, hydrophobicity, *etc.*) on polymer induced liposome fragmentation, polymer solubility was first studied using DLS for series of HMP polymers with 27 ± 2 molar % of PNDG segment (HMP-

0.27) having varying molecular weights with DP_n = 34-100. All the polymers aqueous solutions were prepared using DCM thin film hydration method with a 5 mg/ml polymer concentration. Figure S2.6 shows the normalized DLS G(t) for HMP-0.27 polymers with varying molecular weights. The size distributions obtained by fitting the G(t) using MEM are shown in Figure S2.7. Two size populations were observed for all the samples, indicating that the polymers were not individually dissolved under current sample preparation condition. The population at short decay time was attributed to individually dissolved polymers and the population at the longer decay time was considered as polymer aggregates formed in aqueous solution. The morphologies of selected HMP polymers (100-0.27 and 34-0.29) were analyzed using cryo-TEM in Figure S2.8. The size and homogeneity information of varying HMP copolymers in aqueous solutions were summarized in Table S2.1.

2.2.4 Effect of chain length on liposome fragmentation

To assess the effect of the chain length of HMP on polymer induced liposome fragmentation, a series of HMP polymers (HMP-0.27) having a constant ~ 27 ± 2 % molar percentage of hydrophobic segment but varying chain length (DP_n = 100, 60, 34) were investigated. Polymer aqueous solutions (5 mg/ml) were prepared using DCM thin film hydration method as

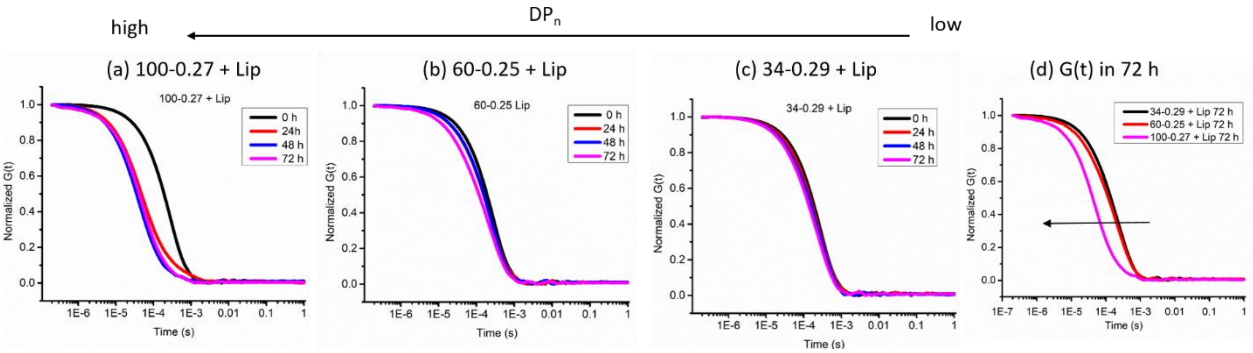

Figure 2.9. (a)-(c) Change of normalized G(t) over 3 days after mixing 5 mg/ml HMP-0.27 polymers with 2.5 mg/ml liposomes (v/v = 1:1); (d) Normalized G(t) for HMP-0.27 and liposome complexes (HMP-0.27+lip) after incubating for 72 h.

described in section 2.1.6. The polymer aqueous solutions were filtered through PES syringe filters (pore size = 0.45 µm) followed by the addition of freshly extruded liposome solutions (2.5 mg/ml) in equal volume (v/v = 1:1) and gentle mixing using a pipette. Liposome fragmentation and size change was investigated by taking aliquot of the solution samples for DLS and SLS over a period of 3 days. Normalized G(t) at different incubation time points for selected liposome and HMP-0.27 mixtures (HMP-0.27+lip) were shown in Figure 2.9 (a) - (c). G(t) with longest polymer (DP_n = 100) exhibited a pronounced shift towards low decay time after incubation for 24 h relative to the shorter polymers with DP_n = 60 and 34, suggesting that long polymer is more effective in inducing liposomes fragmentation. MEM analysis of G(t) (Figure 2. 10 (a)-(c) revealed two size populations for all the samples. The population at low decay time was attributed to the fragmented liposome pieces in the presence of HMP polymer, and the population at higher decay time was presumed to be either residual liposomes or large structural assemblies of liposomes and polymers. Importantly, as the HMP chain length become longer, the intensity of the small size population relative that of the large size population increases accordingly, suggesting that HMPs with longer chain length is more effective in inducing liposome fragmentation relative to the shorter ones.

Total static light scattering (SLS) intensity of HMP-0.27 polymer and liposome mixtures (HMP-0.27+lip) versus time was plotted in Figure 2.10 (d). In comparison of the total light

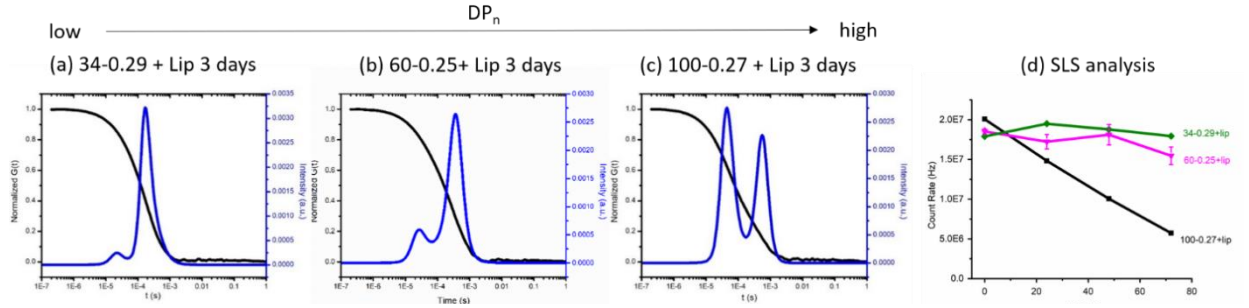

Figure 2.10. (a)-(c) Normalized G(t) with decay time distributions and (d) static light scattering (SLS) intensity change over 3 days for HMP-0.27 polymer and liposome complex (HMP-0.27+ lip) in water. DP_n of HMP-0.27 varies in the range of 34 - 100. The size distribution was analyzed using MEM analysis method.

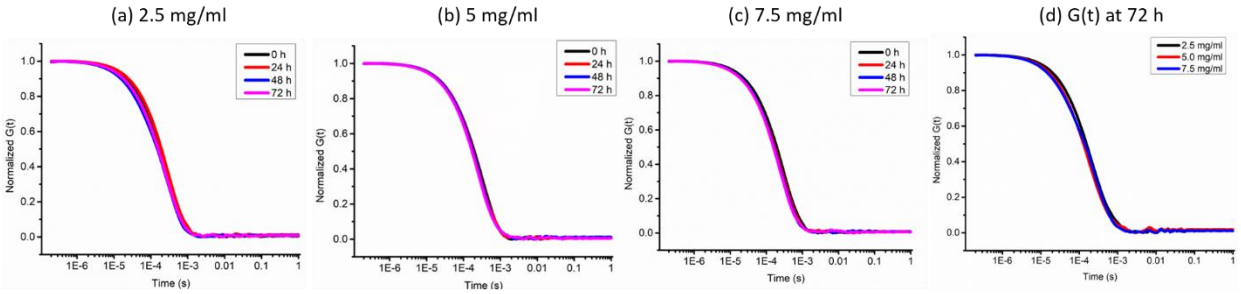

Figure 2.11. Change of G(t) after mixing 2.5 mg/ml liposome aqueous solutions with (a) 5 mg/ml, (b) 10 mg/ml and (c) 15 mg/ml 34-0.29 (v/v = 1:1); (c) Normalized G(t) for 34-0.29 and liposome complexes (34-0.29+lip) after incubating for 72 h.

intensities over 3 days, it was found that as molecular weight increasing from DP_n = 34 to 100, the final intensity decreased accordingly. SLS analysis result further supported that the efficiency of polymer-induced liposome fragmentation was strongly dependent on polymer molecular weight with long polymer (100-0.27) induced faster and greater extent of liposome fragmentation relative to short ones (60-0.25 and 34-0.29). The size and homogeneity information of HMP and lipid complexes were summarized in Table S2.2.

Since short polymer (34-0.29) was limited in inducing liposome fragmentation, higher polymer concentration was applied to enhance liposome fragmentation. 34-0.29 polymer aqueous solutions at concentration of 5 mg/ml, 10 mg/ml and 15 mg/ml were studied. All the polymer aqueous solutions were prepared using DCM thin film hydration method and stirred overnight before adding a constant volume of freshly prepared liposome solution (2.5 mg/ml). The final polymer concentrations are 2.5 mg/ml, 5.0 mg/ml and 7.5 mg/ml respectively. A liposome control group with same liposome concentration as other samples were also set for comparison. DLS G(t) was monitored every 24 h over a period of 3 days and plot of G(t) versus decay time was shown in Figure 2.11. G(t) after 3 days are comparable for the three samples (Figure 2.11 d). Based on MEM analysis of G(t) over 3 days in Figure 2.12, it was found that the intensity at lower decay time increase with polymer concentration from 2.5 mg/ml to 7.5 mg/ml indicating effective

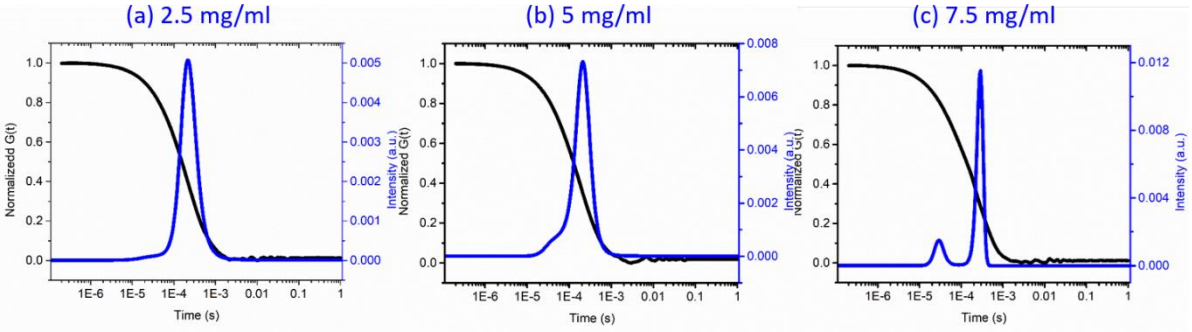

Figure 2.12. DLS decay time distributions for 34-0.29+lip with final polymer concentrations at (a) 2.5 mg/ml, (b) 5.0 mg/ml and (c) 7.5 mg/ml. The decay time distribution was analyzed using MEM analysis method.

liposome fragmentation at the high concentration sample (7.5 mg/ml) (Figure 2.12 c). While tripling the concentration of short polymer 34-0.29 can accelerate the liposome fragmentation, the final extent of fragmentation at 7.5 mg/ml in Figure 2.12 (c) was still lower than 100-0.27 at low concentration of 2.5 mg/ml in Figure 2.10 (c). As a result, it was concluded that shorter chain HMP is not as effective in inducing fragmentation of liposome relative to the longer chain counterparts.

Morphology of the two HMP-0.27+lip complexes, namely 100-0.27+lip and 34-0.29+lip, were characterized using cryo-TEM (in Figure 2.14 (a) (b) (e) (f)) and negative stain TEM (in Figure 2.13 (c) (d) (g) (h)). All the cryo-TEM images shown here are bright filed images. No residual liposomes but small spherical structures were observed in sample 100-0.27+lip in Figure 2.13 (a)-(d) indicating all the liposomes were fragmented into small pieces in the presence of 100-0.27 polymers. By contrast, short fibril structures with a ~ 50 nm average length were found to co-exist with large lipid assembles in sample 34-0.29+lip in Figure 2.13 (e)-(h). Based on the combined results of DLS, SLS and morphology analysis, it was concluded that long polymer (DP_n = 100) induced effective liposome fragmentation with faster and higher extent of fragmentation relative to short ones with DP_n = 34.

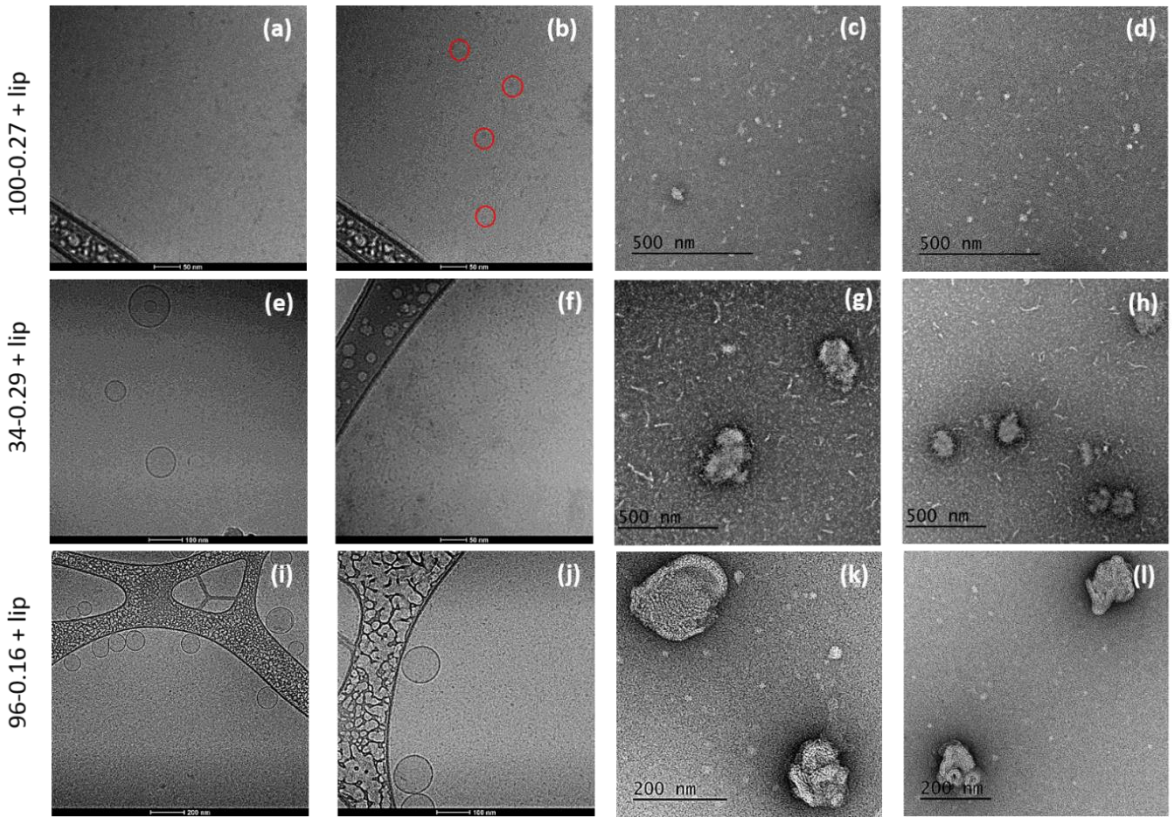

Figure 2.13. (a)-(b) Cryo-TEM characterization on (a)-(b) 100-0.27+lip complex, (e)-(f) 34-0.29 +lip complex, and (i)-(j) 96-0.16+lip complex; Negative stained TEM characterization on (c)-(d) 100-0.27+lip complex, (g)-(h) 34-0.29+lip complex, and (k)-(l) 96-0.16+lip complex.

2.2.5 Effect of polymer hydrophobicity on liposome fragmentation

In this section, the effect of polymer hydrophobicity on liposome fragmentation was investigated by comparing the hydrophilic $PNMeOEt_{99}$ homopolymer (99-0.00), *a.k.a*. unmodified polypeptoids (UMP), with two HMP polymers with similar molecular weight (DP_n = 96 to 100) and varying hydrophobicity (PNDG molar percentage =16% and 27%). Polymer size in aqueous solution was first characterized using DLS with MEM analysis result shown in Figure 2.14. Two size population distributions were observed in both HMP samples and the detailed size information was compared and summarized in Table S2.1. After the addition of liposomes, the size change was monitored using DLS and SLS over 3 days. Normalized G(t) from DLS measurements reveals that more hydrophobic 100-0.27 exhibited a notable shift towards lower decay time after 24 h in Figure

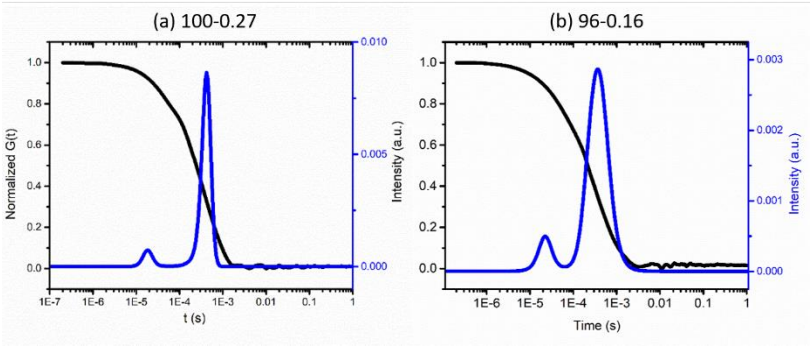

Figure 2.14. DLS normalized G(t) with decay time distributions for 5 mg/ml (a) 100-0.27 and (b) 96-0.16 polymer aqueous solutions. The decay time distribution was analyzed using MEM analysis method.

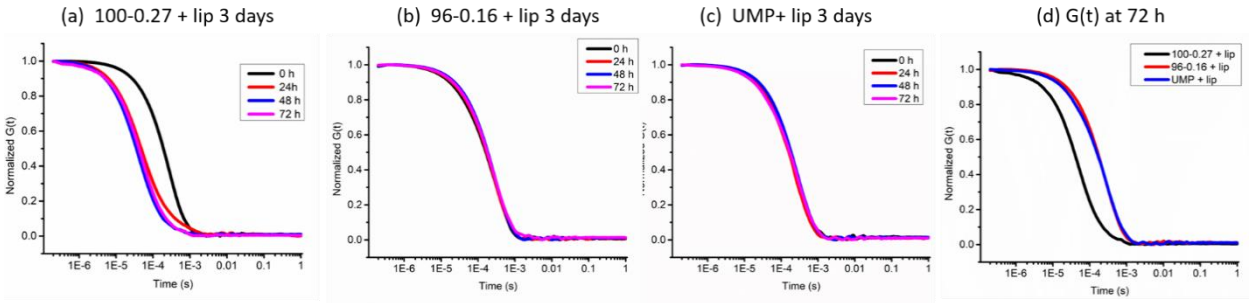

Figure 2.15. Time dependence study on DLS normalized G(t) of polymer and lipid complexes with varying polymer hydrophobicity (De mol % = 0, 16 %, 27 %).

2.15 (a). Whereas no notable shifts for relatively hydrophilic polymers (96-0.16 and 99-0.00) were observed in Figure 2.15 (b) and (c). Based on MEM analysis of G(t) over 3 days in Figure 2.16 (a)-(c), the UMP and lipid complex, namely as 99-0.00+lip, shows no significant fragmentation peak at lower decay in Figure 2.16 (a). In contrast, two HMP samples (96-0.16+lip and 100-0.27+lip) had two size populations with the population at low decay time corresponding to fragmented liposomes ($peak_1$) and the one at higher decay time corresponding to residual liposomes or re-constructed polymer/liposome assembles ($peak_2$) as shown in Figure 2.16 (b)-(c). Furthermore, it can be observed that the intensity of $peak_1$ (I_1) for sample 100-0.27+lip in Figure 2.16 (c) is dramatically higher than I_1 for sample 96-0.16+lip in Figure 2.16 (b). Therefore, it was concluded that the relatively hydrophilic 96-0.16 polymer resulted in less extent of liposome fragmentation relative to the hydrophobic 100-0.27 polymer. The detailed size and homogeneity

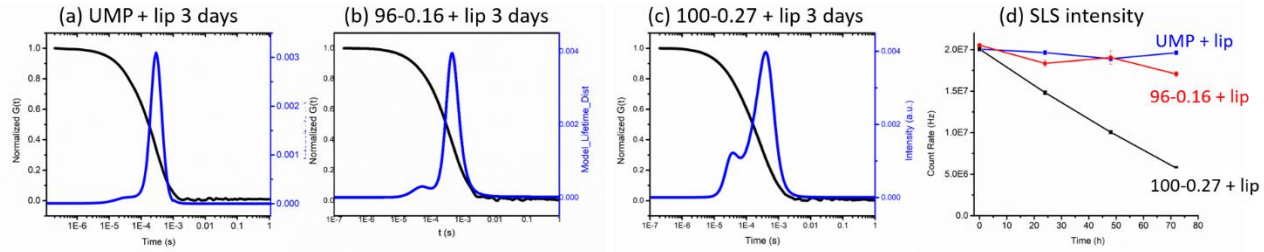

Figure 2.16. DLS G(t) and decay time distributions after incubating liposomes with HMPs having varying polymer hydrophobicity (De mol % = 0, 16 %, 27 %) over 3 days. The decay time distributions were analyzed using MEM analysis method.

information of resultant polymer and lipid complexes were summarized in Table S2.2. SLS experiments were conducted without stirring. Plot of SLS intensity versus time in Figure 2.16 (d) showed that the intensity of UMP 99-0.00 remained at ~ 2.0×10^7 over 3 days, revealing no significant fragmentation occurred in the presence of hydrophilic UMP 99-0.00. By contrast, the intensities of two HMP samples decrease over 3 days, and the intensity of 100-0.27+lip decreased more significantly from ~ 2.0×10^7 to ~ 5.0×10^6, relative to ~ 2.0×10^7 to 1.8×10^7 for 96-0.16+lip over the course of 3 days, further indicating that the more hydrophobic polymer 100-0.27 resulted in more effective liposome fragmentation relative to hydrophilic 96-0.16 polymers. The morphology of UMP and HMP lipid complexes were analyzed using cryo-TEM and negative stained TEM and the results of 100-0.27+lip and 96-0.16+lip were shown in Figure 2.13 (a)-(d) and (i)-(l) respectively. While hydrophobic 100-0.27 completely fragmented liposomes as shown in Figure 2.13 (a)-(d), residual liposomes were still present in sample 96-0.16+lip (Figure 2.13 (i)-(l)), indicating the incomplete liposome fragmentation by hydrophilic 96-0.16 polymer, which is consistent with the DLS and SLS results. Cryo-TEM and negatively stained TEM analysis of UMP and lipid complex (99-0.00+lip) (Figure S2.10) reveals the abundant presence of elongated liposomal structures instead of fragmented liposomes, which agrees with SLS results that unmodified polypeptoid cannot effectively induce liposome fragmentation.

Our combined experimental results indicate that the density of hydrophobic sidechains in HMPs as well as the chain length is important in their effectiveness (*i.e.*, extent and the rate of fragmentation) in inducing liposome fragmentation. The higher the density of hydrophobic sidechains on HMPs can presumably promote membrane deformation and instability by increasing local hydrophobic interaction with the lipid tails in the membrane. In addition, the liposome fragments can presumably be better stabilized by longer chain HMPs than the shorter ones due to reduced entropic penalty associated with the formation of HMP-lipid complexes for the former relative to the latter. This is also consistent with the MD simulation studies on mechanism of SMA copolymer induced membrane fragmentation,[2] the high local contacts between the hydrophobic groups in polymers and acyl chains in the lipid bilayer membranes are the key factor dominating the extent and rate of membrane fragmentation.

2.3 Conclusions

Hydrophobically modified polypeptoids (HMPs) with varying molecular characteristics have been designed and synthesized to fragment synthetic liposomes into nanoscale polymer/lipid complexes towards membrane protein extraction applications. The effects of polymer concentration, chain length, and relative hydrophobicity on liposome fragmentation have been elucidated by a combination of DLS, SLS and EM analysis. DLS and SLS results revealed that HMPs with relatively higher polymer hydrophobicity (De mol % = 27 %) and longer chain length (DP_n=100) can induce more effective liposome fragmentation relative to short polymers (DP_n = 34-60) and hydrophilic polymers with similar chain length (DP_n = 96 with De mol % = 16 %). The HMP induced liposome fragmentation was further investigated using cryo-TEM and negative stained TEM, which also supported that longer HMPs with higher hydrophobicity (100-0.27) can most effectively induce liposome fragmentation. It is hypothesized that a high local hydrophobic

contact between polymers and lipid membranes is critical to accelerate and enhance the extent of liposome fragmentation.

2.4 Future perspective

The combined experimental results demonstrated that the density of hydrophobic sidechains in HMPs as well as the chain length is important in the extent and the rate of liposome fragmentation. Molecular dynamics (MD) simulation study will be important towards understanding the molecular details regarding the roles of polymer chain lengths and the density of local hydrophobic contacts in liposome fragmentation, which represents an important aspect of future work.

While cryo-TEM revealed that HMPs can fragment liposomes to form HMP-and-lipids complexes with ~10 - 20 nm hydrodynamic diameter, the detailed structure of the complex is currently unknown. An important future work will be focused on structural elucidation of HMP-and-lipid complexes using scattering techniques (e.g., SAXS or SANS).

Finally, cryo-TEM studies have shown that the addition of HMP with optimized molecular characteristics (92-0.22) can fragment liposomes based on the Escherichia coli (*a.k.a.* E. Coli) lipid extract (Figure S2.11 (a)) into nanoscale polymer and E. Coli lipid complexes in Figure S2.11 (b). An important aspect of the future work will be focused on investigating the 92-0.22 polymer in the direct extraction of membrane proteins from E. Coli lysate.

2.5 References

1. Livesey, A. K.; Brochon, J. C., Analyzing the distribution of decay constants in pulse-fluorimetry using the maximum entropy method. *Biophysical journal* **1987,** *52* (5), 693-706.

2. Orekhov, P. S.; Bozdaganyan, M. E.; Voskoboynikova, N.; Mulkidjanian, A. Y.; Steinhoff, H.-J.; Shaitan, K. V., Styrene/Maleic Acid Copolymers Form SMALPs by Pulling Lipid Patches out of the Lipid Bilayer. *Langmuir* **2019,** *35* (10), 3748-3758.

CHAPTER 3. INVESTIGATION OF AMPHIPIHLIC POLYPEPTOIDS-FUNCTIONALIZED HALLOYSITE NANOTUBES AS PICKERING EMULSION STABILIZERS FOR OIL REMEDIATION

3.1 Introduction

Large scale oil spills (*e.g.*, Deepwater Horizon) have devastating impacts on the marine and coastal ecosystem (*i.e.*, aquatic species,[1,2,3] vegetation,[4] coastal human populations,[5] *etc.*). Bioremediation is a noninvasive and relatively cost-effective strategy for the oil-spill mitigation. This method relies on dispersants to emulsify the oil plume into discrete oil-in-water droplets formed by wave action.[10,11,12] The formation of oil droplets stimulates biodegradation by providing a larger oil-water interface to be accessed by alkane-degrading organisms.[6,7,8,9] Traditional dispersants consist of a mixture of amphiphilic anionic and non-ionic surfactants with organic solvents. For example, approximately 2.1 million gallons of chemical dispersants were applied for oil emulsification during the Deepwater Horizon oil spills in 2010.[13] The use of large amounts of surfactants and organic solvents has caused serious environmental concerns due to their potential toxicity.[34,35] For example, COREXIT EC 9500, Tween 20, sodium dodecyl sulfate and nonionic surfactant, have been demonstrated to have adverse effects on the population of *Alcanivorax borkumensis*, a dominant hydrocarbon-degrading bacteria in the microcosm that blooms in ocean after oil spills.[23,14,15,16]

Intense research efforts have been dedicated to the development of environmentally benign dispersant systems towards oil-spill remediation by investigating non-surfactant-based emulsion stabilizers and reducing or eliminating the usage of organic solvents.[17,18,19,62] Solid particles are

Chapter 3 is reprinted with permission Yu, T.; Swientoniewski, L.T.; Omarova**,** M.; Li, M.; Negulescu, I. I.; Jiang, N.; Darvish, O. A.; Panchal, A.; Blake, D. A.; Wu, Q.; Lvov, Y. M.; John, V.; Zhang, D. Investigation of Amphiphilic Polypeptoid- Functionalized Halloysites Nanotubes (HNTs) as Stabilizer towards Oil Spill Remediation. *ACS Appl. Mater. Interfaces,* **2019**, *11*, 27944-27953.

known to stabilize the emulsification by being adsorbed at the oil/water interface and creating steric or electrostatic barriers at the interface to impede the droplet coalescence.[20,21,22] Furthermore, in the case of oil spill remediation, it is advantageous that solid particles can stabilize oil-water interface at low particle concentration relative to the traditional surfactants, which may dynamically desorb from the interface at high dilution in the open ocean.[17]

A wide variety of solid particles have been investigated as stabilizers for the oil-in-water emulsion including silica,[24,29,36,61] graphene oxide,[18] carbon black,[17,25] iron oxide,[26,66] nanocrystals[27] and naturally occurring clay particles,[28,30,33,65] *etc.*. Halloysite clay nanotubes (HNTs) are naturally occurring aluminosilicate ($Al_2O_3 \cdot 2SiO_2 \cdot 2H_2O$) clay nanotubes with large specific area, tunable surface chemistry and high thermal and mechanical stabilities.[31,40,60,64] The unique tubular morphology with high aspect ratio is beneficial to the emulsion stability by increasing the detachment energy of particles from the oil-water interface.[32] However, the pristine HNTs are overly hydrophilic and thus cannot effectively stabilize oil-in-water (o/w) emulsions. This is similar to what has been observed for other hydrophilic clay particles. Surface modification is often required in order to control the hydrophilicity-lipophilicity balance (HLB) of the particle surfaces (*e.g.*, silica,[36,37,38,51] graphene oxide,[18] iron oxide,[26,66] carbon black,[39,17] and other clay particles)[19,28,32,63-65] rendering them more effective as oil-in-water emulsion stabilizers. The outer surface of HNTs possesses suitable functional groups (*e.g.*, silanol) which allow for facile chemical modification. In addition, HNTs can be produced in large quantities at relatively low cost, further enhancing their appeal as emulsion stabilizers for oil spill remediation.[41]

Polypeptoids are an emerging class of peptidomimetic polymers that feature *N*-substituted polyglycine backbone.[42,43] Synthesis of well-defined polypeptoids with controlled molecular weight and narrow molecular weight distribution has been developed in the last decade.[42,43]

Previous studies show that polypeptoids are cytocompatible,[47] oxidatively degradable,[48] having tunable HLB characteristics by changing the *N*-substituent structure, and interfacially active in reducing the air-water surface tension.[49] The combination of these favorable attributes make polypeptoid highly promising as polymeric surfactants for o/w emulsion.

In this contribution, we investigated the functionalization of HNTs with amphiphilic polypeptoids and characterized the physical properties of resulting functionalized HNTs that are important for understanding their performance as o/w emulsion stabilizers towards oil spill remediation. Specifically, functionalization of HNTs with amphiphilic polypeptoids was successfully achieved by a surface-initiated ring-opening polymerization method. The functionalized HNTs were found to stabilize the o/w emulsion to varying extent, which is strongly influenced by the HLB characteristics of the grafted polypeptoids. A combination of interfacial tension, contact angle, rheological and microscopic measurements have revealed that functionalization of HNTs with polypeptoids having appropriate hydrophobic content can effectively lower the interfacial tension, enhance the thermodynamic propensity of HNTs to partition at the oil/water interface and increase the emulsion viscosity relative to the pristine HNTs, resulting in more stable o/w emulsions. Cell culture studies have shown that polypeptoid-functionalized HNTs are non-cytotoxic towards *Alcanivorax borkumensis*, the dominant alkane degrading bacterium in the ocean after crude oil-spill. Notably, the functionalized HNTs with higher hydrophobic polypeptoid content (HLB= 12.0-14.3) was found to induce more cell proliferation than those that are less hydrophobic or the pristine HNTs.

3.2 Experimental

3.2.1 General consideration

Halloysite nanotubes were purchased from Applied Minerals Inc., U.S.A. and were first dried at 80 °C under vacuum (30 Hg) overnight and stored in desiccator before use. (3-Aminopropyl) triethoxysilane (APTES) was purchased from Sigma-Aldrich and stored under nitrogen atmosphere after distillation. *Alcanivorax borkumensis* (ATTC-700651^{TM}) was purchased from the American Type Culture Collection, and the freeze-dried cultures were reconstituted according to ATTC instructions using Difco Marine Broth. Agar and fluorescent assay plates (96-well, black, flat bottom, non-treated, polystyrene) purchased from Fisher Scientific. All other chemicals used were purchased from Sigma-Aldrich and used as received unless otherwise noted. All solvents used (*e.g.*, toluene, dichloromethane (DCM), hexanes, and acetonitrile (CH_3CN) were purchased from Sigma-Aldrich with HPLC grades and purified with alumina columns under argon. All *N*-substituted *N*-carboxyanhydride monomers (*i.e.*, Me-NCA, Bu-NCA and De-NCA) were synthesized by adapting a reported procedure.[68] ^{1}H NMR analysis was performed on Bruker AVIII-400, a 400 MHz spectrometer and the chemical shifts in parts per million (ppm) were referenced to the proton impurities of $CDCl_3$. FTIR spectra were collected on a Bruker Alpha FT-IR spectrometer. Samples of varying polypeptoids-grafted-HNTs and p-HNTs were grinded into fine powders before measurement. The sample powders were packed into a firm layer on the diamond crystal with the equipped stainless steel plunger to ensure the good contact with the crystal surface. Spectrum were collected in the range of 4000-400 cm^{-1}. The spectral resolution was set at 4 $cm^{-1}$and the number of scan for both background and sample scans were set as 64. Thermogravimetric analysis (TGA) was performed with ~5 mg of pristine or polymer-grafted HNTs on TA 2950 under nitrogen at a heating rate of 10 °C min^{-1} in the 25 – 600 °C range.

3.2.2 Synthesis of polypeptoid-grafted HNTs

Surface functionalize p-HNTs with (3-aminopropyl) triethoxysilane (APTES) has been adapted to the reported procedure to obtain amino group functionalized HNTs (HNT-NH2).[68] Functionalization of HNTs with amphiphilic polypeptoids were achieved by amine-initiated ring-opening polymerization of the corresponding N-substituted glycine-derived N-carboxyanydride monomers (R-NCAs). A representative procedure for the synthesis of copolypeptoids-grafted-HNTs, $M_{90}B_{10}$-g-HNTs, was presented. In the glovebox, the initiator functionalized HNTs (HNTs-NH_2) (200 mg, 0.68 mmol, 0.09 M) was dissolved in anhydrous dichloromethane (DCM) in a 20 ml scintillation vial. The vial which was capped and parafilmed was then transferred out of the box and sonicated in a sonication bath (Branson 2510 Ultrasonic Cleaner) for 10 min until the particles were fully dispersed and the vial was moved back into the glovebox after sonication. Bu-NCA (27 mg, 0.17 mmol, $[M_2]_0$ = 0.02 M) and Me-NCA (176 mg, 1.53 mmol, $[M_1]_0$ = 0.20 M) were added into the above particle suspension and allowed to stir and mix at 350 rpm at room temperature for 10 min. Then the reaction mixture was heated at 50 °C and stirred at 350 rpm for 72 h. The $M_{90}B_{10}$-g-HNTs particles were precipitated out and collected by centrifuging at 2000 rpm for 10 min and the product were washed with ample DCM until no monomer or random polymer peaks were observed from ^{1}H NMR followed by drying under vacuum (232 mg, 70.1%).

3.2.3 Surface tension measurement

Surface tensions between dodecane and particle aqueous stock solution were measured by the pendant drop method using a standard goniometer (Rame-Hart, model 250). Varying polypeptoids-grafted HNTs and p-HNTs were prepared into 0.5 wt % of stock solutions in artificial sea water (ASW) by sonicating in a sonication bath (Branson 2510 Ultrasonic Cleaner) for 10 min till all the particles were fully dispersed and the samples were then left stirring at 350 rpm for

overnight. A 15 µl of the particle stock solutions were injected into 10 ml of an external n-dodecane phase. The interfacial tension was obtained by analyzing the curvature of the droplet with the DROPimage Advanced Software. Data points were collected every 120 s for 30 min to achieve equilibrium and the data between 12 and 30 min was used in the calculation of the equilibrium interfacial tension. Three independent measurements were performed for each sample and the mean of the triplicate were recorded and plotted versus time in Figure 3.3A and the error bars were generated from the standard deviation of the triplicate measurements.

3.2.4 Three phase contact angle measurement

Three-phase contact angle between *n*-dodecane, ASW and various polypeptoid-grafted HNTs by the compressed disc method using a standard Rame-Hart model 250 goniometer. Around 0.15 g of varying polypeptoid-g-HNTs were compressed into a 20 mm diameter disc with 30 MPa pressure using the Riken high pressure hydraulic equipment for 2 min. The disc was then put into a cuvette cell filled with n-dodecane and 5 µl of artificial sea water (ASW) was placed onto the artificial surface of HNTs substrate with a 21 gauge needle and the three phase contact angle at n-dodecane, ASW and the particle interface was measured at 25°C every 1s, using a drop shape analyzer until the contact angle becomes stabilized. Two independent measurements were carried out for each sample and the mean of the doublet were calculated and recorded.

3.2.5 Steady shear viscosity measurement

The steady shear viscosity experiments were performed with a AR 2000ex Rheometer (TA Instruments Inc.) using a cone-plate geometry (40 mm diameter and 2° cone angle). About 0.6 ml of the emulsion sample was added onto the plate and the gap between cone and plate was set at 52 µm for all the sample measurements. The steady shear viscosity for emulsions stabilized by varying polypeptoid-grafted HNTs (g-HNTs) or pristine HNTs (p-HNTs) were measured under a

steady shear flow with increasing the shear rate successively from ~ 1×10^{-4} to 10.0 s^{-1} at 25 °C. The equilibrium time required to reach steady state between each rate change was set at 60 s for all the samples.

3.2.6 Assessment of emulsion stability by optical microscopy

The mean diameters (D) of the oil droplets in particle stabilized o/w emulsions were characterized by Leica DM6 B upright microscope equipped with Hamamatsu sCMOS camera and LAS X software**.** For each sample, the sizes of at least 200 droplets were analyzed by image J software to obtain the mean diameter (D). The droplets sizes were re-measured again after left the emulsion staying at room temperature for 7 days.

Assessment of Emulsion Stability by Emulsion Index Measurement. All the emulsions generated were separated into a top emulsion layer and a bottom serum layer due to gravitational separation instantly after preparation by vortex. Emulsion Index (EI) is defined as the ratio of the height (E_e) of the top emulsion layer versus the height (E_t) of the total liquid column. The height was measured with a metric ruler (mm) at designated time and three independent measurements were performed at each time point and the mean of the triplicate were recorded. Error bars were generated from the standard deviation of each triplicate. The calculated EI results were plotted versus time in Figure S3.3.

3.2.7 Sample preparation for TEM analysis

TEM analysis were conducted on a JEM-1400 TEM with operating voltage of 80 kV and the images were analyzed with FEI Digital Micrograph software. A stock solution of p-HNTs or g-HNTs in ethanol (0.5 wt %) was prepared by sonicating in a sonication bath (Branson 2510 Ultrasonic Cleaner) for 10 min. A small volume of the stock solution (~5 µl) was added onto a

carbon coated 300 mesh copper grid and blotted with a filter paper. The grid was allowed to dry overnight at room temperature before analysis.

3.2.8 Sample preparation for cryo-TEM analysis

A stock solution of p-HNTs or g-HNTs in ASW (0.5 wt %) was prepared by sonicating for 10 min until all the particles are fully dispersed. A small volume of the stock solution (~5 μL) was added onto a lacey carbon-coated 300 mesh copper TEM grid. FEI Vitrobot was applied for blotting both side of the grid for 1 s, resulting in a thin film remaining on the grid. The grid was then plunged into liquid ethane chilled by liquid nitrogen and transferred into the sample holder for imaging.

3.2.9 Sample preparation for cryo-SEM analysis.

A 10 μl of oil-in-ASW emulsion containing p-HNTs or g-HNTs was loaded on the rivet mounted sample holder followed by plunging into liquid nitrogen to quickly freeze the sample. A flat-edge cold knife was used to fracture the droplet at -130 ℃. After subliming the solvent at about -90 ℃ for 15 min, the system was cooled back down to -130 ℃. The sample was then sputter coated with gold-palladium nano-composite for 120 s at 10 mA to deposit a conductive thin layer on the surface of the sample before imaging analysis.

3.2.10 Cleaving polymer off HNT surface by HF treatment

Hydrofluoric acid (HF) was used to cleave the polymer off the surface of polypeptoid-grafted HNTs. Polymer-grafted HNTs (55.0 mg) were fully dispersed in DMF/H2O (1:1, v:v) (3 ml) by magnetically stirring at 350 rpm for 30 min followed by addition of hydrofluoric acid (HF) aqueous solution (1 ml, 48 wt %). The reaction was allowed to proceed at room temperature for 6 hours with stirring and then neutralized to pH = 7 with the addition of NaOH aqueous solution (1.0 M) in ice bath. The solution was extracted with DCM (3 ml) twice. The organic layers were

separated and the volatile was removed using rotovap to afford the final polymers (10.0 - 17.9 mg, 75.4-100 % recovery yield). For example, the recovery yield for the M90D10-grafted HNTs is calculated as followed. Yield = the mass of the recovered polymers / (the mass of the polymer-grafted HNTs prior to HF treatment × weight percentage of the polymer grafted onto the HNTs based on TGA analysis) = 10.0 mg / (55.0 mg × 24.1 wt %) × 100% = 75.4 wt %.

Cell Culture Study. A liquid inoculum was prepared by culturing A. borkumensis in modified ONR7a supplemented with 1% hexadecane to an OD600 of approximately 0.600. Anadarko crude oil was thrice filtered before use. Growth studies were performed in sterilized 125 ml Erlenmeyer flasks in which 300 μL of Anadarko crude oil was added to 1.2 ml of a 5 mg/ml HNT stock solution in ONR7a and each flask was stirred for 10 seconds to generate Pickering emulsions. The solution was then scale up to 30 ml with modified ONR7a to yield concentration of HNTs in the culture flask of 0.2 mg/ml (0.02% w/v) followed by the addition of 300 μL aliquot of the A. borkumensis inoculum. Culture flasks were incubated in dark at 30oC for 48 hours with shaking at 150 rpm. At each designated time point, 1 mlof sample was transferred to an Eppendorf tube and stored at 4oC until the time course was complete. The pH of each harvested sample was also measured using a pH meter.

3.2.11 Resazurin assay

For the resazurin assay,[69] samples were removed from 4^{o}C environment and allowed to warm to room temperature. 100 μl of resazurin solution (0.1 mg/ml in dH_2O) was added to each sample and fully mixed. Samples were incubated for 20 min at room temperature in the dark to allow the cells to metabolize the resazurin into the fluorescent product, resorufin. After incubation, each sample was filtered with 0.22 μm sterile filter to remove the HNTs and cells. The sample was allowed to sit for 10 min in the dark to allow the oil layer to separate. This layer was subsequently

removed by carefully pipetting the top of each sample. Samples were transferred to a black 96-well plate with twice dilution with modified ONR7a. The plates were read on a fluorometer (BioTek Instruments, Inc., SynergyTM 2 Multi-Detection Microplate Reader) coupled with Gen5TM Reader Control and Data Analysis Software for data collection. The fluorescence was plotted versus dilution at each time point and a best-fit linear equation was generated using GraphPad Prism 6.0. The slopes of these lines were plotted versus time after inoculation to generate the growth curves.

3.3 Results and discussion

3.3.1 Synthesis and characterizations of polypeptoid-grafted halloysite nanotubes (g-HNTs)

Functionalization of HNTs with amphiphilic polypeptoids was achieved via the "graft-from" method. Specifically, the exterior surface of pristine HNTs (p-HNTs) was first functionalized with amino groups by treatment with (3-aminopropyl) triethoxysilane (APTES).[50] The amino-functionalized HNTs (HNTs-NH_2) were then used as initiators for the ring-opening polymerization of *N*-substituted glycine-derived *N*-carboxyanhydrides (R-NCAs, R = Me, Bu, De) in varying initial monomer feed ratio (*i.e.*, $[Me]_0$:$[Bu]_0$ or $[Me]_0$:$[De]_0$ = 90:10 and 80:20), thereby producing the corresponding poly(*N*-methyl glycine) (M_x) homopolymer, poly(*N*-methyl glycine)-*r*-poly(*N*-butyl glycine) (M_xB_y) and poly(*N*-methyl glycine)-*r*-poly(*N*-decyl glycine) (M_xD_y) random copolymer-grafted HNTs (Figure 3.1A) (Note: x and y signify the initial percentage molar fraction of hydrophilic (Me-NCA) and hydrophobic (Bu-NCA or De-NCA) monomers used in the polymerization, respectively). M_{100} homopolymer is highly hydrophilic with good water solubility. The M_xB_y or M_xD_y copolymers are expected to be more hydrophobic as the content of the hydrophobic segments (B or D) increases relative to the M segment. In this study, the initial molar ratio of the monomer relative to HNTs-NH_2 (f= $[M]_0$:$[HNTs\text{-}NH_2]_0$) was kept

constant at 2.5 for the synthesis of both homo- and copolypeptoids-grafted HNTs. All polymerizations were conducted in anhydrous dichloromethane (DCM) at 50 ˚C for 72 h with a stirring rate at 300 rpm and the polypeptoid-grafted HNTs (g-HNTs) were isolated by trice washing with DCM to remove any unreacted monomers, which was verified by ^{1}H NMR analysis of the washing.

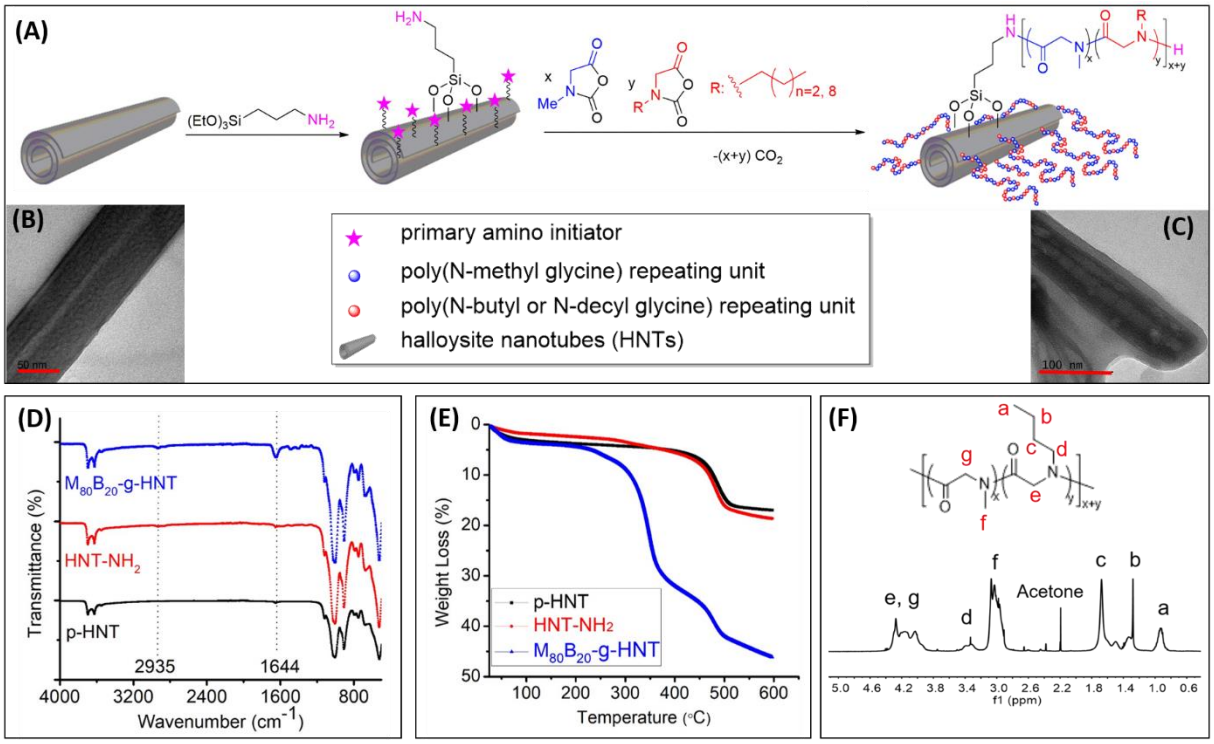

Figure 3.1. (A) Schematics showing the functionalization of HNTs with amphiphilic polypeptoids by the surface-initiated polymerization method; (B) Representative TEM images of p-HNTs and (C) M80B20-g-HNTs in the dry state. The scale bar in (B) and (C) is 50 nm and 100 nm, respectively. (D) FT-IR spectra and (E) Thermograms of pristine HNTs (p-HNT), initiator anchored-HNT (HNTs-NH2) and representative polypeptoid-grafted HNTs (M80B20-g-HNTs) obtained by TGA. FT-IR spectra were vertically shifted for clarify. (F) Representative 1H-NMR spectrum of polypeptoid polymers that were cleaved off from the M80B20-g-HNTs by HF treatment. Detailed chemical shift and integration information were shown in Figure S3.5.

FT-IR spectroscopic analysis of polypeptoid-grafted HNTs in comparison to p-HNTs and initiator anchored-HNTs (*i.e.*, HNTs-NH_2) (Figure 3.1D and Figure S3.1) has revealed the successful grafting of polypeptoids to the HNTs, evidenced by the emergence of 1644 cm^{-1} and 2935 cm^{-1} that are characteristics of the amide and C-H stretching bands of polypeptoids,

respectively. By contrast, these peaks are notably absent for the pristine HNTs (p-HNTs) in the corresponding spectral region. Thermogravimetric analysis (TGA) was also conducted to quantify the extent of polymer grafting on the HNTs (Figure 3.1E and S2-S3). All polypeptoid-grafted HNTs were shown to undergo two-stage decomposition in the 25-600 °C range with the most rapid

Table 3.1. Molecular characteristics of amphiphilic polypeptoids that were grafted onto HNTs by the surface-initiated polymerization method.

Entry #	Grafted Polypeptoids ($M_x(B/D)_y$) [a]	x:y (Theo.) [b]	x:y (Exptl.)[c]	HLB (Exptl.) [d]
1	M_{100}	N/A	N/A	20.0
2	$M_{90}B_{10}$	9.00	9.71	17.2
3	$M_{80}B_{20}$	4.00	4.00	14.3
4	$M_{90}D_{10}$	9.00	8.38	15.0
5	$M_{80}D_{20}$	4.00	4.17	12.0

[a.] Mx signifies the hydrophilic segment poly(N-methyl glycine). By and Dy signify the hydrophobic segment, poly(N-butyl glycine and poly(N-decyl glycine), respectively. The numbers in subscript correspond to the initial molar percentage of the respective monomer. b. x:y (Theo.) corresponds to the initial molar ratio of the hydrophilic and hydrophobic monomers in the polymerization. c. x:y (Exptl.) indicates the experimental molar ratio between the hydrophilic (M) and hydrophobic segment (B or D) in the grafted polypeptoids determined by 1H NMR analysis of the polymers cleaved from the g-HNTs. d. HLB (Exptl.) is the experimental HLB characteristic of the grafted polypeptoids. It is defined as the mass fraction of the hydrophilic segments (M) over the entire polymer [HLB = 20 × (mx/mx+ my), mx: mass of hydrophilic segment (M), mx+my: total mass of both the hydrophilic (M) and hydrophobic (B or D) segments] and is calculated using the molar ratio between the M and B(D) segments determined by 1H NMR analysis.

weight loss temperature at ~ 350 ºC, which corresponds well to the reported decomposition temperature (T_d) of free poly(*N*-alkyl glycine) polymers.[53,67] An increased percentage weight loss from 17.0 wt % for pristine HNTs to 41.1 − 46.2 wt % for various polypeptoid-grafted HNTs was

also observed (Figure S3.2), corresponding to polymer grafting content in the 24.1-29.2 wt% range for the respective polypeptoid-grafted HNTs. In addition, the polymer grafting content can be controlled by adjusting the initial monomer-to-HNTs-NH_2 feed ratio. For example, TGA revealed an increase of percentage weight loss from 46.0 wt % to 57.7 wt % for the poly(*N*-methyl glycine) grafted-HNTs, as the feed ratio is increased from 2.5 to 5 during the synthesis (Figure S3.3).

To further characterize the molecular structure of the grafted polypeptoids, the polypeptoid-grafted HNTs were treated with hydrofluoric acid (HF) to enable the cleavage of the polypeptoids from the HNT. The polymer recovery yield is in the 75 ~100 % range for all samples. Representative ^{1}H NMR spectroscopic analysis of the cleaved polymers ($M_{80}B_{20}$) has confirmed the successful formation of the corresponding copolypeptoids (Figure 3.1F and Figure S3.5). In addition, the relative molar content of the hydrophilic (M) and hydrophobic segments (B or D) on the grafted copolypeptoids agree well with the initial monomer feed ratio (Table 1). As the end-group structures were not readily discernable in the ^{1}H NMR spectra, the absolute molecular weight of the grafted copolypeptoids cannot be determined.

The HLB parameter of grafted polypeptoids is defined as the mass fraction of hydrophilic segments over the entire polymer (HLB = 20× w_h/w, w_h: mass of hydrophilic portion, w: mass of whole polymer, 20 is an arbitrary scaling factor)[52,44,45] and have been calculated using the experimentally determined molar ratio of the M and B(D) segments (Table 3.1). All grafted polypeptoids in this study have HLBs in the 12.0-20.0 range (Table 3.1). A higher HLB value indicates a more hydrophilic polymer and vice versa. For example, poly(*N*-methyl glycine) homopolymer, the most hydrophilic polypeptoid used in this study, has a HLB of 20. In addition, the 3-phase contact angle measurements between *n*-dodecane, artificial sea water (ASW) and various polypeptoid-grafted HNTs (Figure S3.6-S3.7) are consistent with the HLB parameters that

were calculated using the chemical composition of the corresponding polypeptoids. A more hydrophilic polypeptoid was found to correlate to a higher HLB value and a smaller contact angle and vice versa (Figure S3.7).

The morphology of pristine HNTs (p-HNTs) and polypeptoid-grafted HNTs (g-HNTs) in dry state or in solution has been analyzed by transmission electron microscopy (TEM) and cryogenic transmission microscopy (cryo-TEM). Here, $M_{90}B_{10}$-g-HNTs are shown as representative for polymer-grafted HNTs. In contrast to pristine HNTs showing a smooth external surface (Figure 3.1B), both TEM (Figure 3.1C and Figure S3.8) and cryo-TEM (Figure S3.9) analysis of M90B10-g-HNTs sample has revealed a low electron density layer with thickness in the 10 – 40 nm range on the external surface of the HNTs. This is consistent with the successful grafting of polymers on the HNTs by the surface-initiated polymerization method. HR-TEM energy-dispersive X-ray spectroscopy (EDS) analysis of various polypeptoid-grafted HNTs also revealed the emergence of N atom signals and an increased relative atomic content of C and O atom relative to the pristine HNTs, further supporting the successful grafting of polypeptoids onto the HNT surface (Figure S3.4).

3.3.2 Oil-in-water emulsion stability in the presence of polypeptoid-grafted HNTs

To assess the effect of polypeptoid-grafted HNTs (g-HNTs) on the o/w emulsion stability, emulsions of *n*-dodecane in artificial sea water (ASW, 35 g/L NaCl) in the presence of g-HNTs were prepared as followed. Briefly, a suspension of g-HNT (0.5 wt %) was first obtained by dispersing HNTs in the saline water and sonicated in a sonication bath (Branson 2510 Ultrasonic Cleaner) for 10 min at room temperature. *n*-Dodecane was then added into the above saline suspension in a 1:3 (v:v) *n*-dodecane-to-saline water ratio under magnetic stirring at 350 rpm

followed by vortex mixing for 5 min on a Thermolyne Maxi mix II operating at 3000 rpm. The oil-in-water emulsions with pristine-HNTs (p-HNTs) were similarly prepared for comparison.

The emulsion stability was first assessed by measuring the emulsion index (EI) over a period of 14 days at 25 °C. Emulsion index is defined as the ratio of the height (E_e) of the top emulsion layer due to gravitational separation versus the height (E_t) of the total water column.[54] As shown in Figure S3.10, there is no significant change of EI for the emulsions containing the more hydrophobic copolypeptoid-grafted HNTs (*i.e.*, $M_{90}D_{10}$-g-HNTs, $M_{80}B_{20}$-g-HNTs and $M_{80}D_{20}$-g-HNTs), indicating the formation of highly stable emulsions. By contrast, the EI for the emulsions containing the more hydrophilic polypeptoid-grafted HNTs (*i.e.*, M_{100}-g-HNTs and $M_{90}B_{10}$-g-HNTs) decreases significantly from 0.4-0.5 to 0.2-0.3 over the course of 14 days, indicating instability of these emulsions.

The mean diameter (D) of the oil droplets in these freshly prepared emulsions was further characterized by optical microscopic analysis (Figure3.2). The emulsions containing the copolymer-grafted HNTs (*i.e.*, $M_{90}D_{10}$-g-HNTs, $M_{80}B_{20}$-g-HNTs and $M_{80}D_{20}$-g-HNTs) exhibit much smaller mean diameters of the oil droplets (D = 80 ± 20 μm, 90 ± 50 μm or 110 ± 40 μm, respectively) than those with the p-HNTs (D > 500 μm) or homo-polypeptoid (M_{100})-grafted HNTs (D = 180 ± 70 μm). In addition, the size of oil droplets in emulsions containing these copolypeptoid-grafted HNTs is more uniform relative to those with pristine HNTs or homo-polypeptoid-grafted HNTs. Based on these observations, we concluded the use of copolypeptoid-grafted HNTs can more effectively induce the formation of smaller oil droplets relative to the homo-polypeptoid-grafted HNTs or pristine HNTs.

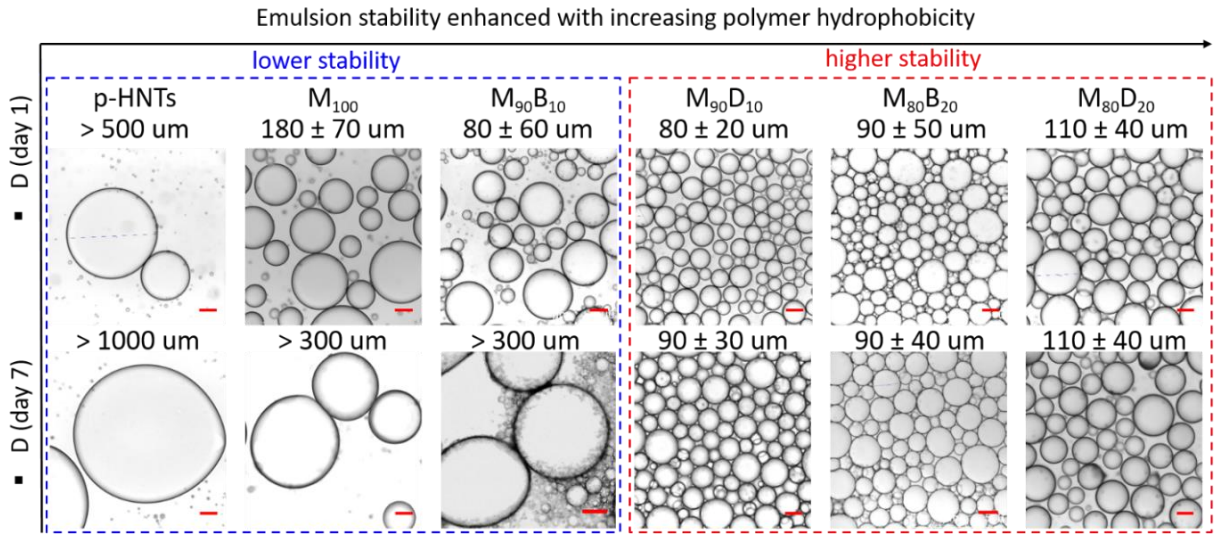

Figure 3.2. Optical microscopy images of *n*-dodecane-in-ASW emulsions in the presence of various polypeptoid-grafted HNTs. The g-HNTs concentrations are 0.5 wt % and the mean diameter (D) ± SD of oil droplets at day 1 and day 7 were measured. The more hydrophobic copolypeptoid ($M_{90}D_{10}$, $M_{80}B_{20}$ or $M_{80}D_{20}$)-grafted HNTs induce smaller oil droplets relative to the homo-polypeptoid (M_{100})-grafted HNTs or pristine HNTs. Scale bar is 100 µm.

To investigate the effect of various HNTs on the emulsion stability over time, the oil droplet sizes in the above emulsions were re-analyzed using optical microscope after 7 days. It was found that the mean diameter of oil droplets in emulsions having p-HNTs, M_{100}-g-HNTs and $M_{90}B_{10}$-g-HNTs increase dramatically to >300 µm after 7 days (Figure 3.2). By contrast, for the three emulsions containing more hydrophobic copolypeptoid-grafted HNTs, *i.e.*, $M_{90}D_{10}$-g-HNTs, $M_{80}D_{20}$-g-HNTs and $M_{80}B_{20}$-g-HNTs, the mean diameters of oil droplets remain nearly unchanged. This indicates that the hydrophobic copolypeptoid-grafted HNTs are more effective in inhibiting the coalescence of oil droplets than the homo-polypeptoid-grafted HNTs or pristine HNTs, resulting in more stable o/w emulsions. This is consistent with the relative stabilities of the emulsions determined by the EI method. These combined results clearly indicate that functionalization of HNTs with amphiphilic polypeptoids having appropriate HLB characteristics

(HLB = 12.0-15.0) is effective in enhancing the performance of HNTs as oil-in-ASW emulsion stabilizers.

Cryo-SEM analysis of the emulsions stabilized by $M_{90}D_{10}$-g-HNTs (e-h, Figure S3.11) or p-HNTs (a-d, Figure S3.11) has revealed that the oil/water interfaces were covered with flocculated HNT particle networks. Polypeptoid-functionalized HNTs were found to form a more extended and interconnected network at the o/w interface (h, Figure S3.11) as compared to the p-HNTs (d, Figure S3.11) presumably owing to enhanced interparticle interactions by polymer functionalization.

3.3.3 Effects of polypeptoid functionalization on O/W interfacial tension

One factor that may influence the above oil-in-ASW emulsion stability is the change of interfacial tension in the presence of different polypeptoid-grafted HNTs. In traditional emulsions, surfactants enhance emulsion stability mainly by reducing the oil-water interfacial tension. By

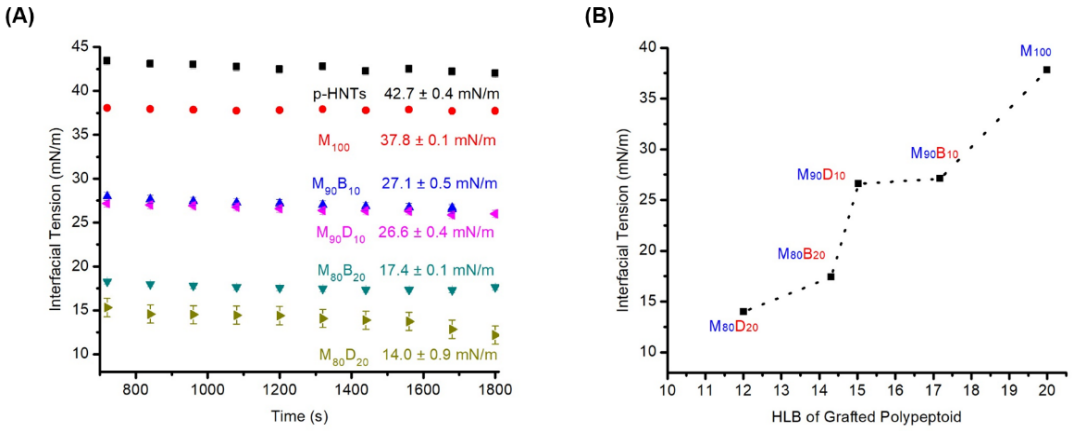

Figure 3.3. (A) Plot of interfacial tension at the n-dodecane/ASW interface in the presence of different polypeptoid-grafted HNTs versus time. The interfacial tension was measured every 120 s for 30 min till equilibrium was reached. The data between 12 and 30 min was used in the calculation of the equilibrium interfacial tension. The results clearly indicate that functionalization of HNTs with amphiphilic polypeptoids can reduce the interfacial tension between n-dodecane and ASW. (B) Plot of interfacial tension versus the experimental HLB characteristic of polypeptoids that were grafted on HNTs (Table 3.1). Decreasing HLB characteristic of the grafted polypeptoids was found to be correlated with reduced interfacial intension, contributing to the enhanced emulsion stability.

contrast, for emulsions stabilized by solid particles (a.k.a. Pickering emulsion), the interfacial tension does not decrease significantly in the presence of solid particles.55 To understand the mechanism of emulsion stabilization by grafted-HNTs, we characterize the dynamic interfacial tension at n-dodecane-ASW interface in the presence of different grafted-HNTs (g-HNTs) or pristine HNTs (p-HNTs) by pendant drop tensiometry.

As shown in Figure 3.3A, the average interfacial tension measured in the presence of pristine HNTs (p-HNTs) (42.7 ± 0.4 mN/m) is comparable to that without any stabilizers (44.5 ± 0.2 mN/m), suggesting that p-HNTs are limited in reducing the interfacial tension. By comparison, the interfacial tension was found to decrease in the presence of polypeptoid-grafted HNTs (g-HNTs). In addition, the interfacial tension appears to be correlated with the HLB characteristics of the grafted polypeptoids. As the HLB decreases from 20.0 (M_{100}-g-HNTs) to 17.2-15.0 ($M_{90}B_{10}$- or $M_{90}D_{10}$-g-HNTs) and 14.3-12.0 ($M_{80}B_{20}$- or $M_{80}D_{20}$-g-HNTs) (Table 3.1), the interfacial tension decreases steadily from ~38 to ~27 and then ~17-14 mN/m (Figure 3.3A). These results clearly indicate that the functionalization of HNTs with amphiphilic polypeptoids with appropriate HLB characteristics can significantly reduce the interfacial tension between *n*-dodecane and ASW, and the extent of reduction in the interfacial tensions can be controlled by tuning the chemical composition of the grafted polypeptoids on HNTs (Figure 3.3B). Furthermore, it appears that the reduction of interfacial tension correlates with an enhancement of emulsion stability except for the emulsion containing $M_{90}B_{10}$-g-HNTs. The emulsion with $M_{90}B_{10}$-g-HNTs was found to become unstable overtime in contrast to that containing $M_{90}D_{10}$-g-HNTs, which has remained stable over time (Figure 3.2). Yet, the interfacial tensions for these two emulsions are comparable (~27 mN/m, Figure 3.3). This clearly suggests that there are other factors in addition to the interfacial tension that contribute to the observed relative o/w emulsion stability.

3.3.4 Effects of polypeptoid functionalization on particle desorption energy

In addition to change the interfacial tension in oil-water emulsion, the detachment energy of solid particles positioning at o/w interface can also contribute to the emulsion stability.[21] When dispersed in a two-phase system, particles prefer to partition at the interface. The desorption energy (ΔG) is defined as the free energy change upon removing particles from the oil/water interface into bulk water phase. The higher the desorption energy is, the more stable the particles are at the interface. This reduces droplet coalescence and enhances the emulsion stability. Particle shape, size and surface chemistry all influence the strength of the desorption energy. Since HNTs can be approximated as cylindrical particles, for oil-in-water emulsion stabilized with cylindrical particles, the desorption energy can be estimated using equation 1 (eq. 1) where r, L, γ_{ow} and θ stand for the cross-section radius and contour length of the cylindrical particle, the oil-water interfacial tension and the three-phase contact angel, respectively.[56,57]

$$\Delta G = 2rL\gamma_{ow}[\sin\theta - \theta cos\theta\left(1+\frac{r}{L}\right)+\frac{r\cos^{2}\theta\sin\theta}{L}] \text{ for } 0^\circ \leq \theta \leq 180^\circ \text{ (eq. 3.1)}$$

Based on TEM analysis of p-HNTs, the average contour length (L) and cross-section radius (r) of HNTs were found to be ~1 μm and ~50 nm, respectively. *n*-Dodecane−ASW interfacial tension was experimentally determined to be 44.5 mN/m^2. Based on these parameters, the dependence of desorption energy of HNT particles on the three-phase contact angle, an indicator of HNT surface wettability, can be theoretically assessed. The plot of theoretical desorption energy (ΔG) versus the three-phase contact angle (θ) (Figure 3.4A) has revealed an initial increase of ΔG in the 0-70° range followed by a decrease of ΔG in the 70-180° range. This clearly indicates that highest desorption energy can be obtained by modification of the surface chemistry of HNT particles to achieve intermediate wettability.

To further assess the detachment energy of the polypeptoid-grafted HNT particles, we have measured the three-phase contact angle between *n*-dodecane, ASW and various polypeptoid-grafted HNTs by the compressed disc method using a standard Rame-Hart model 250 goniometer. As shown in Figure S3.6, the contact angle of p-HNTs was found to be rather small (~10˚), consistent with the surface of p-HNTs being highly hydrophilic. The contact angle was found to increase upon functionalization of polypeptoids. Specifically, the contact angles increased steadily from 42 ± 5° to 146 ± 1° as the hydrophobic content of the polypeptoids was increased (or the HLB parameter of polypeptoids was decreased) (Figure S3.7). This result clearly indicates that the wettability of HNT surface at the oil/water interface can be effectively controlled via the grafting of polypeptoids with varying HLB characteristics. As the grafted polypeptoids become increasingly hydrophobic, the wettability of HNT decreases accordingly.

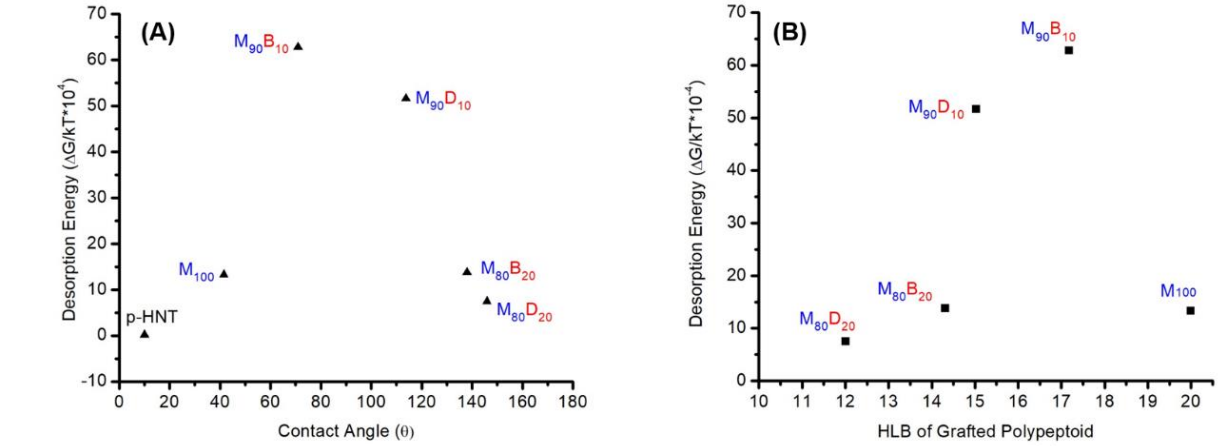

Figure 3.4. (A) Plot of theoretical desorption energy of various HNTs with or without polypeptoids grafting versus three-phase contact angle (θ) (▲). The HNTs are approximated as cylindrical particles having a length-to-radius ratio (L/r) of 20.0 (L= ~1 μm and r= ~50 nm) in the calculation of desorption energy using eq. 1. (B) Plot of the desorption energy versus the HLB parameter of grafted polypeptoids. HNT particles functionalized with copolypeptoids having intermediate HLB characteristics (M90B10 and M90D10) afforded the largest detachment energies.

Using the experimentally determined three-phase contact angle, the desorption energy of g-HNTs that were grafted with different polypeptoids in *n*-dodecane-ASW emulsion have been estimated using eq. 1 (Figure 3.4A). It is found that functionalization of HNTs with polypeptoids has increased the desorption energy of HNT particles to varying degree, relative to that of the pristine HNTs in the *n*-dodecane-ASW emulsion. In particular, HNTs that were grafted with copolypeptoids having an intermediate HLB (*i.e.*, $M_{90}B_{10}$, HLB= 17.2; $M_{90}D_{10}$, HLB=15.0) exhibited the largest desorption energy ($\Delta G = 6.28 \times 10^5$ kT and 5.16×10^5 kT) among all samples, which is 26 times higher than that of the pristine HNTs and 4 times higher than hydrophilic homopolypeptoid (M_{100}-g-HNTs) (Figure 3.4B). While functionalization of HNTs with amphiphilic polypeptoids enhances the thermodynamic propensity of g-HNTs to partition at the oil-water interface, thus contributing to the enhanced stability of the o/w emulsion, the relative strength of the detachment energy of g-HNTs is not well correlated with the relative emulsion stability that was experimentally observed. For example, while the desorption energy of $M_{90}B_{10}$-g-HNTs is higher than that of $M_{80}B_{20}$-g-HNTs, the o/w emulsion containing the former g-HNTs is significantly less stable that that having the latter (*vide supra*, Figure 3.2). Hence, we concluded that while the enhanced propensity of these polypeptoid-grafted HNTs to partition at the oil-water interface may contribute to the enhanced stability of the emulsion but the effect is not as dominant as the change of interfacial tension due to polypeptoid functionalization.

3.3.5 Effects of polypeptoid functionalization on the steady shear viscosity of O/W emulsions

Apart from interfacial tension and particle adsorption at the oil-water interface, another important factor that may contribute to the emulsion stability is the emulsion viscosity at low shear rates. To investigate the effect of polymer grafting on the emulsion viscosity, steady shear experiments of *n*-dodecane-ASW emulsions stabilized by polypeptoid-grafted HNTs or p-HNTs

were conducted in the 10^{-4}-10 s^{-1} shear rate range. Plots of steady shear viscosity versus the shear rate (Figure 3.5A) revealed a shear-thinning behavior for all samples. At the low shear rate range (10^{-4}-10^{-3} s^{-1}), the viscosity decrease was relatively minor, indicative of approaching a Newtonian fluid plateau at this shear range. (Note: shear rate below 10^{-4} s^{-1} is not accessible due to instrumental limitation). The decrease of viscosity with increasing shear rate becomes more pronounced at the intermediate10^{-2}-1 s^{-1} shear rate range. At higher shear rate range (1-10 s^{-1}), the viscosity once again decreases more gradually with increasing shear rate, indicative of approaching the infinite viscosity of these emulsions (*e.g.*, p-HNTs, M_{100}-, $M_{90}B_{10}$- and $M_{90}B_{20}$-g-HNTs). The shear viscosity in the entire shear rate range can be well-fitted with the Cross model using equation 2 (eq. 2) to enable the determination of zero-shear viscosity (Figure 3.5A).[46] In eq. 2, η_γ is the steady shear viscosity and γ is steady shear rate. η_∞ and η_0 stand for infinite shear viscosity and zero shear viscosity, respectively. k is the Cross time constant and n is the Cross rate constant.

$$\eta_\gamma = \eta_\infty + \frac{\eta_0 - \eta_\infty}{1+(k\gamma)^n} \quad \text{(eq. 3.2)}$$

In this model, all samples arrive at a Newtonian fluid regime at the low shear rate and exhibit a plateau shear viscosity which is defined as the zero-shear viscosity. It was found that the stable emulsions (*i.e.*, $M_{80}B_{20}$-g-HNTs, $M_{80}D_{20}$-g-HNTs and $M_{90}D_{10}$-g-HNTs) exhibited much higher zero-shear viscosities (~870 - 5100 Pa·s) than the unstable ones (2.4 - 320 Pa·s for p-HNTs, M_{100}-g-HNTs and $M_{90}B_{10}$-g-HNTs), indicating the important role of zero-shear viscosity in emulsion stability. It is particularly worth noting that the emulsion having $M_{90}B_{10}$-g-HNTs exhibited unusually low zero-shear viscosity (2.4 Pa·s) relative to that having $M_{90}D_{10}$-g-HNTs (5100 Pa·s), in spite of the former exhibiting comparable interfacial tension and higher particle desorption energy relative to the latter. As a result, the low zero-shear viscosity is likely the dominant factor that has contributed to the significantly diminished stability over time for the

former emulsion with $M_{90}B_{10}$-g-HNTs, in contrast to the one having $M_{90}D_{10}$-g-HNTs that remained temporally stable.

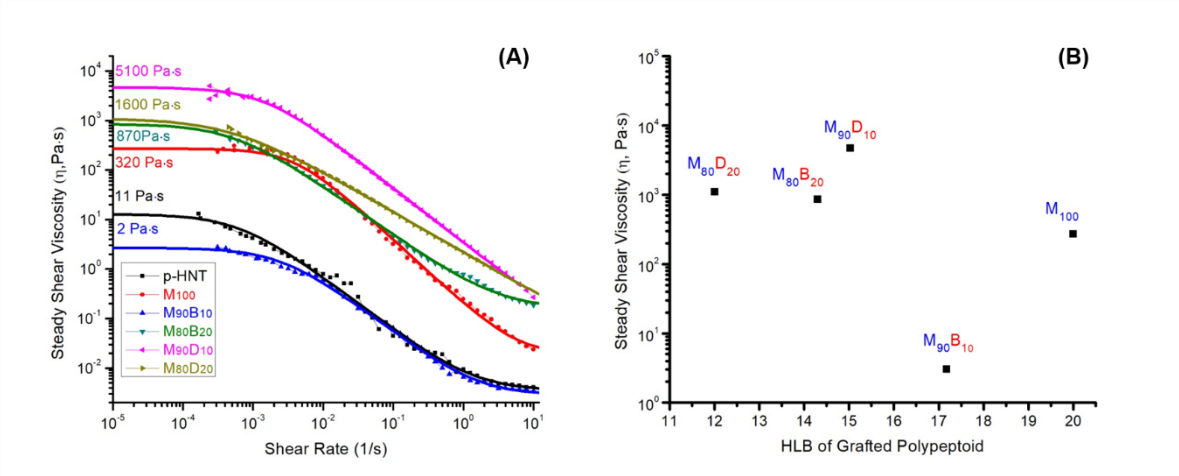

Figure 3.5. (A) Plots of steady shear viscosities (ŋ) versus shear rate for n-dodecane-in-ASW emulsions stabilized by different polypeptoid-grafted HNTs or pristine HNTs in low shear rate range (10-4-10 s-1) and the fitted curve using the Cross model to extrapolate the zero-shear viscosity. (B) Plots of the zero-shear viscosity versus HLB characteristic of polypeptoids grafted onto the HNTs.

It was previously reported that a more viscous continuous phase can reduce the extent of creaming and inhibit oil droplet coalescence according to the Stokes' equation, where the emulsion creaming rate (v) can be estimated by $v = d^2(\rho_o - \rho_w)g/(18\eta)$. Here d represents the diameter of oil droplet, ρ_o and ρ_w represent the density of oil and water respectively, g is the local acceleration of gravity, and ŋ signifies the viscosity of the continuous phase.[58,37,72] In this study, functionalization of HNTs with polypeptoids can significantly alter the HNT inter-connectivity and their partition at the interface versus in the continuous phase, evidenced by cryo-SEM analysis of the emulsions (Figure S3.11). This gives rise to difference in emulsion viscosity, hence resulting in varying emulsion stability against oil droplet coalescence over time.

3.3.6 Effects of polypeptoid-grafted HNTs on *A. borkumensis* cell growth

Alcanivorax borkumensis (*i.e. A. borkumensis*), a hydrocarbon degrading bacterium, is dominant in the microbial communities after several weeks of oil spills.[59] It has been widely used

as the model organism to investigate the dispersants' effects on the population of microbial species. Previous studies have shown that the addition of commonly used surfactants (*e.g.*, COREXIT EC9500A, Lecithin, Tween20, *etc.*) can impact the bacterial adherence to the o/w interface and compromise the *A. borkumensis* viability.[14,15,16] In this work, the cell growth of *A. borkumensis* in the presence of pristine or polypeptoid-grafted HNTs has been investigated to determine their effects on the cell viability. ONR7a was used as a substitute of the seawater for the cell culture of *A. borkumensis*. In brief, ONR7a is a completely synthetic medium that contains all necessary nutrients for the growth of *A. borkumensis* (*e.g.*, nitrogen and phosphorous, *etc.*) except for carbon. The addition of Anadarko crude oil (Figure 3.6) or *n*-hexadecane (Figure S3.12) was used as a carbon source for the cell growth. The cell growth was monitored for 48 h and quantified by fluorescent resazurin assay, an established protocol to monitor live cell viability according to a reported procedure.[33] Two control groups, one with no carbon source and a second without bacteria were used for comparisons.

The cell growth study shown in Figure 3.6A has revealed that HNTs grafted with increasingly hydrophobic polypeptoids inhibit the initial cell growth, resulting in longer lag times relative to the pristine HNTs (p-HNTs) and the control group without any HNTs. However, the maximum cell numbers achieved in the culture were enhanced in the presence of HNTs grafted with more hydrophobic polypeptoids, namely $M_{90}D_{10}$ and $M_{80}D_{20}$. We propose that the increasing lag time may result from the limited initial bacteria attachment at the oil-water interface due to the presence of highly hydrophobic polypeptoid-grafted HNTs. With the gradual formation of biosurfactants and biofilms over time, the interfacial hydrophobicity and structure may have been adjusted to stimulate the bacteria attachment and access to the oil-water interface. As the HNTs grafted with more hydrophobic polypeptoids tend to generate smaller oil droplets with larger

interfacial area than the pristine HNTs, this may also contribute to the larger maximum cell numbers as well as the enhanced cell growth rate. This is further confirmed by plotting the cell growth rate in exponential phase for varying polypeptoid-grafted HNT samples in Figured 3.6B, the cell growth rate was estimated by calculating the tangent between two neighboring measurement time points during the exponential growth stage (Figure 3.6A). From Figure 3.6B, it is observed that the cell growth rate increases with the hydrophobicity of the grafted polypeptoids, and the growth rate of all the polypeptoid-grafted HNTs are higher than the pristine HNTs. Interestingly, for grafted polymers with HLB lower than 17.2, the growth rates are all higher than the control group without any particles stabilizers namely Anadarko Only. In addition to providing larger oil-water interface and better anchoring for bacteria at the interface, the grafted polypeptoids on HNTs can enhance the bacteria cell growth presumably by serving as a nitrogen source, a critical and required nutrient for cell growth. This is evidenced by a notable bacterial cell growth in the presence of polypeptoid-grafted HNTs with endogenous nitrogen source removed from the

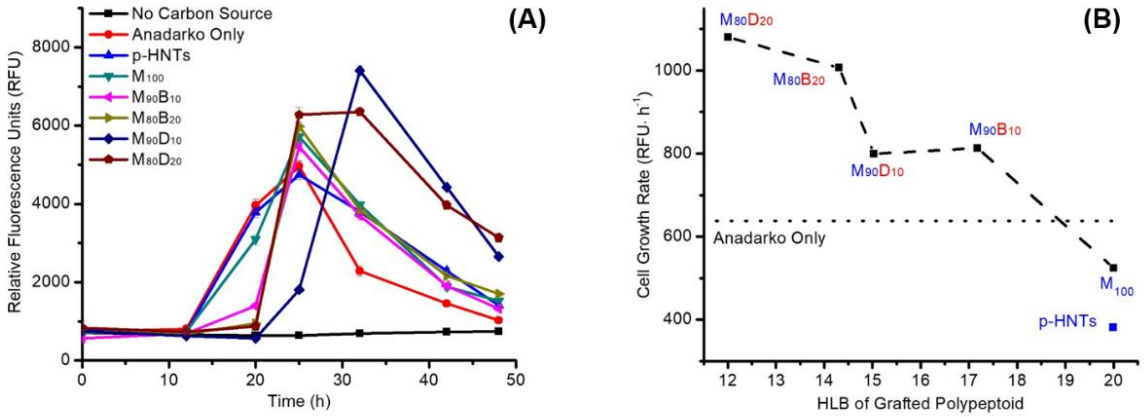

Figure 3.6. (A) Growth of A. borkumensis in modified ONR7a containing 1% Anadarko crude oil and 0.02% w/v of the indicated particles. Points represent mean + SD of the slope of the best fit line from serial dilution of technical replicates. The polymers with increasing hydrophobicity inhibit the initial cell growth, resulting in longer lag time but stimulated cell growth in the exponential growth phase. (B) The cell growth rate (RFU/h) under the exponential growth phase was plotted versus the HLB of grafted-polypeptoids (Table 3.1). The increasing polymer hydrophobicity (lower HLB) enhanced the cell growth rate at exponential growth stage.

ONR7a medium (Figure S3.12). However, it should be noted that the enhancement effect (Figure S3.12) is much less pronounced than when the endogenous nitrogen source is present in the culture medium (Figure 3.6(a)). This suggests that other non-biological factors (*e.g.*, enlarged o/w interfacial area, *etc*.) must have contributed to the significantly enhanced cell growth in the typical ONR7a medium with the endogenous nitrogen source present. The mechanism by which the bacteria metabolize polypeptoids is currently unknown and will be investigated in future. In contrast to traditional surfactants,[14,15,16] polypeptoid-grafted HNTs are non-toxic towards *A. borkumensis* and also stimulate the bacterial growth, significantly enhancing their appeal as alternative emulsion stabilizers for oil remediation.

3.4 Conclusions

We have developed a method to functionalize halloysite nanotubes with amphiphilic polypeptoids by surface-initiated polymerizaiton of *N*-carboxanhydride monomers. Hydrophilicity-lipophilicity balance (HLB) and hence the wettablity of HNT surfaces can be systematically adjusted by controlling the initial feed ratio of hydrophobic and hydrophilic monomers. HNTs funtionalized with polypeptoids having appropriate HLB characterisics (HLB = 12.0-15.0) were found to be significantly more effective stabilizers for the oil/water emulsion relative to the pristine HNTs. Functionalization of HNTs with polypeptoids having appropriate HLB characteristics were found to enhance the emulsion stabilities by 1) effectively reducing the interfacial tension, 2) enhancing the thermodynamic propensity of HNT particles to partition at the oil-water interface as well as 3) increasing the emulsion viscosities to inhibit the oil droplets coalescense. In contrast to traditional surfactants which inhibit the oil-degrading bacterial growth, the polypeptoid-grafted HNTs have been shown to be non-cytotoxic and can promote the bacteria cell growth. This study has highlighted the potential of polypeptoid-functionalized natural clay

particles as a class of environmentally benign and biocompatible emusifier/stabilizer with tunable surface properties for the oil remendiation application.

3.5 References

1. Valentine, D. L.; Kessler, J. D.; Redmond, M. C.; Mendes, S. D.; Heintz, M. B.; Farwell, C.; Hu, L.; Kinnaman, F. S.; Yvon-Lewis, S.; Du, M.; Chan, E. W.; Tigreros, F. G.; Villanueva, C. J., Propane Respiration Jump-Starts Microbial Response to a Deep Oil Spill. *Science* **2010,** *330* (6001), 208-211.

2. Head, I. M.; Jones, D. M.; Röling, W. F. M., Marine microorganisms make a meal of oil. *Nature Reviews Microbiology* **2006,** *4*, 173.

3. Mason, O. U.; Hazen, T. C.; Borglin, S.; Chain, P. S. G.; Dubinsky, E. A.; Fortney, J. L.; Han, J.; Holman, H.-Y. N.; Hultman, J.; Lamendella, R.; Mackelprang, R.; Malfatti, S.; Tom, L. M.; Tringe, S. G.; Woyke, T.; Zhou, J.; Rubin, E. M.; Jansson, J. K., Metagenome, metatranscriptome and single-cell sequencing reveal microbial response to Deepwater Horizon oil spill. *The Isme Journal* **2012,** *6*, 1715.

4. Lin, Q.; Mendelssohn, I. A., Impacts and Recovery of the Deepwater Horizon Oil Spill on Vegetation Structure and Function of Coastal Salt Marshes in the Northern Gulf of Mexico. Environmental Science & Technology **2012,** *46* (7), 3737-3743.

5. Abramson, D. M.; Grattan, L. M.; Mayer, B.; Colten, C. E.; Arosemena, F. A.; Bedimo-Rung, A.; Lichtveld, M., The Resilience Activation Framework: a Conceptual Model of How Access to Social Resources Promotes Adaptation and Rapid Recovery in Post-disaster Settings. *The Journal of Behavioral Health Services & Research* **2015,** *42* (1), 42-57.

6. Das, N.; Chandran, P., Microbial degradation of petroleum hydrocarbon contaminants: an overview. Biotechnology research international **2010,** *2011*, 941810-941810.

7. Leahy, J. G.; Colwell, R. R., Microbial degradation of hydrocarbons in the environment. *Microbiological Reviews* **1990,** *54* (3), 305-315.

8. Kostka, J. E.; Prakash, O.; Overholt, W. A.; Green, S. J.; Freyer, G.; Canion, A.; Delgardio, J.; Norton, N.; Hazen, T. C.; Huettel, M., Hydrocarbon-degrading bacteria and the bacterial community response in gulf of Mexico beach sands impacted by the deepwater horizon oil spill. *Applied and environmental microbiology* **2011,** *77* (22), 7962-7974.

9. Joye, S. B.; Kleindienst, S.; Gilbert, J. A.; Handley, K. M.; Weisenhorn, P.; Overholt, W. A.; Kostka, J. E., Responses of Microbial Communities to Hydrocarbon Exposures. *Oceanography* **2016,** *29* (3), 136-149.

10. Chapman, H.; Purnell, K.; Law, R. J.; Kirby, M. F., The use of chemical dispersants to combat oil spills at sea: A review of practice and research needs in Europe. *Marine Pollution Bulletin* **2007,** *54* (7), 827-838.

11. Sorial, G. A.; Venosa, A. D.; Koran, K. M.; Holder, E.; King, D. W., Oil Spill Dispersant Effectiveness Protocol. II: Performance of Revised Protocol. *Journal of Environmental Engineering* **2004,** *130* (10), 1085-1093.

12. Prince, R. C.; Butler, J. D., A protocol for assessing the effectiveness of oil spill dispersants in stimulating the biodegradation of oil. *Environmental Science and Pollution Research* **2014,** *21* (16), 9506-9510.

13. Kujawinski, E. B.; Kido Soule, M. C.; Valentine, D. L.; Boysen, A. K.; Longnecker, K.; Redmond, M. C., Fate of Dispersants Associated with the Deepwater Horizon Oil Spill. *Environmental Science & Technology* **2011,** *45* (4), 1298-1306.

14. Kleindienst, S.; Seidel, M.; Ziervogel, K.; Grim, S.; Loftis, K.; Harrison, S.; Malkin, S. Y.; Perkins, M. J.; Field, J.; Sogin, M. L.; Dittmar, T.; Passow, U.; Medeiros, P. M.; Joye, S. B., Chemical dispersants can suppress the activity of natural oil-degrading microorganisms. *Proceedings of the National Academy of Sciences* **2015**. *112* (48), 14900-14905.

15. Bookstaver, M.; Bose, A.; Tripathi, A., Interaction of Alcanivorax borkumensis with a Surfactant Decorated Oil–Water Interface. *Langmuir* **2015,** *31* (21), 5875-5881.

16. Abbasi, A.; Bothun, G. D.; Bose, A., Attachment of Alcanivorax borkumensis to Hexadecane-In-Artificial Sea Water Emulsion Droplets. *Langmuir* **2018,** *34* (18), 5352-5357.

17. Saha, A.; Nikova, A.; Venkataraman, P.; John, V. T.; Bose, A., Oil Emulsification Using Surface-Tunable Carbon Black Particles. *ACS Applied Materials & Interfaces* **2013,** *5* (8), 3094-3100.

18. Kim, J.; Cote, L. J.; Kim, F.; Yuan, W.; Shull, K. R.; Huang, J., Graphene Oxide Sheets at Interfaces. *Journal of the American Chemical Society* **2010,** *132* (23), 8180-8186.

19. Dong, J.; Worthen, A. J.; Foster, L. M.; Chen, Y.; Cornell, K. A.; Bryant, S. L.; Truskett, T. M.; Bielawski, C. W.; Johnston, K. P., Modified Montmorillonite Clay Microparticles for Stable Oil-in-Seawater Emulsions. *ACS Applied Materials & Interfaces* **2014,** *6* (14), 11502-11513.

20. Yang, Y.; Fang, Z.; Chen, X.; Zhang, W.; Xie, Y.; Chen, Y.; Liu, Z.; Yuan, W., An Overview of Pickering Emulsions: Solid-Particle Materials, Classification, Morphology, and Applications. *Frontiers in Pharmacology* **2017,** *8* (287), 1-20.

21. Walz, J. Y., Colloidal Particles at Liquid Interfaces Edited by Bernard P. Binks and Tommy S. Horozov (University of Hull, U.K.). Cambridge University Press: Cambridge. 2006. XIV + 504

pp. $145.00. ISBN 0-521-84846-6. *Journal of the American Chemical Society* **2007,** *129* (13), 4106-4107.

22. Hunter, T. N.; Pugh, R. J.; Franks, G. V.; Jameson, G. J., The role of particles in stabilising foams and emulsions. *Advances in Colloid and Interface Science* **2008,** *137* (2), 57-81.

23. Overholt, W. A.; Marks, K. P.; Romero, I. C.; Hollander, D. J.; Snell, T. W.; Kostka, J. E., Hydrocarbon-Degrading Bacteria Exhibit a Species-Specific Response to Dispersed Oil while Moderating Ecotoxicity. *Applied and Environmental Microbiology* **2016,** *82* (2), 518.

24. Binks, B. P.; Philip, J.; Rodrigues, J. A., Inversion of Silica-Stabilized Emulsions Induced by Particle Concentration. *Langmuir* **2005,** *21* (8), 3296-3302.

25. Katepalli, H.; John, V. T.; Bose, A., The Response of Carbon Black Stabilized Oil-in-Water Emulsions to the Addition of Surfactant Solutions. *Langmuir* **2013,** *29* (23), 6790-6797.

26. Magnetic Pickering Emulsions Stabilized by Fe3O4 Nanoparticles. *Langmuir* **2011,** *27* (7), 3308-3316.

27. Perrin, E.; Bizot, H.; Cathala, B.; Capron, I., Chitin Nanocrystals for Pickering High Internal Phase Emulsions. *Biomacromolecules* **2014,** *15* (10), 3766-3771.

28. Omarova, M.; Swientoniewski, L. T.; Tsengam, I. K. M.; Panchal, A.; Yu, T.; Blake, D. A.; Lvov, Y. M.; Zhang, D.; John, V., Engineered Clays as Sustainable Oil Dispersants in the Presence of Model Hydrocarbon Degrading Bacteria: The Role of Bacterial Sequestration and Biofilm Formation. *ACS Sustainable Chemistry & Engineering* **2018,** *6* (11), 14143-14153.

29. Worthen, A. J.; Foster, L. M.; Dong, J.; Bollinger, J. A.; Peterman, A. H.; Pastora, L. E.; Bryant, S. L.; Truskett, T. M.; Bielawski, C. W.; Johnston, K. P., Synergistic Formation and Stabilization of Oil-in-Water Emulsions by a Weakly Interacting Mixture of Zwitterionic Surfactant and Silica Nanoparticles. *Langmuir* **2014,** *30* (4), 984-994.

30. Zhang, J.; Li, L.; Xu, J.; Sun, D., Effect of cetyltrimethylammonium bromide addition on the emulsions stabilized by montmorillonite. *Colloid and Polymer Science* **2014,** *292* (2), 441-447.

31. Lvov, Y.; Wang, W.; Zhang, L.; Fakhrullin, R., Halloysite Clay Nanotubes for Loading and Sustained Release of Functional Compounds. *Advanced Materials* **2015,** *28* (6), 1227-1250.

32. Owoseni, O.; Zhang, Y.; Su, Y.; He, J.; McPherson, G. L.; Bose, A.; John, V. T., Tuning the Wettability of Halloysite Clay Nanotubes by Surface Carbonization for Optimal Emulsion Stabilization. *Langmuir* **2015,** *31* (51), 13700-13707.

33. Panchal, A.; Swientoniewski, L. T.; Omarova, M.; Yu, T.; Zhang, D.; Blake, D. A.; John, V.; Lvov, Y. M., Bacterial proliferation on clay nanotube Pickering emulsions for oil spill bioremediation. *Colloids and Surfaces B: Biointerfaces* **2018,** *164*, 27-33.

34. Fu, J.; Gong, Y.; Zhao, X.; O'Reilly, S. E.; Zhao, D., Effects of Oil and Dispersant on Formation of Marine Oil Snow and Transport of Oil Hydrocarbons. *Environmental Science & Technology* **2014,** *48* (24), 14392-14399.

35. Nyankson, E.; Olasehinde, O.; John, V. T.; Gupta, R. B., Surfactant-Loaded Halloysite Clay Nanotube Dispersants for Crude Oil Spill Remediation. *Industrial & Engineering Chemistry Research* **2015,** *54* (38), 9328-9341.

36. Jiang, J.; Zhu, Y.; Cui, Z.; Binks, B. P., Switchable Pickering Emulsions Stabilized by Silica Nanoparticles Hydrophobized In Situ with a Switchable Surfactant. *Angewandte Chemie* **2013,** *125* (47), 12599-12602.

37. Pi, G.; Li, Y.; Bao, M.; Mao, L.; Gong, H.; Wang, Z., Novel and Environmentally Friendly Oil Spill Dispersant Based on the Synergy of Biopolymer Xanthan Gum and Silica Nanoparticles. *ACS Sustainable Chemistry & Engineering* **2016,** *4* (6), 3095-3102.

38. Fujii, S.; Read, E. S.; Binks, B. P.; Armes, S. P., Stimulus-Responsive Emulsifiers Based on Nanocomposite Microgel Particles. *Advanced Materials* **2005,** *17* (8), 1014-1018.

39. Powell, K. C.; Chauhan, A., Interfacial Tension and Surface Elasticity of Carbon Black (CB) Covered Oil–Water Interface. *Langmuir* **2014,** *30* (41), 12287-12296.

40. Yang, Y.; Chen, Y.; Leng, F.; Huang, L.; Wang, Z.; Tian, W., Recent Advances on Surface Modification of Halloysite Nanotubes for Multifunctional Applications. *Applied Sciences* **2017,** *7* (12), 1215.

41. Joussein, E.; Petit, S.; Churchman, J.; Theng, B.; Righi, D.; Delvaux, B., Halloysite clay minerals – a review. In *Clay Minerals*, **2005;** Vol. 40, p 383.

42. Chan, B. A.; Xuan, S.; Li, A.; Simpson, J. M.; Sternhagen, G. L.; Yu, T.; Darvish, O. A.; Jiang, N.; Zhang, D., Polypeptoid polymers: Synthesis, characterization, and properties. *Biopolymers* **2017,** *109* (1), e23070.

43. Zhang, D.; Lahasky, S. H.; Guo, L.; Lee, C.-U.; Lavan, M., Polypeptoid Materials: Current Status and Future Perspectives. *Macromolecules* **2012,** *45* (15), 5833-5841.

44. Griffin, W. C., Classification of Surface-Active Agents by "HLB". *Journal of the Society of Cosmetic Chemists*, **1949,** *1*, 311–326.

45. Griffin, W. C., Calculation of HLB values of Nonionic Surfactants, *Journal of the Society of Cosmetic Chemist*, **1954**, *5*, 249-256.

46. Cross, M.M. Rheology of non-Newtonian fluids: a new flow equation for pseudoplastic systems. *Journal of Colloidal Science* **1965**, *20* (5), 417-437.

47. Xuan, S.; Lee, C.-U.; Chen, C.; Doyle, A. B.; Zhang, Y.; Guo, L.; John, V. T.; Hayes, D.; Zhang, D., Thermoreversible and Injectable ABC Polypeptoid Hydrogels: Controlling the Hydrogel Properties through Molecular Design. *Chemistry of Materials* **2016,** *28* (3), 727-737.

48. Ulbricht, J.; Jordan, R.; Luxenhofer, R., On the biodegradability of polyethylene glycol, polypeptoids and poly(2-oxazoline)s. *Biomaterials* **2014,** *35* (17), 4848-4861.

49.van Zoelen, W.; Zuckermann, R. N.; Segalman, R. A., Tunable Surface Properties from Sequence-Specific Polypeptoid–Polystyrene Block Copolymer Thin Films. *Macromolecules* **2012,** *45* (17), 7072-7082.

50. Yuan, P.; Southon, P. D.; Liu, Z.; Green, M. E. R.; Hook, J. M.; Antill, S. J.; Kepert, C. J., Functionalization of Halloysite Clay Nanotubes by Grafting with γ-Aminopropyltriethoxysilane. *The Journal of Physical Chemistry C* **2008,** *112* (40), 15742-15751.

51. Zhao, X.; Yu, G.; Li, J.; Feng, Y.; Zhang, L.; Peng, Y.; Tang, Y.; Wang, L., Eco-Friendly Pickering Emulsion Stabilized by Silica Nanoparticles Dispersed with High-Molecular-Weight Amphiphilic Alginate Derivatives. *ACS Sustainable Chemistry & Engineering* **2018,** *6* (3), 4105-4114.

52. Fetsch, C.; Flecks, S.; Gieseler, D.; Marschelke, C.; Ulbricht, J.; van Pée, K.-H.; Luxenhofer, R., Self-Assembly of Amphiphilic Block Copolypeptoids with C2-C5 Side Chains in Aqueous Solution. *Macromolecular Chemistry and Physics* **2015,** *216* (5), 547-560;

53. Fetsch, C.; Luxenhofer, R., Thermal Properties of Aliphatic Polypeptoids. *Polymers* **2013,** *5* (1), 112-117.

54. Wongkongkatep, P.; Manopwisedjaroen, K.; Tiposoth, P.; Archakunakorn, S.; Pongtharangkul, T.; Suphantharika, M.; Honda, K.; Hamachi, I.; Wongkongkatep, J., Bacteria Interface Pickering Emulsions Stabilized by Self-assembled Bacteria–Chitosan Network. *Langmuir* **2012,** *28* (13), 5729-5736.

55. Vignati, E.; Piazza, R.; Lockhart, T. P., Pickering Emulsions: Interfacial Tension, Colloidal Layer Morphology, and Trapped-Particle Motion. *Langmuir* **2003,** *19* (17), 6650-6656

56. Owoseni, O.; Nyankson, E.; Zhang, Y.; Adams, S. J.; He, J.; McPherson, G. L.; Bose, A.; Gupta, R. B.; John, V. T., Release of Surfactant Cargo from Interfacially-Active Halloysite Clay Nanotubes for Oil Spill Remediation. *Langmuir* **2014,** *30* (45), 13533-13541.

57. Creighton, M. A.; Ohata, Y.; Miyawaki, J.; Bose, A.; Hurt, R. H., Two-Dimensional Materials as Emulsion Stabilizers: Interfacial Thermodynamics and Molecular Barrier Properties. *Langmuir* **2014,** *30* (13), 3687-3696.

58. Murakami, R.; Moriyama, H.; Yamamoto, M.; Binks, B. P.; Rocher, A., Particle Stabilization of Oil-in-Water-in-Air Materials: Powdered Emulsions. *Advanced Materials* **2012,** *24* (6), 767-771.

59. Kasai, Y.; Kishira, H.; Sasaki, T.; Syutsubo, K.; Watanabe, K.; Harayama, S., Predominant growth of Alcanivorax strains in oil-contaminated and nutrient-supplemented sea water. *Environmental Microbiology* **2002,** *4* (3), 141-147.

60. Cavallaro, G.; Lazzara, G.; Milioto, S.; Parisi, F.; Sanzillo, V., Modified Halloysite Nanotubes: Nanoarchitectures for Enhancing the Capture of Oils from Vapor and Liquid Phases. *ACS Applied Materials & Interfaces* **2014,** *6* (1), 606-612.

61. Pi, G.; Mao, L.; Bao, M.; Li, Y.; Gong, H.; Zhang, J., Preparation of Oil-in-Seawater Emulsions Based on Environmentally Benign Nanoparticles and Biosurfactant for Oil Spill Remediation. *ACS Sustainable Chemistry & Engineering* **2015,** *3* (11), 2686-2693.

62. Nyankson, E.; Demir, M.; Gonen, M.; Gupta, R. B., Interfacially Active Hydroxylated Soybean Lecithin Dispersant for Crude Oil Spill Remediation. *ACS Sustainable Chemistry & Engineering* **2016,** *4* (4), 2056-2067.

63. Feng, J.; Fan, H.; Zha, D.-a.; Wang, L.; Jin, Z., Characterizations of the Formation of Polydopamine-Coated Halloysite Nanotubes in Various pH Environments. *Langmuir* **2016,** *32* (40), 10377-10386.

64. Ma, W.; Wu, H.; Higaki, Y.; Takahara, A., Halloysite Nanotubes: Green Nanomaterial for Functional Organic-Inorganic Nanohybrids. *The Chemical Record* **2018,** *18* (7-8), 986-999.

65. Jing, H.; Higaki, Y.; Ma, W.; Xi, J.; Jinnai, H.; Otsuka, H.; Takahara, A., Preparation and characterization of polycarbonate nanocomposites based on surface-modified halloysite nanotubes. *Polymer Journal* **2014,** *46*, 307.

66. Flores, J. A.; Pavía-Sanders, A.; Chen, Y.; Pochan, D. J.; Wooley, K. L., Recyclable Hybrid Inorganic/Organic Magnetically Active Networks for the Sequestration of Crude Oil from Aqueous Environments. *Chemistry of Materials* **2015,** *27* (10), 3775-3782.

67. Lee, C.-U.; Li, A.; Ghale, K.; Zhang, D., Crystallization and Melting Behaviors of Cyclic and Linear Polypeptoids with Alkyl Side Chains. *Macromolecules* **2013,** *46* (20), 8213-8223.

CHAPTER 4. DESIGN AND SYNTHESIS OF THERMORESPONSIVE ABC TRIBLOCK COPOLYPEPTOIDS WITH DEUTERATED HYDROPHOBIC SEGMENT FOR ELUCIDATING THE NANOSTRUCTURES AND SELF-ASSEMBLY OF THE ABC THERMORESPONSIVE HYDROGELS

4.1 Introduction

4.1.1 Physically crosslinked injectable hydrogels

Injectable hydrogels have attracted extensive research interest due to the minimal invasive delivery relative to the traditional implantation method. Injectable hydrogels have wide applications in biomedical application e.g. cell or drug carriers, extracellular matrix in tissue engineering, etc. Significant research efforts have been dedicated to design synthetic polymers with tunable chemical structures as injectable hydrogels. Stimuli sensitive synthetic block copolymers are widely used for designing injectable hydrogels, in which the gelation was induced by external stimuli such as pH, temperature, ionic strength, etc. Stimuli sensitive hydrogels can be divided into chemically and physically crosslinked hydrogels. Chemical hydrogels are composed of polymers forming crosslinking via covalent bond under the external stimuli. Physical hydrogels are comprised of supramolecular assembles that are non-covalently crosslinked. In the selective solvent, the block copolymer having both solvophilic and solvophobic segments undergo microphase separation which is driven by the hydrophobic interactions to form micellar structures and the gelation occurred with polymer concentration increase up to critical gelation concentration (CGC). The advantage of physically cross-linked hydrogel (*a.k.a.* physical hydrogel) over chemically cross-linked hydrogels (*a.k.a.* chemical hydrogel) are: 1) the crosslinking condition (e.g., photo irradiation or addition of crosslinking agents) for chemical hydrogel formation may bring damages to local tissues upon hydrogel injection; 2) physical hydrogels generally exhibit relatively smaller volume changes during the gelation relative to chemical hydrogels, which is

beneficial to retain the entrapped drugs or encapsulated cells; 3) compared with chemical hydrogels, the physical hydrogels were appealing due to the high gelation reversibility; 4) the mechanical properties of physical hydrogels can be readily tuned by the molecular design and polymer concentration.[1,2]

4.1.2 Multicompartment physical hydrogels

Inspired by eukaryotic cells with multiple subunits which perform different cellular functions simultaneously,[3] multicompartment physical hydrogels based with multiblock copolymeric micelles have attracted increasing research interest.[4] Multicompartment physical hydrogels are composed with multiblock copolymers assembled into discrete subdomains connected by solvophilic bridges as polymeric networks with distinguishable compartments. Many factors will contribute to the size and structures of multicompartment micelles. For example, the core-corona interfacial energies and the polymer chain conformations which determined by solvent and chemical compositions of different polymer blocks. The external environment (e.g. pH, temperature, etc.) also result in micelles with different shapes and sizes. Different copolymer micellar structures (e.g. spherical or worm-like micelles, vesicles, etc.) can be achieved through molecular design by tuning the chemical structures, molecular weight as well as the polymer architecture.[5-8]

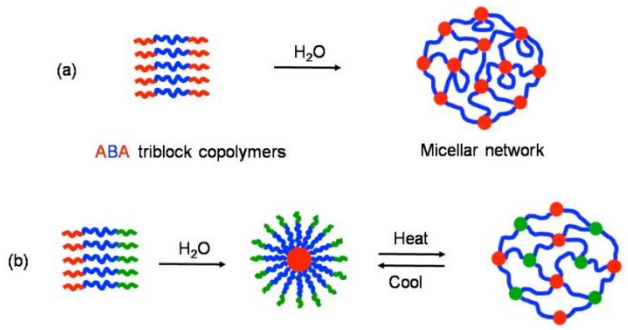

Figure 4.1 Illustration of gelation of (a) ABA and (b) thermoresponsive ABC polymers. Reproduced from Ref.13 with permission from American Chemical Society.

ABC triblock copolymers have been recently designed to form multicompartment hydrogels, in which two immiscible hydrophobic blocks (A and C) are separated by a hydrophilic mid-block (B). ABC triblock copolymers have notable advantage over traditional ABA copolymers in forming structurally defined hydrogel networks. In ABA copolymer, the hydrophobic A end-block associate to form micellar cores above the critical micelle concentration (CMC) with the hydrophilic mid-block back folding to form loops between the same subdomains to form flower shape micelles. With further increase of the polymer concentration, more inter-micellar bridges are formed which contribute to the elasticity of the hydrogel network. Above the critical gelation concentration (CGC), a sharp increase in solution viscosity and thus a formation of solid-like gel is observed due to the extensive formation of inter-micellar bridges.[9,10] However, due to the possible formation of intra-micellar loops and dangling ends, not all hydrophilic blocks are bridged between different subdomains, resulting in network defects and poor gelation efficiency.

The structure of ABA and ABC copolymer-based hydrogels have been studied using a combination of cryo-TEM and small-angle neutron scattering (SANS) experiments. Taribagil et al. investigated the hydrophobicity effect of end blocks on the morphology of hydrogel networks using ABC triblock copolymer of poly(1,2-butadinene)-*b*-poly(ethylene oxide)-*b*-poly(perfluoropropylene oxide) (PB-PEO-PFPO) and ABA triblock copolymer of PB-PEO-PB and PFPO-PEO-PFPO at high polymer concentration of 10 wt % in water. It was found that the structure of hydrophobic domains as well as the morphology of polymeric networks are determined by the interfacial tension between water and the hydrophobic blocks. In PB-PEO-PB and PFPO-PEO-PFPO ABA triblock copolymers, both PB and PFPO hydrophobic end-blocks segregated into domains bridged by PEO midblock. However, PB end-blocks associated into spherical domains as

shown in Figure 4.2 (a), which is in contrast to disk-like domains for PFPO in Figure 4.2 (b). In ABC hydrogel based with PB-PEO-PFPO copolymers, the network structure was determined by the interfacial tensions between two hydrophobic end-blocks. The disk-like PFPO domains (green in Figure 4.2 (c)) were embedded into the bi-continuous PB sheet (red in Figure 4.2 (c)), and both faces of the sheet are cover by PEO loops (blue in Figure 4.2 (c)).[11]

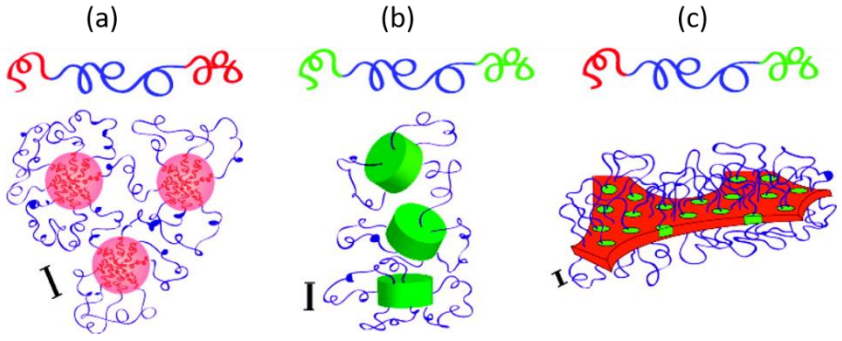

Figure 4.2. Schematic representations showing the dependence of network morphology on the end-groups. 1,2-Polybutadiene (PB), poly(ethylene oxide) (PEO), and poly(perfluoropropylene oxide) (PFPO) have been represented in red, blue, and green, respectively. The scale bars identify a length of 5 nm in each cartoon. Reproduced from Ref.11 with permission from American Chemical Society.

Difference of gelation efficiency between linear ABA and ABC copolymers have been studied. Shunmugam et al. reported the critical gelation concentration (CGC) of ABA hydrogel based on poly(methyl methacrylate)-b-poly[oligo(ethylene glycol)methyl methacrylate]-b-poly(methyl methacrylate) (PMMA-*b*-POEGMA-*b*-PMMA) triblock copolymer is 45 wt % which is significantly higher relative to the ABC hydrogel based with poly (methyl methacrylate)-*b*-poly[oligo(ethylene glycol) methyl methacrylate]-*b*-poly(heptadecafluorodecyl methacrylate) (PMMA-*b*-POEGMA-*b*-PFM) with a 29 wt % CGC.[12] Zhou et al. reported a poly(ethylene-*alt*-propylene)-*b*-poly(ethylene oxide)-*b*-poly(*N*-isopropylacrylamide) (PON) ABC copolymer based thermo-responsive hydrogels and the gelation behavior was compared to that of poly(*N*-isopropylacrylamide)-*b*-poly(ethylene oxide)-*b*-poly(*N*-isopropylacrylamide) (NON) ABA

copolymer. The ABC copolymer exhibits a sharper sol-gel transition with a lower CGC of 1 wt % relative to the ABA copolymer with a 10 wt % CGC.[13]

4.1.3 Thermal responsive polymer based hydrogels

Thermo-responsive hydrogels undergo reversible phase transition from free-flowing solution to free-standing gel (*a.k.a.* sol-gel transition) upon heating above low critical solution temperature (LCST). Thermo-reversible polymers having suitable LCST can form gels at human physiological temperature which is particularly appealing for *in vivo* uses.

Many thermo-responsive polymers have been reported, such as poly(alkyl vinyl ethers),[14,15] functionalized polyglycidols,[16] poly(*N*,*N*-diethylacrylamide) (PDEAM),[20] etc. The most widely investigated thermo-responsive polymer is poly(*N*-isopropylacrylamide) (PNIPAM) with LCST at ~ 32˚C which is close to physiological temperature, and the specific LCST can be readily tuned with the molecular weight and chemical composition.[17-19] Whereas, PNIPAM has limitation in the application of injectable hydrogels: 1) due to the high hydrophobicity of the PNIPAM above LCST, PNIPAM based hydrogel undergo undesired syneresis, resulting in the change of hydrogel structures, mechanical properties and diminished performance in drug encapsulation.[21,22] Copolymers of PNIPAM with relatively hydrophilic segments (*e.g.* poly (2-methacryloyloxyethyl phosphorylcholine) (PMPC), polyethylene glycol (PEG), *etc.*) were designed to enhance the gelation behavior of PNIPAM. In addition, PNIPAM is non-biodegradable *in vivo* which severely limited its applications as injectable hydrogels.[23,24] To address this issue, biodegradable segment such as polylactic acid (PLA), polyester, poly(ε-caprolactone) (PCL)[25,26] have been introduced in the design of copolymers based thermo-reversible hydrogels.

4.1.4 ABC triblock copolypeptoid based thermo-reversible hydrogels

Polypeptoids have been demonstrated as being cytocompatible towards many cell lines,[28,29] and the polyamide backbone are oxidatively degradable under physiologically relevant conditions.[30] Relative to polypeptides, polypeptoids exhibited enhanced proteolytic stability *in vivo*.[31] Recent studies show polypeptoids bearing suitable *N*-substituents can exhibit thermo-responsive behavior in aqueous solutions. For example, poly(*N*-alkyl glycine) with 3 carbons in the *N*-substituents undergo temperature-induced cloud point transition.[32] Xuan et al. reported a series of ABC-type triblock copolypeptoids, *i.e.* poly(*N*-allyl glycine)-*b*-poly(*N*-methyl glycine)-*b*-poly(*N*-decyl glycine) (AMD), which can undergo thermo-reversible sol-gel transitions at a wide range of transition temperatures, depending on their chemical compositions and solution concentration.[27] It was hypothesized that the gelation occurred in a stepwise manner, in which the initial micellization of the triblock copolymer was followed by thermo-induced gelation of end-block A above LCST, resulting in the formation of two-compartment micellar networks. The hydrogel structure was not fully characterized and the gelation mechanism was not unambiguously determined.

In this work, I design, synthesize and characterize 1) ABC hydrogels with varying chemical compositions and chain lengths, 2) and analogous ABC triblock copolymers bearing deuterated hydrophobic block, and 3) conducted structural characterization of the hydrogels by a combination of cryo-TEM, SANS, WAXS methods in collaboration with Dr. Naisheng Jiang. The partially deuterated polymers enable the contrast-matching small angle neutron scattering (SANS) experiments and elucidation of the hydrogel structures.

4.2 Experimental

4.2.1 General considerations

All chemicals and solvents were purchased from Sigma Aldrich and used as received unless otherwise noted. The solvents used for polymerization were further purified by using alumina columns under argon protection. *N*-decyl-d_{21}-amine was synthesized by P. Bonnessen from Center for Nanophase Materials Sciences (CNMS) in Oak Ridge National Lab (ORNL). Deuterium oxide (D_2O, 99.8 atom % D), deuterated dichloromethane (CD_2Cl_2, 99.8 atom % D), deuterated chloroform ($CDCl_3$, 99.95 atom % D), and deuterated dimethyl sulfoxide-d_6 (DMSO-d_6, 99.9 atom % D) were purchased from Cambridge Isotope laboratories. Deionized water for hydrogel preparation was further purified by Nanopure Bioresearch water purification system with a resistance of 17.8-17.9 MΩ·cm from Barnstead Lab Water Products. ^1H and ^2H NMR was collected by Bruker AV-400 III spectrometer at 298K and analyzed using Topspin software. Chemical shifts (δ) given in parts per million (ppm) were referenced to protio impurities of deuterated solvents.

4.2.2 Synthesis of *N*-substituted *N*-carboxyanhydride (NCA) monomers

Three NCA monomers including *N*-allyl glycine derived *N*-carboxyanhydride (Allyl-NCA) and *N*-methyl glycine derived *N*-carboxyanhydride (Me-NCA) and *N*-decyl glycine derived *N*-carboxyanhydride (De-NCA) have been synthesized by adapting a published procedure.[27] ^1H NMR for these monomers were shown in Figure 4.3 and Figure S4.1-S4.3.

4.2.3 Synthesis of deuterated *N*-decyl-d_{21} substituted *N*-carboxyanhydride (Decyl-d_{21}-NCA) monomer

Synthesis of 2-(n-decyl-d21-amino)acetic acid hydrochloride Glyoxylic acid monohydrate (1.168g, 12.69 mmol) was added in CH_2Cl_2 with stirring at 400 rpm until the solid is fully dissolved. *N*-decyl-d_{21}-amine (1.132g, 6.34 mmol) was added into the above solution and the reaction was stirred at 300 rpm at room temperature for overnight. The volatiles were removed

under vacuum to afford a faint yellow oil. 4N HCl aqueous solution (12.68 ml) was added and the mixture was refluxed at 90 ˚C for overnight. The water was removed using rotary evaporation to afford a faint yellow solid which was further purified by recrystallization using methanol/ THF (v/v = 1:8) at 4 ˚C for twice to yield a white solid (Compound **1** in Scheme 4.1) (0.918 g, 56.1 % yield). ^{1}H NMR (δ in DMSO, 400 MHz, ppm): 3.83 (s, -$COCH_2$-), 9.06 (s, -HNHCl). ^{2}H NMR (δ in DMSO, 400 MHz, ppm): 0.74 ppm (t, $CD_3(CD_2)_7CD_2CD_2$-); 1.13 ppm (m, $CD_3(CD_2)_7CD_2CD_2$-).

Synthesis of 2-(*N*,*N*-tert-butoxycarbonyl-n-decyl-d21-amino)acetic acid Compound **1** (Scheme 4.1) (0.918 g, 3.55 mmol), di-tert-butyl dicarbonate (1.937 g, 8.88 mmol) and triethylamine (2.66 ml, 17.75 mmol) were dissolved in DI water (17.75 ml) and stirred at 25 ˚C for 18 h. The reaction mixture was extracted with hexanes (3 × 10 ml) to remove extra di-tert-butyl dicarbonate. Note that an emulsion layer was formed between the aqueous and hexanes phases in the presence of amphiphilic Compound **1**, which was not collected, thus resulting in the partial loss of the products. The aqueous phase was isolated and acidified with 4N HCl till pH = 4 at 0˚C. The aqueous solution was further extracted with ethyl acetate (3 × 10 ml). The separated organic layer was washed with brine and dried over anhydrous $MgSO_4$. After filtration, the volatiles were removed under vacuum to afford the desired product as a colorless oil (Compound **2** in Scheme 4.1) (0.360 g, 30.2 % yield). ^{1}H NMR (δ in $CDCl_3$, 400 MHz, ppm): 3.96 and 3.87 (s, -$COCH_2$-); 1.46 and 1.42 (s, -$(CH_3)_3$). ^{2}H NMR (δ in $CDCl_3$ 400 MHz, ppm): 0.76 ppm (t, $CD_3(CD_2)_7CD_2CD_2$-); 1.17 ppm (m, $CD_3(CD_2)_7CD_2CD_2$-); 1.40 (m, $CD_3(CD_2)_7CD_2CD_2$-), 3.15 (m, $CD_3(CD_2)_7CD_2CD_2$-).

Synthesis of *N*-Decyl-d_{21} *N*-carboxyanhydride Compound **2** (Scheme 4.1) (0.360 g, 1.07 mmol) was dissolved in anhydrous CH_2Cl_2 (5.4 ml, 0.2 M) under nitrogen at 0˚C, and phosphorus

trichloride (78 µl, 0.89 mmol) was added dropwise with a stirring at 300 rpm. Under nitrogen atmosphere, the reaction mixture was stirred at 0˚C for 1 h before warmed to room temperature for additional 3 h. The reaction mixture was concentrated and purified by running a silica plug. A white oily crude product was formed after removing the volatiles under vacuum. In glovebox, the crude product was extracted using anhydrous CH_2Cl_2 (3× 30 ml) and the insoluble residues were filtered off. The collected clear solution was stirred with CaH_2 (40 mg, 0.95 mmol) for 20 min to remove the acidic impurities. Volatiles were removed under vacuum and the crude product was further purified with recrystallization twice with CH_2Cl_2/hexanes (v/v = 1: 10) at -20 ˚C. to afford a white solid (Monomer **M** in Scheme 4.1) (62.7 mg, 22.3 % yield). ^{1}H NMR (δ in $CDCl_3$, 400 MHz, ppm): 4.11 (s, -$COCH_2$-); ^{2}H NMR (δ in $CDCl_3$ 400 MHz, ppm): 0.80 ppm (t, $CD_3(CD_2)_7CD_2CD_2$-); 1.17 ppm (m, $CD_3(CD_2)_7CD_2CD_2$-); 1.51 (m, $CD_3(CD_2)_7CD_2CD_2$-), 3.34 (t, $CD_3(CD_2)_7CD_2CD_2$-).

4.2.4 Synthesis of AMD and AMd triblock copolypeptoids

Poly(*N*-allyl glycine)-*b*-poly(*N*-methyl glycine)-*b*-poly(*N*-decyl glycine), namely as AMD and poly(*N*-allyl glycine)-*b*-poly(*N*-methyl glycine)-*b*-poly(*N*-decyl-d_{21} glycine), namely as AMd were synthesized by the benzyl amine-initiated ring-opening polymerization of the corresponding *N*-substituted *N*-carboxyanhydrides (R-NCAs) in a sequential manner.[271-41-4] A representative procedure for the synthesis of $A_{100}M_{101}D_{10}$ triblock copolypeptoid is shown in Scheme 4.2. In the glovebox, stock solutions of Ally-NCA (M_1, 564 mg, $[M_1]_0$ = 0.4 M), Me-NCA (M_2, 460 mg, $[M_2]_0$ = 0.4 M), De-NCA (M_3, 964 mg, $[M_3]_0$ = 0.4 M) in anhydrous acetonitrile (CH_3CN) were prepared in 10 ml volumetric flasks respectively. Benzyl amine stock solution (I_0, 32.7 mg, $[I]_0$ = 61.03 mM) in anhydrous THF was prepared using a 5 ml volumetric flask. Initiator stock solution I_0 (200 µl, 0.012 mmol, $[M_1]_0$: $[I]_0$ = 100) was added into M_1 (3.05 ml, 0.172 g, 1.22 mmol, $[M_1]_0$ = 0.4 M)

at 50˚C under nitrogen atmosphere for 48 h to reach complete conversion. An aliquot of the reaction mixture was taken to confirm the conversion of polymerization for each block as tracked by monitoring the disappearance of -C=O peak at 1780 cm^{-1} and 1740 cm^{-1} in the reaction aliquots taken over time using FT-IR spectroscopy, prior to the successive additions of Me-NCA (M_2, 3.05 ml, 0.087 g, 1.22 mmol, $[M_2]_0$ = 0.4 M) and De-NCA stock solutions (M_3, 0.305 ml, 0.024 g, 0.122 mmol, $[M_3]_0$ = 0.4 M) in a sequential manner. The polymerization reactions of M and D blocks were conducted at room temperature in anhydrous CH_3CN. (Note: polymerization time varied depending on different $[M_1]_0$: $[M_2]_0$: $[M_3]_0$ and $[M_1+M_2+M_3]_0$: $[I]_0$). After the polymerization was completed, the volatiles were removed under vacuum to afford a crude polymer, which was purified by re-dissolution in DCM and subsequent precipitation in THF. The polymer was isolated by centrifugation and dried under vacuum to yield a white powder (0.205 g, 90.0 %).

The triblock copolymer composition was determined by ^{1}H NMR spectroscopy using end-group analysis. For AMD copolymers, DP_n of each block was calculated based on the integration information of the characteristic peaks. DP_n (A) = (5 × integration of –CH=) / (1 × integration of C_6H_5); DP_n (M) = (5 × integration of ^{a}-CH_3) / (3 × integration of -C_6H_5); DP_n (D) = (5 × integration of -^{b}CH_3) / (3 × integration of -C_6H_5). Here a and b refer to the methyl protons in M and D blocks respectively). For AMd copolymers, the deuteriums at the side chain of d segment are invisible in ^{1}H NMR spectrum, but the -CH_2 on the backbone are still hydrogenated which can be used to conduct the end group analysis to obtain the DP_n of d segment in ^{1}H NMR. Therefore, DP_n (d) = (5 × (integration of -$COCH_2N$-) − DP_n(A) − DP_n(M)) / (2 × integration-C_6H_5).

4.2.5 Size-exclusion chromatography (SEC)

SEC experiments were performed in DMF with 0.1 M LiBr at 25 ℃ with a flow rate of 0.5 ml/min. AMD or AMd polymers were prepared into 5 mg/ml solution in SEC solvent and left to stand for overnight. The polymer solutions were filtered with 0.45 μm PTFE filters before injecting into the SEC system. SEC analysis was performed using an Agilent 1200 system equipped with three Phenomenex 5 μm, 300 × 7.8 mm columns, a Wyatt DAWN EOS multiangle light scattering (MALS) detector (GaAs 30mW laser at λ = 690 nm) and Wyatt OptilabrEX differential refractive index (DRI) detector. The data analysis was performed using Wyatt Astra V 5.3 software. The PDI were obtained using polystyrene standards. The SEC traces were shown in Figure 4.6 and the results of SEC analysis were in Table 4.1.

4.2.6 Preparation of the AMD and AMd aqueous solutions/hydrogels

Aqueous solutions (1 wt % and 5 wt %) of AMD or AMd triblock terpolypeptoids in deuterium oxide (D_2O) (99.8% D_2O, Cambridge Isotope Laboratories, Inc., Andover, MA, USA) or nanopure water were prepared via the "thin film hydration" method.[5, 6] Briefly, the polymers were first dissolved in CH_2Cl_2 in a glass vial. The volatiles were dried under nitrogen flow to yield a formation of polymer thin film. The dried thin film was then hydrated with D_2O or H_2O to achieve the targeted concentration. The solution mixture was subsequently stirred at room temperature for at least 12 hours with the stirring rate of 300 rpm before further characterizations.

4.2.7 Cryo-transmission electron microscopy experiment

Cryo-TEM imaging was conducted using a FEI G2 F30 Tecnai TEM operated at 200 kV. 1 wt % of $A_{100}M_{101}D_{10}$ and $A_{101}M_{107}D_{21}$ polymer aqueous solutions were prepared as described in 4.2.6. To catch the morphology at high temperature, the polymer aqueous solutions were heated at 40˚C for 10 min and 5 μl of the sample was quickly transferred to a 200-mesh lacey carbon grid

(Electron Microscopy Sciences) mounted on the FEI Vitrobot to blot for 2 seconds and quickly quenched into liquid ethane.

4.2.8 Small-angle neutron scattering (SANS) experiment

SANS data were collected using two SANS instruments, namely the NGB 30m-SANS instrument and the NG3 vSANS instrument at the National Institute of Standards and Technology Center for Neutron Research (NCNR) in Gaithersburg, MD. For the NGB 30m-SANS instrument,[7] two neutron wavelengths, λ = 6 Å and λ = 8.4 Å ($\Delta\lambda/\lambda \sim 0.14$) with sample-to-detector distances of 13.2 m, 4.00 m and 1.33 m (wide-angle detector) were used to cover an effective q-range of ~ 0.001 to 0.47 $Å^{-1}$, where q is the scattering vector ($q = 4\pi\sin\theta/\lambda$). For the NG3 vSANS instrument, a neutron wavelength of λ = 11 Å ($\Delta\lambda/\lambda \sim 0.12$) with sample-to-detector distances of 4.5 m and 18.5 m were used to cover an effective q-range of ~ 0.0013 to 0.48 $Å^{-1}$. All samples were measured in custom-made titanium cells with quartz windows and a path length of 2 mm, which were mounted on a temperature-controlled multiple position sample holder. The temperature of the sample holder was controlled by using a water circulation bath system in a range of 15 - 60 °C with accuracy better than 0.1 °C. To ensure the equilibrium of the samples at the given temperatures, we waited for 30 min prior to each SANS measurements. A typical SANS data reduction protocol was used to correct for empty sample cell, background radiation, detector sensitivity, instrument dark current and sample transmission by using the Igor Pro 6.37 software (WaveMetrics, Inc., Lake Oswego, OR, USA) incorporated with data reduction macros.[8] Note that the incoherent scattering of solvent (i.e. D_2O or D_2O/H_2O mixture) was not subtracted from each data, but was included as an q-independent background term in the model fitting. The reduced one-dimensional SANS intensity profiles I(q) vs. q were scaled to an absolute cross section (units of cm^{-1}).

Additional SANS data were collected using the Bio-SANS instrument[9] of the High Flux Isotope Reactor (HFIR) at Oak Ridge National Laboratory (Oak Ridge, TN). Two neutron wavelengths, λ = 6 Å and λ = 18 Å with $\Delta\lambda/\lambda \sim 0.15$, and sample-to-detector distances of 15.5 m (small-angle detector) and 1.1m (wide-angle detector) were used to cover an effective *q*-range of $\sim$ 0.001 to 0.8 $Å^{-1}$. Both detectors are two-dimensional (2D) position-sensitive detectors configured to provide a wide q-coverage in a single setting. All samples were measured in quartz "banjo" cells (Hellma USA, Plainview, NY) with a path length of 2 mm mounted on a temperature-controlled multiple position sample holder. A typical SANS data reduction protocol was used to correct for instrument dark current, detector sensitivity, detector geometry, incident beam normalization and sample transmission by using the facility supplied data reduction software Mantid.[10] Reduced data were azimuthally averaged and merged from the two-detector setting to produce the one-dimensional SANS intensity profiles I(*q*) vs. *q* and scaled to absolute units.

The SasView software package (version 4.2.2) available at https://www.sasview.org/ was utilized to fit the data with suitable models. Instrumental smearing effects for SANS are included during SANS data analysis by convolving the scattering intensity with the SANS instrumental resolution function,[8] which are included in the SasView program.

4.3 Results and discussion

4.3.1 Synthesis and characterization of AMD and AMd triblock copolypeptoids

Poly(*N*-allyl glycine)-*b*-poly(*N*-methyl glycine)-*b*-poly(*N*-decyl glycine) (AMD) triblock copolypeptoids have been synthesized using benzyl amine-initiated ring-opening polymerization of the corresponding *N*-substituted *N*-carboxyanhydrides (R-NCAs) in a sequential manner by adapting a reported procedure as shown in Scheme 4.2.[27] ^{1}H NMR of Al-, Me-, and De-NCA monomers were shown in Figure 4.3 (a)-(c), and the detailed chemical

shift and integration information were included in Figure S4.1-S4.3. Two AMD polymers with targeted composition of $A_{100}M_{100}D_{10}$ and $A_{100}M_{100}D_{20}$ were designed and synthesized to elucidate the effect of chain length and crystallization of hydrophobic segment (D) on the micellar morphology.

Scheme 4.1. Synthetic scheme of Decyl-d_{21}-NCA monomer

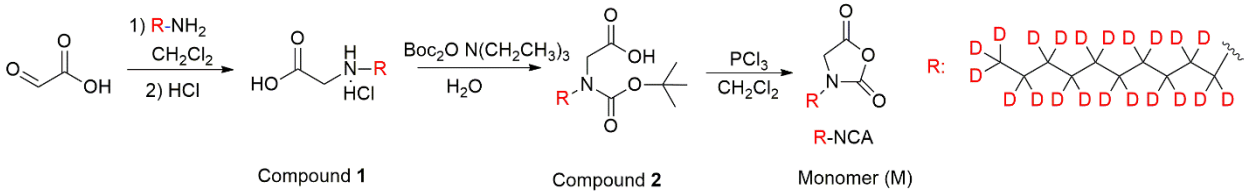

Scheme 4.2. Synthetic scheme for AMD and AMd triblock copolypeptoids.

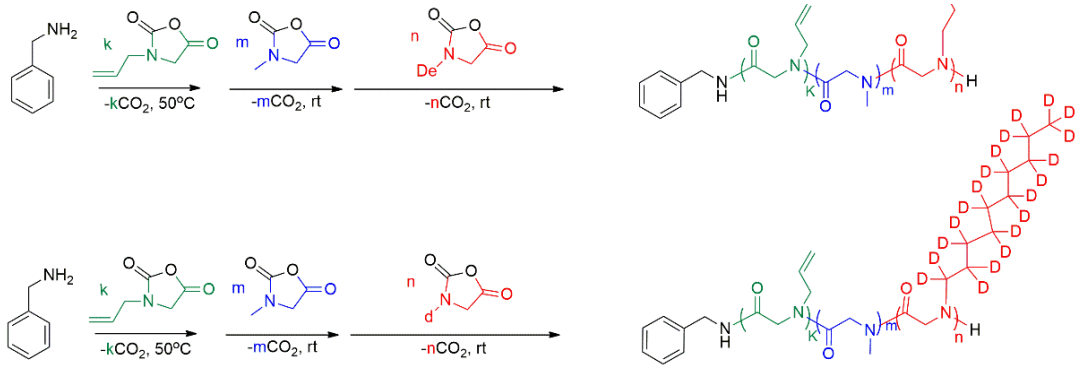

To further investigate the thermally induced structural evolution of AMD polymer in aqueous solutions, we intended to conduct temperature-dependent SANS as well as contrast matching SANS experiments using AMd, which is analogous to AMD polymers bearing deuterated D segments. To enable the contrast matching SANS experiments, De-NCA monomer with deuterated decyl *N*-substituent was synthesized (*a.k.a.* De-d_{21}-NCA) for the first time by adapting a reported procedure outlined in Scheme 4.1.[27] The molecular structures of the precursors (Compound **1** and **2**) and De-d_{21}-NCA monomer (M) were verified by a combination of ^{1}H and ^{2}H NMR spectral analysis (Figure S4.4-S4.9). The chemical shifts of the De-d_{21}-NCA precursors (*i.e.*

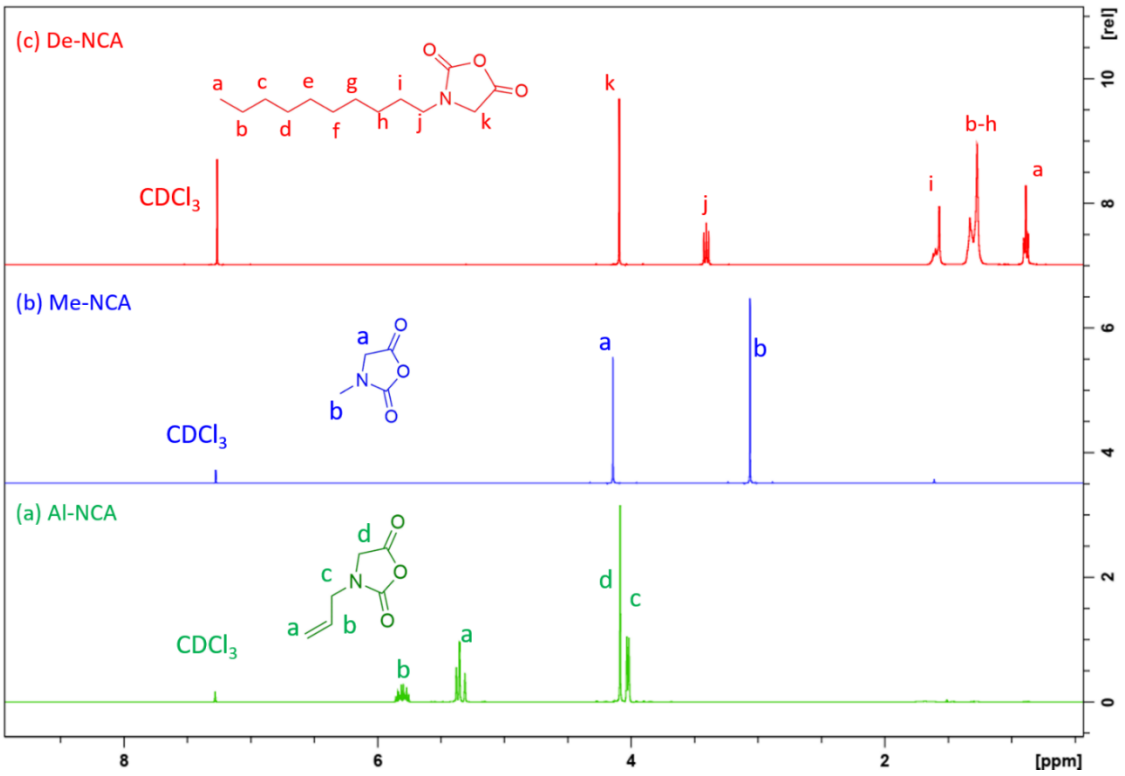

Figure 4.3. ^{1}H NMR spectra of (a) Al-NCA, (b) Me-NCA and (c) De-NCA monomers in $CDCl_3$.

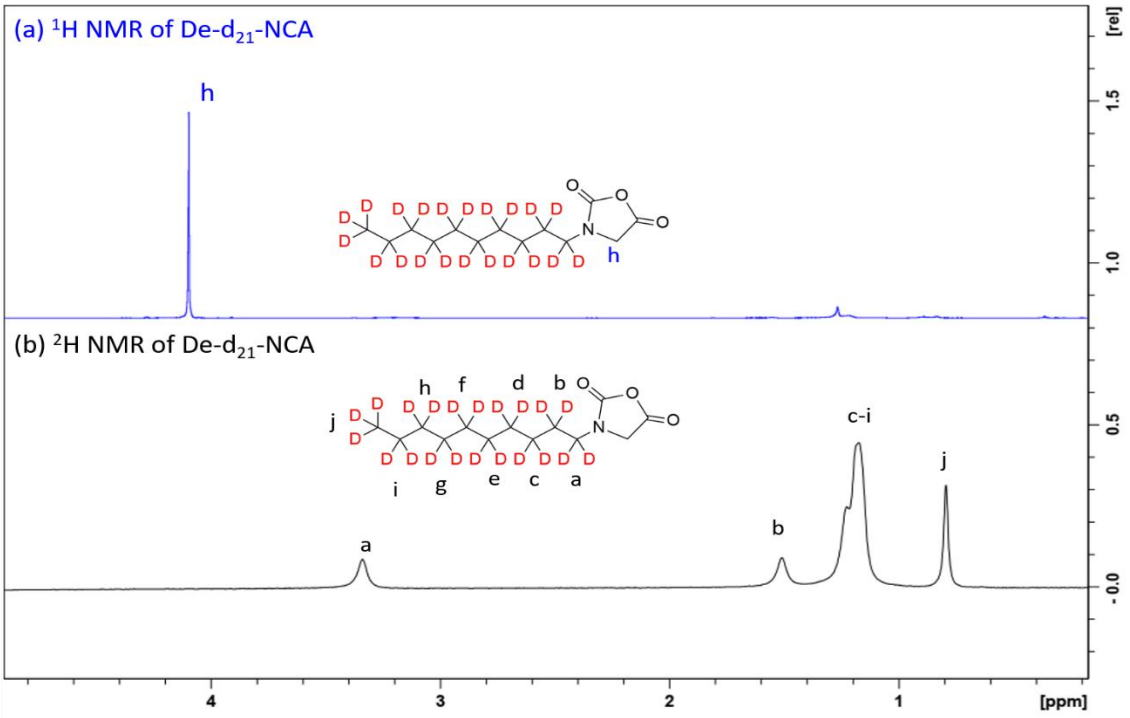

Figure 4.4. (a)^{1}H-NMR and (b) ^{2}H-NMR spectra of De-d_{21}-NCA monomer in $CDCl_3$.

Compound **1**, Compound **2)** in ^{1}H and ^{2}H NMR spectra are summarized in section 4.2.3. For De-d_{21}-NCA monomer, only the -$COCH_2$- protons appeared at 4.11 ppm in the ^{1}H NMR spectrum (Figure 4.4 (a)). The deuterated *N*-$C_{10}d_{21}$ group that are invisible in the ^{1}H NMR spectrum can be clearly observed in the ^{2}H NMR spectrum (Figure 4.4 (b)). The deuterium signals due to *N*-$C_{10}d_{21}$ group appeared in the similar chemical shift range in the ^{2}H NMR spectrum (Figure 4.4 (b)) as the protons of *N*-$C_{10}H_{21}$ group of De-NCA in ^{1}H NMR spectrum (Figure S4.3), supporting the successful synthesis of De-d_{21}-NCA.

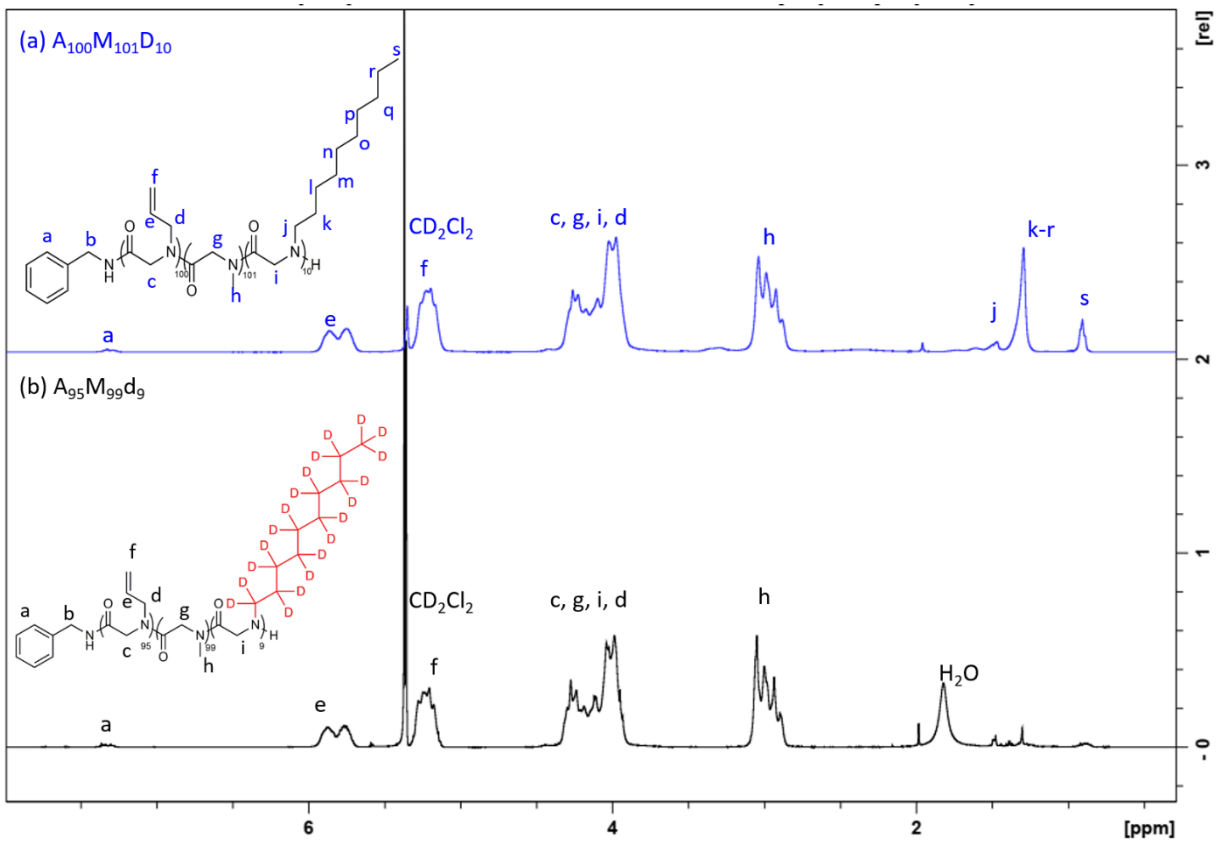

Figure 4.5. ^{1}H NMR spectra of (a) $A_{100}M_{101}D_{10}$ and (b) $A_{95}M_{99}d_9$ in CD_2Cl_2.

AMd polymers were synthesized using benzyl amine-initiated ring opening polymerization with the same initial monomer-to-initiator ratio of $[M_1]_0$:$[M_2]_0$:$[M_3]_0$:$[I]_0$ as AMD polymers, and the polymer compositions were verified by end-group analysis using ^{1}H NMR spectroscopy. Note

that the end group analysis for AMd and AMD copolymers are different. The methods to calculate DP_n (A) and DP_n (B) are the same for both AMD and AMd copolymers: DP_n (A) = (5 × integration of –CH=) / (1 × integration of C_6H_5); DP_n (M) = (5 × integration of ^{a}-CH_3) / (3 × integration of -C_6H_5), where a refer to the methyl protons in M block. By contrast, the method to calculate DP_n (D) and DP_n (d) are different. For AMD copolymers, DP_n (D) = (5 × integration of -$^{b}CH_3$) / (3 × integration of -C_6H_5). Here b refers to the methyl protons in D block. For AMd copolymers, since

Table 4.1 Molecular characteristics of AMD and AMd triblock copolypeptoids

Samples[a]	$[M_1]_0$:$[M_2]_0$:$[M_3]_0$:$[I]_0$[b]	M_n (theor.) (kDa)[c]	M_n (NMR) (kDa)[d]	M_n (SEC) (kDa)[e]	PDI[e]
$A_{100}M_{101}D_{10}$	100:100:10	18.9	18.9	37.0	1.08
$A_{95}M_{99}d_9$	100:100:10	18.9	18.2	43.1	1.15
$A_{101}M_{107}D_{21}$	100:100:20	20.8	21.6	37.8	1.11
$A_{96}M_{105}d_{18}$	100:100:20	20.8	20.7	45.3	1.18

[a.] The numbers in subscripts correspond to the DP_n of each individual block determined by end-group analysis using ^{1}H NMR spectroscopy in CD_2Cl_2. b. Initial monomer-to-initiator ratio. c. Theoretical molecular weights were calculated from the initial monomer-to-initiator ratio. d. M_n determined by ^{1}H NMR analysis. e. M_n and PDI determined by the SEC-DRI method using polystyrene standards (0.1 M LiBr/DMF at 25˚C).

the deuteriums at the side chain of d segment are invisible in ^{1}H NMR spectrum (Figure 4.5 (b)), but the -CH_2 on the backbone are still hydrogenated which can be used to conduct the end group analysis to obtain the DP_n (d) in ^{1}H NMR. Therefore, DP_n (d) = (5 × (integration of -$COCH_2$N-) − DP_n(A) − DP_n(M)) / (2 × integration-C_6H_5). The ^{1}H NMR spectra of AMD and AMd copolymers were shown in Figure S4.10-S4.13 and the polymer compositions determined by end-group analysis were summarized in Table 4.1, which agree well with the targeted compositions. The

polymer size and distributions were analyzed using SEC-DRI in DMF with 0.1 M LiBr at 25 ˚C, and the results in Figure 4.6 show that all polymers exhibit narrow distributions with low polydispersity in the 1.08-1.18 range, indicating that polymerization has occurred in a controlled manner (Table 4.1, Figure 4.6).

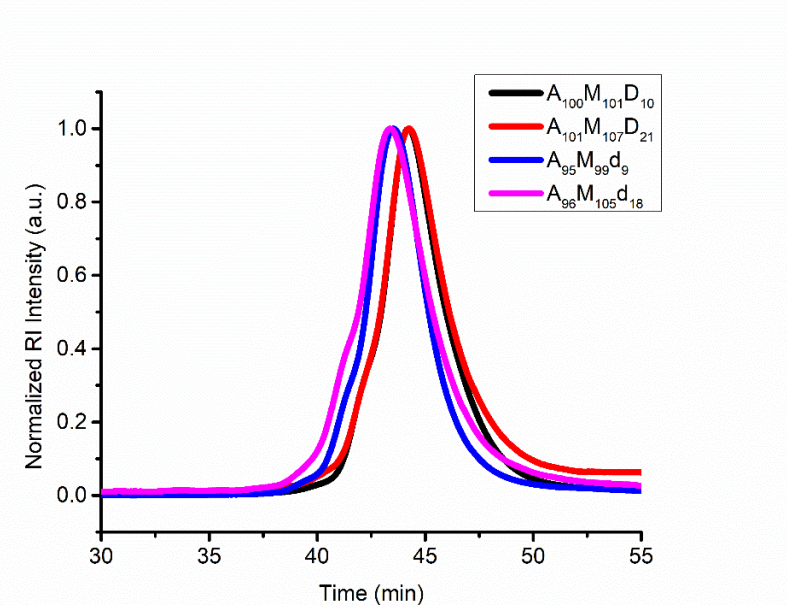

Figure 4.6. SEC-DRI chromatograms of AMD and AMd triblock copolypeptoids in DMF with 0.1 M LiBr at 25℃.

4.3.2 Structural evolution of AMD triblock copolypeptoids in aqueous solutions

The preparation of polymer solutions and the corresponding hydrogels were described in section 4.2.6. Both AMD and AMd triblock copolypeptoids used in this study undergo thermo-reversible gelation in D_2O or H_2O by visual observation. The 5 wt % solutions of AMD form freestanding opaque gels upon heating in the 30 - 40 ˚C range, which return to a free-flowing liquid state after cooled down to room temperature. To better understand the structural evolution during the sol-gel transition, temperature-dependent SANS experiments and cryo-TEM analysis of aqueous solutions of selected AMD and AMd copolymers were conducted.

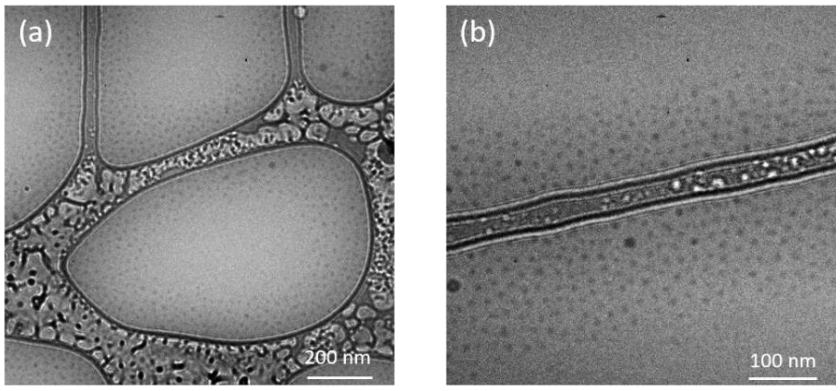

Figure 4.7. Representative cryo-TEM images of $A_{100}M_{101}D_{10}$ (a, b) in aqueous solutions (1wt %) vitrified from 40 ˚C ($T>T_{gel}$).

It was previously shown that the sol-gel transition temperature for 1 wt % $A_{92}M_{94}D_{12}$ polymer solutions is at ~ 27.2°C, and the polymer segregated into spherical micelles with an average diameter of 13 ± 1 nm at $T < T_{gel}$.[27] As a result, the SANS data of an aqueous solution of $A_{100}M_{101}D_{10}$ (1wt %) were first collected at 20°C and 60°C, which is below and above the gelation temperature (T_{gel}), respectively, as shown in Figure 4.8 (a). In collaboration with Dr. Naisheng Jiang, the SANS data were further analyzed to obtain the relevant structural parameters of the polymer solutions. At 20 °C, the SANS profile can be well fitted with a typical core-shell spherical micelle model developed by Pedersen and co-worker,[35-37] in which the total coherent scattering is

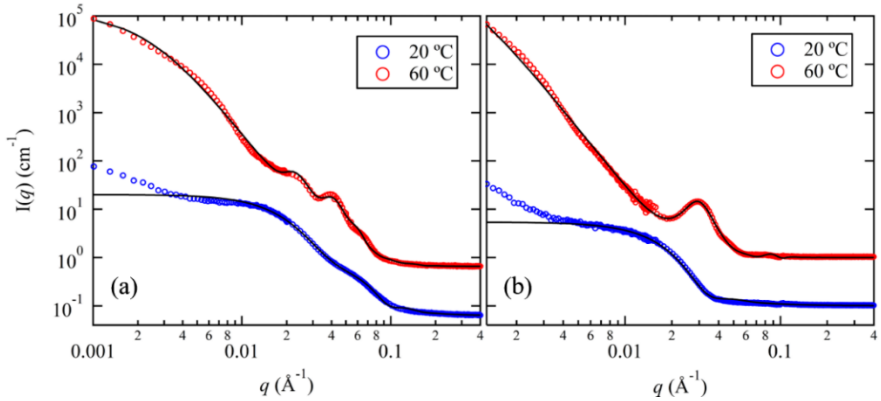

Figure 4.8. SANS profiles of (a) 1 wt % $A_{100}M_{101}D_{10}$ in D_2O and (b) 1 wt % $A_{95}M_{99}d_9$ in D_2O/H_2O with 93.8 % D_2O (*i.e.*, d contrast matched condition) measured at 20 °C ($T<T_{gel}$) and 60 °C ($T>T_{gel}$). The solid curves correspond to the best-fits to the data. The profiles at 60 °C were shifted vertically for clarity by multiplying 10.

described as a function of a micelle form factor and a monodisperse hard-sphere structure factor. The core radius (R_c) = 4.5 ± 0.2 nm and the radius of gyration of the Gaussian corona chains ($R_{g,chain}$) = 5.0 ± 0.2 nm was obtained based on the fitting result. The average aggregation number (N_{agg}) of polymer chains in a single micelle of $A_{100}M_{101}D_{10}$ was estimated as N_{agg} = 92. The hard-sphere radius (R_{hs}) is estimated to be 6.1 ± 0.2 nm, which is in good agreement with the size obtained from cryo-TEM analysis which is 6.5 ± 0.5 nm. The overall micellar size (R_{hs}) obtained is much less than $R_c + 2R_{g,chain}$, indicating a high degree of interpenetration of $A_{100}M_{101}$ corona chains among micelles.

Upon heating the free-flowing 1wt % $A_{100}M_{101}D_{10}$ micellar solution to $T > T_{g,}$ (T = 60 °C), two distinct scattering peaks at q = 0.022 and 0.040 $Å^{-1}$ appeared as shown in Figure 4.8 (a), which corresponds to the d_1 and d_2 spacing in Figure 4.9 (c) respectively, indicating the occurrence of two distinct compartments in the hydrogel networks.[38] As illustrated in Figure 4.9 (c), the thermo-responsive A block dehydrated into a discrete micellar domain upon heating at $T > T_{gel}$. Therefore, the dehydrated A and hydrophobic D domains are alternatively segregated and bridged by the hydrophilic M segments, giving rise to two characteristic length scales in the spatial correlation corresponding to the two scattering peaks at 60 °C in Figure 4.8 (a). In addition, cryo-TEM analysis of 1wt % $A_{100}M_{101}D_{10}$ aqueous solution vitrified from temperature (i.e., 40°C) above the gelation temperature (Figure 4.7 (a) and (b)) also revealed the presence of spherical micelles with an average radius of 7 ± 1 nm, consistent with the formation of micellar networks.

To further elucidate the structure of micellar domains of A block, the contrast matching analysis of d segment was conducted by SANS using a site-selectively deuterated analog of $A_{100}M_{101}D_{10}$ polymer bearing deuterated hydrophobic segment, *i.e.* $A_{95}M_{99}d_9$ block copolymers. To contrast matching the d segment, H_2O (6.2 v%) was mixed with the background solvent D_2O

(93.8 v %) to match the scattering length density of the target deuterated d segment. By contrast matching the d segment, the deuterated d block micellar structures become invisible under neutron, and the scattering profile is only predominated by the domains from dehydrated A block.

As shown in Figure 4.8 b, when the d block is contrast matched, the scattering peak at q = 0.040 $Å^{-1}$ from the micellar core-shell structure disappeared at T = 20 ˚C ($T < T_{gel}$). Upon heating the solution to T = 60 ˚C ($T > T_{gel}$), only one major scattering peak is discernible at $q \approx 0.03$ $Å^{-1}$ in the intermediate q range. Since the hydrophobic d spheres are contrast-matched out, the observed single scattering peak is related to the spatial correlation of the dehydrated A spheres, which serve as one of the physically cross-linked junctions in the hydrogel network. Based on the fitting result, the core radius of dehydrated A sphere ($R_{c, A}$) is 7.2 nm at 60 ˚C which still contains 50.0 vol% of D_2O, indicating A is only partial dehydrated. The number fraction ratio, *i.e.*, total number of A spheres relative to D sphere, was estimated to be 0.72, which suggests that D form slightly more junction points than A blocks in the two-compartment network.

The temperature-dependence of the SANS curves for $A_{100}M_{101}D_{10}$ in D_2O and $A_{95}M_{99}d_9$ in D_2O/ H_2O at $T > T_{gel}$ were shown in Figure 4.9. For $A_{100}M_{101}D_{10}$ in Figure 4.9 (a), a continuous intensity increase as a function of temperature for the primary scattering peak near q = 0.022 $Å^{-1}$ was observed, while the secondary peak near q = 0.040 $Å^{-1}$ remain nearly unchanged during the heating process. Since the primary peak is mainly associated with the spatial correlation among D spheres, the increase of the primary peak intensity reveals the enhanced inter-micellar ordering of D domains with increasing temperature. For $A_{95}M_{99}d_9$ in Figure 4.9 (b), when the d block is contrast matched, the dehydrated A spheres dominate the SANS intensity near mid-q region. The single scattering peak from dehydrated A domains gradually intensifies and shifts towards lower q with increase of temperature. Based on the fitting result, the core radius of A sphere ($R_{c, A}$)

gradually increases from 6.0 nm with aggregation numbers $N_{agg,\,A}$ = 34 at 30 °C to $R_{c,\,A}$ = 7.2 nm with $N_{agg,\,A}$ = 47 at 60 °C, indicating the A block assembled into larger aggregated micelles with temperature increase.

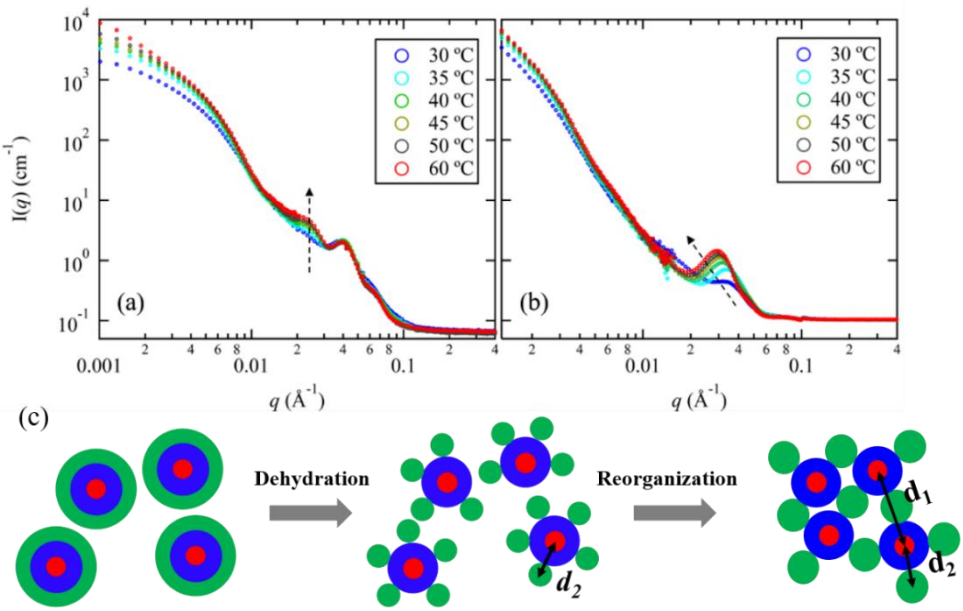

Figure 4.9. (a) SANS profiles of 1 wt % $A_{100}M_{101}D_{10}$ in D2O and (b) 1 wt % $A_{95}M_{99}d_9$ in D_2O/H_2O with 93.8 % D_2O (i.e., d contrast matched condition) measured during heating process at T > T_{gel}. (c) Proposed structural change of AMD during temperature induced sol-to-gel transition.

Based on the above results, the structural evolution of the hydrogel network as a function of temperature can be concluded. At T < $T_{g,}$ AMD polymers aggregated into core-shell spherical micelles. With temperature increase above $T_{gel,}$ the A block dehydrated to form spherical micellar domains. With temperature further increase, the A spheres continue to dehydrate and more A blocks are aggregated into lager micellar cores. This process facilitates the reorganization of the D spheres, leading to more ordered inter-micellar structures in the two-compartment hydrogel network, as illustrated in Figure 4.9 (c).

4.3.3 Effect of core-forming D block content on the micellar morphology

We further investigated the effect of molar fraction of core-forming D block on the structures of the two-compartment hydrogel networks using the SANS method. Previously cryo-

TEM analysis has revealed the presence of rod-shaped micelles in the aqueous solution of $A_{98}M_{98}D_{18}$ copolymers (molar fraction of D segment = 8.9%) below the gelation temperature.[27] This is in contrast to that for the $A_{92}M_{94}D_{12}$ copolymers (molar fraction of D segment = 4.7%) solution where only spherical micelles were observed below the gelation temperature. It is hypothesized that longer or higher molar fraction of comb-shaped D segments can promote crystallization within the micellar core, resulting in the formation of elongated micellar building

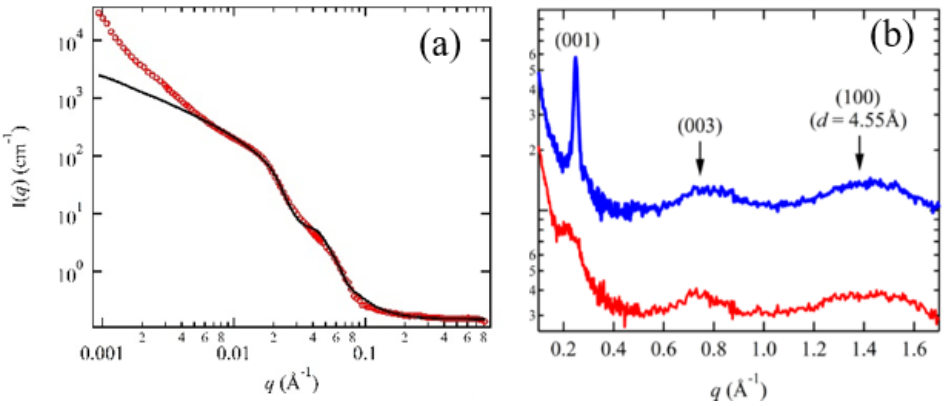

Figure 4.10. SANS profiles of (a) 1 wt % $A_{100}M_{107}D_{21}$ in D_2O measured at 20 °C ($T < T_{gel}$). The solid curves correspond to the best-fits to the data. The profiles at 60 °C were shifted vertically for clarity by multiplying 10. (b) WAXD intensity profiles for the $A_{95}M_{99}d_9$ (red line) and $A_{96}M_{105}d_{18}$ (blue line) in 1 wt % aqueous solution measured at 20 °C.

block in the network.[33,34.] In this study, we further characterized the solution structure of $A_{101}M_{107}D_{21}$ copolymer (molar fraction of D segment = 9.2%) that has comparable composition as that of $A_{98}M_{98}D_{18}$ copolymer above the gelation temperature by the SANS and cryo-TEM methods.

The SANS profiles of $A_{101}M_{107}D_{21}$ polymers in water (1wt %) collected at 20 ˚C can be well fitted using a core-shell cylindrical micelle model[33,39,40] with the radius of the cylindrical core estimated to be 4.5 ± 0.2 nm, as shown in Figure 4.10 (a). The formation of cylindrical micelles was presumably driven by the formation of liquid crystalline domain of D segments. Wide-angle X-ray diffraction (WAXD) analysis of an aqueous solution of $A_{96}M_{105}d_{18}$ copolymers revealed the presence of a sharp diffraction peak (001) at q = 0.22 $Å^{-1}$ that are characteristics of liquid crystalline

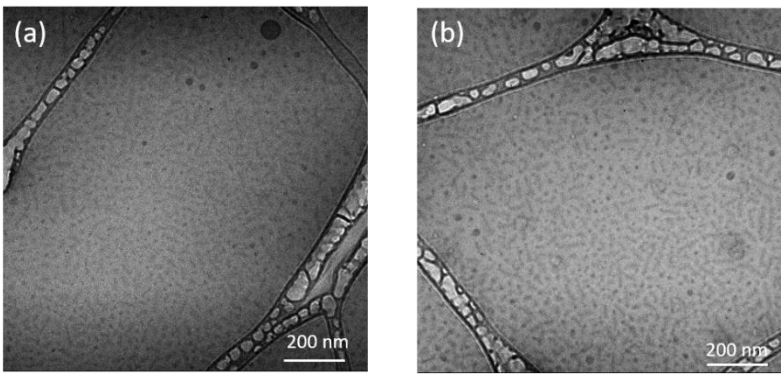

Figure 4.11. Representative cryo-TEM images of $A_{101}M_{107}D_{21}$ (a, b) in aqueous solutions (1wt %) vitrified from 40 ˚C ($T>T_{gel}$).

packing of the comb-shaped polypeptoid polymers (d segments) (Figure 4.10). This is in in sharp contrast to the aqueous solution of $A_{95}M_{99}d_9$ where the (001) diffraction peak at q = 0.22 $Å^{-1}$ is significantly diminished. In addition, while WAXD peaks typically associated with the higher order diffraction (003) or (100) diffraction are discernable at q= 0.75 and 1.4 $Å^{-1}$, these diffractions are weak and ill-defined, indicating the lack of long-range ordering in the cylindrical micellar cores of $A_{96}M_{105}d_{18}$.[33,34]

In addition, cryo-TEM analysis of 1wt % $A_{101}M_{107}D_{21}$ aqueous solution vitrified from temperature (i.e., 40°C) above the gelation temperature (Figure 4.11 (a) and (b)) also revealed the presence of a mixture of spherical and cylindrical micelles. The cylindrical micelles are presumably from hydrophobic D block, which exhibited an average cross-sectional radius of 4 ± 1 nm (T = 40 ˚C) by cryo-TEM analysis, which is comparable to that (4.2 ± 0.2 nm) (T= 60˚C) determined by SANS analysis. The average length of the cylindrical micelles is estimated to be ~ 50 nm by cryo-TEM analysis.

4.4 Conclusions

In this work, AMD thermoresponsive triblock polymers with varying chemical compositions and their site-selectively deuterated counterparts have been synthesized and characterized. SANS and cryo-TEM analysis were conducted to elucidate the structural changes

during the sol-gel transition of these polymers in aqueous solution. Analogous AMD polymers bearing deuterated hydrophobic block (d) were synthesized to further verify the bi-compartmental micellar network structure of the hydrogels by contrast-matching SANS experiments. At room temperature, the triblock copolypeptoids self-assemble into core-shell type of micelles with either spherical or cylindrical shape in aqueous solution, as determined by the molar fraction of core-forming D block. When heated above the gelation temperature (T_{gel}), the formation of two-compartment hydrogel network consisting of distinct micellar cores of dehydrated A and hydrophobic D was unambiguously revealed. The detailed structural parameters of the network were obtained by SANS model fitting. At $T > T_{gel}$, the hydrogel was shown to undergo continuous structural reorganization with increasing temperature, leading to more ordered bicompartmental micellar networks.

4.5 References

1. He, C.; Kim, S. W.; Lee, D. S., In situ gelling stimuli-sensitive block copolymer hydrogels for drug delivery. *Journal of Controlled Release* **2008,** *127* (3), 189-207.

2. Pertici, V.; Trimaille, T.; Gigmes, D., Inputs of Macromolecular Engineering in the Design of Injectable Hydrogels Based on Synthetic Thermoresponsive Polymers. *Macromolecules* **2020,** *53* (2), 682-692.

3. Ringsdorf, H.; Lehmann, P.; Weberskirch, R. Book of Abstracts, 217th National Meeting of the American Chemical Society, Anaheim, CA, March 221-225, 1999.

4. Lodge, T. P.; Rasdal, A.; Li, Z.; Hillmyer, M. A. Simultaneous, Segregated Storage of Two Agents in a Multicompartment Micelle. J. Am. Chem. Soc. *2005*, 127, 17608-17609.

5. Won, Y. Y.; Brannan, A. K.; Davis, H. T.; Bates, F. S. Cryogenic Transmission Electron Microscopy (Cryo-TEM) of Micelles and Vesicles Formed in Water by Poly(ethylene oxide)-Based Block Copolymers. J. Phys. Chem. B *2002*, 106, 3354-3364.

6. Kubowicz, S.; Baussard, J. F.; Lutz, J. F.; Thunemann, A. F.; von Berlepsch, H.; Laschewsky, Multicompartment Micelles Formed by Self-Assembly of Linear ABC Triblock Copolymers in Aqueous Medium. *A. Angew. Chem., Int. Ed.* **2005**, *44*, 5262-5265.

7. Von Berlepsch, H.; Bottcher, C.; Skrabania, K.; Laschewsky, A. Complex domain architecture of multicompartment micelles from a linear ABC triblock copolymer revealed by cryogenic electron tomography. Chem. Commun. *2009*, 2290-2292.

8. Fang, B.; Walther, A.; Wolf, A.; Xu, Y.; Yuan, J.; Muller, A. H. E. Undulated Multicompartment Cylinders by the Controlled and Directed Stacking of Polymer Micelles with a Compartmentalized Corona. Angew. Chem., Int. Ed. *2009*, 48, 2877-2880.

9. Kelarakis, A.; Yuan, X.; Mai, S.; Yang, Y.; Booth, C. Aqueous micellar solutions of a triblock copolymer of ethylene oxide and 1,2-butylene oxide, $B_{12}E_{114}B12$. Scaling the viscoelasticity of fluid and gel. Phys. Chem. Chem. Phys. *2003*, 5, 2628-2634.

10. Kelarakis, A.; Havredaki, V.; Yuan, X.; Chaibundit, C.; Booth, C. Aqueous Gels of Triblock Copolymers of Ethylene Oxide and 1,2-Butylene Oxide (Type BEB) Studied by Rheometry. Macromol. Chem. Phys *2006*, 207, 903-909.

11. Taribagil, R. R.; Hillmyer, M. A.; Lodge, T. P., Hydrogels from ABA and ABC Triblock Polymers. *Macromolecules* **2010,** *43* (12), 5396-5404.

12. Shunmugam, R.; Smith, C. E.; Tew, G. N. Synthesis of Multicompartment Nanoparticles of ABC Miktoarm Star Polymers by Seeded RAFT Dispersion Polymerization J. Polym. Sci., Part A: Polym. Chem. *2007*, 45, 2601-2608.

13. Zhou, C.; Hillmyer, M. A.; Lodge, T. P., Efficient Formation of Multicompartment Hydrogels by Stepwise Self-Assembly of Thermoresponsive ABC Triblock Terpolymers. *Journal of the American Chemical Society* **2012,** *134* (25), 10365-10368.

14. D. Theiss, T. Schmidt and K.-F. Arndt, Temperature-sensitive poly(vinyl methyl ether) hydrogel beads. *Macromol. Symp.*, **2004,** *210*, 465–474.

15. Reichelt, R.; Schmidt, T. ; Kuckling, D.; Arndt, K.F. Structural characterization of temperature-sensitive hydrogels by field emission scanning electron microscopy (FESEM). *Macromol.Symp.,* **2004**, *210*, 501–511.

16. Utrata-Wesolek, A.; Trzebicka, B.; Dworak, A.; Ivanova, S.; Christova, D. Thermoresponsive hydrogels of hydrophobically modified polyglycidol. *e-Polymers*, **2007,** 19.

17. Xia, Y.; Yin, X.; Burke, N. A. D.; Stover, H. D. H. Thermal Response of Narrow-Disperse Poly(*N*-isopropylacrylamide) Prepared by Atom Transfer Radical Polymerization. Macromolecules *2005*, 38, 5937-5943

18. Liu, H.; Zhu, X. Lower critical solution temperatures of N-substituted acrylamide copolymers in aqueous solutions. Polymer *1999*, 40, 6985-6990.

19. Cao, Y.; Zhu, X.; Luo, J.; Liu, H. Effects of Substitution Groups on the RAFT Polymerization of *N*-Alkylacrylamides in the Preparation of Thermosensitive Block Copolymers. Macromolecules *2007,* 40, 6481-6488

20. Angelopoulos, S. A.; Tsitsilianis, C., Thermo-Reversible Hydrogels Based on Poly(N,N-diethylacrylamide)-block-poly(acrylic acid)-block-poly(N,N-diethylacrylamide) Double Hydrophilic Triblock Copolymer. *Macromolecular Chemistry and Physics* **2006,** *207* (23), 2188-2194.

21. Hacker, M. C.; Klouda, L.; Ma, B. B.; Kretlow, J. D.; Mikos, A. G. Synthesis and Characterization of Injectable, Thermally and Chemically Gelable, Amphiphilic Poly(N -Isopropylacrylamide)-Based Macromers. *Biomacromolecules* **2008,** *9,* 1558-1570.

22. Teodorescu, M.; Andrei, M.; Turturica, G.; Stanescu, P. O.; Zaharia, A.; Sarbu, A. Novel Thermoreversible Injectable Hydrogel Formulations Based on Sodium Alginate and Poly(N-Isopropylacrylamide). *Int. J. Polym. Mater. Polym. Biomater.* **2015,** *64,* 763-771.

23. H. Feil, Y.H. Bae, J. Feijen, S.W. Kim, Effect of copolymer hydrophilicity and ionization on the lower critical solution temperature of N-isopropylacrylamide copolymers, *Macromolecules* **1993**, *26,* 2496–2500.

24. F. Kohori, K. Sakai, T. Aoyagi, M. Yokoyama, Y. Sakurai, T. Okano, Preparation and characterization of thermally responsive block copolymer micelles comprising poly(N-isopropylacrylamide-b-D,L-lactide). *Journal of Controlled Release* **1998**, *55,* 87–98.

25. Pertici, V.; Pin-Barre, C.; Rivera, C.; Pellegrino, C.; Laurin, J.; Gigmes, D.; Trimaille, T. Degradable and Injectable Hydrogel for Drug Delivery in Soft Tissues. Biomacromolecules 2019, 20, 149-163.

26. Gan, J.; Guan, X.; Zheng, J.; Guo, H.; Wu, K.; Liang, L.; Lu, M., Biodegradable, thermoresponsive PNIPAM-based hydrogel scaffolds for the sustained release of levofloxacin. *RSC Advances* **2016,** *6* (39), 32967-32978.

27. Xuan, S.; Lee, C.-U.; Chen, C.; Doyle, A. B.; Zhang, Y.; Guo, L.; John, V. T.; Hayes, D.; Zhang, D., Thermoreversible and Injectable ABC Polypeptoid Hydrogels: Controlling the Hydrogel Properties through Molecular Design. *Chemistry of Materials* **2016,** *28* (3), 727-737.

28. Lahasky, S. H.; Hu, X.; Zhang, D. Thermoresponsive Poly(α-peptoid)s: Tuning the Cloud Point Temperatures by Composition and Architecture. *ACS Macro Lett.* **2012,** *1,* 580-584.

29. Fetsch, C.; Flecks, S.; Gieseler, D.; Marschelke, C.; Ulbricht, J.; van Pee, K.; Luxenhofer, R.

Self-Assembly of Amphiphilic Block´ Copolypeptoids with C2-C5 Side Chains in Aqueous Solution. *Macromol. Chem. Phys.* **2015**, *216*, 547-560.

30. Ulbricht, J.; Jordan, R.; Luxenhofer, R. On the Biodegradability of Polyethylene Glycol, Polypeptoids and Poly(2-oxazoline)s. *Biomaterials* **2014**, *35*, 4848-4861.

31. Zhang, D.; Lahasky, S. H.; Guo, L.; Lee, C.-U.; Lavan, M. Polypeptoid Materials: Current Status and Future Perspectives. *Macromolecules* **2012**, *45*, 5833-5841.

32. Robinson, J. W.; Secker, C.; Weidner, S.; Schlaad, H. Thermoresponsive Poly(N-C3 glycine)s. *Macromolecules* **2013,** *46* (3), 580-587.

33. Jiang, N.; Yu, T.; Darvish, O. A.; Qian, S.; Mkam Tsengam, I. K.; John, V.; Zhang, D., Crystallization-Driven Self-Assembly of Coil–Comb-Shaped Polypeptoid Block Copolymers: Solution Morphology and Self-Assembly Pathways. *Macromolecules* **2019,** *52* (22), 8867-8877.

34. Greer, D. R.; Stolberg, M. A.; Kundu, J.; Spencer, R. K.; Pascal, T.; Prendergast, D.; Balsara, N. P.; Zuckermann, R. N. Universal relationship between molecular structure and crystal structure in peptoid polymers and prevalence of the cis backbone conformation. *J. Am. Chem. Soc.* **2018,** *140*, (2), 827–833.

35. Lee, C.-U.; Li, A.; Ghale, K.; Zhang, D. Crystallization and melting behaviors of cyclic and linear polypeptoids with alkyl side chains. *Macromolecules* **2013,** 46, (20), 8213-8223.

36. Lee, C.-U.; Smart, T. P.; Guo, L.; Epps, T. H.; Zhang, D. Synthesis and characterization of amphiphilic cyclic diblock copolypeptoids from n-heterocyclic carbene-mediated zwitterionic polymerization of n-substituted n-carboxyanhydride. *Macromolecules* **2011,** 44, (24), 9574-9585.

37. Greer, D. R.; Stolberg, M. A.; Kundu, J.; Spencer, R. K.; Pascal, T.; Prendergast, D.; Balsara, N. P.; Zuckermann, R. N. Universal relationship between molecular structure and crystal structure in peptoid polymers and prevalence of the cis backbone conformation. *J. Am. Chem. Soc.* **2018,** 140, (2), 827–833.

38. Zhou, C.; Toombes, G. E. S.; Wasbrough, M. J.; Hillmyer, M. A.; Lodge, T. P. Structure of two-compartment hydrogels from thermoresponsive abc triblock terpolymers. *Macromolecules* **2015,** 48, (16), 5934-5943.

39. Pedersen, J. S.; Gerstenberg, M. C. Scattering Form Factor of Block Copolymer Micelles. *Macromolecules* **1996**, *29*, 1363−1365.

40. Pedersen, J. S. Form factors of block copolymer micelles with spherical, ellipsoidal and cylindrical cores. *J. Appl. Crystallogr*. **2000**, *33*, 637−640.

APPENDIX A. COPYRIGHT RELEASES

A.1. Copyright release for Chapter 3

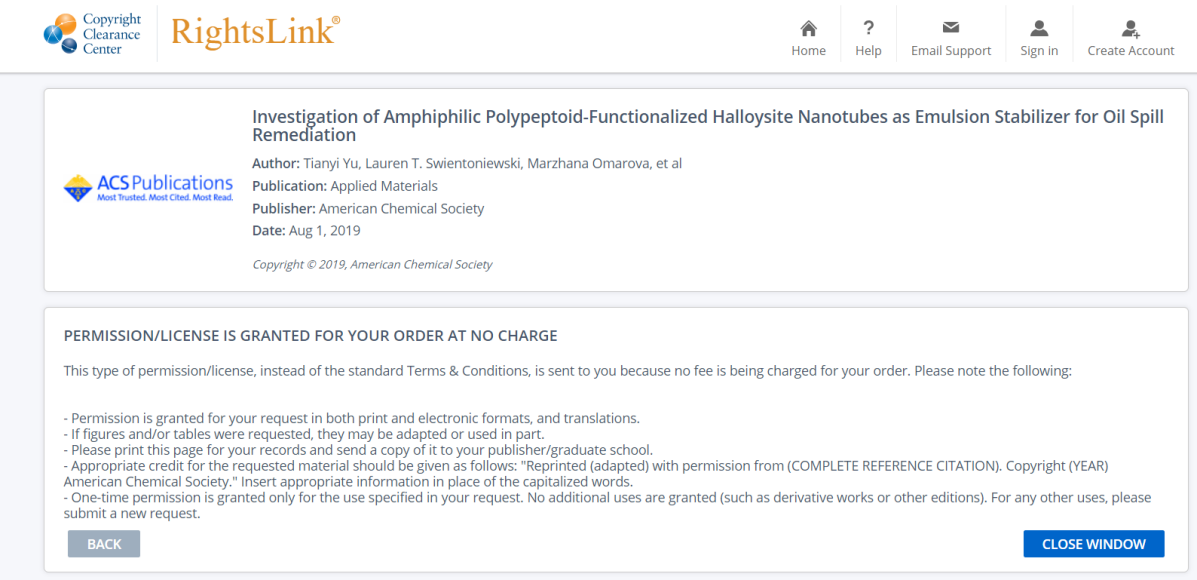

A.2. Permission to use Figure 4.1

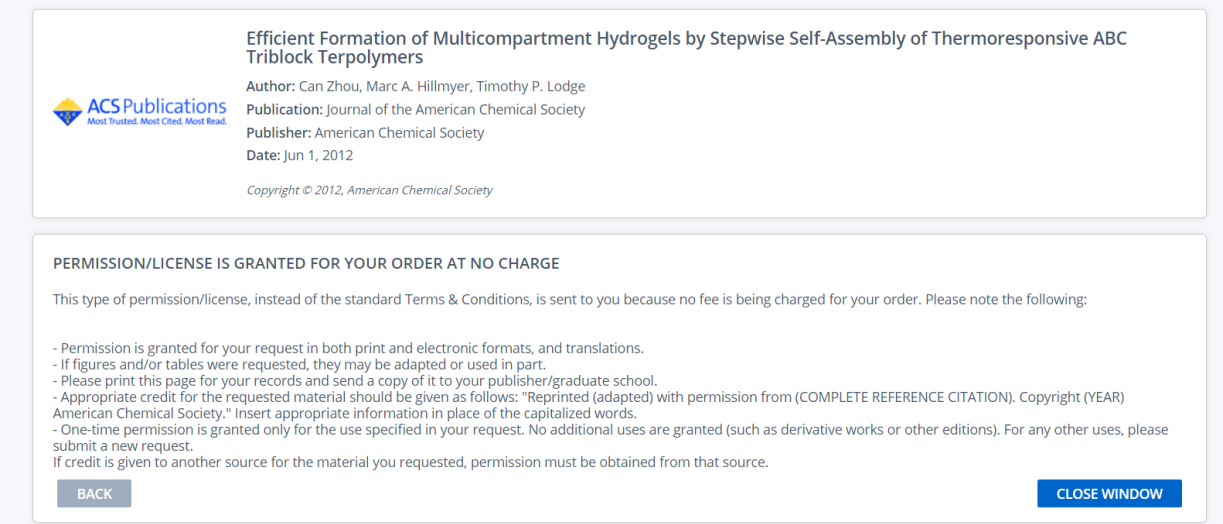

Efficient Formation of Multicompartment Hydrogels by Stepwise Self-Assembly of Thermoresponsive ABC Triblock Terpolymers

Author: Can Zhou, Marc A. Hillmyer, Timothy P. Lodge
Publication: Journal of the American Chemical Society
Publisher: American Chemical Society
Date: Jun 1, 2012

PERMISSION/LICENSE IS GRANTED FOR YOUR ORDER AT NO CHARGE

This type of permission/license, instead of the standard Terms & Conditions, is sent to you because no fee is being charged for your order. Please note the following:

- Permission is granted for your request in both print and electronic formats, and translations.
- If figures and/or tables were requested, they may be adapted or used in part.
- Please print this page for your records and send a copy of it to your publisher/graduate school.
- Appropriate credit for the requested material should be given as follows: "Reprinted (adapted) with permission from (COMPLETE REFERENCE CITATION). Copyright (YEAR) American Chemical Society." Insert appropriate information in place of the capitalized words.
- One-time permission is granted only for the use specified in your request. No additional uses are granted (such as derivative works or other editions). For any other uses, please submit a new request.

If credit is given to another source for the material you requested, permission must be obtained from that source.

BACK CLOSE WINDOW

A.3. Permission to use Figure 4.2

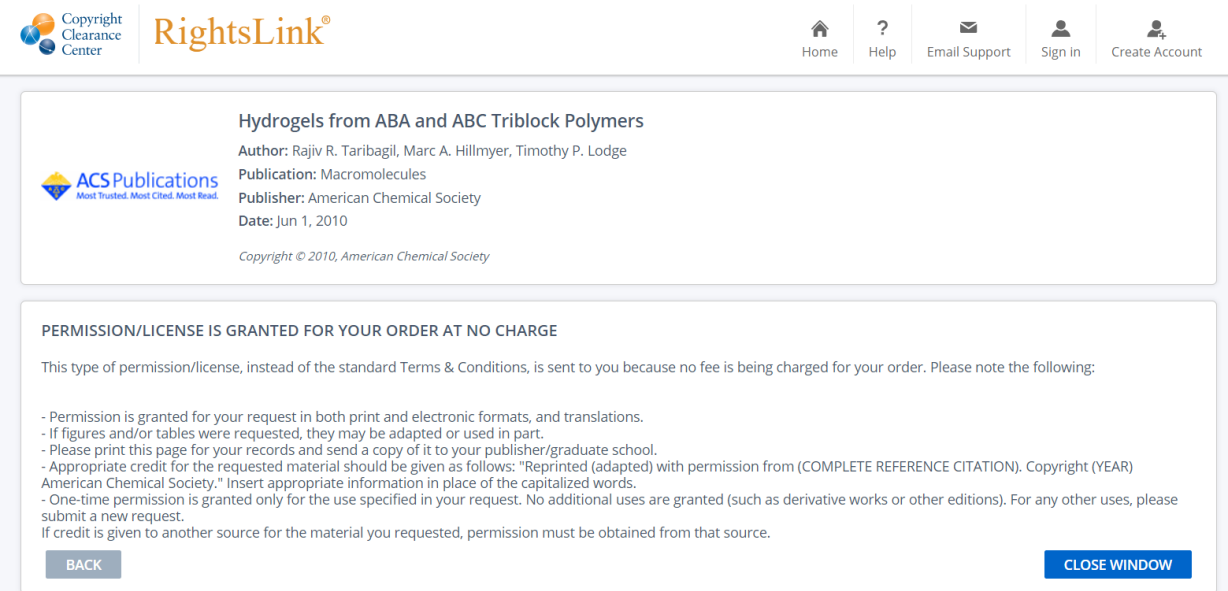

APPENDIX B. SUPPLEMENTAL INFORMATION FOR CHAPTER 2

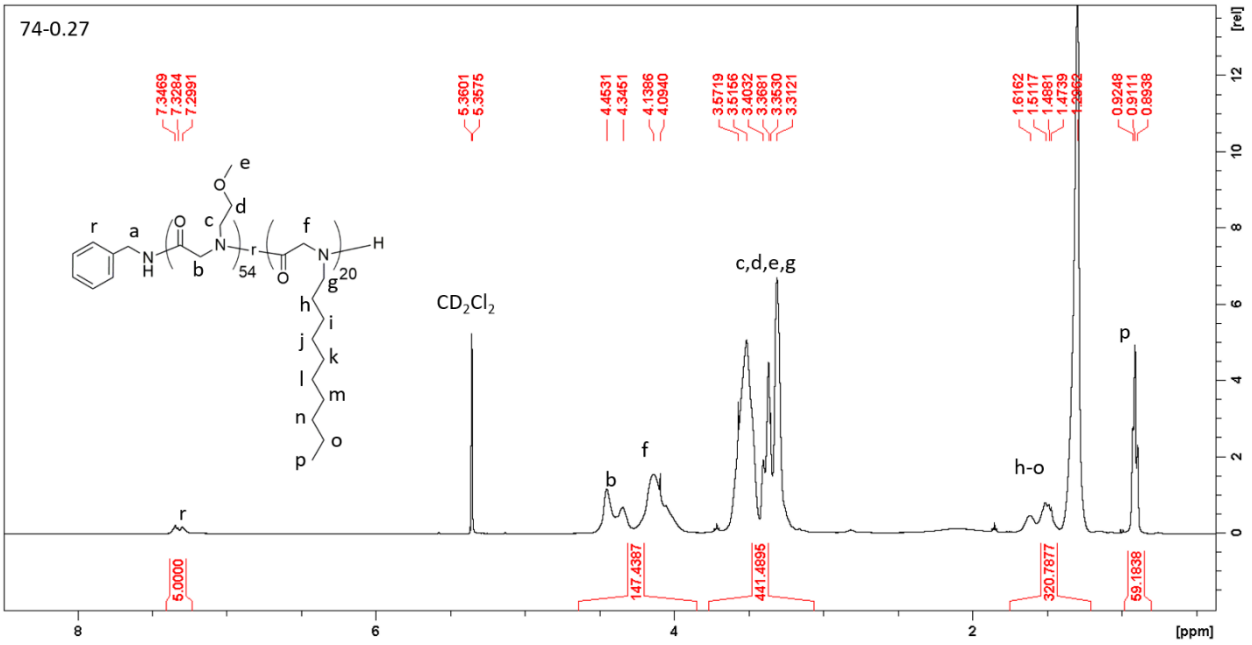

Figure S2.1. ^{1}H NMR spectrum of PNMeOEtG$_{54}$-*r*-PNDG$_{20}$ (74-0.27) random copolypeptoid in CD_2Cl_2

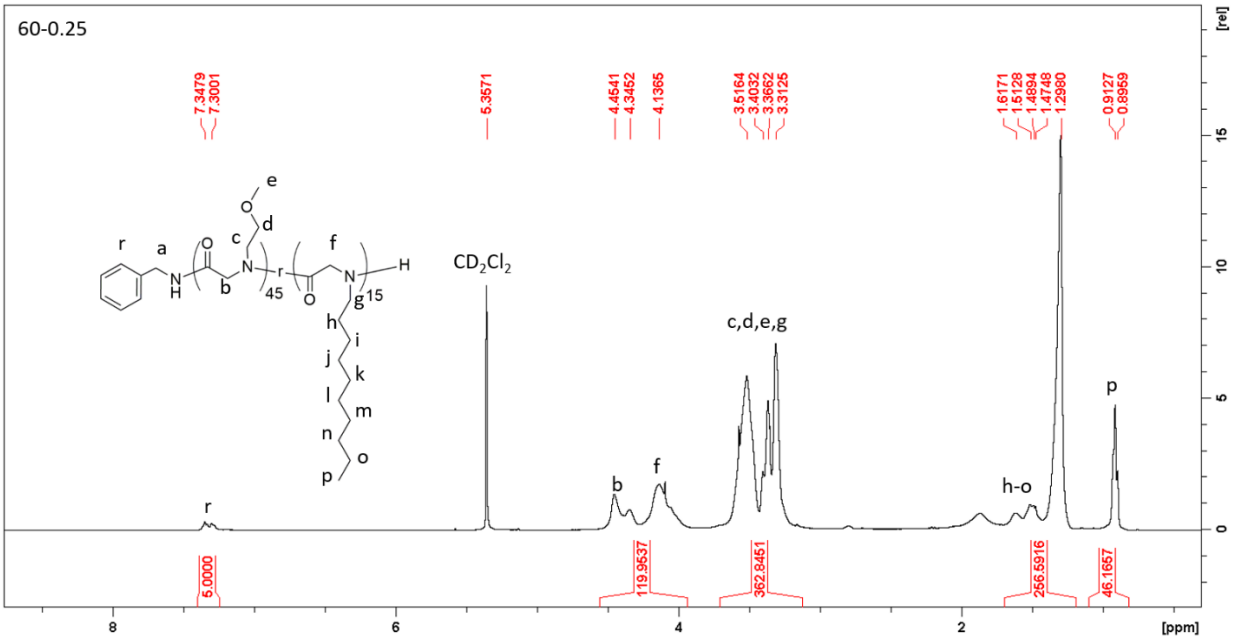

Figure S2.2. ^{1}H NMR spectrum of PNMeOEGt$_{45}$-*r*-PNDG$_{15}$ (60-0.25) random copolypeptoid in CD_2Cl_2.

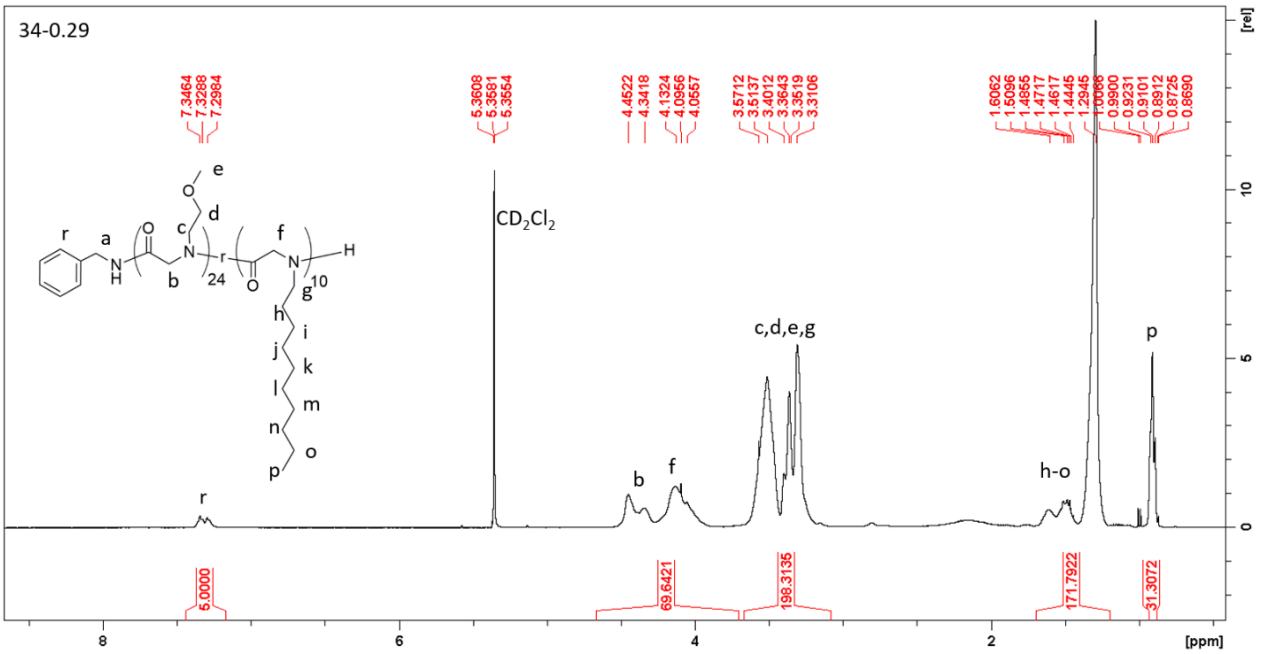

Figure S2.3. ^{1}H NMR spectrum of PNMeOEtG$_{24}$-*r*-PNDG$_{10}$ (34-0.29) random copolypeptoid in CD_2Cl_2

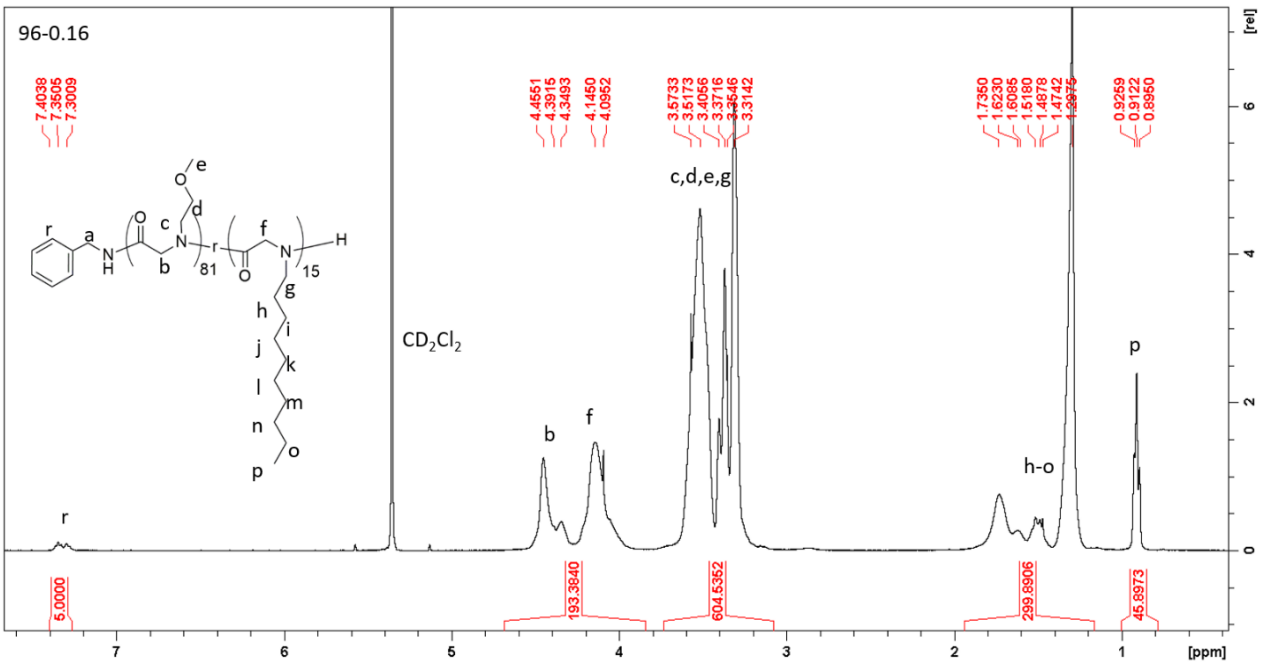

Figure S2.4. ^{1}H NMR spectrum of PNMeOEtG$_{81}$-*r*-PNDG$_{15}$ (96-0.16) random copolypeptoid in CD_2Cl_2.

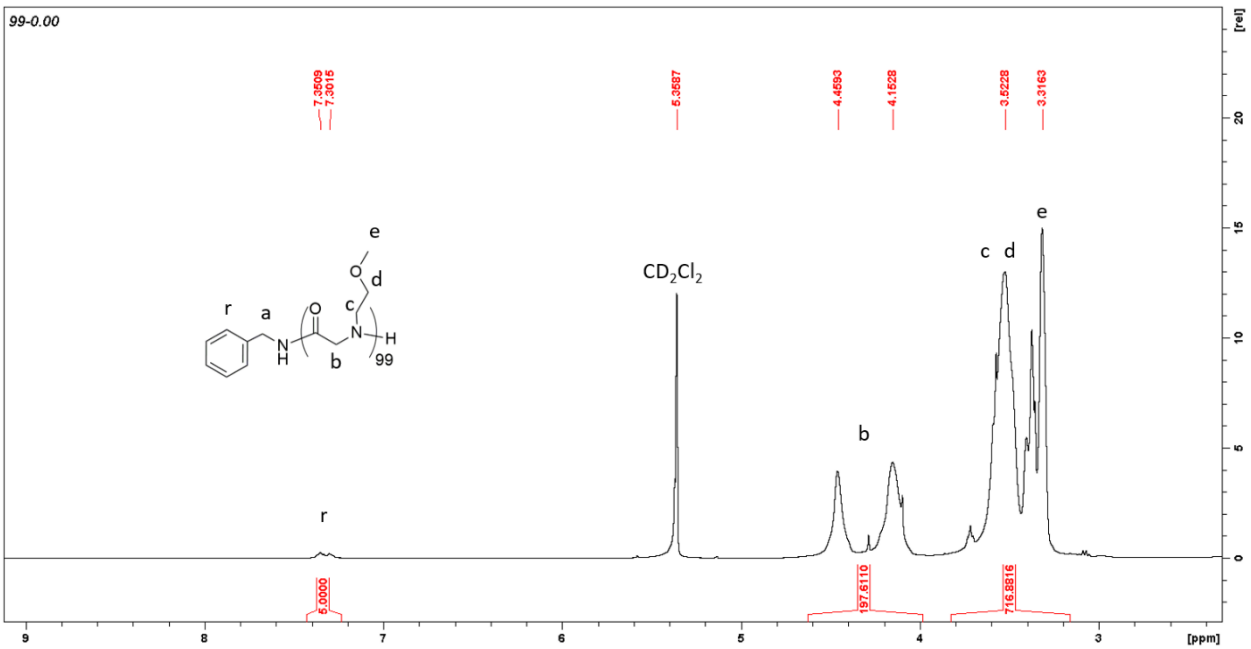

Figure S2.5. ^{1}H NMR spectrum of the PNMeOEt$_{99}$ (99-0.00) random copolypeptoid in CD_2Cl_2.

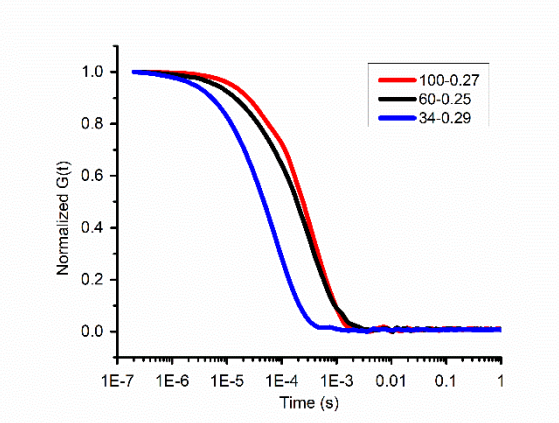

Figure S2.6. Normalized G(t) for HMP-0.27 polymers (DP_n = 34- 100) aqueous solution at 5 mg/ml.

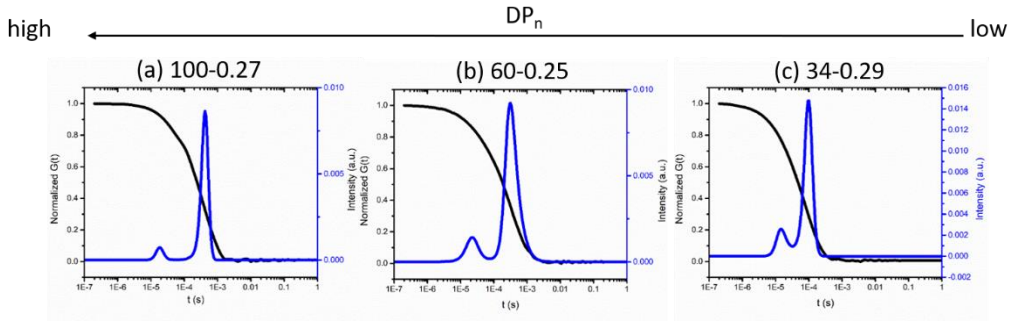

Figure S2.7. Normalized G(t) and decay time distributions for HMP-0.27 polymers with varying molecular weights (DP_n = 34 - 100) in water at 5mg/ml. The decay time distribution was analyzed using MEM analysis method.

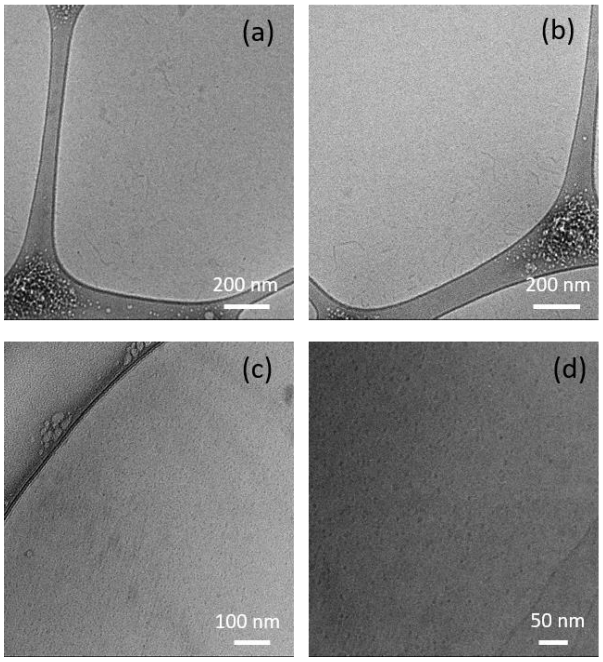

Figure S2.8. Cryo-TEM images of 5 mg/ml aqueous solutions of (a)-(b) 100-0.27 and (c)-(d) 34-0.29 polymers.

Table S2.1. Sizes of HMPs in aqueous solutions

polymer[a]	R_{h1} (nm)[b]	R_{h2} (nm)[c]
100-0.27	3.8 ± 0.3	84.5 ± 0.2
60-0.25	4.9 ± 0.4	72.1 ± 0.4
34-0.29	3.5 ± 0.4	20.1 ± 0.3
96-0.16	3.9 ± 0.4	75.8 ± 0.5

[a.] The sizes of HMP polymers at 5 mg/ml in aqueous solutions were measured by DLS and analyzed using MEM methods. Polymer aqueous solutions were prepared using DCM thin film hydration method followed by stirring at 350 rpm at 25˚C for overnight and filtered through 0.45 µm PES syringe filters before DLS measurement. [b.] R_{h1} represents the hydrodynamic radius corresponding to the intensity distribution peak at lower decay time. [c.] R_{h2} represents the hydrodynamic radius corresponding to the intensity distribution peak at higher decay time.

Table S2.2. Sizes of HMPs and lipid complexes (HMP+lip)

polymer/lipid complex	R_{h1} (nm)[a]	R_{h2} (nm)
100-0.27+lip	9.2 ± 0.5	102.3 ± 0.5
60-0.25+lip	7.2 ± 0.6	70.5 ± 0.5
34-0.29+lip	4.9 ± 0.5	33.6 ± 0.4
96-0.16+lip	11.4 ± 0.7	125.3 ± 0.2
99-0.00+lip	N/A	76.1 ± 0.4

[a.] The sizes of HMP polymer and lipid complexes (HMP+lip) were analyzed using MEM analysis method based on the results of DLS measurements. [b.] R_{h1} refers to the hydrodynamic radius corresponding to the intensity distribution peak at lower decay time. [c.] R_{h2} refers to the hydrodynamic radius corresponding to the peak at higher decay time.

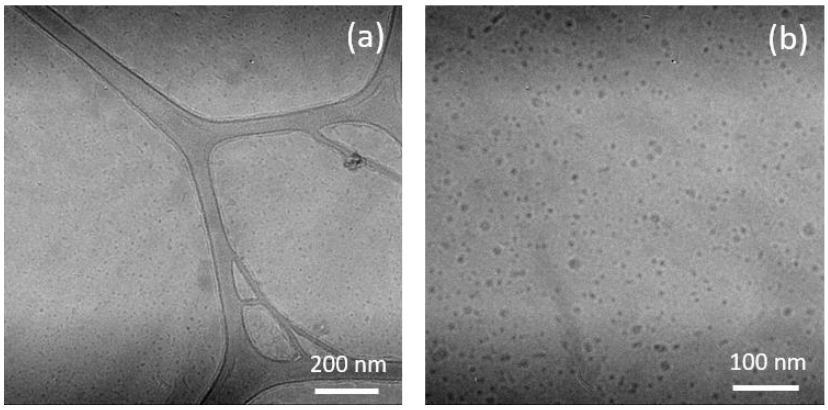

Figure S2.9. Cryo-TEM images of 60-0.25+lip after incubating polymer with liposomes for 3 days.

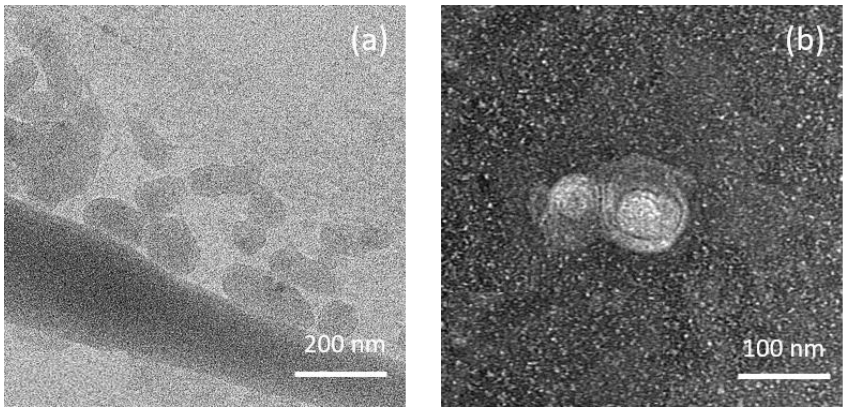

Figure S2.10. (a) Cryo-TEM and (b) negative stained TEM images of 99-0.00+lip

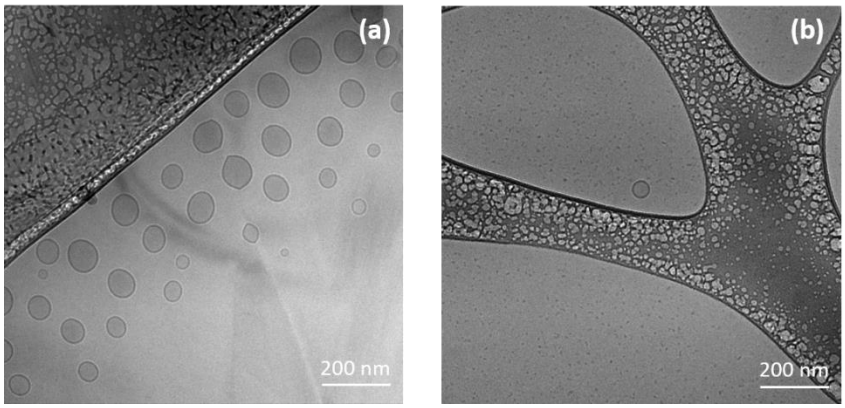

Figure S2.11. Cryo-TEM images E. Coli liposomes (a) before and (b) after addition of 92-0.22 polymers.

APPENDIX C. SUPPLEMENTAL INFORMATION FOR CHAPTER 3

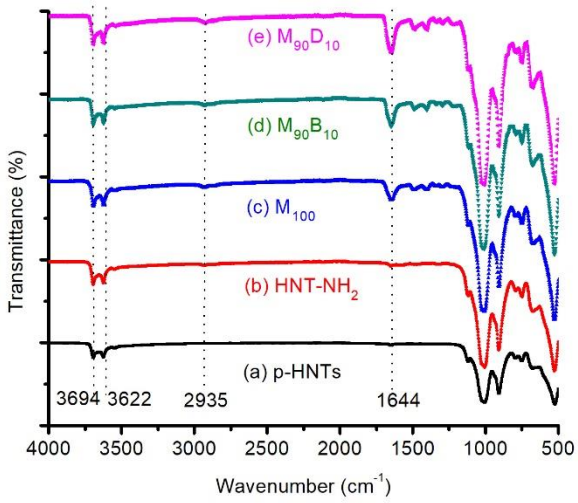

Figure S3.1. FT-IR spectra of (a) the pristine HNTs (p-HNTs), (b) initiator modified HNTs (HNT-NH_2) and homo- or copolypeptoid-grafted HNTs [*i.e.*, (c) M_{100}; (d) $M_{90}B_{10}$; (e) $M_{90}D_{10}$] respectively.

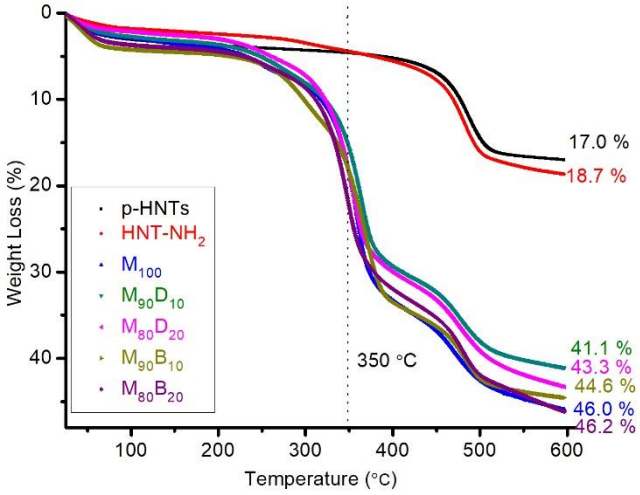

Figure S3.2. Thermograms of pristine HNTs (p-HNTs) and varying polypeptoid-grafted HNTs (g-HNTs) prepared with same initial monomer-to-HNTs-NH_2 feed ratio (f = 2.5) from TGA. The most rapid weight loss temperature is at ~ 350 °C, in agreement with the reported decomposition temperature (T_d) of free poly(*N*-alkylglycine).[70,71]

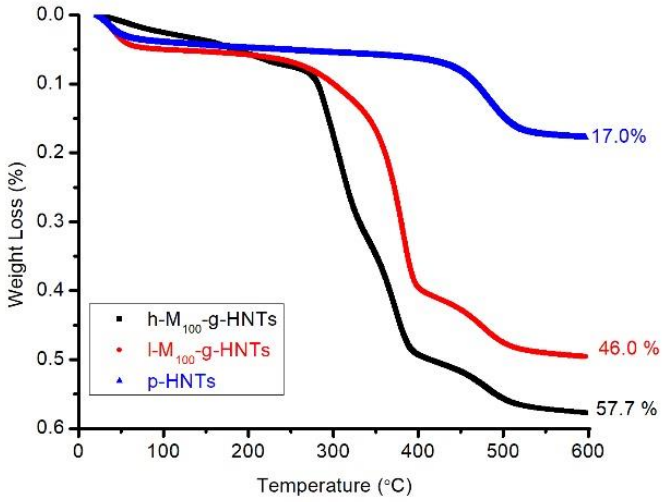

Figure S3.3. Thermograms of pristine HNTs (p-HNTs) and two M_{100}-g-HNTs samples that were prepared by using two different initial monomer-to-initiator molar ratio (*i.e.*, f = 2.5 for l-M_{100}-g-HNTs and f = 5 for h-M_{100}-g-HNTs) by TGA. The weight percentages of polypeptoids grafted on the g-HNTs were shown to increase from 29.0% to 40.7% as the initial monomer-to-HNT-NH_2 ratio increases from 2.5 to 5.

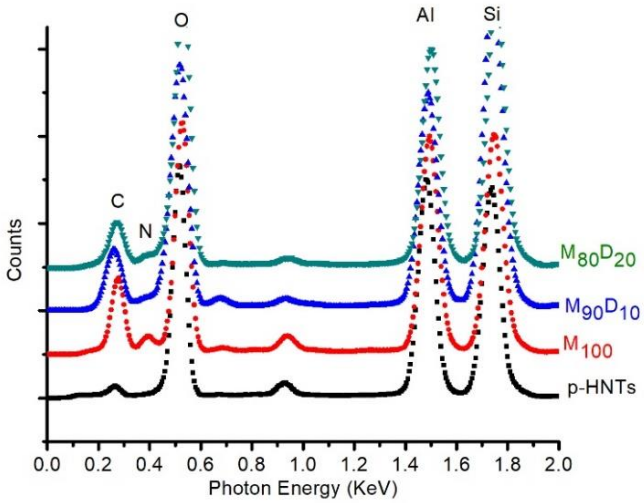

Figure S3.4. Energy-dispersive X-ray spectroscopic (EDS) analysis of p-HNTs, M_{100}-, $M_{90}D_{10}$- and $M_{80}D_{20}$-g-HNTs samples. The emergence of N atom signals and an increased relative atomic content of C and O atom relative to the pristine HNTs support the successful grafting of polypeptoids onto the HNT surface. The C signals of the p-HNTs were due to the carbon coating on the TEM grid.

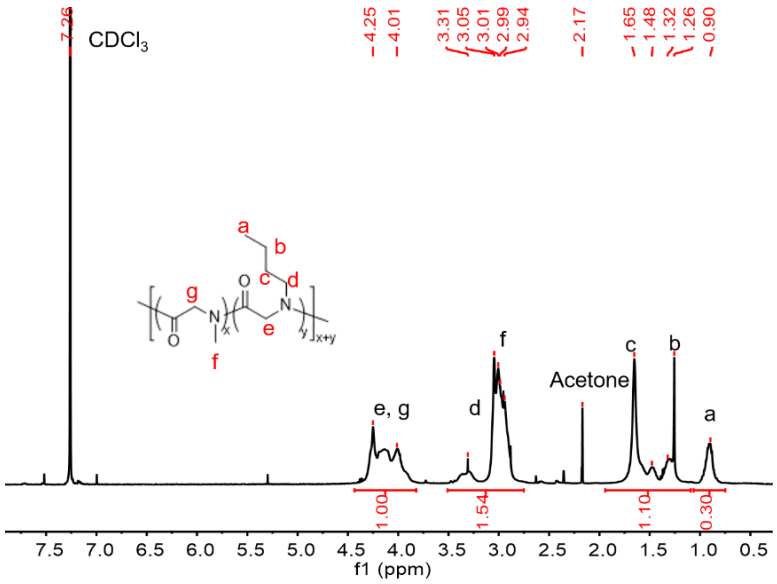

Figure S3.5. Full ^{1}H-NMR spectrum of the $M_{80}B_{20}$ polymer that was cleaved off from $M_{80}B_{20}$-g-HNTs by HF treatment.

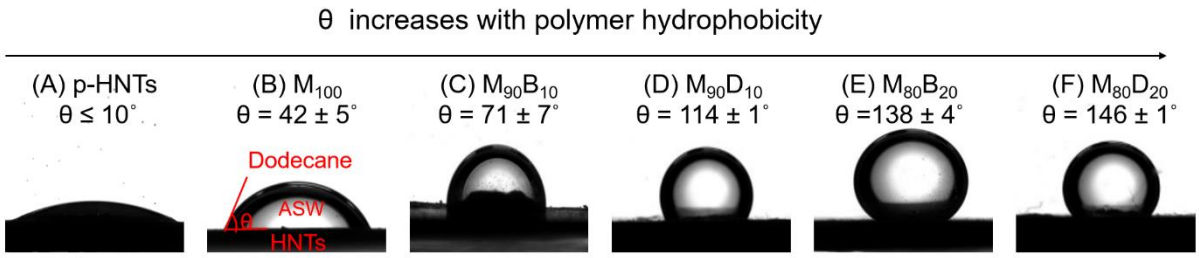

Figure S3.6. Three-phase contact angle (θ) measurement amongst *n*-dodecane, artificial sea water (ASW) and pristine-HNT (p-HNTs) or various polypeptoids-grafted HNTs. θ was found to increase from (a) < 10 ° for p-HNTs to (b) 42 ± 5 ° for the homo-polypeptoid-grafted HNTs (M_{100}) and further up to 146 ± 1˚ for copolypeptoid-grafted HNTs ($M_{80}D_{20}$). This indicates that the wettability of the HNTs at the oil-water interface can be effectively controlled by the grafting of polypeptoids with varying HLB characteristics on the HNT surface.

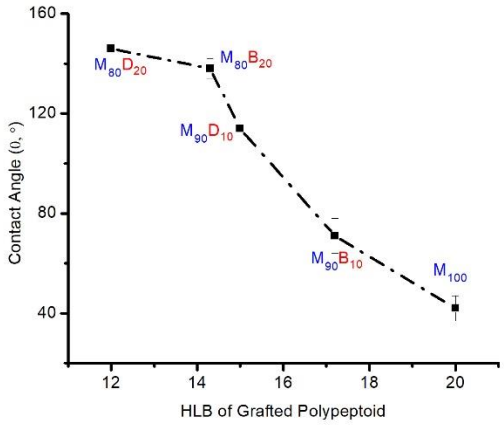

Figure S3.7. Plot of 3-phase contact angle amongst *n*-dodecane, artificial sea water (ASW) and various polypeptoid-grafted HNTs versus the HLB parameter of the corresponding polypeptoids (Table 3.1).

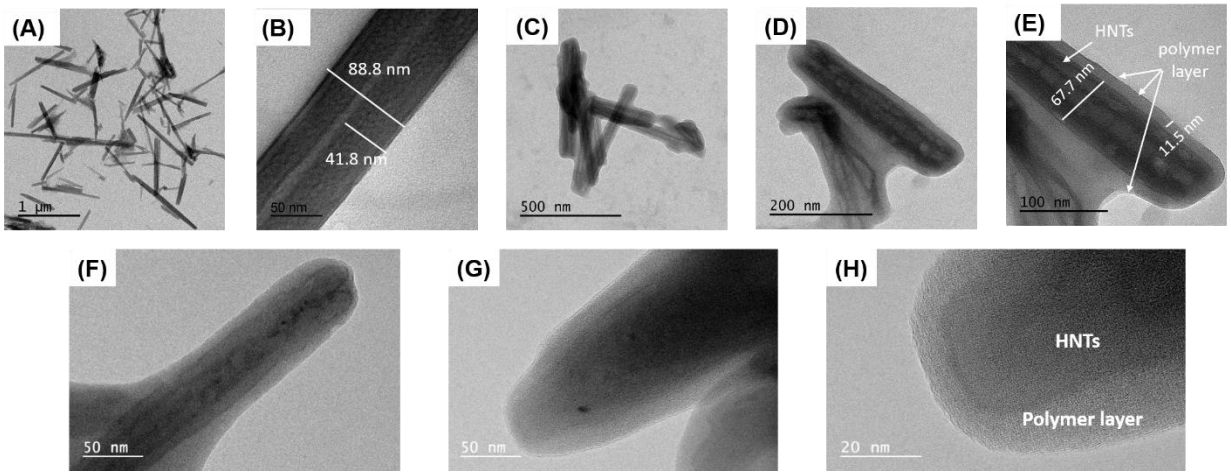

Figure S3.8. Additional TEM images of (A, B) p-HNTs, (C-E) $M_{90}B_{10}$-g-HNTs and (F-H) $M_{90}D_{10}$-g-HNTs in dry state. In contrast to pristine HNTs showing a smooth external surface (A, B), a low electron density layer on the external surface of the g-HNTs were observed indicating the successful polymer grafting (C-H).

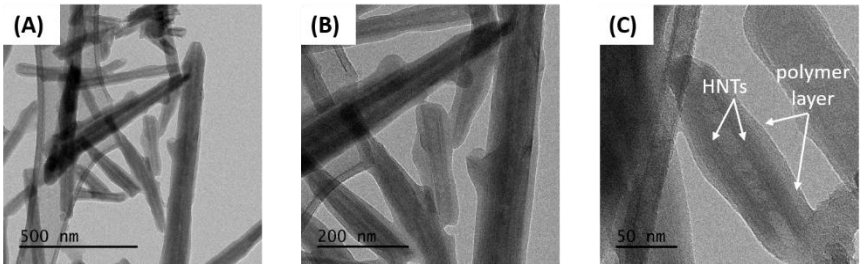

Figure S3.9. Cryo-TEM images of $M_{90}B_{10}$-g-HNTs in artificial saline water (0.5 wt%).

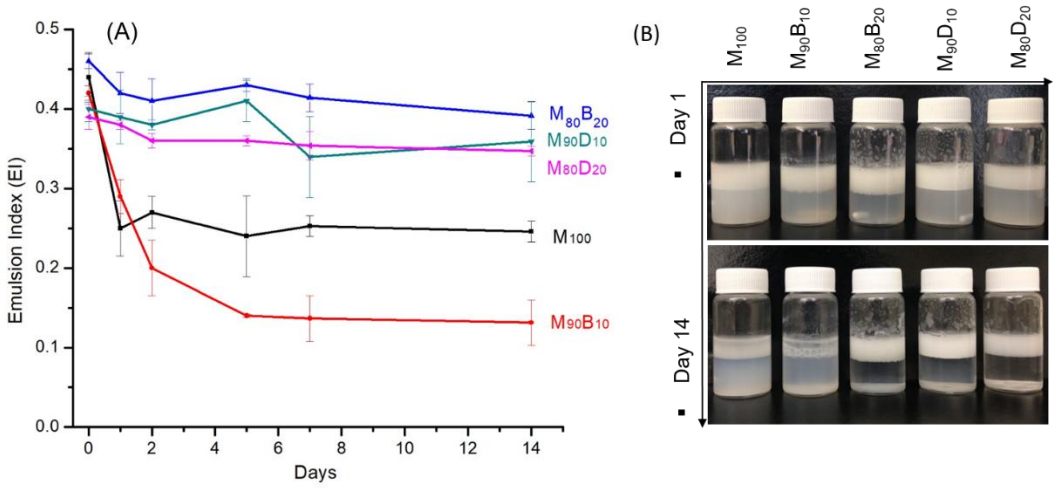

Figure S3.10. (A) Plot of emulsion index (EI) versus time for oil-in-ASW emulsions containing p-HNTs, M_{100}-, $M_{90}B_{10}$-, $M_{80}B_{20}$-, $M_{90}D_{10}$- and $M_{80}D_{20}$-g-HNTs respectively. (B) Optical images show the oil-in-ASW emulsions containing the respective p-HNTs or g-HNTs at 1 h (day 1) or 336 h (day 14) time point.

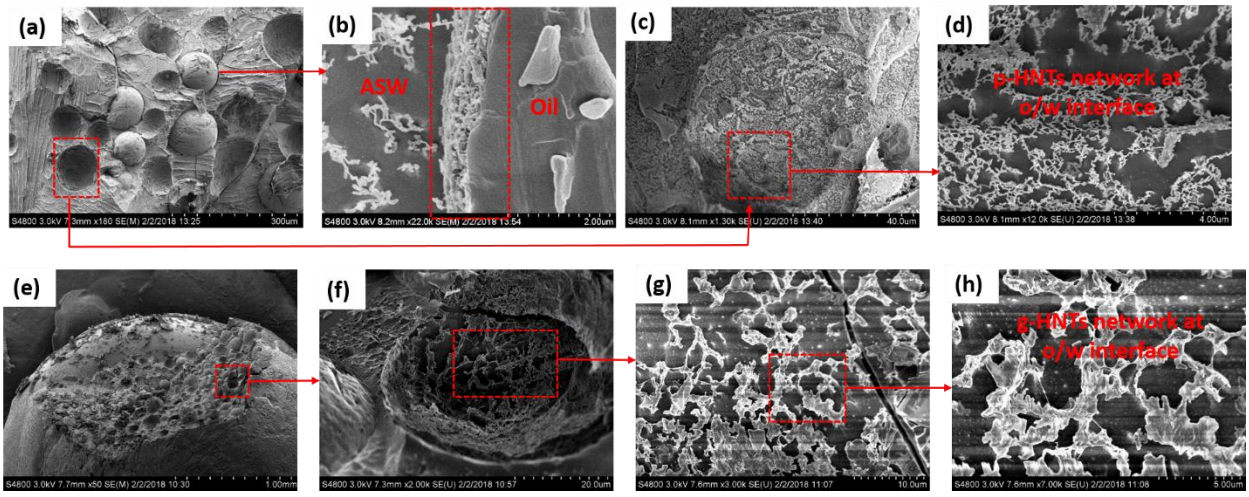

Figure S3.11. (a-d) Cryo-SEM images of the oil-water interfaces of *n*-dodecane/saline water emulsion stabilized by pristine-HNTs or (e-h) $M_{90}D_{10}$-g-HNTs, respectively. The oil-water interfaces were found to be covered with the flocculated HNT particle networks. In addition, the morphology of the particles differs before (a-d) and after (e-h) polymer functionalization. Polymer functionalization of HNTs has resulted in a more extended and interconnected HNT particle networks at the o/w interfaces.

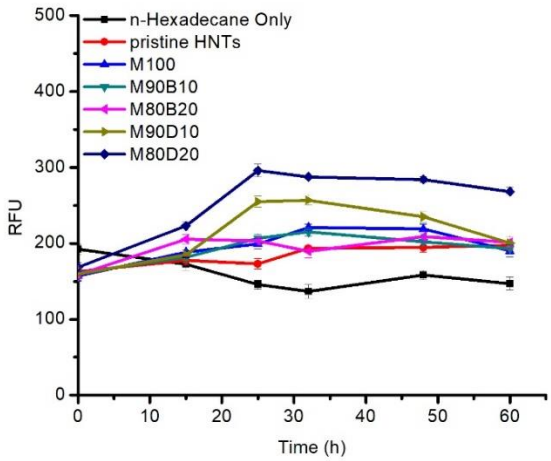

Figure S3.12. A. borkumensis cell growth study in the presence of p-HNTs, M100-, M90B10-, M80B20-, M90D10- and M80D20-g-HNTs respectively without any endogenous nitrogen source in the ONR7a culture medium. 1% w/v n-hexadecane was added in each sample as carbon source. One control group was designed without any HNTs particles added, named as n-hexadecane Only. The grafted polypeptoids on HNTs can also enhance the bacteria cell growth presumably by serving as a nitrogen source, evidenced by a notable bacterial cell growth in the presence of polypeptoid-grafted HNTs without endogenous nitrogen source in the ONR7a medium. However, the enhancement effect here is much less pronounced than when the endogenous nitrogen source is present in the culture medium (Figure 3.6(a)).

Table S3.1. A summary of fitting parameters for the plots of steady shear viscosities (ŋ) versus shear rate for *n*-dodecane-in-ASW emulsions stabilized by different polypeptoid-grafted HNTs or pristine HNTs in low shear rate range (10^{-4}-10 s^{-1}) (Figure 3.5A) by using the Cross model.[a]

Entry #	Sample Name	HLB (Exptl.) [b]	η_0 [c] (Pa·s)	η_∞ [d] (mPa·s)	K [e] (s)	n [f]	Adj. R-Square [g]
1	p-HNT	N/A	11 ± 2	3.7 ± 0.3	1365 ± 300	1.08 ± 0.03	0.983
2	M_{100}-g-HNT	20.0	320 ± 20	16 ± 2	300 ± 30	1.30 ± 0.02	0.993
3	$M_{90}B_{10}$-g-HNT	17.2	2.4 ± 0.1	3.0 ± 0.2	330 ± 40	1.10 ± 0.02	0.994
4	$M_{90}D_{10}$-g-HNT	15.0	5100 ± 200	0	780 ± 40	1.090 ± 0.004	0.999
5	$M_{80}B_{20}$-g-HNT	14.3	870 ± 80	152 ± 9	1900 ± 300	0.99 ± 0.01	0.997
6	$M_{80}D_{20}$-g-HNT	12.0	1600 ± 200	0	3700 ± 700	0.800 ± 0.006	0.998

a. The steady shear viscosity is fitted by Orthogonal Distance Regression (ODR) in OriginPro with Cross model. The Cross model equation is: $\eta_\gamma = \eta_\infty + \frac{\eta_0 - \eta_\infty}{1+(k\gamma)^n}$, where ŋγ is the steady shear viscosity and γ is steady shear rate. b. HLB (Exptl.) is the experimental HLB characteristic of the grafted polypeptoids. It is defined as the mass fraction of the hydrophilic segments (M) over the entire polymer [HLB = 20 × (mx/mx+ my), mx: mass of hydrophilic segment (M), mx+my: total mass of both the hydrophilic (M) and hydrophobic (B or D) segments] and is calculated using the molar ratio between the M and B(D) segments determined by 1H NMR analysis. c. ŋ0 stands for zero shear viscosity. d. ŋ∞ represents infinite shear viscosity. e. k is the Cross time constant. f. n is the Cross rate index which is an important indicator measuring the dependence of viscosity on the shear rate in the shear-thinning region. Here, n was found to decrease with increasing hydrophobicity of the grafted polypeptoids from n=1.30 ± 0.02 for M100 (HLB=20.0) to n=0.80 ± 0.006 for M80D20 (HLB=12.0). g.Adjusted R-square value of the fitting is calculated using the Origin software.

APPENDIX D. SUPPLEMENTAL INFORMATION FOR CHAPTER 4

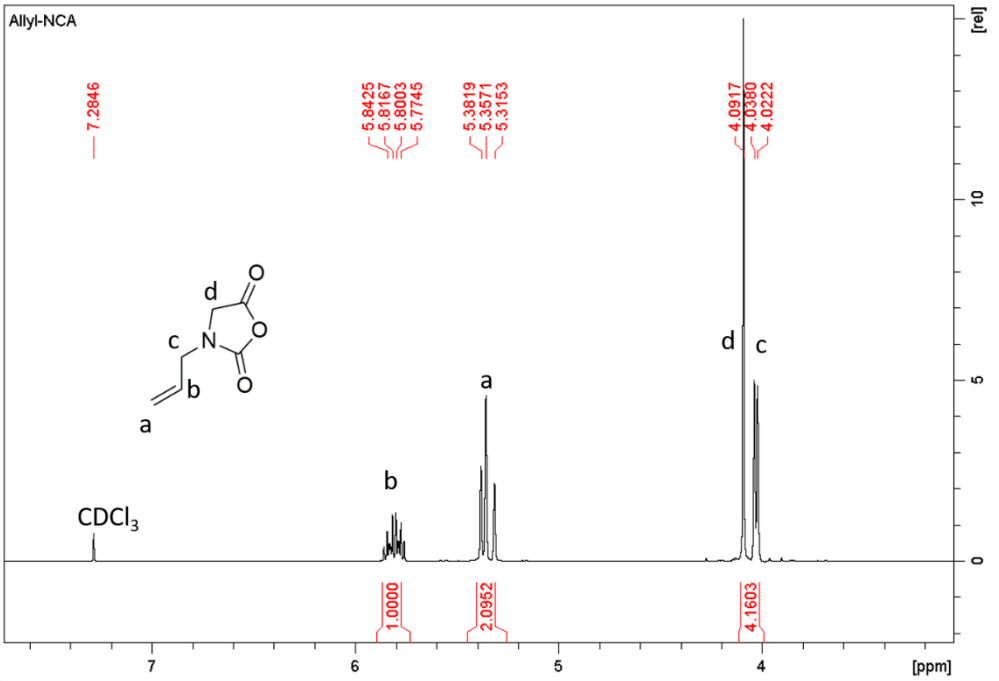

Figure S4.1. ^{1}H NMR spectrum of Allyl-NCA monomer in $CDCl_3$.

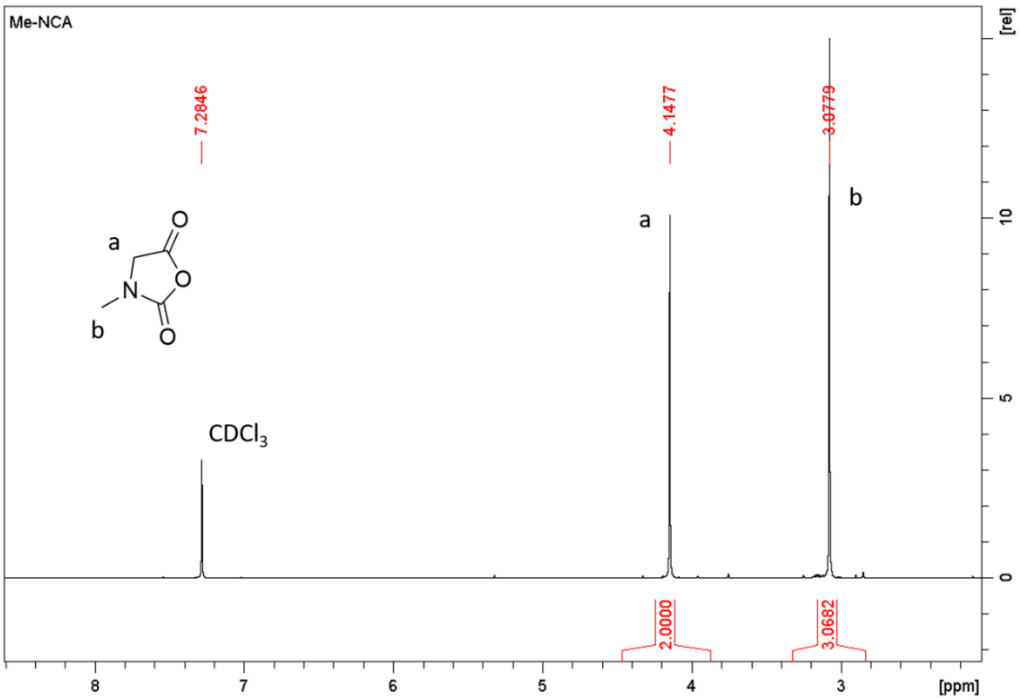

Figure S4.2. ^{1}H NMR spectrum of Me-NCA monomer in $CDCl_3$.

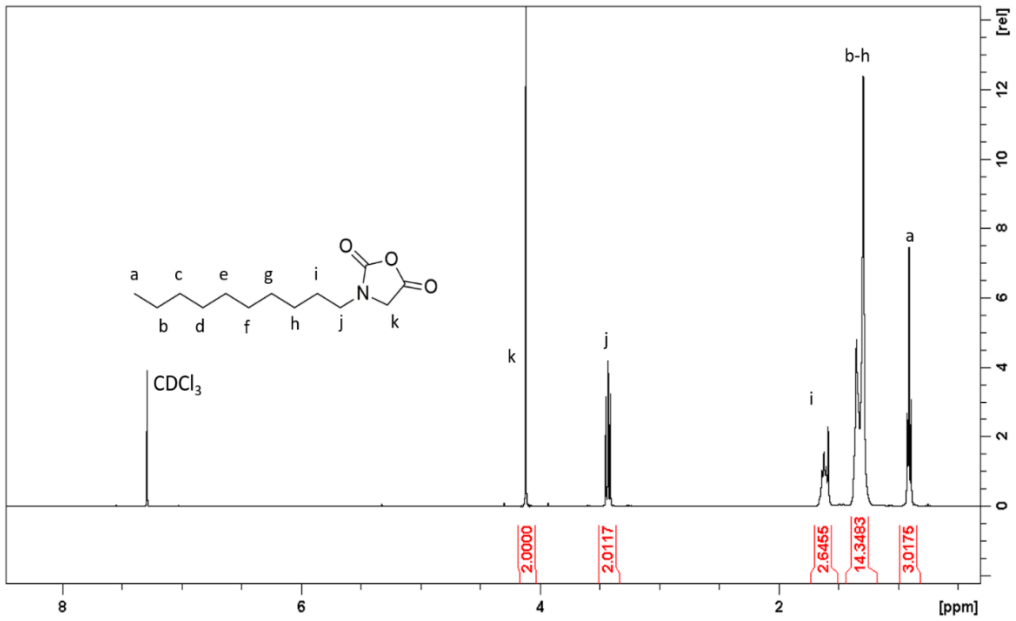

Figure S4.3. ^{1}H NMR spectrum of Decyl-NCA monomer in $CDCl_3$.

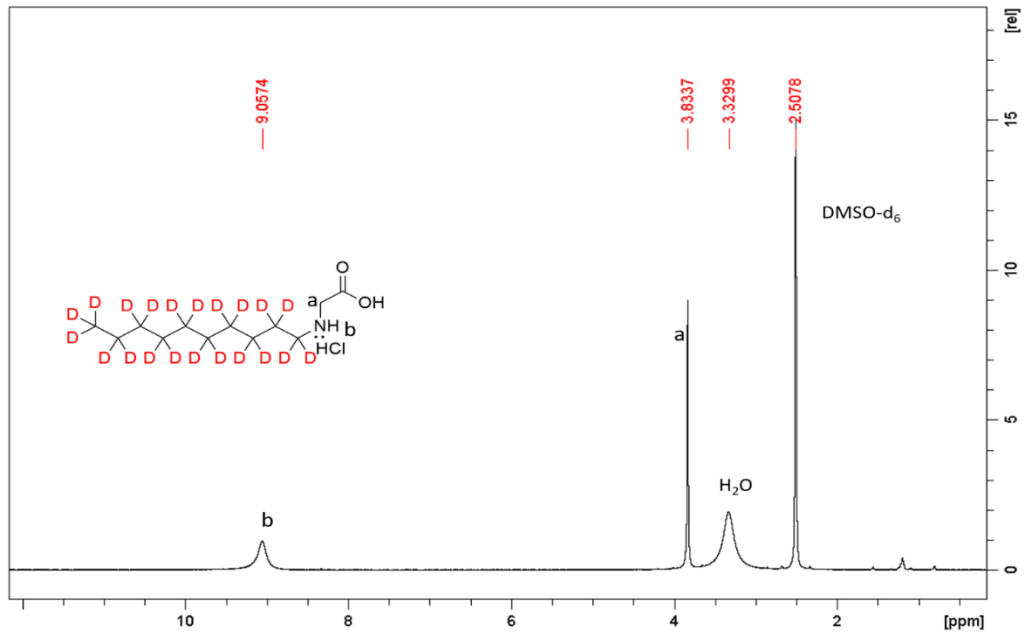

Figure S4.4. ^{1}H NMR spectrum of 2-(*N*,*N*-tert-butoxycarbonyl-n-decyl-d_{21}-amino)acetic acid (Compound **1**) in DMSO-d_6.

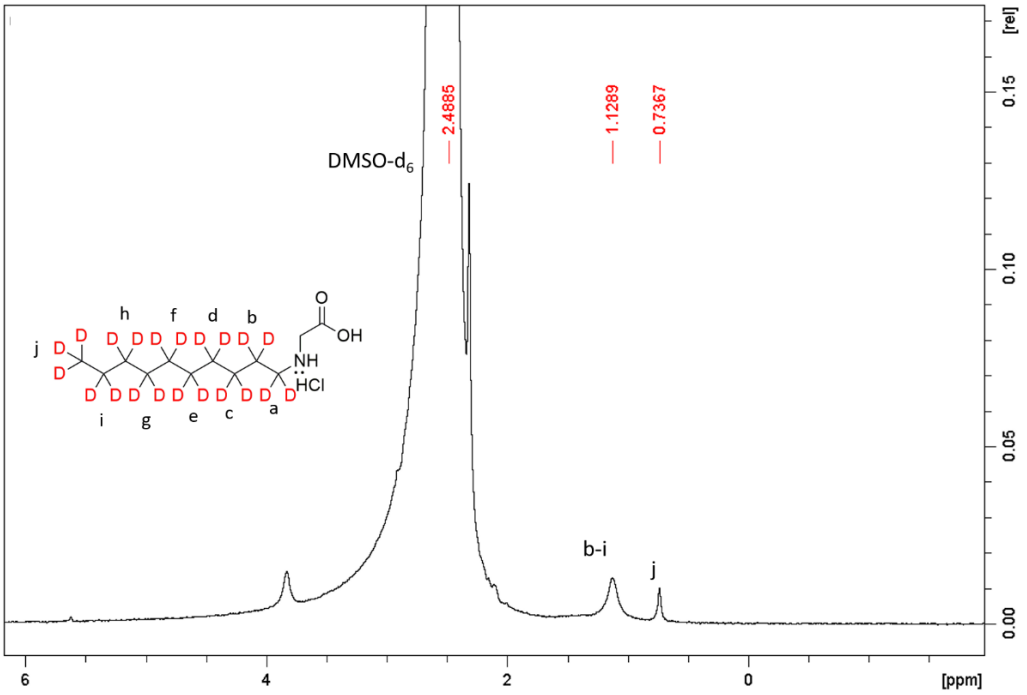

Figure S4.5. ^{2}H NMR spectrum of 2-(N,N-tert-butoxycarbonyl-n-decyl-d$_{21}$-amino)acetic acid (Compound **1**) in DMSO-d$_{6}$.

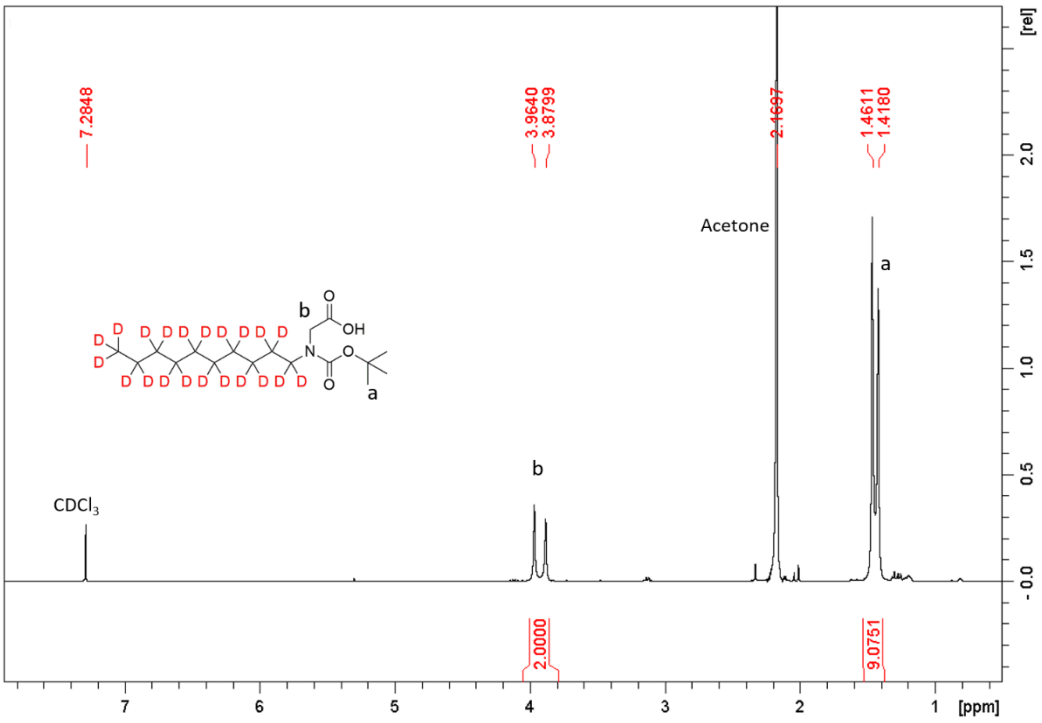

Figure S4.6. ^{1}H NMR spectrum of 2-(*N*,*N*-tert-butoxycarbonyl-n-decyl-d$_{21}$-amino)acetic acid (Compound **2**) in $CDCl_3$

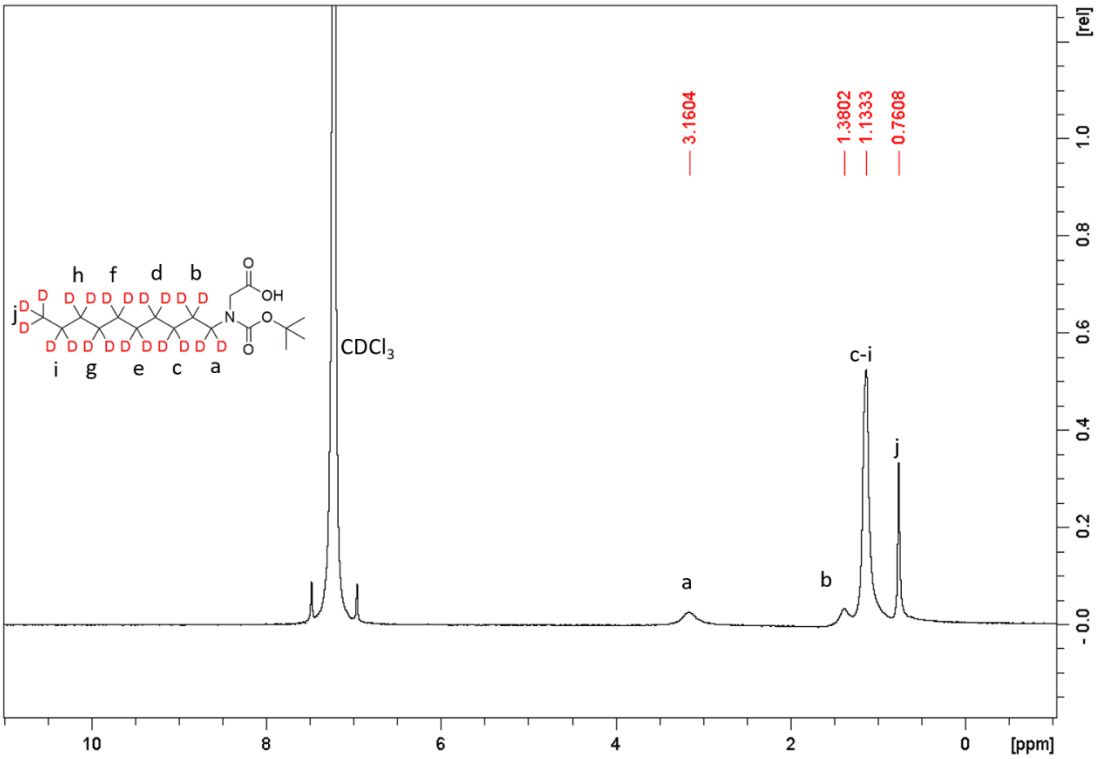

Figure S4.7. ^{2}H NMR spectrum of 2-(N,N-tert-butoxycarbonyl-n-decyl-d_{21}-amino)acetic acid (Compound **2**) in $CDCl_3$.

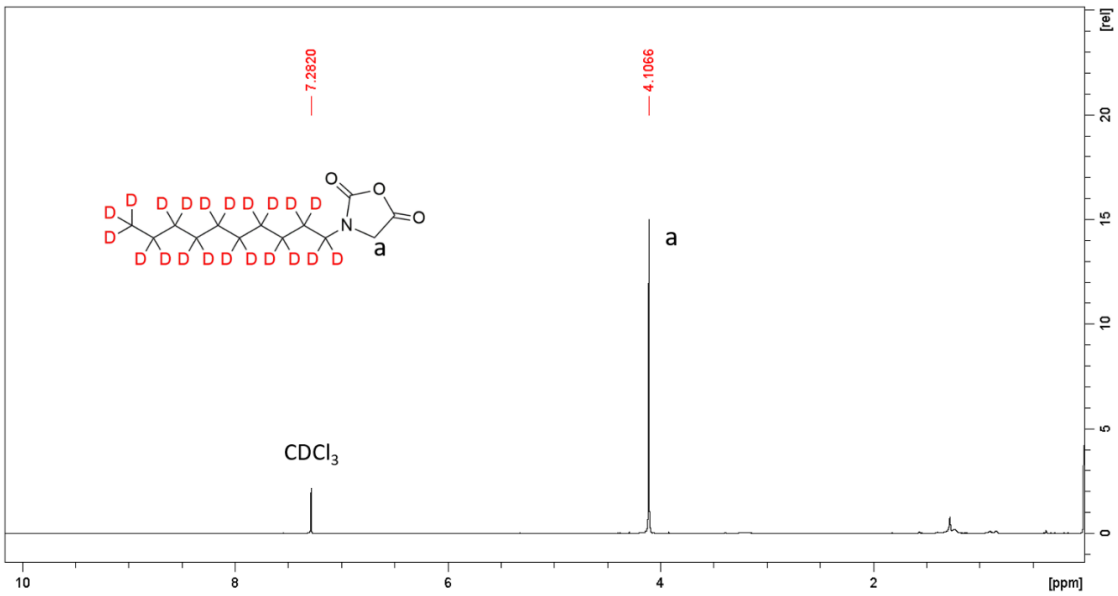

Figure S4.8 ^{1}H NMR spectrum of Decyl-d_{21}-NCA in $CDCl_3$.

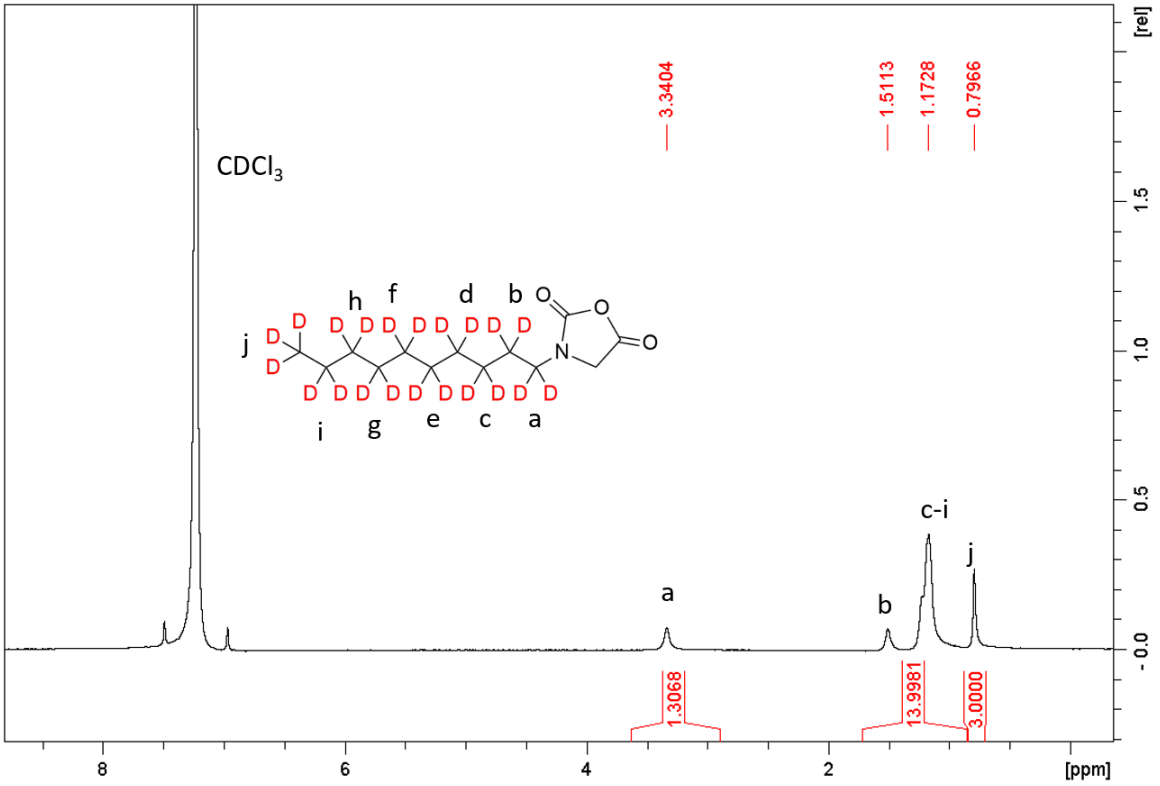

Figure S4.9. ^{2}H NMR spectrum of Decyl-d_{21}-NCA in $CDCl_3$.

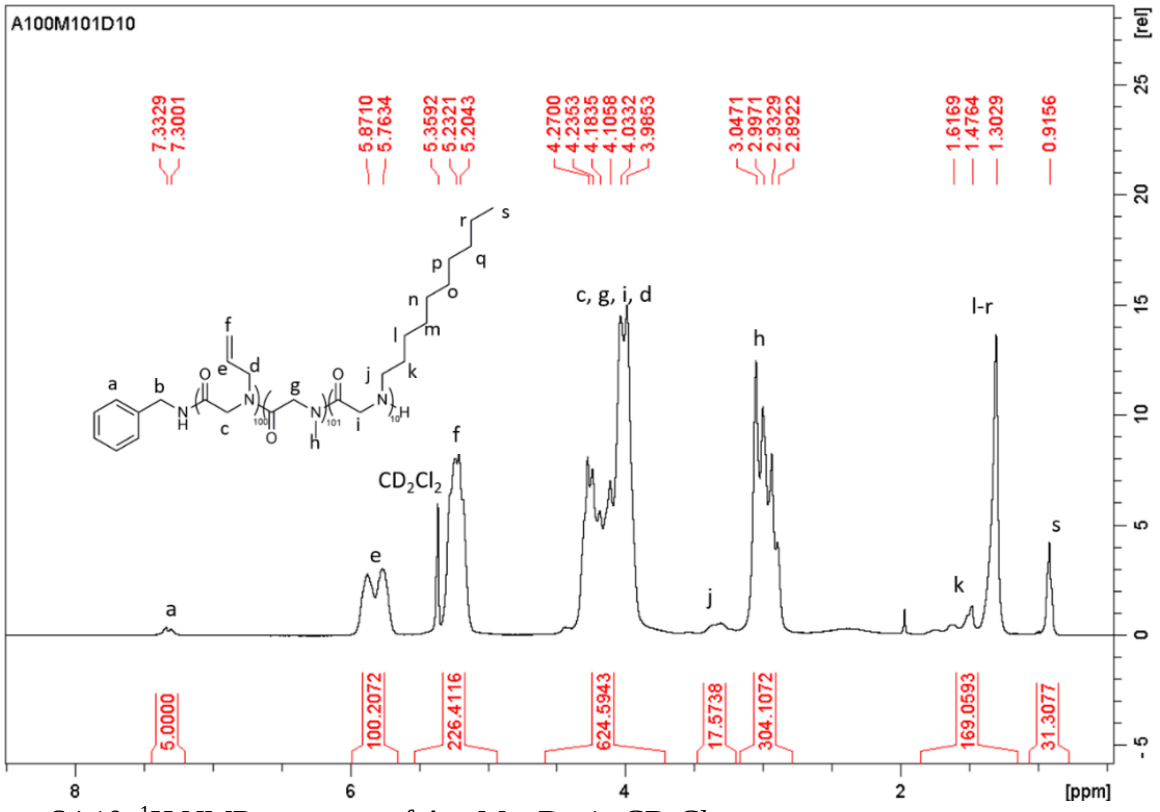

Figure S4.10. ^{1}H NMR spectrum of $A_{100}M_{101}D_{10}$ in CD_2Cl_2.

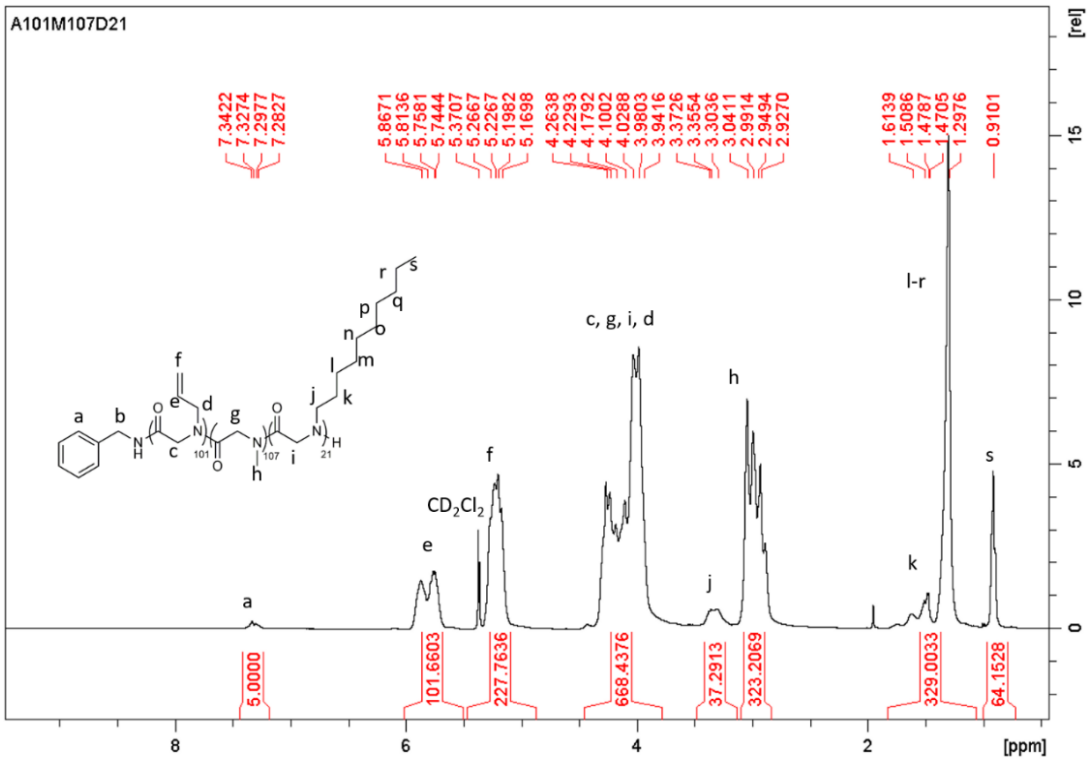

Figure S4.11. ^{1}H NMR spectrum of $A_{101}M_{107}D_{21}$ in CD_2Cl_2.

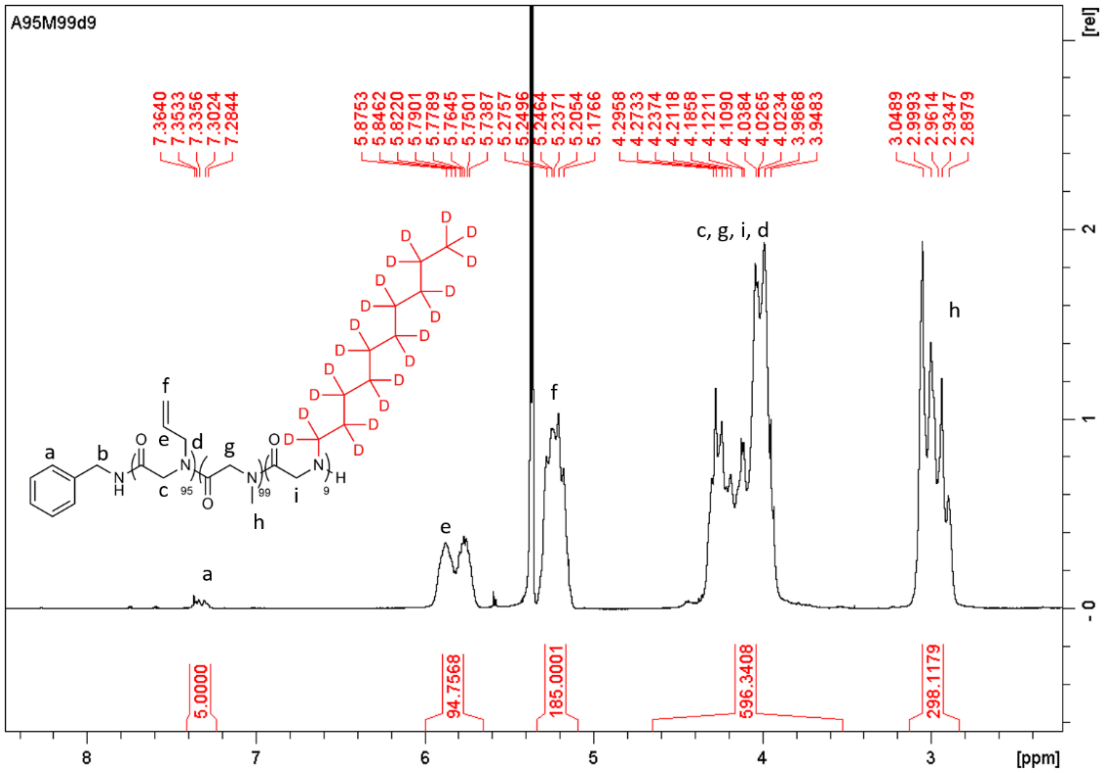

Figure S4.12. ^{1}H NMR spectrum of $A_{95}M_{99}d_9$ in CD_2Cl_2.

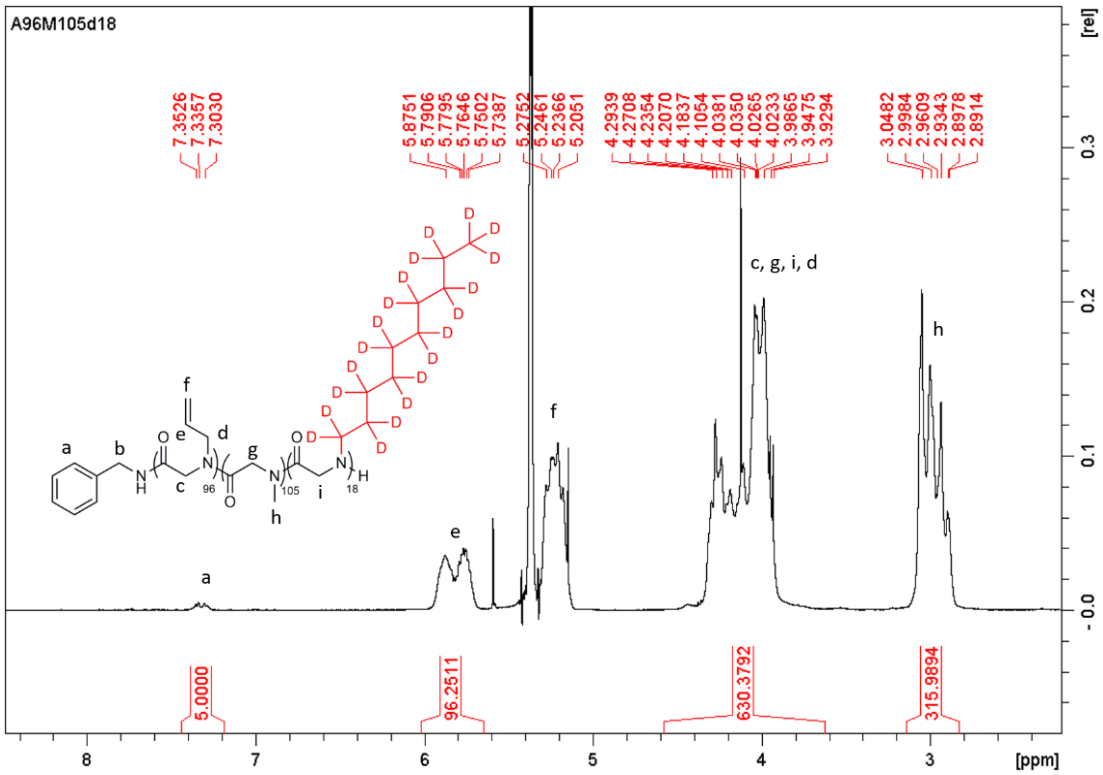

Figure S4.13. ^{1}H NMR spectrum of $A_{96}M_{105}d_{18}$ in CD_2Cl_2.

REFERENCES

Alicja, U.-W.; Barbara, T.; Andrzej, D.; Sijka, I.; Darinka, C., Thermoresponsive hydrogels of hydrophobically modified polyglycidol. *e-Polymers* **2007,** *7* (1), 019.

Angelopoulos, S. A.; Tsitsilianis, C., Thermo-Reversible Hydrogels Based on Poly(N,N-diethylacrylamide)-block-poly(acrylic acid)-block-poly(N,N-diethylacrylamide) Double Hydrophilic Triblock Copolymer. *Macromolecular Chemistry and Physics* **2006,** *207* (23), 2188-2194.

Atlas, R. M.; Bartha, R., Hydrocarbon Biodegradation and Oil Spill Bioremediation. In *Advances in Microbial Ecology*, Marshall, K. C., Ed. Springer US: Boston, MA, 1992; pp 287-338.

Atlas, R. M.; Hazen, T. C., Oil Biodegradation and Bioremediation: A Tale of the Two Worst Spills in U.S. History. *Environmental Science & Technology* **2011,** *45* (16), 6709-6715.

Banerjee, S.; Pal, T. K.; Guha, S. K., Probing molecular interactions of poly(styrene-co-maleic acid) with lipid matrix models to interpret the therapeutic potential of the co-polymer. *Biochimica et Biophysica Acta (BBA) - Biomembranes* **2012,** *1818* (3), 537-550.

Barnaba, C.; Sahoo, B. R.; Ravula, T.; Medina-Meza, I. G.; Im, S.-C.; Anantharamaiah, G. M.; Waskell, L.; Ramamoorthy, A., Cytochrome-P450-Induced Ordering of Microsomal Membranes Modulates Affinity for Drugs. *Angewandte Chemie International Edition* **2018,** *57* (13), 3391-3395.

Bayburt, T. H.; Grinkova, Y. V.; Sligar, S. G., Self-Assembly of Discoidal Phospholipid Bilayer Nanoparticles with Membrane Scaffold Proteins. *Nano Letters* **2002,** *2* (8), 853-856.

Bayburt, T. H.; Sligar, S. G., Self-assembly of single integral membrane proteins into soluble nanoscale phospholipid bilayers. *Protein Science* **2003,** *12* (11), 2476-2481.

Bayburt, T. H.; Sligar, S. G., Membrane protein assembly into Nanodiscs. *FEBS Letters* **2010,** *584* (9), 1721-1727.

Bazzacco, P.; Sharma, K. S.; Durand, G.; Giusti, F.; Ebel, C.; Popot, J.-L.; Pucci, B., Trapping and Stabilization of Integral Membrane Proteins by Hydrophobically Grafted Glucose-Based Telomers. *Biomacromolecules* **2009,** *10* (12), 3317-3326.

Berlepsch, H. v.; Böttcher, C.; Skrabania, K.; Laschewsky, A., Complex domain architecture of multicompartment micelles from a linear ABC triblock copolymer revealed by cryogenic electron tomography. *Chemical Communications* **2009,** (17), 2290-2292.

Binks, B. P.; Philip, J.; Rodrigues, J. A., Inversion of Silica-Stabilized Emulsions Induced by Particle Concentration. *Langmuir* **2005,** *21* (8), 3296-3302.

Binks, B. P.; Whitby, C. P., Nanoparticle silica-stabilised oil-in-water emulsions: improving emulsion stability. *Colloids and Surfaces A: Physicochemical and Engineering Aspects* **2005,** *253* (1), 105-115.

Boldog, T.; Grimme, S.; Li, M.; Sligar, S. G.; Hazelbauer, G. L., Nanodiscs separate chemoreceptor oligomeric states and reveal their signaling properties. *Proceedings of the National Academy of Sciences* **2006,** *103* (31), 11509.

Bookstaver, M.; Bose, A.; Tripathi, A., Interaction of Alcanivorax borkumensis with a Surfactant Decorated Oil–Water Interface. *Langmuir* **2015,** *31* (21), 5875-5881.

Borch, J.; Torta, F.; Sligar, S. G.; Roepstorff, P., Nanodiscs for Immobilization of Lipid Bilayers and Membrane Receptors: Kinetic Analysis of Cholera Toxin Binding to a Glycolipid Receptor. *Analytical Chemistry* **2008,** *80* (16), 6245-6252.

Brouillette, C. G.; Jones, J. L.; Ng, T. C.; Kercret, H.; Chung, B. H.; Segrest, J. P., Structural studies of apolipoprotein A-I/phosphatidylcholine recombinants by high-field proton NMR, nondenaturing gradient gel electrophoresis, and electron microscopy. *Biochemistry* **1984,** *23* (2), 359-367.

Burridge, K. M.; Harding, B. D.; Sahu, I. D.; Kearns, M. M.; Stowe, R. B.; Dolan, M. T.; Edelmann, R. E.; Dabney-Smith, C.; Page, R. C.; Konkolewicz, D.; Lorigan, G. A., Simple Derivatization of RAFT-Synthesized Styrene–Maleic Anhydride Copolymers for Lipid Disk Formulations. *Biomacromolecules* **2020,** *21* (3), 1274-1284.

Cantor, R. S., Lipid Composition and the Lateral Pressure Profile in Bilayers. *Biophysical Journal* **1999,** *76* (5), 2625-2639.

Cao, Y.; Zhu, X. X.; Luo, J.; Liu, H., Effects of Substitution Groups on the RAFT Polymerization of N-Alkylacrylamides in the Preparation of Thermosensitive Block Copolymers. *Macromolecules* **2007,** *40* (18), 6481-6488.

Chae, P. S.; Gotfryd, K.; Pacyna, J.; Miercke, L. J. W.; Rasmussen, S. G. F.; Robbins, R. A.; Rana, R. R.; Loland, C. J.; Kobilka, B.; Stroud, R.; Byrne, B.; Gether, U.; Gellman, S. H., Tandem Facial Amphiphiles for Membrane Protein Stabilization. *Journal of the American Chemical Society* **2010,** *132* (47), 16750-16752.

Chan, B. A.; Xuan, S.; Li, A.; Simpson, J. M.; Sternhagen, G. L.; Yu, T.; Darvish, O. A.; Jiang, N.; Zhang, D., Polypeptoid polymers: Synthesis, characterization, and properties. *Biopolymers* **2017,** *109* (1), e23070.

Chapman, H.; Purnell, K.; Law, R. J.; Kirby, M. F., The use of chemical dispersants to combat oil spills at sea: A review of practice and research needs in Europe. *Marine Pollution Bulletin* **2007,** *54* (7), 827-838.

Colard, C. A. L.; Teixeira, R. F. A.; Bon, S. A. F., Unraveling Mechanistic Events in Solids-Stabilized Emulsion Polymerization by Monitoring the Concentration of Nanoparticles in the Water Phase. *Langmuir* **2010,** *26* (11), 7915-7921.

Craig, A. F.; Clark, E. E.; Sahu, I. D.; Zhang, R.; Frantz, N. D.; Al-Abdul-Wahid, M. S.; Dabney-Smith, C.; Konkolewicz, D.; Lorigan, G. A., Tuning the size of styrene-maleic acid copolymer-lipid nanoparticles (SMALPs) using RAFT polymerization for biophysical studies. *Biochimica et Biophysica Acta (BBA) - Biomembranes* **2016,** *1858* (11), 2931-2939.

Creighton, M. A.; Ohata, Y.; Miyawaki, J.; Bose, A.; Hurt, R. H., Two-Dimensional Materials as Emulsion Stabilizers: Interfacial Thermodynamics and Molecular Barrier Properties. *Langmuir* **2014,** *30* (13), 3687-3696.

Cremaldi, J.; Ejaz, M.; Oak, S.; Holleran, M. K.; Roberts, K.; Cheng, G.; Wang, Y.; Grayson, S. M.; John, V.; Pesika, N. S., Polymer grafted hard carbon microspheres at an oil/water interface. *Journal of Colloid and Interface Science* **2016,** *470*, 31-38.

Cui, Y.; Threlfall, M.; van Duijneveldt, J. S., Optimizing organoclay stabilized Pickering emulsions. *Journal of Colloid and Interface Science* **2011,** *356* (2), 665-671.

Cui, Y.; van Duijneveldt, J. S., Microcapsules Composed of Cross-Linked Organoclay. *Langmuir* **2012,** *28* (3), 1753-1757.

Dalal, K.; Nguyen, N.; Alami, M.; Tan, J.; Moraes, T. F.; Lee, W. C.; Maurus, R.; Sligar, S. S.; Brayer, G. D.; Duong, F., Structure, Binding, and Activity of Syd, a SecY-interacting Protein. *Journal of Biological Chemistry* **2009,** *284* (12), 7897-7902.

D'Andrea, M. A.; Reddy, G. K., Health Consequences among Subjects Involved in Gulf Oil Spill Clean-up Activities. *The American Journal of Medicine* **2013,** *126* (11), 966-974.

Das, N.; Chandran, P., Microbial Degradation of Petroleum Hydrocarbon Contaminants: An Overview. *Biotechnology Research International* **2011,** *2011*.

Dekker, N.; Merck, K.; Tommassen, J.; Verheij, H. M., In Vitro Folding of Escherichia Coli Outer-Membrane Phospholipase A. *European Journal of Biochemistry* **1995,** *232* (1), 214-219.

Denisov, I. G.; Baas, B. J.; Grinkova, Y. V.; Sligar, S. G., Cooperativity in Cytochrome P450 3A4: LINKAGES IN SUBSTRATE BINDING, SPIN STATE, UNCOUPLING, AND PRODUCT FORMATION. *Journal of Biological Chemistry* **2007,** *282* (10), 7066-7076.

Denisov, I. G.; Grinkova, Y. V.; Lazarides, A. A.; Sligar, S. G., Directed Self-Assembly of Monodisperse Phospholipid Bilayer Nanodiscs with Controlled Size. *Journal of the American Chemical Society* **2004,** *126* (11), 3477-3487.

Denisov, I. G.; Sligar, S. G., Nanodiscs for structural and functional studies of membrane proteins. *Nature Structural & Molecular Biology* **2016,** *23* (6), 481-486.

Denisov, I. G.; Sligar, S. G., Nanodiscs in Membrane Biochemistry and Biophysics. *Chemical Reviews* **2017,** *117* (6), 4669-4713.

Dong, J.; Worthen, A. J.; Foster, L. M.; Chen, Y.; Cornell, K. A.; Bryant, S. L.; Truskett, T. M.; Bielawski, C. W.; Johnston, K. P., Modified Montmorillonite Clay Microparticles for Stable Oil-in-Seawater Emulsions. *ACS Applied Materials & Interfaces* **2014,** *6* (14), 11502-11513.

Dörr, J. M.; Koorengevel, M. C.; Schäfer, M.; Prokofyev, A. V.; Scheidelaar, S.; van der Cruijsen, E. A. W.; Dafforn, T. R.; Baldus, M.; Killian, J. A., Detergent-free isolation, characterization, and functional reconstitution of a tetrameric K⁺ channel: The power of native nanodiscs. *Proceedings of the National Academy of Sciences* **2014,** *111* (52), 18607.

Dörr, J. M.; Scheidelaar, S.; Koorengevel, M. C.; Dominguez, J. J.; Schäfer, M.; van Walree, C. A.; Killian, J. A., The styrene–maleic acid copolymer: a versatile tool in membrane research. *European Biophysics Journal* **2016,** *45* (1), 3-21.

Duan, H.; Civjan, N. R.; Sligar, S. G.; Schuler, M. A., Co-incorporation of heterologously expressed Arabidopsis cytochrome P450 and P450 reductase into soluble nanoscale lipid bilayers. *Archives of Biochemistry and Biophysics* **2004,** *424* (2), 141-153.

Dubansky, B.; Whitehead, A.; Miller, J. T.; Rice, C. D.; Galvez, F., Multitissue Molecular, Genomic, and Developmental Effects of the Deepwater Horizon Oil Spill on Resident Gulf Killifish (Fundulus grandis). *Environmental Science & Technology* **2013,** *47* (10), 5074-5082.

43. Durbin, D. M.; Jonas, A., The Effect of Apolipoprotein A-II on the Structure and Function of Apolipoprotein A-I in a Homogeneous Reconstituted High Density Lipoprotein Particle. *Journal of Biological Chemistry* **1997,** *272* (50), 31333-31339.

Fang, B.; Walther, A.; Wolf, A.; Xu, Y.; Yuan, J.; Müller, A. H. E., Undulated Multicompartment Cylinders by the Controlled and Directed Stacking of Polymer Micelles with a Compartmentalized Corona. *Angewandte Chemie International Edition* **2009,** *48* (16), 2877-2880.

Feil, H.; Bae, Y. H.; Feijen, J.; Kim, S. W., Effect of comonomer hydrophilicity and ionization on the lower critical solution temperature of N-isopropylacrylamide copolymers. *Macromolecules* **1993,** *26* (10), 2496-2500.

Fetsch, C.; Flecks, S.; Gieseler, D.; Marschelke, C.; Ulbricht, J.; van Pée, K.-H.; Luxenhofer, R., Self-Assembly of Amphiphilic Block Copolypeptoids with C2-C5 Side Chains in Aqueous Solution. *Macromolecular Chemistry and Physics* **2015,** *216* (5), 547-560.

Fetsch, C.; Luxenhofer, R., Thermal Properties of Aliphatic Polypeptoids. *Polymers* **2013,** *5* (1).

Frolov, V. A.; Shnyrova, A. V.; Zimmerberg, J., Lipid Polymorphisms and Membrane Shape. *Cold Spring Harbor Perspectives in Biology* **2011,** *3* (11).

Fujii, S.; Read, E. S.; Binks, B. P.; Armes, S. P., Stimulus-Responsive Emulsifiers Based on Nanocomposite Microgel Particles. *Advanced Materials* **2005,** *17* (8), 1014-1018.

Gan, J.; Guan, X.; Zheng, J.; Guo, H.; Wu, K.; Liang, L.; Lu, M., Biodegradable, thermoresponsive PNIPAM-based hydrogel scaffolds for the sustained release of levofloxacin. *RSC Advances* **2016,** *6* (39), 32967-32978.

Gao, Y.; Cao, E.; Julius, D.; Cheng, Y., TRPV1 structures in nanodiscs reveal mechanisms of ligand and lipid action. *Nature* **2016,** *534* (7607), 347-351.

Gelot, A.; Friesen, W.; Hamza, H. A., Emulsification of oil and water in the presence of finely divided solids and surface-active agents. *Colloids and Surfaces* **1984,** *12*, 271-303.

Glück, J. M.; Koenig, B. W.; Willbold, D., Nanodiscs allow the use of integral membrane proteins as analytes in surface plasmon resonance studies. *Analytical Biochemistry* **2011,** *408* (1), 46-52.

Greer, D. R.; Stolberg, M. A.; Kundu, J.; Spencer, R. K.; Pascal, T.; Prendergast, D.; Balsara, N. P.; Zuckermann, R. N., Universal Relationship between Molecular Structure and Crystal Structure in Peptoid Polymers and Prevalence of the cis Backbone Conformation. *Journal of the American Chemical Society* **2018,** *140* (2), 827-833.

Grinkova, Y. V.; Denisov, I. G.; Sligar, S. G., Engineering extended membrane scaffold proteins for self-assembly of soluble nanoscale lipid bilayers. *Protein Engineering, Design and Selection* **2010,** *23* (11), 843-848.

Gruner, S. M., Intrinsic curvature hypothesis for biomembrane lipid composition: a role for nonbilayer lipids. *Proceedings of the National Academy of Sciences* **1985,** *82* (11), 3665.

Gulati, S.; Jamshad, M.; Knowles, Timothy J.; Morrison, Kerrie A.; Downing, R.; Cant, N.; Collins, R.; Koenderink, Jan B.; Ford, Robert C.; Overduin, M.; Kerr, Ian D.; Dafforn, Timothy R.; Rothnie, Alice J., Detergent-free purification of ABC (ATP-binding-cassette) transporters. *Biochemical Journal* **2014,** *461* (2), 269-278.

Guo, L.; Lahasky, S. H.; Ghale, K.; Zhang, D., N-Heterocyclic Carbene-Mediated Zwitterionic Polymerization of N-Substituted N-Carboxyanhydrides toward Poly(α-peptoid)s: Kinetic, Mechanism, and Architectural Control. *Journal of the American Chemical Society* **2012,** *134* (22), 9163-9171.

Guo, L.; Zhang, D., Cyclic Poly(α-peptoid)s and Their Block Copolymers from N-Heterocyclic Carbene-Mediated Ring-Opening Polymerizations of N-Substituted N-Carboxylanhydrides. *Journal of the American Chemical Society* **2009,** *131* (50), 18072-18074.

Hacker, M. C.; Klouda, L.; Ma, B. B.; Kretlow, J. D.; Mikos, A. G., Synthesis and Characterization of Injectable, Thermally and Chemically Gelable, Amphiphilic Poly(N-isopropylacrylamide)-Based Macromers. *Biomacromolecules* **2008,** *9* (6), 1558-1570.

Hagn, F.; Etzkorn, M.; Raschle, T.; Wagner, G., Optimized Phospholipid Bilayer Nanodiscs Facilitate High-Resolution Structure Determination of Membrane Proteins. *Journal of the American Chemical Society* **2013,** *135* (5), 1919-1925.

Hardin, N. Z.; Ravula, T.; Mauro, G. D.; Ramamoorthy, A., Hydrophobic Functionalization of Polyacrylic Acid as a Versatile Platform for the Development of Polymer Lipid Nanodisks. *Small* **2019,** *15* (9), 1804813.

He, C.; Kim, S. W.; Lee, D. S., In situ gelling stimuli-sensitive block copolymer hydrogels for drug delivery. *Journal of Controlled Release* **2008,** *127* (3), 189-207.

Head, I. M.; Jones, D. M.; Röling, W. F. M., Marine microorganisms make a meal of oil. *Nature Reviews Microbiology* **2006,** *4*, 173.

Hunter, T. N.; Pugh, R. J.; Franks, G. V.; Jameson, G. J., The role of particles in stabilising foams and emulsions. *Advances in Colloid and Interface Science* **2008,** *137* (2), 57-81.

Jamshad, M.; Charlton, J.; Lin, Y.-P.; Routledge, Sarah J.; Bawa, Z.; Knowles, Timothy J.; Overduin, M.; Dekker, N.; Dafforn, Tim R.; Bill, Roslyn M.; Poyner, David R.; Wheatley, M., G-protein coupled receptor solubilization and purification for biophysical analysis and functional studies, in the total absence of detergent. *Bioscience Reports* **2015,** *35* (2).

Jamshad, M.; Grimard, V.; Idini, I.; Knowles, T. J.; Dowle, M. R.; Schofield, N.; Sridhar, P.; Lin, Y.; Finka, R.; Wheatley, M.; Thomas, O. R. T.; Palmer, R. E.; Overduin, M.; Govaerts, C.; Ruysschaert, J.-M.; Edler, K. J.; Dafforn, T. R., Structural analysis of a nanoparticle containing a lipid bilayer used for detergent-free extraction of membrane proteins. *Nano Research* **2015,** *8* (3), 774-789.

Jiang, J.; Zhu, Y.; Cui, Z.; Binks, B. P., Switchable Pickering Emulsions Stabilized by Silica Nanoparticles Hydrophobized In Situ with a Switchable Surfactant. *Angewandte Chemie* **2013,** *125* (47), 12599-12602.

Jiang, N.; Yu, T.; Darvish, O. A.; Qian, S.; Mkam Tsengam, I. K.; John, V.; Zhang, D., Crystallization-Driven Self-Assembly of Coil–Comb-Shaped Polypeptoid Block Copolymers: Solution Morphology and Self-Assembly Pathways. *Macromolecules* **2019,** *52* (22), 8867-8877.

Jonas, A., [32] Reconstitution of high-density lipoproteins. In *Methods in Enzymology*, Academic Press: 1986; Vol. 128, pp 553-582.

Joye, S. B.; Kleindienst, S.; Gilbert, J. A.; Handley, K. M.; Weisenhorn, P.; Overholt, W. A.; Kostka, J. E., Responses of Microbial Communities to Hydrocarbon Exposures. *Oceanography* **2016,** *29* (3), 136-149.

Kasai, Y.; Kishira, H.; Sasaki, T.; Syutsubo, K.; Watanabe, K.; Harayama, S., Predominant growth of Alcanivorax strains in oil-contaminated and nutrient-supplemented sea water. *Environmental Microbiology* **2002,** *4* (3), 141-147.

Katepalli, H.; John, V. T.; Bose, A., The Response of Carbon Black Stabilized Oil-in-Water Emulsions to the Addition of Surfactant Solutions. *Langmuir* **2013,** *29* (23), 6790-6797.

Kelarakis, A.; Havredaki, V.; Yuan, X.-F.; Chaibundit, C.; Booth, C., Aqueous Gels of Triblock Copolymers of Ethylene Oxide and 1,2-Butylene Oxide (Type BEB) Studied by Rheometry. *Macromolecular Chemistry and Physics* **2006,** *207* (10), 903-909.

Kelarakis, A.; Yuan, X.-F.; Mai, S.-M.; Yang, Y.-W.; Booth, C., Aqueous micellar solutions of a triblock copolymer of ethylene oxide and 1,2-butylene oxide, B12E114B12. Scaling the viscoelasticity of fluid and gel. *Physical Chemistry Chemical Physics* **2003,** *5* (12), 2628-2634.

Kim, J.; Cote, L. J.; Kim, F.; Yuan, W.; Shull, K. R.; Huang, J., Graphene Oxide Sheets at Interfaces. *Journal of the American Chemical Society* **2010,** *132* (23), 8180-8186.

Kleindienst, S.; Seidel, M.; Ziervogel, K.; Grim, S.; Loftis, K.; Harrison, S.; Malkin, S. Y.; Perkins, M. J.; Field, J.; Sogin, M. L.; Dittmar, T.; Passow, U.; Medeiros, P. M.; Joye, S. B., Chemical dispersants can suppress the activity of natural oil-degrading microorganisms. *Proceedings of the National Academy of Sciences* **2015**.

Knowles, T. J.; Finka, R.; Smith, C.; Lin, Y.-P.; Dafforn, T.; Overduin, M., Membrane Proteins Solubilized Intact in Lipid Containing Nanoparticles Bounded by Styrene Maleic Acid Copolymer. *Journal of the American Chemical Society* **2009,** *131* (22), 7484-7485.

Kohori, F.; Sakai, K.; Aoyagi, T.; Yokoyama, M.; Sakurai, Y.; Okano, T., Preparation and characterization of thermally responsive block copolymer micelles comprising poly (N-isopropylacrylamide-b-DL-lactide). *Journal of controlled release* **1998,** *55* (1), 87-98.

Kubowicz, S.; Baussard, J.-F.; Lutz, J.-F.; Thünemann, A. F.; von Berlepsch, H.; Laschewsky, A., Multicompartment Micelles Formed by Self-Assembly of Linear ABC Triblock Copolymers in Aqueous Medium. *Angewandte Chemie International Edition* **2005,** *44* (33), 5262-5265.

Kujawinski, E. B.; Kido Soule, M. C.; Valentine, D. L.; Boysen, A. K.; Longnecker, K.; Redmond, M. C., Fate of Dispersants Associated with the Deepwater Horizon Oil Spill. *Environmental Science & Technology* **2011,** *45* (4), 1298-1306.

Lahasky, S. H.; Hu, X.; Zhang, D., Thermoresponsive Poly(α-peptoid)s: Tuning the Cloud Point Temperatures by Composition and Architecture. *ACS Macro Letters* **2012,** *1* (5), 580-584.

Lahasky, S. H.; Hu, X.; Zhang, D., Thermoresponsive poly (α-peptoid) s: tuning the cloud point temperatures by composition and architecture. *ACS Macro Letters* **2012,** *1* (5), 580-584.

Leahy, J. G.; Colwell, R. R., Microbial degradation of hydrocarbons in the environment. *Microbiological Reviews* **1990,** *54* (3), 305-315.

Lee, C.-U.; Li, A.; Ghale, K.; Zhang, D., Crystallization and Melting Behaviors of Cyclic and Linear Polypeptoids with Alkyl Side Chains. *Macromolecules* **2013,** *46* (20), 8213-8223.

Lee, C.-U.; Smart, T. P.; Guo, L.; Epps, T. H.; Zhang, D., Synthesis and Characterization of Amphiphilic Cyclic Diblock Copolypeptoids from N-Heterocyclic Carbene-Mediated Zwitterionic Polymerization of N-Substituted N-Carboxyanhydride. *Macromolecules* **2011,** *44* (24), 9574-9585.

Lee, S. C.; Khalid, S.; Pollock, N. L.; Knowles, T. J.; Edler, K.; Rothnie, A. J.; R.T.Thomas, O.; Dafforn, T. R., Encapsulated membrane proteins: A simplified system for molecular simulation. *Biochimica et Biophysica Acta (BBA) - Biomembranes* **2016,** *1858* (10), 2549-2557.

Lee, S. C.; Knowles, T. J.; Postis, V. L. G.; Jamshad, M.; Parslow, R. A.; Lin, Y.-p.; Goldman, A.; Sridhar, P.; Overduin, M.; Muench, S. P.; Dafforn, T. R., A method for detergent-free isolation of membrane proteins in their local lipid environment. *Nature Protocols* **2016,** *11* (7), 1149-1162.

Leitz, A. J.; Bayburt, T. H.; Barnakov, A. N.; Springer, B. A.; Sligar, S. G., Functional reconstitution of β2-adrenergic receptors utilizing self-assembling Nanodisc technology. *BioTechniques* **2006,** *40* (5), 601-612.

Li, L.; Chen, J.; Mishra, V. K.; Kurtz, J. A.; Cao, D.; Klon, A. E.; Harvey, S. C.; Anantharamaiah, G. M.; Segrest, J. P., Double Belt Structure of Discoidal High Density Lipoproteins: Molecular Basis for Size Heterogeneity. *Journal of Molecular Biology* **2004,** *343* (5), 1293-1311.

Li, S.; Nie, H.; Gu, S.; Han, Z.; Han, G.; Zhang, W., Synthesis of Multicompartment Nanoparticles of ABC Miktoarm Star Polymers by Seeded RAFT Dispersion Polymerization. *ACS Macro Letters* **2019,** *8* (7), 783-788.

Lindhoud, S.; Carvalho, V.; Pronk, J. W.; Aubin-Tam, M.-E., SMA-SH: Modified Styrene–Maleic Acid Copolymer for Functionalization of Lipid Nanodiscs. *Biomacromolecules* **2016,** *17* (4), 1516-1522.

Liu, H. Y.; Zhu, X. X., Lower critical solution temperatures of N-substituted acrylamide copolymers in aqueous solutions. *Polymer* **1999,** *40* (25), 6985-6990.

Livesey, A. K.; Brochon, J. C., Analyzing the distribution of decay constants in pulse-fluorimetry using the maximum entropy method. *Biophysical journal* **1987,** *52* (5), 693-706.

Lodge, T. P.; Rasdal, A.; Li, Z.; Hillmyer, M. A., Simultaneous, Segregated Storage of Two Agents in a Multicompartment Micelle. *Journal of the American Chemical Society* **2005,** *127* (50), 17608-17609.

Logez, C.; Damian, M.; Legros, C.; Dupré, C.; Guéry, M.; Mary, S.; Wagner, R.; M'Kadmi, C.; Nosjean, O.; Fould, B.; Marie, J.; Fehrentz, J.-A.; Martinez, J.; Ferry, G.; Boutin, J. A.; Banères, J.-L., Detergent-free Isolation of Functional G Protein-Coupled Receptors into Nanometric Lipid Particles. *Biochemistry* **2016,** *55* (1), 38-48.

Lvov, Y.; Wang, W.; Zhang, L.; Fakhrullin, R., Halloysite Clay Nanotubes for Loading and Sustained Release of Functional Compounds. *Advanced Materials* **2015,** *28* (6), 1227-1250.

Marin, V. L.; Bayburt, T. H.; Sligar, S. G.; Mrksich, M., Functional Assays of Membrane-Bound Proteins with SAMDI-TOF Mass Spectrometry. *Angewandte Chemie International Edition* **2007,** *46* (46), 8796-8798.

Mason, O. U.; Hazen, T. C.; Borglin, S.; Chain, P. S. G.; Dubinsky, E. A.; Fortney, J. L.; Han, J.; Holman, H.-Y. N.; Hultman, J.; Lamendella, R.; Mackelprang, R.; Malfatti, S.; Tom, L. M.; Tringe, S. G.; Woyke, T.; Zhou, J.; Rubin, E. M.; Jansson, J. K., Metagenome, metatranscriptome and single-cell sequencing reveal microbial response to Deepwater Horizon oil spill. *The Isme Journal* **2012,** *6*, 1715.

Matz, C. E.; Jonas, A., Micellar complexes of human apolipoprotein A-I with phosphatidylcholines and cholesterol prepared from cholate-lipid dispersions. *Journal of Biological Chemistry* **1982,** *257* (8), 4535-4540.

May, S., Protein-induced bilayer deformations: the lipid tilt degree of freedom. *European Biophysics Journal* **2000,** *29* (1), 17-28.

Mi, L.-Z.; Grey, M. J.; Nishida, N.; Walz, T.; Lu, C.; Springer, T. A., Functional and Structural Stability of the Epidermal Growth Factor Receptor in Detergent Micelles and Phospholipid Nanodiscs. *Biochemistry* **2008,** *47* (39), 10314-10323.

Morrison, K. A.; Akram, A.; Mathews, A.; Khan, Z. A.; Patel, J. H.; Zhou, C.; Hardy, D. J.; Moore-Kelly, C.; Patel, R.; Odiba, V.; Knowles, T. J.; Javed, M.-u.-H.; Chmel, N. P.; Dafforn, T. R.; Rothnie, A. J., Membrane protein extraction and purification using styrene–maleic acid (SMA) copolymer: effect of variations in polymer structure. *Biochemical Journal* **2016,** *473* (23), 4349-4360.

Mouritsen, O. G., Lipids, curvature, and nano-medicine. *European Journal of Lipid Science and Technology* **2011,** *113* (10), 1174-1187.

Murakami, R.; Moriyama, H.; Yamamoto, M.; Binks, B. P.; Rocher, A., Particle Stabilization of Oil-in-Water-in-Air Materials: Powdered Emulsions. *Advanced Materials* **2012,** *24* (6), 767-771.

Nagle, J. F.; Tristram-Nagle, S., Structure of lipid bilayers. *Biochimica et Biophysica Acta (BBA) - Reviews on Biomembranes* **2000,** *1469* (3), 159-195.

Nath, A.; Atkins, W. M.; Sligar, S. G., Applications of Phospholipid Bilayer Nanodiscs in the Study of Membranes and Membrane Proteins. *Biochemistry* **2007,** *46* (8), 2059-2069.

Noordam, P. C.; Killian, A.; Oude Elferink, R. F. M.; de Gier, J., Comparative study on the properties of saturated phosphatidylethanolamine and phosphatidylcholine bilayers: Barrier characteristics and susceptibility to phospholipase A2 degradation. *Chemistry and Physics of Lipids* **1982,** *31* (2), 191-204.

Olivera, N. L.; Nievas, M. L.; Lozada, M.; del Prado, G.; Dionisi, H. M.; Siñeriz, F., Isolation and characterization of biosurfactant-producing Alcanivorax strains: hydrocarbon accession strategies and alkane hydroxylase gene analysis. *Research in Microbiology* **2009,** *160* (1), 19-26.

Oluwole, A. O.; Danielczak, B.; Meister, A.; Babalola, J. O.; Vargas, C.; Keller, S., Solubilization of Membrane Proteins into Functional Lipid-Bilayer Nanodiscs Using a Diisobutylene/Maleic Acid Copolymer. *Angewandte Chemie International Edition* **2017,** *56* (7), 1919-1924.

Orekhov, P. S.; Bozdaganyan, M. E.; Voskoboynikova, N.; Mulkidjanian, A. Y.; Steinhoff, H.-J.; Shaitan, K. V., Styrene/Maleic Acid Copolymers Form SMALPs by Pulling Lipid Patches out of the Lipid Bilayer. *Langmuir* **2019,** *35* (10), 3748-3758.

Orwick, M. C.; Judge, P. J.; Procek, J.; Lindholm, L.; Graziadei, A.; Engel, A.; Gröbner, G.; Watts, A., Detergent-Free Formation and Physicochemical Characterization of Nanosized Lipid–Polymer Complexes: Lipodisq. *Angewandte Chemie International Edition* **2012,** *51* (19), 4653-4657.

Orwick-Rydmark, M.; Lovett, J. E.; Graziadei, A.; Lindholm, L.; Hicks, M. R.; Watts, A., Detergent-Free Incorporation of a Seven-Transmembrane Receptor Protein into Nanosized Bilayer Lipodisq Particles for Functional and Biophysical Studies. *Nano Letters* **2012,** *12* (9), 4687-4692.

Overington, J. P.; Al-Lazikani, B.; Hopkins, A. L., How many drug targets are there? *Nature Reviews Drug Discovery* **2006,** *5* (12), 993-996.

Owoseni, O.; Nyankson, E.; Zhang, Y.; Adams, S. J.; He, J.; McPherson, G. L.; Bose, A.; Gupta, R. B.; John, V. T., Release of Surfactant Cargo from Interfacially-Active Halloysite Clay Nanotubes for Oil Spill Remediation. *Langmuir* **2014,** *30* (45), 13533-13541.

Owoseni, O.; Zhang, Y.; Su, Y.; He, J.; McPherson, G. L.; Bose, A.; John, V. T., Tuning the Wettability of Halloysite Clay Nanotubes by Surface Carbonization for Optimal Emulsion Stabilization. *Langmuir* **2015,** *31* (51), 13700-13707.

Panchal, A.; Swientoniewski, L. T.; Omarova, M.; Yu, T.; Zhang, D.; Blake, D. A.; John, V.; Lvov, Y. M., Bacterial proliferation on clay nanotube Pickering emulsions for oil spill bioremediation. *Colloids and Surfaces B: Biointerfaces* **2018,** *164*, 27-33.

Park, S. H.; Berkamp, S.; Cook, G. A.; Chan, M. K.; Viadiu, H.; Opella, S. J., Nanodiscs versus Macrodiscs for NMR of Membrane Proteins. *Biochemistry* **2011,** *50* (42), 8983-8985.

Paulin, S.; Jamshad, M.; Dafforn, T. R.; Garcia-Lara, J.; Foster, S. J.; Galley, N. F.; Roper, D. I.; Rosado, H.; Taylor, P. W., Surfactant-free purification of membrane protein complexes from bacteria: application to the staphylococcal penicillin-binding protein complex PBP2/PBP2a. *Nanotechnology* **2014,** *25* (28), 285101.

Pedersen, J. S., Form factors of block copolymer micelles with spherical, ellipsoidal and cylindrical cores. *Journal of Applied Crystallography* **2000,** *33* (3), 637-640.

Pedersen, J. S.; Gerstenberg, M. C., Scattering form factor of block copolymer micelles. *Macromolecules* **1996,** *29* (4), 1363-1365.

Perrin, E.; Bizot, H.; Cathala, B.; Capron, I., Chitin Nanocrystals for Pickering High Internal Phase Emulsions. *Biomacromolecules* **2014,** *15* (10), 3766-3771.

Pertici, V.; Pin-Barre, C.; Rivera, C.; Pellegrino, C.; Laurin, J. r. m.; Gigmes, D.; Trimaille, T., Degradable and injectable hydrogel for drug delivery in soft tissues. *Biomacromolecules* **2018,** *20* (1), 149-163.

Pertici, V.; Trimaille, T.; Gigmes, D., Inputs of Macromolecular Engineering in the Design of Injectable Hydrogels Based on Synthetic Thermoresponsive Polymers. *Macromolecules* **2020,** *53* (2), 682-692.

Pi, G.; Li, Y.; Bao, M.; Mao, L.; Gong, H.; Wang, Z., Novel and Environmentally Friendly Oil Spill Dispersant Based on the Synergy of Biopolymer Xanthan Gum and Silica Nanoparticles. *ACS Sustainable Chemistry & Engineering* **2016,** *4* (6), 3095-3102.

Popot, J. L.; Althoff, T.; Bagnard, D.; Banères, J. L.; Bazzacco, P.; Billon-Denis, E.; Catoire, L. J.; Champeil, P.; Charvolin, D.; Cocco, M. J.; Crémel, G.; Dahmane, T.; de la Maza, L. M.; Ebel, C.; Gabel, F.; Giusti, F.; Gohon, Y.; Goormaghtigh, E.; Guittet, E.; Kleinschmidt, J. H.; Kühlbrandt, W.; Le Bon, C.; Martinez, K. L.; Picard, M.; Pucci, B.; Sachs, J. N.; Tribet, C.; van Heijenoort, C.; Wien, F.; Zito, F.; Zoonens, M., Amphipols From A to Z. *Annual Review of Biophysics* **2011,** *40* (1), 379-408.

Postis, V.; Rawson, S.; Mitchell, J. K.; Lee, S. C.; Parslow, R. A.; Dafforn, T. R.; Baldwin, S. A.; Muench, S. P., The use of SMALPs as a novel membrane protein scaffold for structure study by negative stain electron microscopy. *Biochimica et Biophysica Acta (BBA) - Biomembranes* **2015,** *1848* (2), 496-501.

Powell, K. C.; Chauhan, A., Interfacial Tension and Surface Elasticity of Carbon Black (CB) Covered Oil–Water Interface. *Langmuir* **2014,** *30* (41), 12287-12296.

Prabudiansyah, I.; Kusters, I.; Caforio, A.; Driessen, A. J. M., Characterization of the annular lipid shell of the Sec translocon. *Biochimica et Biophysica Acta (BBA) - Biomembranes* **2015,** *1848* (10, Part A), 2050-2056.

Prade, E.; Mahajan, M.; Im, S.-C.; Zhang, M.; Gentry, K. A.; Anantharamaiah, G. M.; Waskell, L.; Ramamoorthy, A., A Minimal Functional Complex of Cytochrome P450 and FBD of Cytochrome P450 Reductase in Nanodiscs. *Angewandte Chemie International Edition* **2018,** *57* (28), 8458-8462.

Prince, R. C.; Butler, J. D., A protocol for assessing the effectiveness of oil spill dispersants in stimulating the biodegradation of oil. *Environmental Science and Pollution Research* **2014,** *21* (16), 9506-9510.

Ravula, T.; Hardin, N. Z.; Bai, J.; Im, S.-C.; Waskell, L.; Ramamoorthy, A., Effect of polymer charge on functional reconstitution of membrane proteins in polymer nanodiscs. *Chemical Communications* **2018,** *54* (69), 9615-9618.

Ravula, T.; Hardin, N. Z.; Di Mauro, G. M.; Ramamoorthy, A., Styrene maleic acid derivates to enhance the applications of bio-inspired polymer based lipid-nanodiscs. *European Polymer Journal* **2018,** *108*, 597-602.

Ravula, T.; Hardin, N. Z.; Ramadugu, S. K.; Cox, S. J.; Ramamoorthy, A., Formation of pH-Resistant Monodispersed Polymer–Lipid Nanodiscs. *Angewandte Chemie International Edition* **2018,** *57* (5), 1342-1345.

Ravula, T.; Hardin, N. Z.; Ramamoorthy, A., Polymer nanodiscs: Advantages and limitations. *Chemistry and Physics of Lipids* **2019,** *219*, 45-49.

Ravula, T.; Ishikuro, D.; Kodera, N.; Ando, T.; Anantharamaiah, G. M.; Ramamoorthy, A., Real-Time Monitoring of Lipid Exchange via Fusion of Peptide Based Lipid-Nanodiscs. *Chemistry of Materials* **2018,** *30* (10), 3204-3207.

Ravula, T.; Ramadugu, S. K.; Di Mauro, G.; Ramamoorthy, A., Bioinspired, Size-Tunable Self-Assembly of Polymer–Lipid Bilayer Nanodiscs. *Angewandte Chemie International Edition* **2017,** *56* (38), 11466-11470.

Reichelt, R.; Schmidt, T.; Kuckling, D.; Arndt, K.-F., Structural characterization of temperature-sensitive hydrogels by field emission scanning electron microscopy (FESEM). *Macromolecular Symposia* **2004,** *210* (1), 501-511.

Ren, J., Application in the Field of Biomedical Materials. In *Biodegradable Poly(Lactic Acid): Synthesis, Modification, Processing and Applications*, Ren, J., Ed. Springer Berlin Heidelberg: Berlin, Heidelberg, 2010; pp 240-272.

Rigaud, J. L.; Levy, D.; Mosser, G.; Lambert, O., Detergent removal by non-polar polystyrene beads. *European Biophysics Journal* **1998,** *27* (4), 305-319.

Robertson, E. J.; Olivier, G. K.; Qian, M.; Proulx, C.; Zuckermann, R. N.; Richmond, G. L., Assembly and molecular order of two-dimensional peptoid nanosheets through the oil–water interface. *Proceedings of the National Academy of Sciences* **2014,** *111* (37), 13284.

Robinson, J. W.; Secker, C.; Weidner, S.; Schlaad, H., Thermoresponsive Poly (N-C3 glycine) s. *Macromolecules* **2013,** *46* (3), 580-587.

Rothnie, A. J., Detergent-Free Membrane Protein Purification. In *Heterologous Expression of Membrane Proteins: Methods and Protocols*, Mus-Veteau, I., Ed. Springer New York: New York, NY, 2016; pp 261-267.

Rothnie, A. J., Detergent-Free Membrane Protein Purification. *Methods Mol Biol* **2016,** *1432*, 261-7.

Rouck, J. E.; Krapf, J. E.; Roy, J.; Huff, H. C.; Das, A., Recent advances in nanodisc technology for membrane protein studies (2012–2017). *FEBS Letters* **2017,** *591* (14), 2057-2088.

Saha, A.; Nikova, A.; Venkataraman, P.; John, V. T.; Bose, A., Oil Emulsification Using Surface-Tunable Carbon Black Particles. *ACS Applied Materials & Interfaces* **2013,** *5* (8), 3094-3100.

Sanii, B.; Haxton, T. K.; Olivier, G. K.; Cho, A.; Barton, B.; Proulx, C.; Whitelam, S.; Zuckermann, R. N., Structure-Determining Step in the Hierarchical Assembly of Peptoid Nanosheets. *ACS Nano* **2014,** *8* (11), 11674-11684.

Scheidelaar, S.; Koorengevel, Martijn C.; Pardo, Juan D.; Meeldijk, Johannes D.; Breukink, E.; Killian, J. A., Molecular Model for the Solubilization of Membranes into Nanodisks by Styrene Maleic Acid Copolymers. *Biophysical Journal* **2015,** *108* (2), 279-290.

Seddon, A. M.; Curnow, P.; Booth, P. J., Membrane proteins, lipids and detergents: not just a soap opera. *Biochimica et Biophysica Acta (BBA) - Biomembranes* **2004,** *1666* (1), 105-117.

Shen, P. S.; Yang, X.; DeCaen, P. G.; Liu, X.; Bulkley, D.; Clapham, D. E.; Cao, E., The Structure of the Polycystic Kidney Disease Channel PKD2 in Lipid Nanodiscs. *Cell* **2016,** *167* (3), 763-773.e11.

Shi, L.; Shen, Q.-T.; Kiel, A.; Wang, J.; Wang, H.-W.; Melia, T. J.; Rothman, J. E.; Pincet, F., SNARE Proteins: One to Fuse and Three to Keep the Nascent Fusion Pore Open. *Science* **2012,** *335* (6074), 1355.

Silva, R. A. G. D.; Huang, R.; Morris, J.; Fang, J.; Gracheva, E. O.; Ren, G.; Kontush, A.; Jerome, W. G.; Rye, K.-A.; Davidson, W. S., Structure of apolipoprotein A-I in spherical high density lipoproteins of different sizes. *Proceedings of the National Academy of Sciences* **2008,** *105* (34), 12176.

Smith, A. A. A.; Autzen, H. E.; Laursen, T.; Wu, V.; Yen, M.; Hall, A.; Hansen, S. D.; Cheng, Y.; Xu, T., Controlling Styrene Maleic Acid Lipid Particles through RAFT. *Biomacromolecules* **2017,** *18* (11), 3706-3713.

Sorial, G. A.; Venosa, A. D.; Koran, K. M.; Holder, E.; King, D. W., Oil Spill Dispersant Effectiveness Protocol. II: Performance of Revised Protocol. *Journal of Environmental Engineering* **2004,** *130* (10), 1085-1093.

Swainsbury, D. J. K.; Scheidelaar, S.; Foster, N.; van Grondelle, R.; Killian, J. A.; Jones, M. R., The effectiveness of styrene-maleic acid (SMA) copolymers for solubilisation of integral membrane proteins from SMA-accessible and SMA-resistant membranes. *Biochimica et Biophysica Acta (BBA) - Biomembranes* **2017,** *1859* (10), 2133-2143.

Tao, H.; Lee, S. C.; Moeller, A.; Roy, R. S.; Siu, F. Y.; Zimmermann, J.; Stevens, R. C.; Potter, C. S.; Carragher, B.; Zhang, Q., Engineered nanostructured β-sheet peptides protect membrane proteins. *Nature Methods* **2013,** *10* (8), 759-761.

Taribagil, R. R.; Hillmyer, M. A.; Lodge, T. P., Hydrogels from ABA and ABC Triblock Polymers. *Macromolecules* **2010,** *43* (12), 5396-5404.

Teodorescu, M.; Andrei, M.; Turturică, G.; Stănescu, P. O.; Zaharia, A.; Sârbu, A., Novel Thermoreversible Injectable Hydrogel Formulations Based on Sodium Alginate and Poly(N-Isopropylacrylamide). *International Journal of Polymeric Materials and Polymeric Biomaterials* **2015,** *64* (15), 763-771.

Theiss, D.; Schmidt, T.; Arndt, K.-F., Temperature-sensitive poly(vinyl methyl ether) hydrogel beads. *Macromolecular Symposia* **2004,** *210* (1), 465-474.

Tribet, C.; Audebert, R.; Popot, J.-L., Amphipols: Polymers that keep membrane proteins soluble in aqueous solutions. *Proceedings of the National Academy of Sciences* **1996,** *93* (26), 15047.

Ulbricht, J.; Jordan, R.; Luxenhofer, R., On the biodegradability of polyethylene glycol, polypeptoids and poly(2-oxazoline)s. *Biomaterials* **2014,** *35* (17), 4848-4861.

Ulbricht, J.; Jordan, R.; Luxenhofer, R., On the biodegradability of polyethylene glycol, polypeptoids and poly (2-oxazoline) s. *Biomaterials* **2014,** *35* (17), 4848-4861.

Valentine, D. L.; Kessler, J. D.; Redmond, M. C.; Mendes, S. D.; Heintz, M. B.; Farwell, C.; Hu, L.; Kinnaman, F. S.; Yvon-Lewis, S.; Du, M.; Chan, E. W.; Tigreros, F. G.; Villanueva, C.

J., Propane Respiration Jump-Starts Microbial Response to a Deep Oil Spill. *Science* **2010,** *330* (6001), 208-211.

van Zoelen, W.; Zuckermann, R. N.; Segalman, R. A., Tunable Surface Properties from Sequence-Specific Polypeptoid–Polystyrene Block Copolymer Thin Films. *Macromolecules* **2012,** *45* (17), 7072-7082.

Vanaken, T.; Foxall-Vanaken, S.; Castleman, S.; Ferguson-Miller, S., [3] Alkyl glycoside detergents: Synthesis and applications to the study of membrane proteins. In *Methods in Enzymology*, Academic Press: 1986; Vol. 125, pp 27-35.

Vargas, C.; Arenas, R. C.; Frotscher, E.; Keller, S., Nanoparticle self-assembly in mixtures of phospholipids with styrene/maleic acid copolymers or fluorinated surfactants. *Nanoscale* **2015,** *7* (48), 20685-20696.

Vignati, E.; Piazza, R.; Lockhart, T. P., Pickering Emulsions: Interfacial Tension, Colloidal Layer Morphology, and Trapped-Particle Motion. *Langmuir* **2003,** *19* (17), 6650-6656.

Walz, J. Y., Colloidal Particles at Liquid Interfaces Edited by Bernard P. Binks and Tommy S. Horozov (University of Hull, U.K.). Cambridge University Press: Cambridge. 2006. XIV + 504 pp. $145.00. ISBN 0-521-84846-6. *Journal of the American Chemical Society* **2007,** *129* (13), 4106-4107.

Wang, J.; Liu, G.; Wang, L.; Li, C.; Xu, J.; Sun, D., Synergistic stabilization of emulsions by poly(oxypropylene)diamine and Laponite particles. *Colloids and Surfaces A: Physicochemical and Engineering Aspects* **2010,** *353* (2), 117-124.

Won, Y.-Y.; Brannan, A. K.; Davis, H. T.; Bates, F. S., Cryogenic Transmission Electron Microscopy (Cryo-TEM) of Micelles and Vesicles Formed in Water by Poly(ethylene oxide)-Based Block Copolymers. *The Journal of Physical Chemistry B* **2002,** *106* (13), 3354-3364.

Wongkongkatep, P.; Manopwisedjaroen, K.; Tiposoth, P.; Archakunakorn, S.; Pongtharangkul, T.; Suphantharika, M.; Honda, K.; Hamachi, I.; Wongkongkatep, J., Bacteria Interface Pickering Emulsions Stabilized by Self-assembled Bacteria–Chitosan Network. *Langmuir* **2012,** *28* (13), 5729-5736.

Xia, Y.; Yin, X.; Burke, N. A. D.; Stöver, H. D. H., Thermal Response of Narrow-Disperse Poly(N-isopropylacrylamide) Prepared by Atom Transfer Radical Polymerization. *Macromolecules* **2005,** *38* (14), 5937-5943.

Xuan, S.; Lee, C.-U.; Chen, C.; Doyle, A. B.; Zhang, Y.; Guo, L.; John, V. T.; Hayes, D.; Zhang, D., Thermoreversible and Injectable ABC Polypeptoid Hydrogels: Controlling the Hydrogel Properties through Molecular Design. *Chemistry of Materials* **2016,** *28* (3), 727-737.

Xue, M.; Cheng, L.; Faustino, I.; Guo, W.; Marrink, S. J., Molecular Mechanism of Lipid Nanodisk Formation by Styrene-Maleic Acid Copolymers. *Biophysical Journal* **2018,** *115* (3), 494-502.

Yah, W. O.; Takahara, A.; Lvov, Y. M., Selective Modification of Halloysite Lumen with Octadecylphosphonic Acid: New Inorganic Tubular Micelle. *Journal of the American Chemical Society* **2012,** *134* (3), 1853-1859.

Yang, Y.; Fang, Z.; Chen, X.; Zhang, W.; Xie, Y.; Chen, Y.; Liu, Z.; Yuan, W., An Overview of Pickering Emulsions: Solid-Particle Materials, Classification, Morphology, and Applications. *Frontiers in Pharmacology* **2017,** *8* (287).

Yasuhara, K.; Arakida, J.; Ravula, T.; Ramadugu, S. K.; Sahoo, B.; Kikuchi, J.-i.; Ramamoorthy, A., Spontaneous Lipid Nanodisc Fomation by Amphiphilic Polymethacrylate Copolymers. *Journal of the American Chemical Society* **2017,** *139* (51), 18657-18663.

Zhang, D.; Lahasky, S. H.; Guo, L.; Lee, C.-U.; Lavan, M., Polypeptoid Materials: Current Status and Future Perspectives. *Macromolecules* **2012,** *45* (15), 5833-5841.

Zhang, J.; Li, L.; Xu, J.; Sun, D., Effect of cetyltrimethylammonium bromide addition on the emulsions stabilized by montmorillonite. *Colloid and Polymer Science* **2014,** *292* (2), 441-447.

Zhang, M.; Huang, R.; Ackermann, R.; Im, S.-C.; Waskell, L.; Schwendeman, A.; Ramamoorthy, A., Reconstitution of the Cytb5–CytP450 Complex in Nanodiscs for Structural Studies using NMR Spectroscopy. *Angewandte Chemie International Edition* **2016,** *55* (14), 4497-4499.

Zhang, Q.; Ma, X.; Ward, A.; Hong, W.-X.; Jaakola, V.-P.; Stevens, R. C.; Finn, M. G.; Chang, G., Designing Facial Amphiphiles for the Stabilization of Integral Membrane Proteins. *Angewandte Chemie International Edition* **2007,** *46* (37), 7023-7025.

Zhang, R.; Sahu, I. D.; Bali, A. P.; Dabney-Smith, C.; Lorigan, G. A., Characterization of the structure of lipodisq nanoparticles in the presence of KCNE1 by dynamic light scattering and transmission electron microscopy. *Chemistry and Physics of Lipids* **2017,** *203*, 19-23.

Zhang, R.; Sahu, I. D.; Liu, L.; Osatuke, A.; Comer, R. G.; Dabney-Smith, C.; Lorigan, G. A., Characterizing the structure of lipodisq nanoparticles for membrane protein spectroscopic studies. *Biochimica et Biophysica Acta (BBA) - Biomembranes* **2015,** *1848* (1, Part B), 329-333.

Zhang, Y.; Xuan, S.; Owoseni, O.; Omarova, M.; Li, X.; Saito, M. E.; He, J.; McPherson, G. L.; Raghavan, S. R.; Zhang, D.; John, V. T., Amphiphilic Polypeptoids Serve as the Connective Glue to Transform Liposomes into Multilamellar Structures with Closely Spaced Bilayers. *Langmuir* **2017,** *33* (11), 2780-2789.

Zhou, C.; Hillmyer, M. A.; Lodge, T. P., Efficient Formation of Multicompartment Hydrogels by Stepwise Self-Assembly of Thermoresponsive ABC Triblock Terpolymers. *Journal of the American Chemical Society* **2012,** *134* (25), 10365-10368.

Zhou, C.; Toombes, G. E.; Wasbrough, M. J.; Hillmyer, M. A.; Lodge, T. P., Structure of two-compartment hydrogels from thermoresponsive ABC triblock terpolymers. *Macromolecules* **2015,** *48* (16), 5934-5943.

Zhou, J.; Qiao, X.; Binks, B. P.; Sun, K.; Bai, M.; Li, Y.; Liu, Y., Magnetic Pickering Emulsions Stabilized by Fe3O4 Nanoparticles. *Langmuir* **2011,** *27* (7), 3308-3316.

VITA

Tianyi Yu was born in Shandong, China. She attended East China University of Science and Technology in Shanghai, China, and gained her B.Eng. degree in Polymer Science and Engineering in 2012. She attended the M.S. program in Department of Polymer Science at The University of Akron in Ohio in 2011 and gained her M.S. degree in Polymer Science in 2013. She joined the Ph.D. program in Department of Chemistry at Louisiana State University in 2015. She conducted her graduate research under the supervision of Professor Donghui Zhang and successfully defended her Ph.D. dissertation on Oct 16th, 2020.